Charles University in Prague
Faculty of Mathematics and Physics
Institute of Theoretical Physics

Ph.D. Thesis

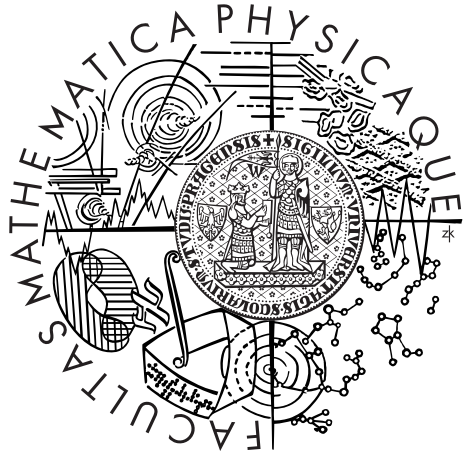

Billiard time machine

Jindřich Dolanský
Supervisor: doc. RNDr. Jiří Langer, CSc.
Field of study: F–12 General physics

Acknowledgements

First of all, I wish to thank to Pavel Krtouš for his guidance, support and large number of helpful discussions during my Ph.D. studies. I would equally like to thank to my supervisor, Jiří Langer, for his help and inspiring comments during the preparation of this work.

In Prague, January 2011

Contents

Title: *Billiard time machine*
Author: *Jindřich Dolanský*
Department: *Institute of Theoretical Physics*
Supervisor: *doc. RNDr. Jiří Langer, CSc.*
Supervisor's e-mail address: *Jiri.Langer@mff.cuni.cz*
Abstract: *In this work we investigate a simple interacting system of an elastic particle in the non-relativistic spacetime with a nontrivial causal structure realized by a wormhole with a time shift. We require that standard local physical laws hold, and search for their globally consistent solutions, i.e, we assume the validity of the principle of self-consistency. If there were nontrivial set of initial conditions which would violate this principle, the system would be logically inconsistent. We show that the investigated system is not inconsistent in this sense, i.e., that all standard initial conditions have a globally consistent evolution. Even for the so called dangerous initial conditions which threaten to result into the paradoxical situation a consistent solution exists. In this case, the paradoxical collision-free trajectory is superseded by a special consistent self-colliding trajectory. Moreover, we demonstrate that more than one globally consistent evolution exists for a wide class of initial conditions. Thus, the evolution of the described system is not unique due to the nontrivial causal structure of the spacetime. We find and analyze all solutions with multiple self-collisions for the point-particle, and all trajectories with one self-collision for the finite ball. Thanks to the chosen model we are able carry out a detailed explicit analysis of the structure of solutions. This elaborated model can be reused for another analysis, for example, study of systems with multiple self-collisions of the finite ball, which can be necessary for resolution of open problems.*
Keywords: *wormhole time machines, principle of self-consistency, conical space, evolution of the system, self-collision, self-intersection, dangerous initial conditions, paradoxical self-intersection, dangerous self-collision*

Název práce: *Stroj času jako kulečník*
Autor: *Jindřich Dolanský*
Katedra: *Ústav teoretické fyziky*
Školitel: *doc. RNDr. Jiří Langer, CSc.*
Školitelova e-mailová adresa: *Jiri.Langer@mff.cuni.cz*
Abstrakt: *V této práci zkoumáme jednoduchý interagující systém dokonale pružné částice v nerelativistickém časoprostoru s netriviální kauzální strukturou uskutečněnou červí dírou s časovým posunem. Požadujeme platnost standardních lokálních fyzikálních zákonů a hledáme globálně konzistentní řešení, t.j., předpokládáme, že platí princip self-konzistence. Jestliže by existovala netriviální množina počátečních hodnot, která by porušovala tento princip, systém by byl logicky nekonzistentní. Ukážeme, že zkoumaný systém není nekonzistentní v tomto smyslu, t.j., že pro všechny počáteční podmínky existují globálně konzistentní řešení. Dokonce i pro potenciálně paradoxní podmínky, které by mohly vyústit v nekonzistentní situace, lze nalézt konzistentní řešení. V tomto případě jsou nesrážkové paradoxní trajektorie nahrazeny speciálními konzistentními srážkovými trajektoriemi. Demonstrujeme, že pro širokou množinu počátečních dat existuje více než jedno globálně konzistentní řešení. Vývoj popisovaného systému není jednoznačný díky netriviální kauzální struktuře daného časoprostoru. Najdeme a analyzujeme všechna řešení pro libovolný počet self-srážek bodové částice a všechna řešení pro jednu self-srážku konečné koule. Díky zvolenému časoprostoru můžeme provést detailní a explicitní analýzu struktury řešení. Zpracovaný model může být využit k dalšímu studiu, například systému s libovolným počtem self-srážek pro konečnou kouli, a vyřešení některých neuzavřených problémů.*
Klíčová slova: *červoděrové stroje času, princip self-konzistence, kónický prostor, self-srážka, self-průsečík, potenciálně paradoxní počáteční podmínky, paradoxní self-průsečík*

Chapter 1

Introduction

Time travel is a phenomenon which has been attracting interest both in fiction and general discussions for a long time. However, only after a formulation of the theory of relativity could such considerations be investigated on a more scientific and solid basis.

Already, the special relativity shows that different observers experience different times and one of them can "travel" to the future of the other one by means of his relative motion (e.g., an astronaut returning from a trip to the centre of our galaxy after spending 40 years in a spaceship comes to the Earth where more than 50,000 years have elapsed). Obviously, traveling (communicating) *back* in time is equivalent to exceeding the speed of light in special relativity as clearly illustrated, e.g., in [1].

Thanks to the general theory of relativity a possibility opens that an observer could travel even to his own past – his worldline could pass through a geometrically or topologically nontrivial area to a region where the worldline originally started [2, 3]. Worldlines which even cross themselves are called *closed timelike curves (CTCs)* and it is customary to say that spacetimes with CTCs contain *time machines*[4, 5].

1.1 The principle of self-consistency

Spacetimes with time machines are causally nontrivial – in such spacetimes one can send a signal to one's own past or even try to influence the past – which immediately opens a question of consistency of standard physical laws as we know them. On a formal level, it is the question of the existence of solutions of physical equations of motion and the question of whether the initial value problem is well-possessed. On a less formal level, these problems can be phrased as the well-known "grandfather paradox," suggested, e.g., in [6, 7, 8]: in spacetimes with time machines, one has to face a logical riddle of what happens if one travels to his own past and kills his grandfather. Consequently, one would never be born, and therefore, one could not travel to the past.

This is a clearly inconsistent situation which suggests that spacetimes with CTCs are pathological and they should be excluded from serious scientific consideration. However, a system containing live beings is too complicated by too many unknown physical laws, and therefore, one cannot be sure that the inconsistency of the grand-father paradox

is really inescapable. Hence, there have been attempts to reinterpret this paradox as a badly formulated problem, since the initial conditions are affected by the outcome of the experiment. A consistent solution of this problem could be an existence of a law which always prevents the grandson from killing his grandfather [9, 10].

To formulate this point (for much simpler systems) more precisely new terms have to be introduced. Let us consider a spacetime containing a time machine and we want to study a system with well-known local physical laws (e.g.,a point particle, or electromagnetic field). We do not change these local laws, i.e. we require that they hold locally in any small spacetime domain (by the principle of correspondence any sufficiently small spacetime domain resembles spacetime of special relativity where we know the local physics). However, in addition to the local laws we also require the so-called *principle of self-consistency* [11, 12, 13]. Namely, a *globally consistent* solution of local laws must exist. It means, that we allow the system to propagate itself to its own past; however, it must be done in a *consistent* way with the original evolution in the past.

The key question of studies of time machines is whether such globally consistent evolutions exist for given local laws and whether these global evolutions are sufficiently generic. More accurately, it is questioned if there exist consistent solutions for all, or, at least, for almost all standard initial data. Otherwise, if the local laws have no globally consistent solution, the spacetime would be clearly pathological and we could rule it out from our consideration. Similarly, the pathology would be serious if the local physical laws had only few globally consistent solutions.

This point could be stated more clearly if one considers a spacetime which is causally nice up to some moment (formally: globally hyperbolic up to some Cauchy hypersurface) and a time machine forms only after this moment. The spacetime thus contains CTCs, however they are bounded and one cannot travel to an arbitrary far past. In such a spacetime one would like to have a globally consistent solution of local laws for *any* standard initial conditions formulated in causally nice past (i.e., before the time machine was formed). In other words, it should not influence or restrict us now (when, let's assume, time machines do not exist) if somebody in a far future invents and constructs a time machine. On other hand, if the existence of a time machine in a future would restrict initial condition in causally regular past we would consider such a spacetime pathological.

In the last two decades physicists have considered various spacetimes with CTCs and studied the consistency of different physical systems in these spacetimes. Surprisingly, such studies have shown that for a simple physical system pathology of spacetimes is not so severe and the equations of motion can be consistently solved. Let us mention the results for a system of interacting particles [14, 11, 15] or the scalar field theory [12, 16] where it was shown that standard local laws have globally consistent solutions even in the presence of CTCs. Another surprising result of such studies is that the existence of time machines does not usually restrict a number of consistent solution, but on the contrary, it leads to a possibility of more than one globally consistent solution for given initial values. In spacetimes with time machines, we thus usually lose the uniqueness of the evolution [14].

As an example, especially in [14], the system of the billiard balls in spacetime with wormholes has been studied. This system allows a straightforward reformulation of the grandfather paradox: the ball could be sent through the time machine in such a way

that it hits itself and thus prevents itself to enter the time machine. Although it seems that such "paradoxical" initial conditions do not lead to a consistent evolution of the system, it was shown that such solution(s) really exist(s).

1.2 Wormholes-based time machines

Let us shortly review basic knowledge on wormholes since we will use it to define the time machine spacetime. The simplest way how to construct relativistic spacetimes with CTCs is to consider a wormhole which can be then deformed to a time machine – such a procedure is described in detail, e.g., in reference [4]. The wormhole can be viewed as a shortcut between two spatial places which could be very distant in the surrounding space. The entries into the wormhole are called *mouths* of the wormhole. A simple spatial wormhole can be obtained by cutting out two spheres in a three dimensional space and gluing the surfaces of these holes together, cf. figure 2.1a. We thus obtain a topologically and geometrically nontrivial space which is not a simply connected space, and the geometry on the glued surface is not flat.

Spacetimes with nontrivial topology contain curves noncontractible into a point, i.e. curves passing through the (traversable) wormhole. However, the topological censorship theorem states that in any asymptotically flat, globally hyperbolic spacetime such that every inextendible null geodesics satisfies the ANEC (Averaged Null Energy Condition), every causal curve from past null infinity to future null infinity is contractible into a causal curve that lies in a topologically trivial neighbourhood of infinity, i.e., it lies entirely in asymptotically flat region and does not pass through the nontrivial topology, [17, 18]. In other words, it prohibits causal curves passing through the wormhole and leaving it any time in future, i.e., any active probing of the topology of space is forbidden.

Loosely rephrased, any asymptotically flat, globally hyperbolic spacetime containing a traversable wormhole and satisfying the Einstein field equations must violate the ANEC (for at least one inextendible null geodesics). It has been shown, in [4], that there has to be present enough "exotic" matter, which violates the ANEC (also the AWEC – Averaged Weak Energy Condition), to maintain the traversable wormhole. Because the wormhole is made of the "exotic" matter the traveller moving through it at very high speed measures negative energy density accompanied by violation of the weak energy condition (also by the other energy conditions, [19]) which causes the wormhole to act like a diverging lens. The precise conditions under which traversable wormholes spacetimes would be permitted are mainly subject of quantum field theory and have not been resolved yet [6].

In order to turn wormhole into time machine a time shift between the mouths has to be induced. It can be done, for example, by placing the mouths into different gravitational potentials [20], or by accelerating one mouth of the wormhole relative to the other [4]. Immediately as the time shift between the mouths becomes greater than their spatial distance in the outer spacetime the connected regions turn out to be causally connected through the wormhole (CTCs form).

Commonly, two kinds of time machine spacetimes are distinguished: Either CTCs emerge at some time (for example, the Morris-Thorne-Yurtsever time machine space-

time [19]), or CTCs are always present (the eternal time machine spacetime). The first case implies that the spacetime is divided by the Cauchy horizon into region without the CTCs (before the first CTC forms) and with the CTCs (after the first CTC emerges). This null hypersurface divides spacetime into globally hyperbolic part where we can uniquely predict outcomes of our experiments and into non-globally hyperbolic where outcomes of experiments could be influenced by information from the future. The second case implies that CTCs can be chosen through each spacetime point, and so there is no spacelike Cauchy hypersurface where initial values used to be defined. Hence, it is not possible to pose the initial problem in the usual manner. Though in some cases we can pose the initial value problem at past null infinity if we can suppose that spacetime is asymptotically flat [16].

1.3 Plan of the work

In this work, we will consider the system of a self-interacting particle in non-relativistic spacetime with the time machine. Thanks to a special time machine configuration which significantly simplifies the analysis we will be able to solve the equations of motion explicitly. This allow us show that any initial conditions, even such that lead to an apparently inconsistent solution which mimics discussed grandfather paradox, have globally consistent evolutions, and that such solutions of local laws are not, in general, unique. After we present the time machine spacetime and determine possible self-interactions, we will discuss by turns one collision of the point-particle, one collision of the finite ball, and multiple collisions of the point-particle.[1] For easier understanding and possibility of formulation of a particular issue we will occasionally vary from the billiard ball to the limit of point-particle in the text. Let us outline contents of all chapters as follow one after another.

In the next chapter we will introduce a conical space which will serve as an arena for particles' trajectories. Then we will establish time shift on the space by identifying the mouths of the wormhole with different (external) times. This will provide us the desired time machine configuration to study particles' trajectories.

The third chapter will be devoted to rules of motion. Notions of self-intersections and self-collisions will be introduced. Then we will describe dangerous initial conditions which could lead to paradoxical situations. Next, rules of self-collisions will be analyzed and possible types of self-collisions will be found. Finally, we will specify the geometry of self-collisions and investigate another symmetry resulting from the conical geometry.

In the fourth chapter we will introduce parameters for initial trajectories and define quantities to describe self-collisions on these trajectories. We will neglect radius of the particle and concentrate on trajectories and self-collisions of point-like particles. In this case, the discussion simplifies considerably since particle's motion turns out to be scale invariant. Later, in chapter 5, we will include into consideration the nonzero radius to gain full account of self-collisions for billiard ball-like particles. First, we will study collision-free trajectories. Next, we will specify the conditions for self-collisions and formulate equations of motion for the point particle with one self-collision. Thus, we

[1] The first two cases have been summarized within articles [21, 22], attached as appendices H and I, while publication concerning the multiple collisions is being prepared.

will consider at most one self-collision though there can occur multiple self-collisions which will be subject of the chapter 6. Then, we will find and discuss globally consistent solutions of equations of motion. Finally, a non-uniqueness of the evolutions in the presence of time machines will be demonstrated for the point particle model.

In the fifth chapter the discussion will be extended to the case of a non-relativistic, freely moving solid ball with finite radius. We will concentrate on the self-collision occurring closest to the vertex and assume the same range of the apex angle as in the previous chapter. We will show that the free trajectories given by the dangerous initial conditions can be replaced by the trajectories possessing self-collisions to avoid the paradoxical situations. This will result into the conservation of the number of solutions for given initial data, i.e., it will be shown that their number is the same for dangerous initial data as for generic ones. Finally, we will express geometrical restrictions imposing constraints on initial values which guarantee that the ball fits in the conical space.

In the last chapter we will give a comprehensive explanation of multiple self-collisions interspaced by multiple self-intersections. In other words, a point particle coming from a distant region of the conical space passes many times through the wormhole and self-collides repeatedly before leaving to the distant region again. Because of the complexity of corresponding expressions increases considerably we will consider only the case of point-like particles. The possibility of multiple self-collisions and self-intersections enlarges a number of solutions for given initial data and more complicated methods will be employed to describe and interpret corresponding solutions.

Chapter 2

Conical spacetime with time machine

In this chapter we will introduce a conical space which will serve as the arena for particles' trajectories. Then we will identify the mouths of the wormhole with a time shift whereby we will obtain the conical space with a time machine. This will provide us the background to study trajectories in presence of the time machine.

2.1 The non-relativistic case

In the spacetime picture, we have to specify also the moments of time when both mouths are identified. It seems natural to assume that they are identified at the same time, but it is not necessary. In the relativistic setup, it is even not clear what "at the same moment" means. The times of identification of both mouths must be specified explicitly on both sides. Of course, we have the restriction, that time must run continuously through the wormhole, i.e., locally, for the observer sitting in the wormhole, clocks on both sides must tick at the same rate without any jumps.

Let us assume as an example two mouths in the Minkowski spacetime which are at rest with respect to the same inertial frame, but they are identified with a time shift Δt equal, say, to one hour. Time on both sides of the wormhole runs in the same rate, so going through the wormhole does not affect an observer in any specific way. However, going through the wormhole, the observer arrives one hour to the future (or to the past, depending on the direction) with respect to the global inertial frame. Depending on the distance of both mouths in the surrounding space such a configuration may form the time machine: if the observer traveling through the wormhole one hour into the past is able to return through the surrounding space to his original position in less than one hour, he can form CTC, i.e., he can return to his own past and meet himself.

However, we will restrict ourselves to *non-relativistic* situation in this work as we will study elastic collisions of *finite rigid spherical balls*. Thus, we will assume that the speed of light is infinite, and it determines a unique notion of simultaneity and thus it allows us to define a global time – at least, before introducing a time machine. We also assume that the space is locally Euclidean.

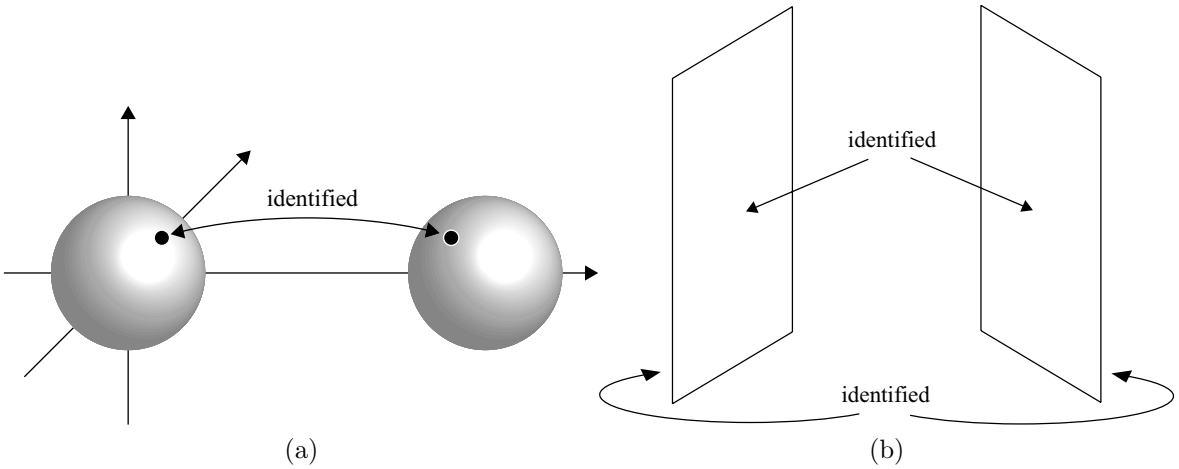

Figure 2.1: **Spatial representation of two simple wormholes.** (a) A wormhole formed by identification of two spherical holes in the surrounding Euclidean space. Surfaces of both spheres are isometrically identified. Since the external curvature of these surfaces is non-vanishing, the geometry near the glued spherical surface is not flat. (b) A wormhole obtained by gluing two planar sections (which, could be obtained from (a) by squeezing the spheres into very thin planes). The external curvature is vanishing with the exception of the boundary of the planar sections and the geometry through the wormhole is thus flat.

To construct the wormhole two space regions must be identified again. However, because the proposed spacetime is non-relativistic the "twin paradox" effect cannot be used to induce time shift between two mouths as discussed above. On the other hand, in this case, thanks to the global simultaneity, we uniquely know what it means when both mouths of the wormhole are identified at the same time. If we identify them with any nonvanishing time shift Δt we immediately obtain the time machine, since the passage through the wormhole takes us to a different moment of time with respect to the global time of the surrounding spacetime. Of course, it destroys the standard causal structure of the non-relativistic spacetime (a clear distinction between future and past), but despite this we will keep using and referring to the original notion of the simultaneity and to the global time of the surrounding space.

2.2 Conical space

In this work, we consider an even simpler situation of the wormhole with planar mouths instead of spherical ones, cf. fig. 2.1(a). Namely, we cut out from the space two planar sections which we identify as in figure 2.1(b). Since we use *flat planar* sections, their identification is geometrically trivial, i.e., spacetime in them is flat everywhere, the space is locally Euclidean, without matter. Here we have ignored problematic boundaries of our planar sections. The whole curvature of the mouths is squeezed to the borders of the planar sections which can be understood as a kind of solid frames on which the traversable parts of the wormhole are spanned.

To avoid a discussion of the wormhole boundary we assume that the planar sections are much larger than the scales of our experiments. In this approximation we can

even assume that the planar sections are infinite. As an idealization, we consider the mouths of our wormhole to be two half-planes with a common boundary line, called the *axis*. These two half-planes form an angle γ. If we identify them (first, say, at the same moment of time) the space between them becomes a locally Euclidean space with a conical singularity localized on the axis. Indeed, if we restrict ourselves to the two-dimensional picture and ignore the direction parallel to the axis, our space forms a cone with the vertex angle γ.

Notice that only such a trajectory can intersect itself which closes a loop situated in a plane perpendicular to the axis. Such a loop can be always superposed to the outer trajectories (the initial and final trajectory) lying also in a plane. Let us assume that both the loop and outer trajectories are bound to the same plane as momentum is not changed by rotation of the outer trajectories. Thus, we will restrict our study to particles moving perpendicularly to the axis, i.e., we will consider motion within the two-dimensional cone.

Of course, this is a over idealized situation. We should keep in mind that the mouths of the wormhole are large but finite, so somewhere very far from the axis, the conical part of the space ends and goes over to the full Euclidean space. But in most of our discussion, we restrict ourselves only to the part of the space between the mouths of the wormhole. We thus effectively work in the conical space with angle γ around the axis.

Let us stress that in our original construction the mouths of the wormhole are special and privileged – given by the position of the wormhole. However, after enlarging them to the semi-infinite size and restricting ourselves only to the conical space between mouths, we can no longer localize the position of the mouths by local experiments. The geometry through the mouths is locally Euclidean, as it is anywhere else. We thus obtained a space which is axially symmetric with respect to the rotation around the axis (it has also translation symmetry along the axis and it is static). The position of the wormhole can be identified only on scales larger than the wormhole, from the surrounding globally Euclidean space – however, this region is very far and we do not consider it.

Finally, we assume that the vertex angle γ of the cone is smaller than π since only for such angles we obtain interesting situations when the straight trajectory of a free particle intersects itself. Indeed, on the cone with $\gamma < \pi$ a straight line intersects itself at least once. To be specific, for $\gamma \in [\frac{\pi}{n+1}, \frac{\pi}{n})$, the straight line intersects itself n-times alternately on two opposite radial lines, i.e. separated by the half of the vertex angle $\gamma/2$, thanks to the conical geometry. In figure 2.2 we can see the straight trajectory within the conical space for two different values of the vertex angle: For $\gamma \in (\pi/2, \pi)$, fig. 2.2(a,b), the trajectory intersects itself just once, while for $\gamma \in (\pi/5, \pi/4]$, 2.2(c,d), it intersects itself four times. In the next chapters it will be explained why the angle in each intersection is equal to $\pi - j\gamma$ (for $j \in [1, \mathrm{Quotient}(\pi, \gamma)]$) and decreases by γ as it recedes from the vertex. Notice also that we have employed two distinct representations which will be used throughout the text: First, we can unfold the cone into an angle in a plane within which are straight trajectories represented by straight lines, cf. fig. 2.2(a,c). However, we can rescale angular coordinates bounded in the interval $[-\gamma/2, \gamma/2]$ by the factor $2\pi/\gamma$ in such a way that it cover full range $[-\pi, \pi]$, cf. fig. 2.2(b,d). In such a case, which we call "bird's eye view" case, straight trajectories are represented as loops winding around the vertex and escaping the cone eventually.

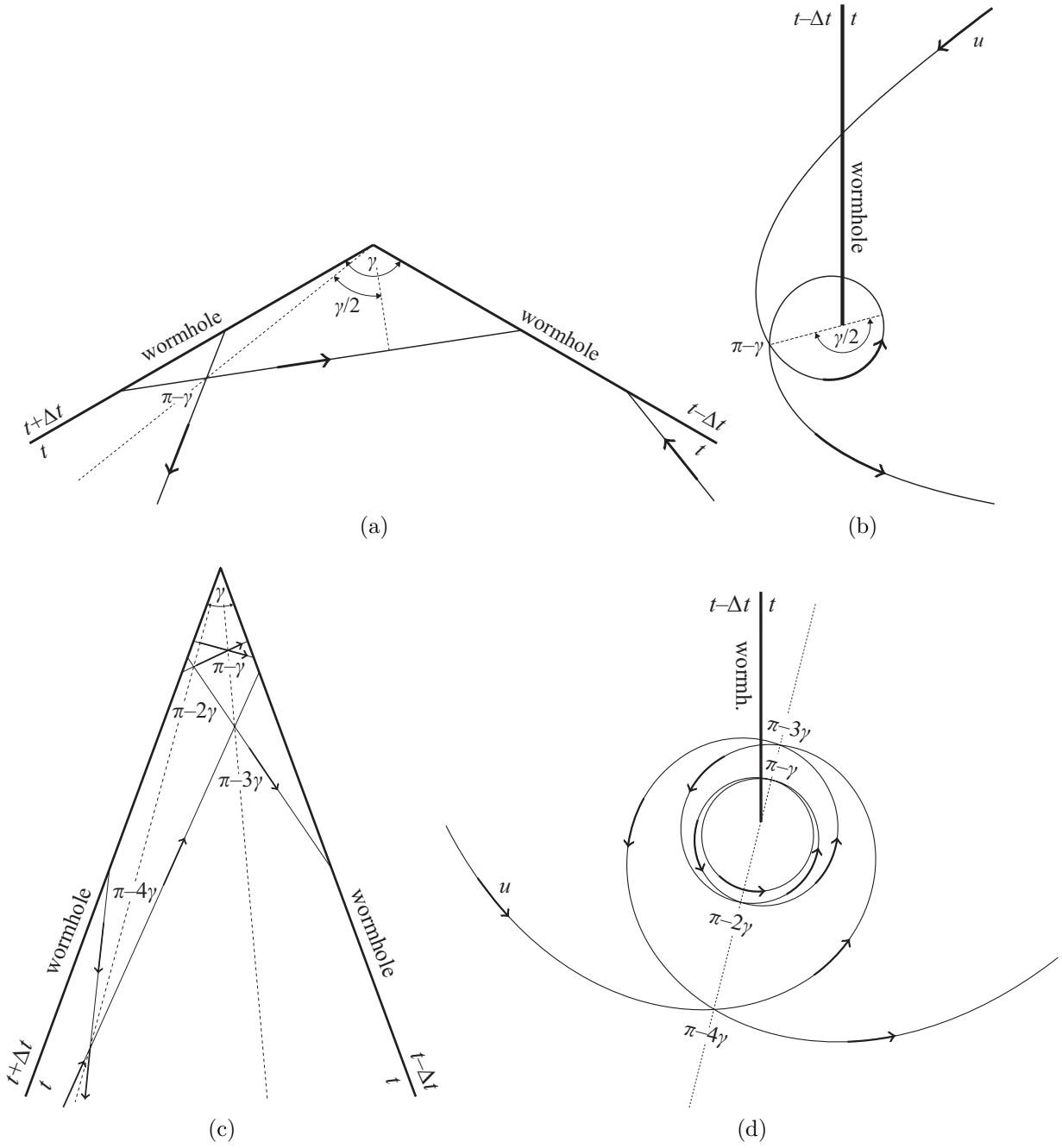

Figure 2.2: **Straight line on the cone.** We assume that the angle γ around the vertex of the cone is smaller than π since only for such angles we obtain interesting situations when the straight trajectory of a free particle intersects itself. To be specific, for $\gamma \in [\frac{\pi}{n+1}, \frac{\pi}{n})$ the straight line intersects itself n-times alternately on two opposite radial lines, i.e., separated by the half of the vertex angle $\gamma/2$, thanks to the conical geometry. We can see the straight trajectory within the conical space for two different values of the vertex angle: (a,b) For $\gamma \in (\pi/2, \pi)$ the trajectory intersects itself just once, while (c,d) for $\gamma \in (\pi/5, \pi/4]$ it intersects itself four times. In the next chapters it will be explained why the angle in each intersection is equal to $\pi - j\gamma$ (for $j \in [1, \text{Quotient}(\pi, \gamma)]$) and decreases by γ as it recedes from the vertex. Notice also that we have employed two distinct representations which will be used throughout the text: In (a,c) we have unfolded the cone into an angle in a plane within which are straight trajectories represented by straight lines. In (b,d) we have rescaled angular coordinates bounded in the interval $[-\gamma/2, \gamma/2]$ by the factor $2\pi/\gamma$ in such a way that it cover full range $[-\pi, \pi]$. In this case of "bird's eye view", straight trajectories are represented as loops winding around the vertex and escaping the cone eventually.

2.3 Conical time machine

In the previous paragraph we have assumed the identification of both mouths at the same moment of a global time. Since we want to study a conical space with a time machine, we have to identify the two planar mouths with a time difference Δt. After such an identification the spacetime is still locally Euclidian, even through the wormhole, (except the axis, of course), but endowed with a strange causal structure. Hypersurfaces of simultaneity (visualized in the standard spacetime diagram as horizontal planes) propagate through the wormhole and form "helical" surfaces winding around the vertex. This indicates that the spacetime contains CTCs. The particle moving toward the wormhole reads that the external time t increases continuously until it enters the wormhole mouth. But by crossing one of the mouths the external time t either increases by Δt into $t + \Delta t > t$, or decreases by $-\Delta t$ into $t - \Delta t < t$.

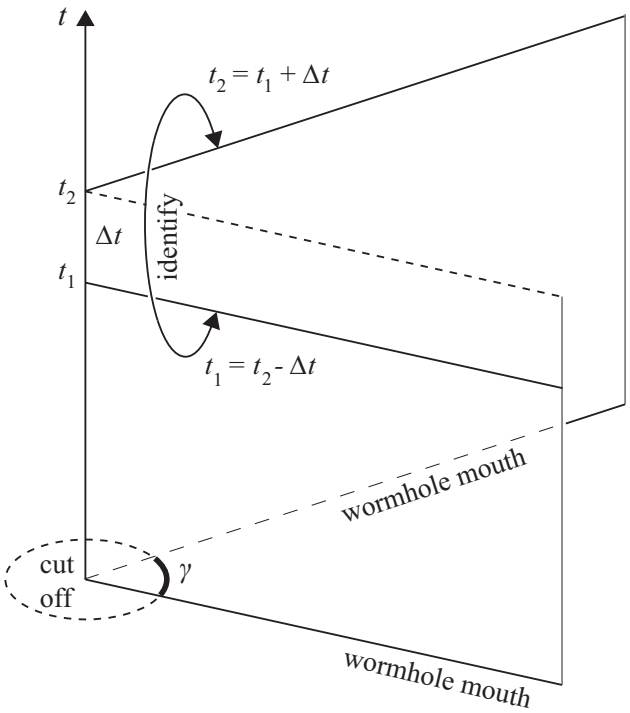

Figure 2.3: **A spacetime diagram of the conical time machine.** The vertical direction is temporal, horizontal planes correspond to the hypersurface of simultaneity of the original spacetime (the third spatial direction is suppressed). Two half-planes forming the boundary of the conical spacetime represent the history of the mouths of the wormhole, and they are identified with a time shift Δt.

This can be visualized in the non-relativistic spacetime diagram in figure 2.3. Here, two spatial directions perpendicular to the axis are represented by horizontal directions; the direction parallel to the axis is suppressed. The vertical direction corresponds to time. Semi-planar mouths of the wormhole at one moment are thus depicted as horizontal semi-lines, their time evolution as vertical half-planes. The identification of two such half-planes is not on the same vertical level, but with the vertical shift Δt. We assume that going through the wormhole in counterclockwise direction takes us time $\Delta t > 0$ to the past, in clockwise direction to the future.

Chapter 3

Rules of motion in the conical space

In the just described non-relativistic conical spacetime with the time machine where $\gamma < \pi$ a trajectory of a free particle must intersect itself if it moves along a straight line. If the trajectory crosses itself in different times we will speak about *self-intersection*. If the particle intersects its trajectory exactly at the same time, which is allowed thanks to time shift Δt gained in the wormhole, it hits itself and we speak about *self-collision*. In this case, two versions of the same particle collide: the *younger* version of the ball coming from infinity hits the *older* version coming from the wormhole; after the collision, the younger version flies to the wormhole and the older one flies away to infinity.

The particle could be sent through the time machine in such a way that it hits itself, and thus prevents itself to enter the time machine, cf. fig. 3.1. Obviously, this is physical representation of the grandfather paradox described above, cf. section 1.1. Thus, the paradoxical situation is represented by the particle which occurs twice at the same time at the same place, i.e., at the point of self-intersection of the initial (collision-free) trajectory. However, the particle moving along the same initial trajectory can collide with itself consistently as it was shown in [14]. Search for such (self-colliding) solutions – superseding paradoxical ones – will be considerable task of this work. The initial conditions, respectively initial trajectories, which can, but need not, lead to the paradoxical situations will be called the *dangerous initial conditions*, respectively *dangerous trajectories*. Only if we want to indicate such initial conditions which would result into the inconsistent, i.e., paradoxical, situations we will call them the *paradoxical initial conditions*, respectively the *paradoxical initial trajectory*. Accordingly, we will use the term the *paradoxical self-intersection*.

However, it turns out that for these dangerous initial conditions we can find a consistent solution with a self-collision which is fine-tuned in such a way that the self-interacting particle consistently moves through the time machine. To convince ourselves that it is really true we first investigate a general particle motion with one self-collision and later also with multiple self-collisions. In the following we analyze rules of self-collisions of such a particle and determine possible types of self-collisions. Then we specify the geometry of self-collisions and we investigate another symmetry resulting from the conical geometry.

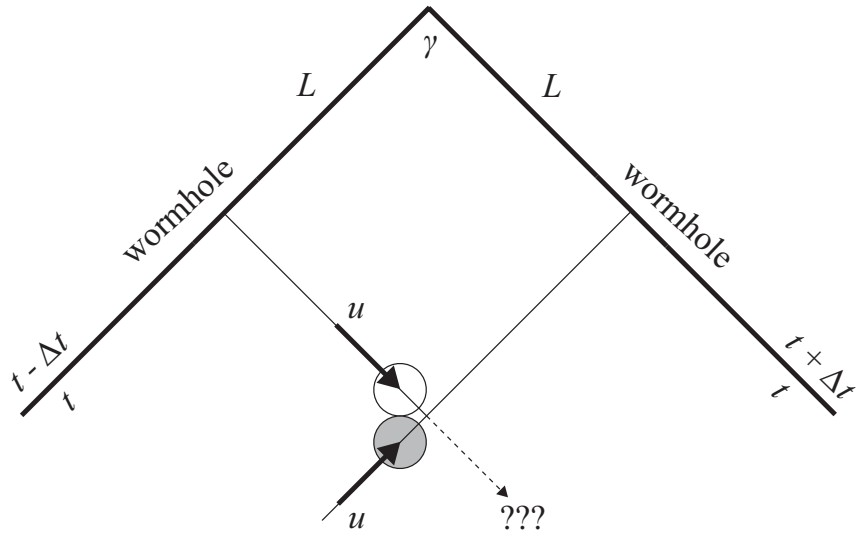

Figure 3.1: **The ball self-colliding inconsistently in the conical space with time shift Δt.** The (gray version of) ball comes from a distant region and enters the wormhole (in a distance L from the axis of the cone) without any self-collision. It leaves (now in white) the time machine (in the distance L from the axis again) in such a way that it hits itself inconsistently. Thus, this situation represents an inconsistent evolution which is the direct analogue of the well-known grandfather paradox.

3.1 Self-collision types

First, we will investigate a motion of a particle which can interact with a similar particle by the elastic collision described by the standard non-relativistic local laws. Namely, we assume the validity of the local conservation of energy and momentum. To study elastic collisions we consider finite rigid spherical balls of radius R (this is also the main reason for the restriction to the non-relativistic case). Then, we realize that the velocity of the particle remains fixed as it passes through the time machine. We receive that there exist two types of self-collisions. Next, we employ conical geometry which forbids one of these types. Finally, we separate physical from spurious self-collisions for the allowed type.

Let us examine self-collisions within the center of mass system: incoming younger version of the particle with velocity $\vec{U}$ collides with its older version with velocity $\vec{V}$, which came from the wormhole, whereby they acquire velocities $\vec{U}'$ and $\vec{V}'$ respectively. In the center of mass system velocities must satisfy

$$\vec{U} + \vec{V} = 0 \quad \text{and} \quad \vec{U}' + \vec{V}' = 0.$$

In this system we introduce the counterclockwise orthogonal basis of vectors $\vec{e}_{\parallel}$ and $\vec{e}_{\perp}$ *at the moment* of collision on which $\vec{U}$, $\vec{V}$ and $\vec{U}'$, $\vec{V}'$ can be spanned. The first vector $\vec{e}_{\parallel}$ goes through centers of balls and the origin is located at the contact point, see fig. 3.2. Moreover, the parallel basis vector $\vec{e}_{\parallel}$ is correlated with regard to the wormhole in such a way that it points in the counterclockwise direction, i.e., if extended it would intersect the "right" mouth through which objects travel to the past. If we project velocities

into these two directions we obtain

$$\vec{U} = -U_{\parallel}\vec{e}_{\parallel} + U_{\perp}\vec{e}_{\perp}\ , \qquad \vec{V} = U_{\parallel}\vec{e}_{\parallel} - U_{\perp}\vec{e}_{\perp},$$

and

$$\vec{U}' = U_{\parallel}\vec{e}_{\parallel} + U_{\perp}\vec{e}_{\perp}\ , \qquad \vec{V}' = -U_{\parallel}\vec{e}_{\parallel} - U_{\perp}\vec{e}_{\perp}.$$

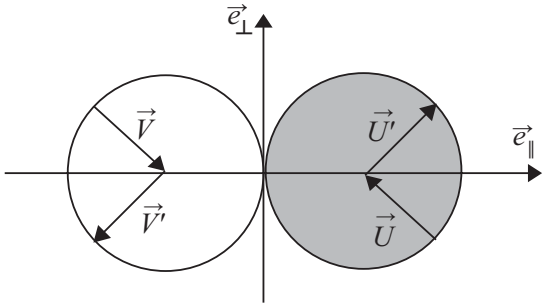

Figure 3.2: **The self-collision of two versions of the ball in the center of mass system.** The counterclockwise orthogonal basis of vectors $\vec{e}_{\parallel}$ and $\vec{e}_{\perp}$ *at the moment* of collision where the first vector $\vec{e}_{\parallel}$ goes through centers of balls and the origin is located at the contact point. The parallel basis vector $\vec{e}_{\parallel}$ is correlated with regard to the wormhole in such a way that it points in the counterclockwise direction, i.e., if extended it would intersect the "right" mouth through which objects travel to the past.

After we express the velocity of the center of mass with respect of wormhole frame in the basis of vectors $\vec{e}_{\parallel}$ and $\vec{e}_{\perp}$

$$\vec{w} = w_{\parallel}\vec{e}_{\parallel} + w_{\perp}\vec{e}_{\perp},$$

we can add it to velocities in the center of mass frame,

$$\vec{u} = \vec{U} + \vec{w}\ , \qquad \vec{u}' = \vec{U}' + \vec{w},$$
$$\vec{v} = \vec{V} + \vec{w}\ , \qquad \vec{v}' = \vec{V}' + \vec{w},$$

to receive velocities in the wormhole system. Since the magnitude of velocity is not changed by passage through the wormhole, $u' = v$, we receive also $u = v'$ due to energy conservation law. Then we can write

$$(\vec{U} + \vec{w})^2 = (\vec{V}' + \vec{w})^2,$$

which implies that (after we split velocities into directions $\vec{e}_{\parallel}$ and $\vec{e}_{\perp}$)

$$w_{\perp}U_{\perp} = 0.$$

It leads to the two alternatives: Either $w_{\perp} = 0$ and then

$$\vec{w} = w_{\parallel}\vec{e}_{\parallel},\ \vec{U} \text{ arbitrary}, \tag{3.1}$$

or $U_{\perp} = 0$ and then

$$\vec{U} = U_{\parallel}\vec{e}_{\parallel},\ \vec{w} \text{ arbitrary}. \tag{3.2}$$

3.1.1 Mirror exchange self-collision

Let us to analyze the first alternative (3.1). We can write out velocities in components as

$$\vec{u} = (-U_\parallel + w_\parallel)\vec{e}_\parallel + U_\perp \vec{e}_\perp \ , \qquad \vec{v} = (U_\parallel + w_\parallel)\vec{e}_\parallel - U_\perp \vec{e}_\perp,$$

$$\vec{u}' = (U_\parallel + w_\parallel)\vec{e}_\parallel + U_\perp \vec{e}_\perp \ , \qquad \vec{v}' = (-U_\parallel + w_\parallel)\vec{e}_\parallel - U_\perp \vec{e}_\perp.$$

Summing velocity vectors $\vec{u}$ and $\vec{v}$ we find that

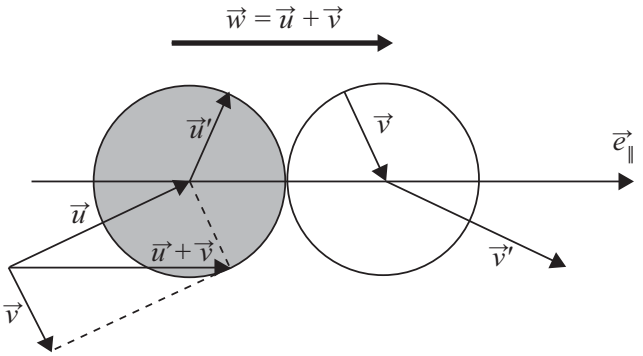

Figure 3.3: **The self-collision with exchange of mirror reflected velocities.** Since the axes of the center of mass frame coincide with the axes of the wormhole frame with the origin at the contact point *at the moment* of self-collision we can depict the self-collision within the "same" axes $\vec{e}_\parallel$ and $\vec{e}_\perp$ using the wormhole frame velocities. The centers of both versions of the particle lie along the line given by $\vec{u} + \vec{v}$ in the instant of self-collision, eq. (3.4). The mirror exchange self-collision is characterized by the exchange of mirror reflected directions of velocities: The younger version with velocity $\vec{u}$ acquires mirror reflected component of $\vec{v}$ along the direction $\vec{e}_\parallel$ while the older version with velocity $\vec{v}$ acquires mirror reflected $\vec{e}_\parallel$-component of $\vec{u}$.

$$\vec{u} + \vec{v} = 2w_\parallel \vec{e}_\parallel, \tag{3.4}$$

i.e., centers of both versions of the particle lie along the line given by $\vec{u}+\vec{v}$ at the instant of self-collision. Notice that axes of the center of mass frame coincide with axes of the wormhole frame with the origin at the contact point *at the moment* of self-collision. Thus we can depict the self-collision within the "same" axes $\vec{e}_\parallel$ and $\vec{e}_\perp$, see figure 3.3, using wormhole frame velocities.

From expressions (3.3) and (3.4) we can infer that the corresponding self-collision causes exchange of magnitudes of velocities between the two versions of the particle while they acquire mirror reflected component of the velocity of the other particle along the direction $\vec{e}_\parallel$ given by the vector $\vec{u} + \vec{v}$. We will call this type of self-collision the *mirror exchange self-collision* in accord with [14], see fig. 3.3: The younger version with velocity $\vec{u}$ acquires mirror reflected component of $\vec{v}$ along the direction $\vec{e}_\parallel$ while the older version with velocity $\vec{v}$ acquires mirror reflected $\vec{e}_\parallel$-component of $\vec{u}$.

3.1.2 Velocity exchange self-collision

According to the condition (3.2) we formulate analogical relations

$$\vec{u} = (-U_{\parallel} + w_{\parallel})\vec{e}_{\parallel} + w_{\perp}\vec{e}_{\perp} \ , \qquad \vec{v} = (U_{\parallel} + w_{\parallel})\vec{e}_{\parallel} + w_{\perp}\vec{e}_{\perp},$$

$$\vec{u}' = (U_{\parallel} + w_{\parallel})\vec{e}_{\parallel} + w_{\perp}\vec{e}_{\perp} \ , \qquad \vec{v}' = (-U_{\parallel} + w_{\parallel})\vec{e}_{\parallel} + w_{\perp}\vec{e}_{\perp}.$$

In this case, the two versions of the particle exchange both directions and magnitudes of their velocities and we will call it the *velocity exchange self-collision*. The centers of

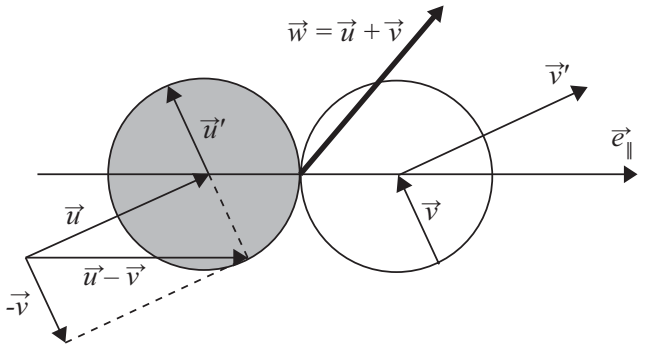

Figure 3.4: **Velocity exchange self-collision.** In the case of velocity exchange self-collisions, the two versions of the particle exchange both directions and magnitudes of their velocities. The centers of both versions of the particle are now located along the line given by the vector $\vec{u} - \vec{v}$.

both versions of the particle are now located along the line given by the vector

$$\vec{u} - \vec{v} = 2U_{\parallel}\vec{e}_{\parallel}.$$

The corresponding situation illustrating velocity exchange self-collisions is visualized in figure 3.4.

However, velocity exchange self-collisions cannot take place within the conical space because of the conservation of momentum between the self-collision (i.e., that the particle moves along straight trajectory within the conical geometry). Indeed, from (3.5) we can see that initial and final velocities of the particle moving between the self-collision through the wormhole are equal, $\vec{v} = \vec{u}'$. However, the transfer through the wormhole changes direction of the particle by the angle γ. Only within the cylinder space which represents the degenerated case of the conical space for $\gamma = 0$ velocity exchange self-collisions could occur, see figure 3.5

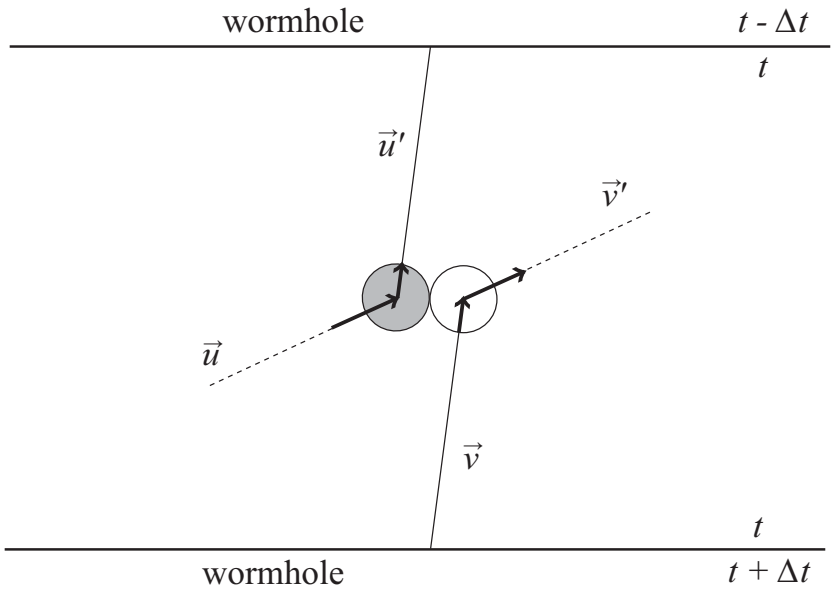

Figure 3.5: **Velocity exchange self-collision within the unfolded cylinder, $\gamma = 0$.** Velocity exchange self-collisions cannot take place within the conical space because conservation of momentum between the self-collision (i.e., that the particle moves along straight trajectory within the conical geometry) does not allow it. The particle traveling through the wormhole changes the direction by the angle γ which is inconsistent with $\vec{v} = \vec{u}'$. Only within the cylinder space which represents the degenerated case of the conical space for $\gamma = 0$ velocity exchange self-collisions can occur.

3.2 Symmetry of inner trajectories

Let us consider mirror exchange self-collisions within the conical space with time shift and for simplicity we suppose that radius of the particle vanishes. We will show that self-collisions are symmetrical with respect to corresponding radial lines, see figure 3.6(a). Notice, however, that investigated symmetries hold for particles with finite radius, $R > 0$, as well.

The particle must enter and leave the wormhole in the same distance L from the vertex of the cone. In order to preserve straightness of the trajectory the angle α (between the inner incoming trajectory and the wormhole) has to be complement of the angle $\beta = \pi - \alpha$ (between the inner outgoing trajectory and the wormhole). Moreover, we notice that points A (axis of the cone), E (location where the particle enters wormhole), C (location of the self-collision) and X (location where the particle quits wormhole) determine tetragon and all four points lie on the same circle (thanks to the complementarity of opposite angles $\alpha + \beta = \pi$, $\gamma + (\Xi + \Theta) = \pi$). Next, $|XV| = |VE| = L$, which implies

$$\frac{L}{\sin \Xi} = \frac{r}{\sin \beta} = \frac{r}{\sin \alpha} = \frac{L}{\sin \Theta} ,$$

see figure 3.6(a). Angles $\Xi, \Theta \in [0, \pi/2]$, and thus we receive equality of angles

$$\sin \Xi = \sin \Theta \Rightarrow \Xi = \Theta = \frac{\pi - \gamma}{2},$$

again using the complementarity $\Xi+\Theta = \pi-\gamma$. Thus trajectory of the particle between the self-collision – defined by the velocities $\vec{u}'$ and $\vec{v}$ – must be symmetrical with respect to the radial line. Here, the symmetry is understood in the conical space which neglects a position of the wormhole.

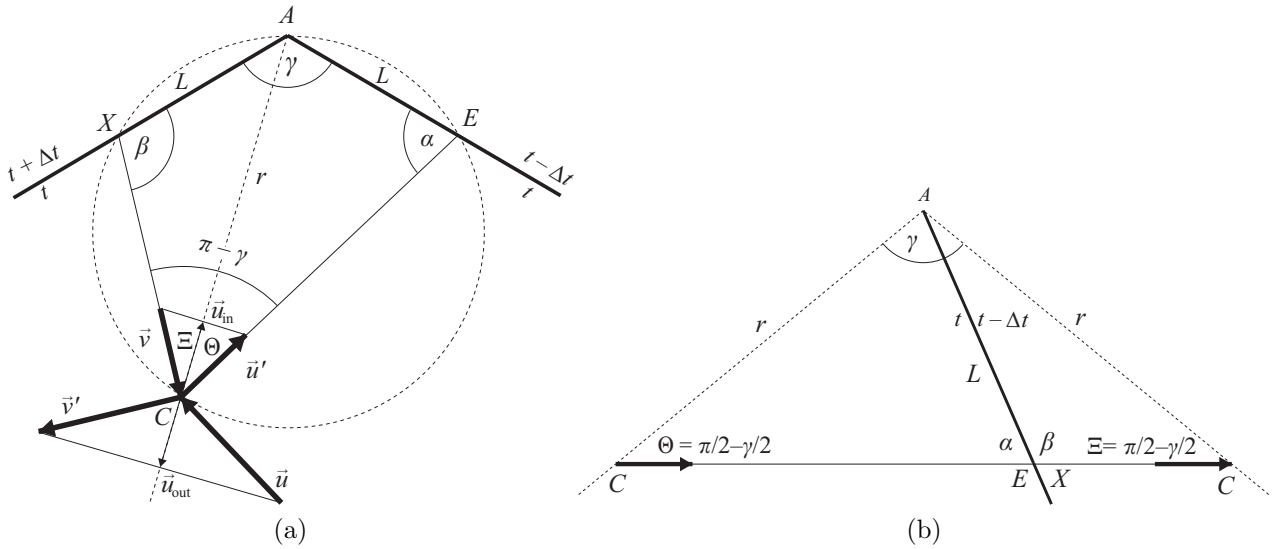

Figure 3.6: **Self-collisions are symmetric with respect to the radial line.** (a) The conical space is illustrated as an angle, boundary of which represent mouthes of the wormhole and should be identified. The self-collision is symmetrical with respect to the radial line. Projections of inner velocities and outer velocities are equal, $u_{\text{in}} = u_{\text{out}}$. (b) The trajectory between the self-collision is a straight line, which can be clearly demonstrated if we cut the conical space not along the wormhole but along the radial line going through the self-collision. The wormhole is than depicted as another radial line. Since the particle passes the wormhole freely, its trajectory must be straight across the wormhole line. It starts and ends at the self-collision which is represented as two points on the boundary semi-lines at the distance r from the vertex.

Symmetry of the inner trajectory between the self-collision can be also shown due to the triangle which arises by different unfolding of the conical space into the plane, see figure 3.6(b). The trajectory between the self-collision is a straight line, which can be clearly demonstrated if we cut the conical space not along the wormhole but along the radial line going through the self-collision. The original wormhole is than depicted as another radial line. Since the particle passes the wormhole freely, its trajectory must be straight across the wormhole line at the distance L from the vertex. It starts and ends at the self-collision which is represented as two points on the boundary semi-lines at the distance r from the vertex. The same geometry applies also for a segment of the collision-free trajectory between its self-intersection. Thus the triangle is isosceles with two angles equal to $\frac{\pi-\gamma}{2}$.

3.2.1 Equality of projections of inner and outer velocities

Let us show also that the radial projection vector $\vec{u}_{\text{in}}$ of the inner velocities $\vec{u}', \vec{v}$ has the same magnitude as the radial projection vector $\vec{u}_{\text{out}}$ of the outer velocities $\vec{u}, \vec{v}'$, see

figure 3.6(a). Since the particle preserves its velocity while passing wormhole, $u' = v$, and $\vec{u}'$ a $\vec{v}$ are symmetrical with respect to the radial line, their projections are identical and equal to u_{in}. Due to energy conservation law, $u = v'$, and momentum conservation law, $\vec{u} + \vec{v} = \vec{u}' + \vec{v}'$, also velocities $\vec{u}$ a $\vec{v}'$ are symmetrical and determine identical projection u_{out}. After we rearrange terms in conservation of momentum law we find that

$$2\vec{u}_{\text{in}} = \vec{u}' - \vec{v} = -(\vec{v}' - \vec{u}) = -2\vec{u}_{\text{out}}. \tag{3.6}$$

Thus, we have determined the geometry of self-collisions: Due to the conical geometry self-collisions are symmetrical with respect to the radial line.

3.3 Two types of mirror exchange self-collisions

Finally, we will distinguish two subtypes of mirror exchange self-collisions for finite balls. Remind that the direction of the vector $\vec{e}_{\parallel}$ is fixed with respect to the wormhole, i.e., it points to the "right" mouth of the wormhole, and thus it can be used to define the left-hand side and the right-hand side within the wormhole frame. The first type represents the situation when the older version of the ball touches the younger one by its rear part, i.e., the younger version must collide from the left side, $\vec{r}_u - \vec{r}_v = -2R\vec{e}_{\parallel}$. Let us denote such a case as the self-collision of the *type I* – the configuration of type I

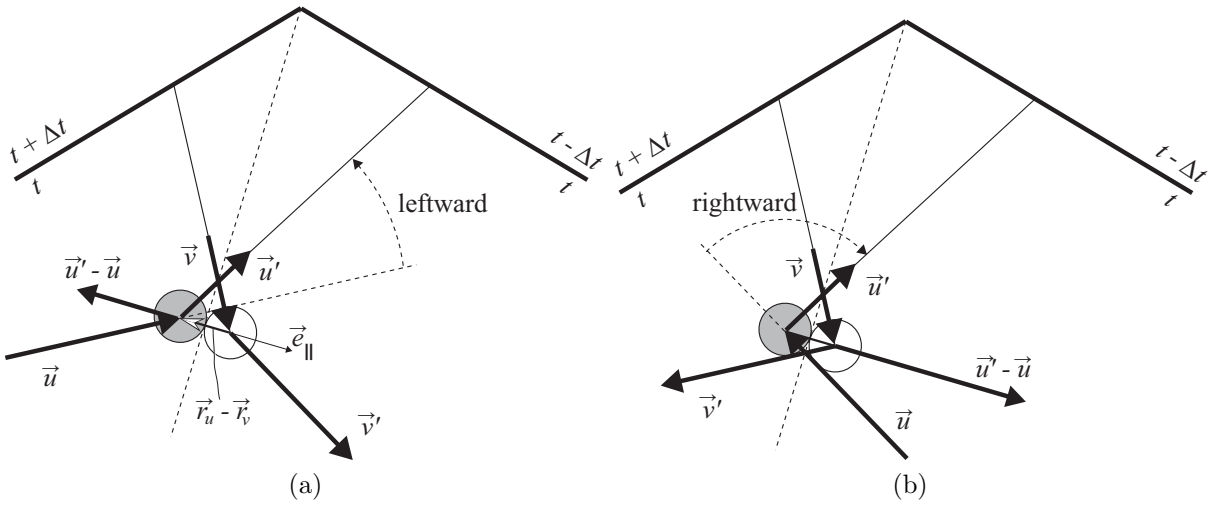

Figure 3.7: **Self-collisions of type I.** The configuration of type I represents a situation in which the younger version (in gray) is on the left side while the older version (in white) is on the right side with respect to the radial line. (a) The physical self-collision. The momentum transfer is positive and the trajectory of the particle is deflected leftward. (b) The spurious self-collision. The momentum transfer is negative and the trajectory of the particle is deflected rightward. However, the spurious self-collision cannot occur, otherwise the ball would self-collide before it would reach the illustrated position. In other words, even if we allowed spurious self-collisions (negative momentum transfer) they would have not been acceptable geometrically.

is illustrated in figure 3.7(a). The second type represents the situation when the older version touches the younger version by its frontal part, i.e., the younger version of the

particle must occupy the right side, $\vec{r}_u - \vec{r}_v = +2R\vec{e}_\parallel$. We will denote this case as the self-collision of the *type II* – the configuration of type II is illustrated in figure 3.8(a).

Let us mention that the momentum transfer $\vec{u}' - \vec{u}$ (happening along the line of centers of balls) is positive, if it points to the direction $\vec{r}_u - \vec{r}_v = -2R\vec{e}_\parallel$ at the moment of the self-collision. For example, if the younger version of the ball settles on the left of the older version (type I) then the momentum transfer $\vec{u}' - \vec{u}$ must point to the left (since balls bounce off one another instead of attracting mutually). Oppositely, if the younger version is on the right (type II) then the momentum transfer must point to the right.

In the case of self-collisions of type I, the positive momentum transfer means that $\mathrm{sign}[(\vec{u}' - \vec{u}) \cdot \vec{e}_\parallel] = -1$. The trajectory of the particle after the self-collision is directed to the wormhole closer to the vertex than if it followed the collision-free trajectory, i.e. it is deflected leftward, figure 3.7(a). We will say that the particle undergoes the *physical* self-collision of type I. If the momentum transfer is negative, i.e., $\mathrm{sign}[(\vec{u}' - \vec{u}) \cdot \vec{e}_\parallel] = +1$, the trajectory is deflected rightward, figure 3.7(b), and we say that the self-collision of type I is *spurious*. However, even if we allowed spurious self-collisions (negative momentum transfer) they would not been acceptable geometrically. As can be seen from figures 3.7(b) and 3.8(b) balls would collide before they would reach anticipated positions, and thus spurious self-collisions can not occur.

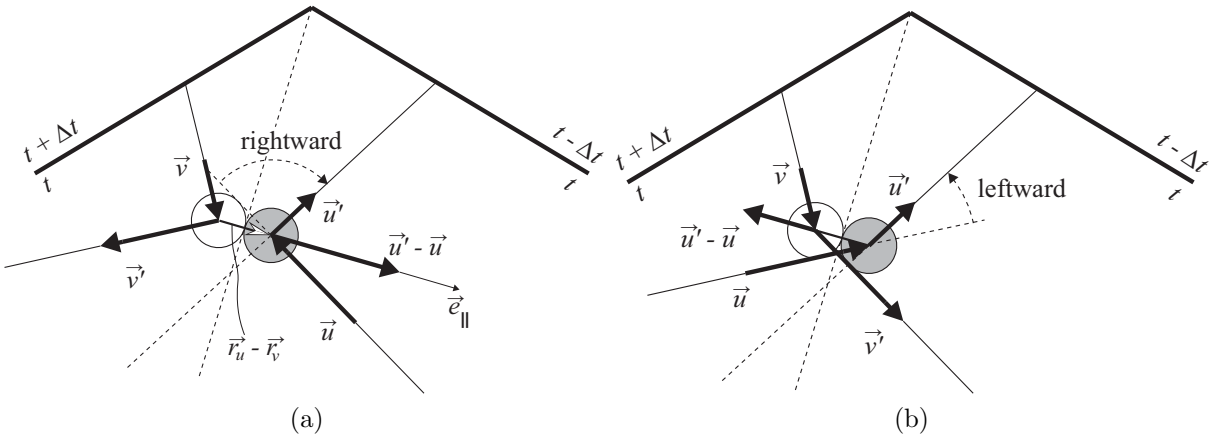

Figure 3.8: **Self-collisions of type II.** The configuration of type II represents a situation in which the older version is on the left side while the younger version is on the right side with respect to the radial line. (a) The physical self-collision. The momentum transfer is positive and the trajectory of the particle is deflected rightward. (b) The spurious self-collision. The momentum transfer is negative and the trajectory of the particle is deflected leftward. Analogously to type I, the spurious self-collision can not occur, otherwise the ball would self-collide before it would reach the illustrated position.

If the momentum transfer $\vec{u}' - \vec{u}$ is positive for self-collisions of type II, i.e., $\mathrm{sign}[(\vec{u}' - \vec{u}) \cdot \vec{e}_\parallel] = +1$, then the trajectory of the particle is directed to the wormhole further from the vertex than if it moved along the collision-free trajectory. In this case, the particle is deflected rightward, figure 3.8(a), and thus the corresponding self-collision of type II is *physical*. If the momentum transfer is negative, i.e., $\mathrm{sign}[(\vec{u}' - \vec{u}) \cdot \vec{e}_\parallel] = -1$, and the trajectory is deflected leftward, the self-collision of type II is *spurious*, figure 3.8(b).

Chapter 4

Point particle: one self-collision

Let us introduce parameters for initial trajectories and define quantities to describe self-collisions on these trajectories. We will neglect radius R of the particle for now, and concentrate on trajectories and self-collisions of point-like particles, i.e., $R \to 0$.[1] In this case, the discussion simplifies considerably since it turns out to be scale invariant. Later, in chapter 5, we will include into consideration the radius R to gain full account of self-collisions for billiard ball-like particles. First, we will study collision-free trajectories. Next, we will specify the conditions for self-collisions and find consistent solutions for motion of the point-particle with one self-collision. More accurately, we will consider the innermost self-collision only, though there can occur multiple self-collisions which will be subject of the chapter 6. For the angle γ lies in the interval $(\pi/2, \pi)$ there is allowed only one self-intersection along the collision-free trajectory, cf. section 2.2, and hence we will consider only conical spaces with the vertex angle within this range.

4.1 Model parameters

Let us suppose that a particle incomes along an initial trajectory from the Euclidean space outside the cone. The trajectory of the particle can be determined by two initial parameters: the *impact parameter* ρ, which gives the distance of the initial trajectory from the vertex of the cone, and the *magnitude of initial velocity* $u > 0$, see figure 4.1. We adopt the convention that the impact parameter ρ is positive if the particle circles the cone in the counterclockwise direction (with respect to the vertex of the cone) and it is negative if it circles the cone in the clockwise direction.

Of course, the parameters u and ρ do not determine the initial trajectory uniquely since they do not specify its angular location around the axis and its temporal location. Hence, we have to define two additional parameters which ensure the desired uniqueness. However, the conical space is symmetrical under rotations and it is static, so the character of the motion is not affected by its angular and temporal location. Thus, the geometry of the self-collision does not depend on these additional parameters which will be subject of paragraph 4.6.

[1] Such a system has been the main subject of [22] (appendix I).

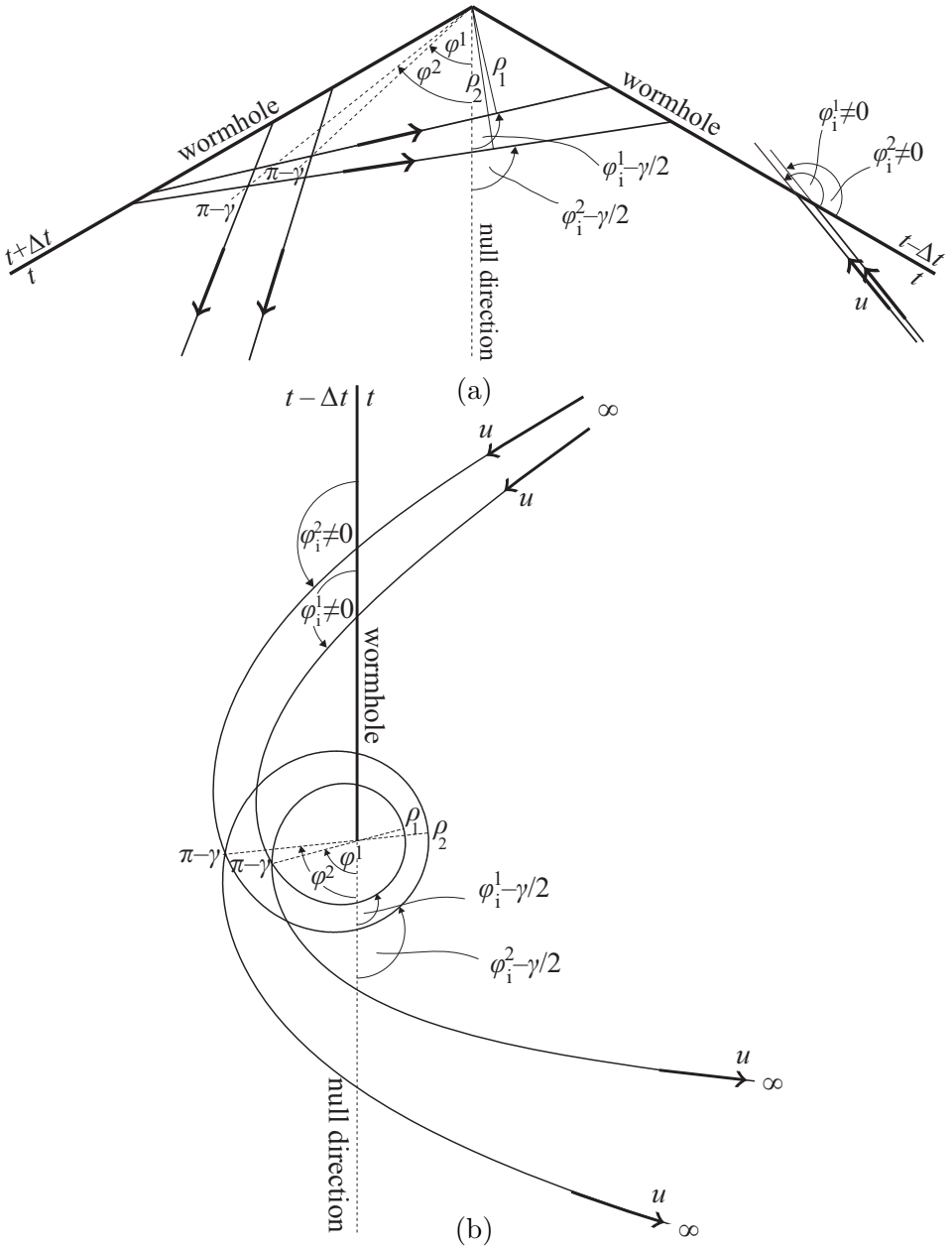

Figure 4.1: **Parameters of the initial trajectory.** Diagram illustrates the typical situation when the particle starts from a distant Euclidean region, approaches the conical space, circles it without self-collision and leaves it for the distant Euclidean region. The trajectory of the particle can be determined by two initial parameters aside from the angular parameter φ_i encoding its orientation with respect to the wormhole, respectively the null direction: the *impact parameter* ρ which gives the distance of the initial trajectory from the vertex of the cone, and the *magnitude of initial velocity* $u > 0$. More specifically, figure shows two collision-free trajectories given by different values of the impact parameter, $\rho^1 \neq \rho^2$, starting from one point, passing through the wormhole under different angles $\varphi_\mathrm{i}^1 \neq \varphi_\mathrm{i}^2$, intersecting themselves on two different radial lines, given by angles $\varphi^1 \neq \varphi^2$ (between the lines and the null direction), and diverging mutually as approaching infinity. Also we can see that holding fixed $\rho^{1,2}$ and varying position of the angle $\varphi^{1,2}$ corresponds to the rotating of the starting point, i.e. rotating the Euclidean space around the conical space, or rotating of the cone with respect to the Euclidean space. Notice that both couples of pairs φ_i^1 and φ_i^2, respectively angles φ^1 and φ^2, are used to determine initial trajectories uniquely. (a) The cone is unfolded into the plane angle. (b) The cone from the "bird's eye view".

For a special choice of initial data the particle moving along the initial trajectory may self-interact. A typical self-colliding trajectory in the conical space with a time machine is illustrated in fig. 4.3. A point-particle is approaching the wormhole from the infinity with a velocity u, it collides with the version of itself which already passed through the time machine, and with a velocity v moves toward the wormhole. After passing it and self-colliding with itself, it moves with the velocity u back to the infinity.

The self-collision can be parametrized by its *radial distance* r from the axis and by the orientated *scattering angle* $\omega \in [-\pi/2, \pi/2]$ between the outgoing trajectory and the radial direction. Thanks to the symmetry of the self-collision with respect to the radial direction, the angle ω also determines the direction of the incoming trajectory, and it is thus a half of the angle between incoming and outgoing trajectories. From the same reasons, the outgoing particle also has the velocity u and the impact parameter ρ. The domain of the angle ω is constrained by rules of motion in the conical space. Namely, the particle moving along the initial trajectory with the velocity $u > 0$ must be approaching the vertex, while the particle moving along the final trajectory with the same velocity must be receding from the vertex.

The collision parameters ω and r encode the same information as the initial parameters ρ and u. The sign of the angle ω corresponds to the sign of the initial impact parameter ρ, while quantities u and r are both positive. Therefore, we can relate couples of these parameters

$$\begin{pmatrix} \rho \\ u \end{pmatrix} \leftrightarrow \begin{pmatrix} \omega \\ r \end{pmatrix}, \qquad \text{or} \qquad \begin{pmatrix} \omega \\ u \end{pmatrix} \leftrightarrow \begin{pmatrix} \rho \\ r \end{pmatrix}, \tag{4.1}$$

where the first assignment relates the parameters of the incoming trajectory u, ρ and parameters of the self-collision r, ω, while the second map binds together length parameters r, ρ and the parameters ω, u which will be useful when we analyze self-colliding solutions. To keep orientation of the trajectory the first parameter should be the orientated quantity (ρ or ω), while the second should be the positive quantity (u or r).

4.2 Collision-free trajectories

The initial trajectory, described above, represents a generic physical solution if it does not self-interact, i.e., it passes along the collision-free trajectory. The collision-free trajectory can take the particle to the past, or to the future, according to the direction in which it passes the wormhole. If the collision-free trajectory has a negative impact parameter, $\rho < 0$, the time machine takes the particle to the future, while if the collision-free trajectory is defined by positive impact parameter, $\rho > 0$, it takes the particle back in time by $-\Delta t$.

There are two ways in which the particle can travel back in time without self-collision, see figure 4.2. From obvious reason the particle is depicted with a finite radius. Either the movement around the cone takes shorter time than the time thus gained, namely $\Delta t > s/u$, in which case the older version of the particle (i.e., the one that already passed the wormhole) moves through the point of intersection as the first, figure 4.2(a). This case we will call of type I. Or, the orbit around the cone takes longer time than time thus gained, $\Delta t < s/u$, in which case the older version of the particle

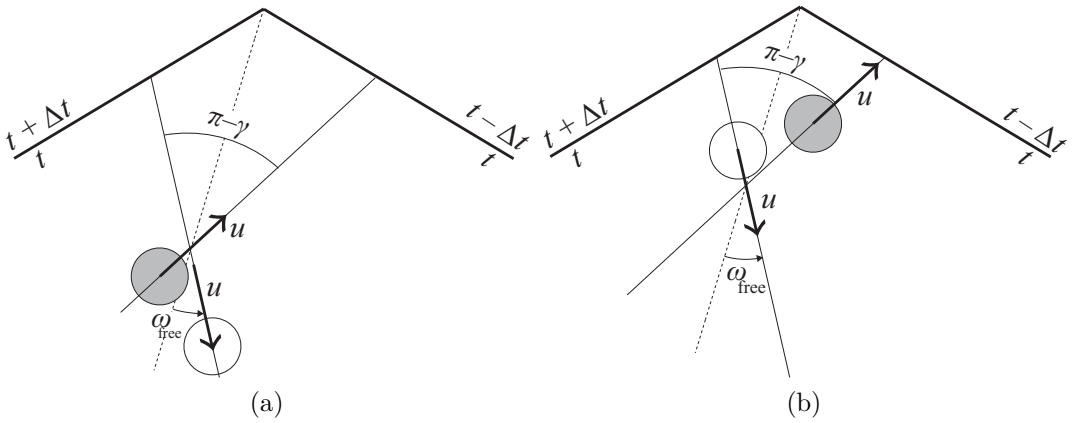

Figure 4.2: **Two types of collision-free trajectories passing the time machine to the past.** (a) If time s/v spent by the ball between the self-collision is smaller than the time shift Δt, i.e., $s/u < \Delta t$, then the younger version of the ball goes through the point of intersection later than the older version. Such a collision-free trajectory to the past is of type I. (b) On the contrary, if $s/u > \Delta t$, then the older version of the ball goes through the point of intersection later than the younger version of the ball. Such a collision-free trajectory to the past is of type II.

gets late with respect to the younger version of the particle which moves through the point of intersection as the first, figure 4.2(b). This case we will call of type II.

For the collision-free trajectory we can define analogous quantities r and ω which refer to the point of self-intersection instead of self-collision. In this case, the impact parameter of the inner trajectory between the self-intersection, or the self-collision, denoted by $\rho_{\rm in}$, equals to the initial value, $\rho_{\rm in} = \rho$, and the angle ω is fully given by the conical geometry

$$\omega = \omega_{\rm free} \equiv \frac{\pi - \gamma}{2},$$

cf. section 3.2. Obviously, the direction of the collision-free trajectory to the future is determined by the additive inverse value $\omega = -\omega_{\rm free} \equiv \frac{\gamma-\pi}{2}$. The length s of the straight trajectory between its self-intersection is given also by the conical geometry as can be seen in figure 4.3,

$$s = 2\rho \tan \frac{\gamma}{2}.$$

The time needed to circle the cone is thus $\frac{s}{u} = \frac{2\rho \tan \gamma/2}{u}$.

4.3 Trajectories with self-collisions

From the definitions of parameters ρ, r, ω we immediately see that, for both self-interacting and collision-free trajectories, ρ in terms of r and ω is given by the simple geometry

$$\rho = r \, \sin \omega \, , \tag{4.2}$$

and hence also

$$\rho_{\rm in} = r\,\sin\omega_{\rm free} = r\,\cos\frac{\gamma}{2}\,.$$

For a trajectory between the self-collision the inner velocity v is given by the condition

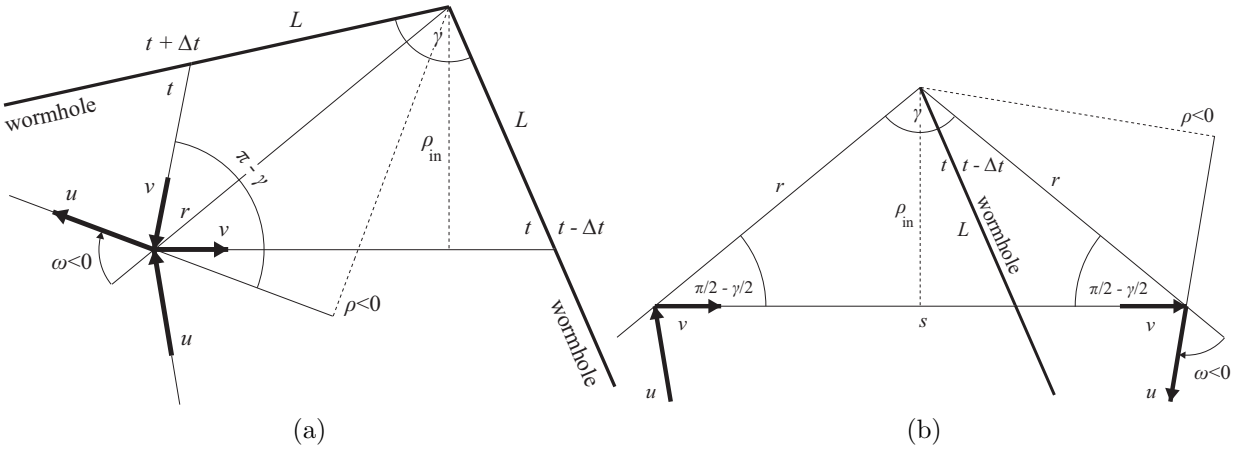

Figure 4.3: **Geometry of self-colliding trajectory and its parameters.** (a) A typical self-colliding trajectory in the conical space with time machine. A point-particle is approaching the wormhole from infinity with a velocity u and impact parameter ρ; it collides with the version of itself which has already passed through the time machine, and with a velocity v moves toward the wormhole. After passing the wormhole and self-colliding with itself, it moves with the velocity u back to infinity. The self-collision occurs at the distance r from the axis, and the outgoing trajectory forms with the radial direction the orientated angle ω. Thanks to symmetry of the self-collision with respect to the radial direction, the angle ω is half of the angle between the incoming and outgoing trajectory. The domain of the angle ω is constrained by the rules of motion in the conical space. The radial distance r of self-collision is related to ω by constraint (4.2). (b) The same situation depicted in a map which cuts the conical space not along the wormhole but along the radial direction through the self-collision. The length s of the straight trajectory between its self-intersection is given by $s = 2\rho_{\rm in}\tan\frac{\gamma}{2} = 2r\sin\frac{\gamma}{2}$.

that the particle has to travel the distance s in time Δt, i.e.,

$$v = \frac{s}{\Delta t} = \frac{2r\sin\frac{\gamma}{2}}{\Delta t} = \frac{2\rho}{\Delta t}\frac{\sin\frac{\gamma}{2}}{\sin\omega}\,, \tag{4.3}$$

where we expressed the length s using the radial distance r, see figure 4.3, which is given in terms of ρ and ω by equation (4.2).

The remaining relation between parameters ρ, u, and r, ω follows from the equation for the self-collision, namely from the momentum and energy conservation during the self-collision. It turns to be equivalent to the conservation of the radial momentum during the self-collision, cf. eq. (3.6). Comparing the radial momentum of the particle between the self-collision given by $v\sin\frac{\gamma}{2}$ and the radial momentum of the incoming trajectory $u\cos\omega$ we receive equation

$$u\cos\omega = v\sin\frac{\gamma}{2}\,, \tag{4.4}$$

which relates the incoming velocity u to the inner velocity v along the trajectory between the self-collision. Notice that for $\omega \in (\frac{\gamma-\pi}{2}, \frac{\pi-\gamma}{2})$ the younger version is accelerated up

by the self-collision, while for $\omega \in [-\frac{\pi}{2}, \frac{\gamma-\pi}{2}) \cup (\frac{\pi-\gamma}{2}, \frac{\pi}{2}]$ the younger version is slowed down.

Substituting expression (4.3) into (4.4) we obtain ω in terms of ρ and u

$$\sin(2\omega) = \frac{4\rho \sin^2 \frac{\gamma}{2}}{u\Delta t} \, . \tag{4.5}$$

If we retype the above equation as

$$\cos\omega = \frac{2r \sin^2 \frac{\gamma}{2}}{u\triangle t},$$

and compare with modified geometric constraint (4.2)

$$\cos^2\omega = 1 - \frac{\rho^2}{r^2},$$

we receive the quartic equation for r

$$4r^4 \sin^4 \frac{\gamma}{2} - r^2(\triangle tu)^2 + \rho^2(\triangle tu)^2 = 0,$$

with two positive roots

$$r = \frac{\triangle tu}{2\sqrt{2}\sin^2 \frac{\gamma}{2}} \sqrt{1 \pm \sqrt{1 - \frac{16\rho^2 \sin^4 \frac{\gamma}{2}}{(\triangle tu)^2}}}, \tag{4.6}$$

i.e., we have also r in terms of ρ and u.

Oppositely, equation (4.2) along with expression of the initial velocity

$$u = \frac{2r \sin^2 \frac{\gamma}{2}}{\Delta t \cos\omega} \, ,$$

employing eqs. (4.3), (4.4), gives ρ and u in terms of r and ω, i.e., the first relation in (4.1). Moreover, we can also rewrite equations (4.2) and (4.5) as functions of the angle ω and the velocity u as

$$\rho = \frac{u\Delta t \sin\omega \cos\omega}{2\sin^2 \frac{\gamma}{2}} \, , \tag{4.7}$$

and

$$r = \frac{u\Delta t \cos\omega}{2\sin^2 \frac{\gamma}{2}} \, , \tag{4.8}$$

which represent the second relation in (4.1), i.e., r and ρ in terms of u and ω. Notice that both functions are periodical in the angle ω.

Dividing these equations by $u\Delta t$ we obtain relations for dimensionless quantities (distances measured in units of $u\Delta t$) which do not depend on the velocity u anymore. It means that point-particle configurations with different initial velocities u are related just by a simple rescaling. Hence, we will fix u and concentrate on the relation between ρ, r, and ω. In figures 4.4 and 4.5 we can see the function $\rho = \rho(\omega)$ and the parametric curve $[\rho(\omega), r(\omega)]$ in the plane r-ρ for $\omega \in [-\pi, \pi]$. From these graphs we can easily read the desired dependencies $\omega(\rho)$ and $r(\rho)$.

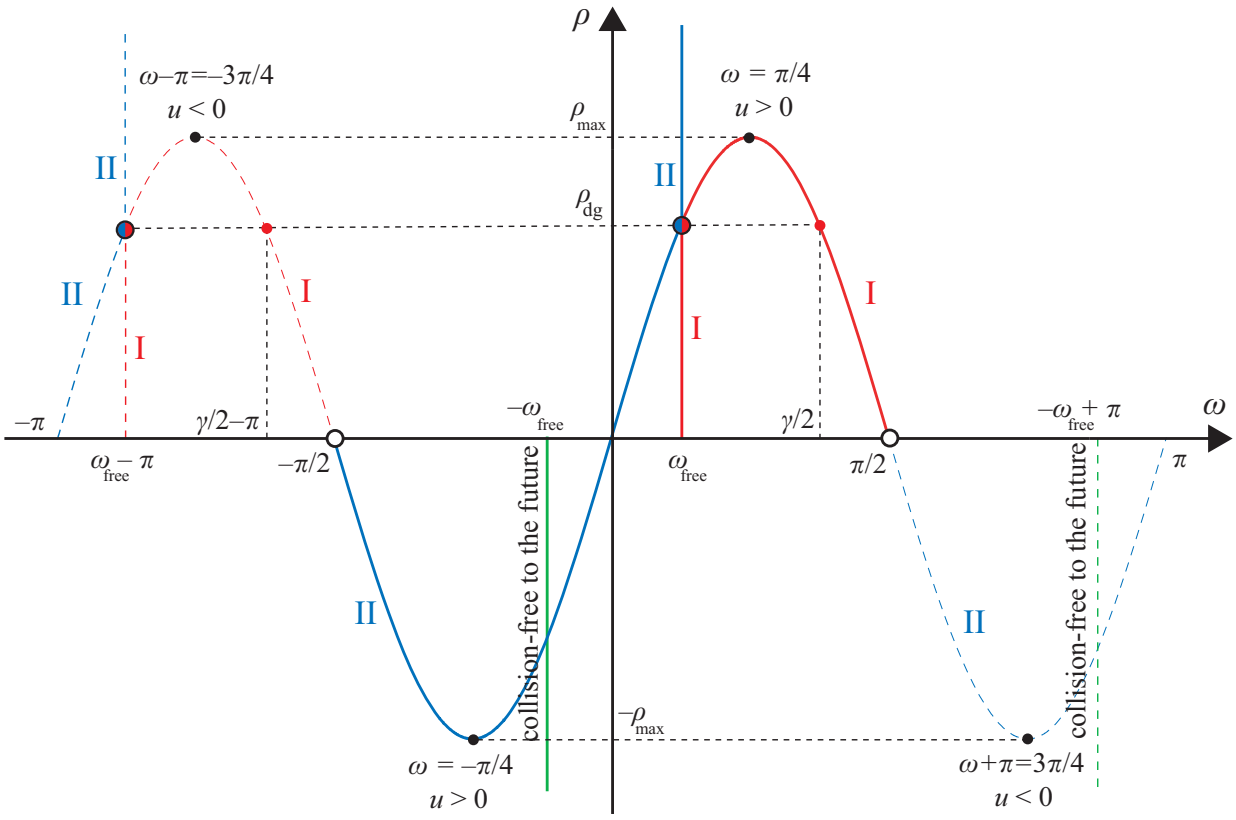

Figure 4.4: **The ρ-ω diagram of solutions for a point-particle.** Each point of the graph in the ρ-ω plane for $\omega \in [-\pi, \pi]$ represents a consistent solution for a point-particle with at most one self-collision, cf. eq. (4.7). The initial velocity u is fixed (it changes only a scale of the solutions) except for its sign. The sign of u defines two different parametrizations. The part of graph with $\omega \in [-\pi/2, \pi/2]$ (depicted by solid lines) corresponds to the positive initial velocity parametrization, $u > 0$. The collision-free solutions are represented by the straight vertical lines $\omega = \pm\omega_{\text{free}}$. The line $\omega = \omega_{\text{free}}$ corresponds to collision-free trajectories to the past and the line $\omega = -\omega_{\text{free}}$ (in green) corresponds to collision-free trajectories to the future. The collision-free solutions with $\rho < \rho_{\text{dg}}$ (in red) are of type I while the solutions with $\rho > \rho_{\text{dg}}$ (in blue) are of type II. The sinusoidal part of the graph represents the solutions with one self-collisions. The part with $\omega > \omega_{\text{free}}$ (in red) represents self-collisions of type I while the part with $\omega < \omega_{\text{free}}$ (in blue) represents self-collisions of type II. We can see how collision-free solution of type I (II) changes into self-colliding solution of type I (II) for dangerous values $\omega = \omega_{\text{free}}$ and $\rho = \rho_{\text{dg}}$. The point $(\rho = \rho_{\text{dg}}, \omega = \omega_{\text{free}})$ represents both the paradoxical self-intersection and the (geometrically indistinguishable) consistent self-collision. In the (following) discussion of finite ball we will find that the paradoxical self-intersection is superseded by the self-colliding solution at this point. The (red) point $(\rho_{\text{dg}}, \gamma/2)$ represents regular trajectory though starting with the dangerous value $(\rho_{\text{dg}}$. Notice that self-collisions are possible only for $|\rho| < \rho_{\max}$ and that points $(\rho, \omega) = (0, -\pi/2), (0, \pi/2)$ are taken out of the graph since they represent self-collisions with vanishing projections of velocities which take place vanishingly close to the axis. The union of intervals $\omega \in [-\pi, -\pi/2) \cup (\pi/2, \pi]$ corresponds to the negative initial velocity parametrization, $u < 0$, with curves depicted by dashed lines, cf. paragraph 4.7. Clearly, all considered phenomena have their images in this parametrization.

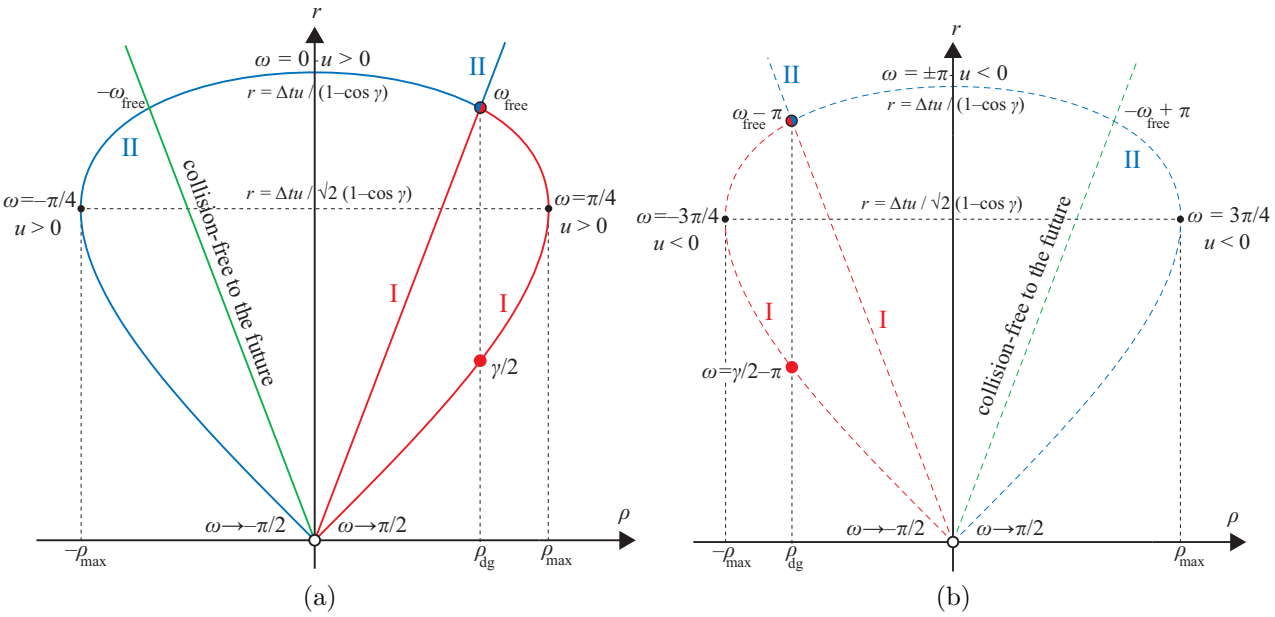

Figure 4.5: **The r-ρ diagram of solutions for a point-particle.** Each point of the graph in the r-ρ plane represents a consistent solution for a point-particle with at most one self-collision. The scattering angle $\omega \in [-\pi, \pi]$ represents the parameter of the curves defined by eqs. (4.7) and (4.8). The radial lines $\omega = \pm\omega_{\rm free}$ represent the collision-free solutions. The self-colliding solutions are depicted by the parametric curves $[\rho(\omega), r(\omega)]$. The type of the (collision-free, self-colliding) solutions is indicated in a similar manner as in fig. 4.4. The sign of the velocity u defines two different parametrizations represented by mirror reflected graphs. (a) The positive initial velocity parametrization with $\omega \in (-\pi/2, \pi/2)$ where curves are depicted by solid lines. (b) The negative initial velocity parametrization with $\omega \in [-\pi, -\pi/2) \cup (\pi/2, \pi]$ where curves are drawn by dashed lines.

The equation (4.7) also determines the interval of the impact parameter ρ for which the self-interaction is possible. Clearly, $\rho \in [-\rho_{\rm max}, \rho_{\rm max}]$ with

$$\rho_{\rm max} \equiv \frac{\Delta t u}{4 \sin^2 \gamma/2}, \tag{4.9}$$

which we get by substitution $\omega = \frac{\pi}{4}$. Similarly, from eq. (4.8) for the radial distance of the self-collision r we find $r \in [0, \frac{\Delta t u}{2 \sin^2 \gamma/2}]$. Trajectories outside this region cross themselves too far from the axis with the time shift too short to self-interact. Notice that equation (4.4) implies that solutions $(\rho, \omega) = (0, -\pi/2), (0, \pi/2)$ represent self-collisions with vanishing projections of velocities which take place with zero distance from the axis, $r = 0$, cf. fig. 4.5, and hence we consider such solutions as singular. This is why we take these two cases out of the set of solutions, see corresponding white points in figs. 4.4 and 4.5.

4.4 Dangerous trajectories

Let us turn attention to the dangerous initial conditions mentioned earlier, cf. section 3. Clearly, the dangerous initial parameters would be those for which the self-

intersection becomes the self-collision. It means that $\omega = \omega_{\text{free}}$ and $v = u$. Thus, inequality $\Delta t \neq s/u$ for collision-free trajectories is replaced by equality $\Delta t = s/u$. Substituting $\omega = \omega_{\text{free}}$ and $v = u$ into (4.3) leads to

$$u_{\text{dg}}\Delta t = 2\rho_{\text{dg}} \tan\frac{\gamma}{2} ,$$

where u_{dg}, ρ_{dg} denotes the dangerous values of the initial parameters.

For such initial parameters the collision-free trajectory degenerates to the paradoxical situation, when the particle would have to pass through itself, which is, moreover, indistinguishable from the self-colliding solution, when the particle would self-interact without exchange of any momentum, cf. points $(\rho_{\text{dg}}, \omega_{\text{free}})$ in diagrams 4.4 and 4.5. In other words, geometry of the paradoxical self-intersection and dangerous self-collision, i.e., consistent self-collision for the dangerous parameters, is identical in the case of the point-like particle. Therefore, the exact behavior of the particle, in this case, cannot be solved on the level of a point-particle model but can be found by investigating finite balls as we will do in the next section 5. It will be shown that paradoxical collision-free trajectories are replaced by consistent self-colliding solutions and that the number of solutions within the impact parameter interval $[-\rho_{\max}, \rho_{\max}]$ is conserved. Notice, however, that there exists one regular solution for the dangerous parameters depicted by (red) points $(\rho_{\text{dg}}, \frac{\gamma}{2})$ in figures 4.4 and 4.5.

4.5 Number of solutions

Inspecting figures 4.4 and 4.5 we find that for any $\rho \in (-\infty, +\infty)$ there is always one collision-free trajectory – except the value ρ_{dg}. Two self-colliding solutions exist within $\rho \in [-\rho_{\max}, \rho_{\max}]$ except the case of maximal (minimal) value of the impact parameter, $\rho = \pm\rho_{\max}$, when two self-colliding solutions coincide. Thus, for $\rho \in (-\rho_{\max}, \rho_{\max}) - \{\rho_{\text{dg}}\}$ there are three solutions – one of them corresponding to the collision-free trajectory, and two of them corresponding to self-colliding trajectories. The two self-colliding solutions add up to $\pm\frac{\pi}{2}$ and represent completely different evolutions of the system. All three situations are depicted in figure 4.6. We can see that the first solution represents the self-collision nearer the vertex where the particle self-collides with larger ω, while the second solution represents self-collision farther from the vertex where the particle self-collides with smaller ω.

We can observe that the point $(\rho_{\text{dg}}, \omega_{\text{free}})$ separates two types I and II of collision-free trajectories to the past discussed in paragraph 4.2. Moreover, the direction ω_{free} represents the boundary value between self-collisions of type I and II, cf. section 3.3. Thus, for self-collisions of type I, for which trajectories get deflected leftward with respect to the collision-free trajectory, is

$$\omega > \omega_{\text{free}} ,$$

while for self-collisions of type II, for which trajectories get deflected rightward, holds

$$\omega < \omega_{\text{free}} .$$

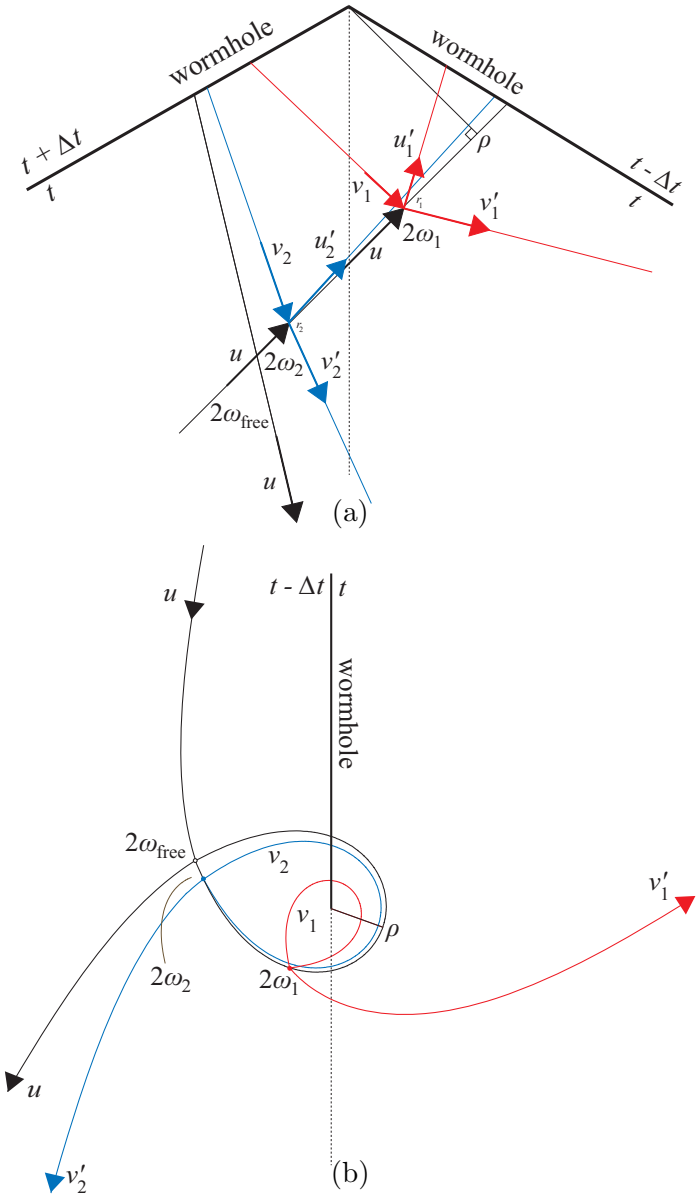

Figure 4.6: **Three possible solutions for given initial conditions of a point-like particle.** For $\rho \in (-\rho_{\max}, \rho_{\max})$, $\rho \neq \rho_{\rm dg}$ there are three solutions – one of them corresponding to the collision-free trajectory, and two of them corresponding to self-colliding trajectories. Here two self-colliding solutions with $\omega > 0$ (red and blue trajectories) and one collision-free solution to the past with $\omega = \omega_{\rm free}$ (the black trajectory) are plotted. One of the self-colliding trajectories is close to the free trajectory (it coincides in the limit $\rho \to \rho_{\rm dg}$); another is rather different. (a) The cone unfolded into a plane angle. (b) Bird's eye view of the cone.

Hence, in the limit $R \to 0$ of the point-particle, the point $(\rho_{\rm dg}, \omega_{\rm free})$ represents transition between (collision-free, self-colliding) solutions of type I and II. This can be seen in figs. 4.4 and 4.5 where collision-free solution of type I (II) changes continuously into self-colliding solution of type I (II) varying the impact parameter ρ through the value $\rho_{\rm dg}$. Self-colliding (collision-free) solutions of type I are depicted as red lines, while self-colliding (collision-free) solutions of type II are depicted as blue lines.

We can summarize that the point-particle model documents a non-uniqueness of

the evolutions in the presence of time machines. Since this model is not rich enough to investigate structure of trajectories corresponding to dangerous initial values we extend discussion to the case of finite balls in the following chapter.

4.6 Asymptotic behavior of the outer trajectories

The asymptotic behavior of the incoming and outgoing trajectories determines how many times the outer trajectories pass through the wormhole. For the case of one self-collision, the number of wormhole passages differs depending on if inequality $|\omega| < \frac{\gamma}{2}$, or if $|\omega| > \frac{\gamma}{2}$ holds. However, this number may vary with the angle between the self-collision and wormhole which is considered bellow.

4.6.1 Orientation of the wormhole

Till now we have concentrated on the local geometry of self-collision in which case we have ignored its angular position with respect to the wormhole. Thus, the self-collisions determined by the same parameters ω and r but rotated differently with respect to the axis have not been distinguished, cf. pars. 2.2 and 4.1. However, when discussing the asymptotic behavior of the incoming and outgoing trajectories, the angular position with respect to the wormhole must be taken into account since it affects the number of wormhole passages, and consequently the total time contribution of the trajectory.

The angular position of self-collision can be defined by choosing the orientation φ of the wormhole mouths (keeping the angular position φ_{i} of the incoming trajectory fixed), where we measure with respect to the *null radial direction* which is *opposite* to the wormhole, and making the identification of points with φ differing by an integer multiple of γ. The typical orientation given by $\varphi = \pm\frac{\gamma}{2}$ can be varied by adding the angle $\psi \in (-\frac{\gamma}{2}, \frac{\gamma}{2})$ whereby $\varphi = \pm\frac{\gamma}{2} + \psi$. Examples of different orientations of the wormhole mouths can be seen in fig. 4.8. Alternatively, we could fix the orientation of the wormhole mouths, for example $\psi = 0$, and vary the orientation φ_{i} of the incoming trajectory.

4.6.2 Covering space

However, we first describe the motion without a reference to the wormhole mouths. It can be done in the simplest way employing the *totally covering space* for the conical space. Namely, instead of the conical space with angular coordinate $\varphi \in (-\frac{\gamma}{2}, \frac{\gamma}{2})$ we use the space without any restriction on φ, i.e., a helical surface winding around the axis infinitely. The original conical space is then obtained by the identification of points which differ in coordinate φ by an integer multiple of γ.

In this covering space, the trajectory can be described as follows. Let us assume a particle incoming along the null direction, $\varphi_{\mathrm{i}} = 0$, with the impact parameter ρ and the initial velocity u. The self-collision C for such a trajectory always happens on the circle which we call the *collision circle*. It has the center S on the radial line $\varphi = 0$, it passes

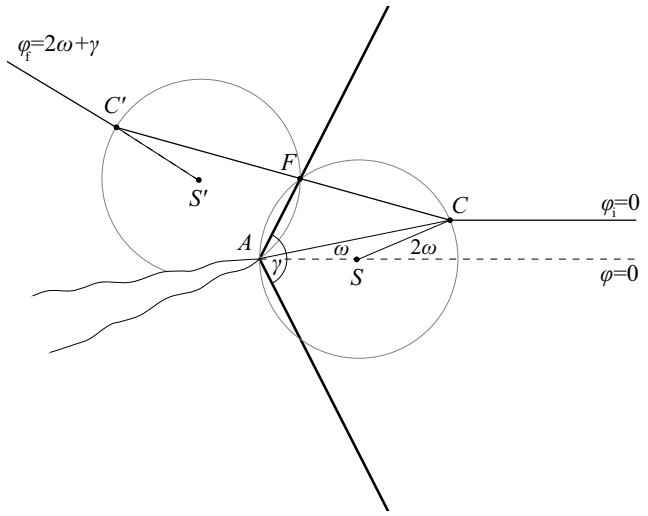

Figure 4.7: **Self-colliding trajectory in the totally covering space.** The particle incoming along the direction $\varphi_{\mathrm{i}} = 0$ with the impact parameter ρ is deflected at the point of self-collision C. The point C must lie on the collision circle with the center S on the radial line $\varphi = 0$, it passes through the axis A, and its radius is $\rho_{\max}$. The trajectory continues toward the point C', which is obtained by a counterclockwise rotation of the point C around A by angle γ. In the original conical space, points C and C' are identified and correspond to the point of self-collision. From C', the trajectory continues in the direction which aims from the center S' of the rotated collision circle. The direction of the inner trajectory goes through the focusing point F. The diagram shows only a part of the totally covering space.

through the axis, and its radius is $\rho_{\max}$, cf. fig. 4.7. For $\rho \in (-\rho_{\max}, \rho_{\max})$, the incoming trajectory intersects this circle twice, which corresponds to two possible self-colliding solutions, cf. par. 4.5. The angular coordinate φ of self-collision is given exactly by the scattering angle ω. At the point of self-collision C the trajectory is deflected, and it continues toward the point C', which can be obtained by a counterclockwise rotation of the point C around the axis by angle γ, cf. fig. 4.7. In the covering space, C and C' are different points; however, in the original conical space these points are identified as the point of self-collision – of course, the particle must pass the point of self-collision twice. Finally, from C' the particle continues through the covering space in the direction which aims from the center S' of the rotated collision circle, cf. fig. 4.7. Thus, the angular parameter of the outgoing trajectory is given by

$$\varphi_{\mathrm{f}} = \varphi_{\mathrm{i}} + 2\omega + \gamma,$$

in the covering space.

4.6.3 Total time contribution

The typical quantity, which depends on the angular position of self-collision, is the total time ΔT gained in the wormhole during the whole scattering process. It can be read out in the covering space from the angular coordinate φ_{f} of the outgoing trajectory – if it belongs to n-th copy of the wormhole in the covering space, $n \in \mathbf{Z}$, the particle

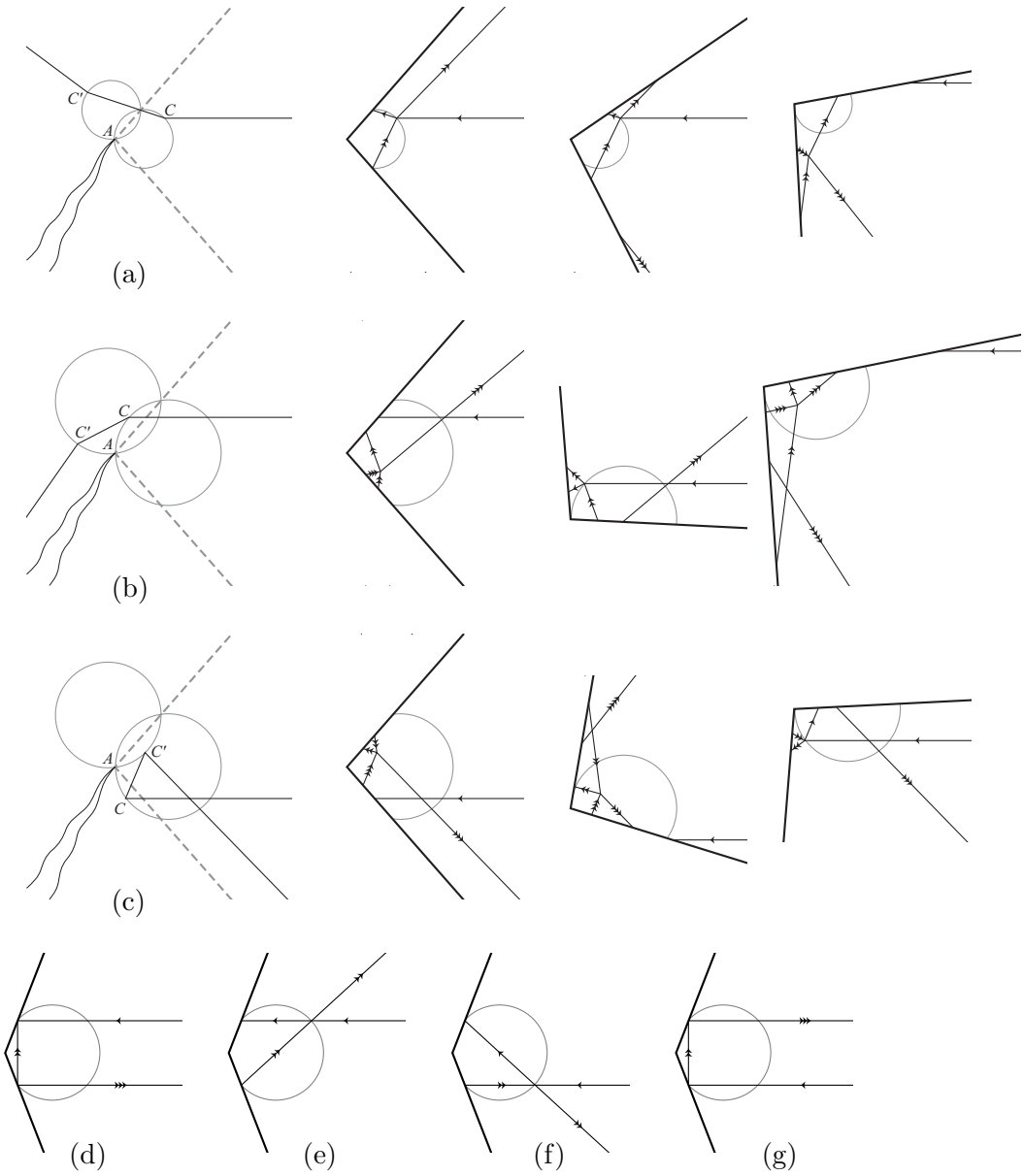

Figure 4.8: **Examples of the self-colliding trajectories** Diagrams show trajectories with various choices of the impact parameter ρ, or, equivalently, with a different scattering angle ω. The angle ω also parameterizes the position of the self-collision on the collision circle. Diagrams (a,b,c) represent typical cases $\omega \in (0, \frac{\pi}{4})$, $\omega \in (\frac{\gamma}{2}, \frac{\pi}{2})$, and $\omega \in (-\frac{\pi}{2}, -\frac{\gamma}{2})$, respectively. The diagram in the first column depicts the trajectory in the totally covering space, the second column shows the trajectory in the conical space with the wormhole centered on the direction of the incoming trajectory ($\psi = 0$), and the third and the fourth columns correspond to other orientations of the wormhole. The diagrams (d,e,f,g) depict special choices of the trajectory, namely, those with $\omega = \frac{\gamma}{2}$, $\omega = \omega_{\text{free}}$, $\omega = -\omega_{\text{free}}$, and $\omega = -\frac{\gamma}{2}$, respectively, in all of them with the wormhole centered on the incoming trajectory. The arrows indicate passages through the wormhole; however, they do not count the time shift, since the particle can travel through the time machine in both directions. We can observe that the structure of the trajectory can change substantially with various choices of the impact parameter and of the incoming direction with respect to the wormhole. For example, the particle can self-collide after passing through the wormhole, both into the past and future, or it can move through the wormhole after the self-collision.

gains the time shift $\Delta T = -n\Delta t$:

$$\varphi_{\rm f} \in \left(-\frac{\gamma}{2} + \psi + n\gamma, \frac{\gamma}{2} + \psi + n\gamma\right) \;\Rightarrow\; \Delta T = -n\Delta t \; . \tag{4.10}$$

Taking into account the restrictions on γ, ψ and ω, the total time shift can be $-3\Delta t \leq \Delta T \leq \Delta t$. Some of the representative trajectories are depicted in fig. 4.8.

The total time shift ΔT can be similarly calculated for the collision-free trajectories. In this case, the direction of the outgoing trajectory in the covering space is $\varphi_{\rm f} = \pi$ for the trajectories passing the wormhole to the past, and $\varphi_{\rm f} = -\pi$ for the trajectories passing the wormhole to the future. The condition (4.10) gives that the trajectory traveling to the past, $\rho > 0$, gains the time shift $\Delta T = -\Delta t$ for $\psi \in (-\frac{\gamma}{2}, \frac{3}{2}\gamma - \pi)$, or it can pass the wormhole twice, $\Delta T = -2\Delta t$, if $\psi \in (\frac{3}{2}\gamma - \pi, \frac{\gamma}{2})$. Similarly, for $\rho < 0$, the particle gains the time shift $\Delta T = \Delta t$ for $\psi \in (\pi - \frac{3}{2}\gamma, \frac{\gamma}{2})$ and $\Delta T = 2\Delta t$ for $\psi \in (-\frac{\gamma}{2}, \pi - \frac{3}{2}\gamma)$.

4.6.4 Congruence

Those particles which approach the time machine along the null direction $\varphi_{\rm i} = 0$ (with various $\rho \in (-\rho_{\max}, \rho_{\max})$, thus forming congruence with "plane-wave" wavefront) self-collide on the common colliding circle and, in the end, leave in the directions which point out from the common point S', cf. fig. 4.9. In the covering space, the original plane-wave congruence of particles scatters to the circular-wave congruence, but the particles are phase shifted. They fly in radial directions, but the wavefront of the congruence at one moment does not form a circle since the particles start to move in the radial directions in various times. Indeed, the incoming particles reach the collision circle in various times and, therefore, their self-collisions do not occur simultaneously. However, for large final times the wavefront after scattering approaches the circle.

Let us mention an interesting feature of the trajectories of the discussed congruence: all inner trajectories (between the self-collisions) have a direction going through one focusing point F, cf. fig. 4.9. For $\omega \in (-\frac{\gamma}{2}, \frac{\gamma}{2})$ they even pass through this point. The congruence (between the self-collisions) thus focuses in this point. However, the particles do not pass the focusing point at the same moment as can be verified by writing down this time explicitly

$$t(\omega) = \frac{\Delta t}{2\sin\frac{\gamma}{2}} \left(\frac{\sin^2\omega}{\sin\frac{\gamma}{2}} + \frac{\sin(\frac{\gamma}{2} - \omega)}{\cos\omega} \right) \; ,$$

depending on the scattering angle ω. At least, times t are maximal, respectively minimal, for limiting values of ω, i.e.,

$$t \xrightarrow{\omega \to \pm\pi/2} \pm\infty \; ,$$

which guarantees that particles with different ρ do not "traverse" each other. Notice also that the focusing point and the collision point coincide for the dangerous initial conditions determined by $u_{\rm dg}$ and $\rho_{\rm dg}$.

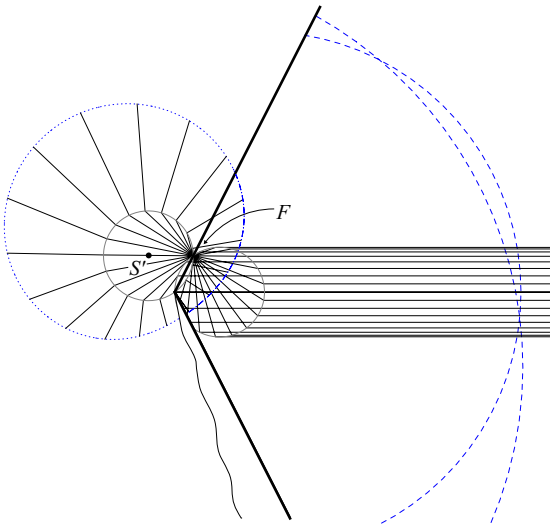

Figure 4.9: **Scattering of the plane-wave congruence of particles in the totally covering space** Congruence of particles coming along $\varphi_{\mathrm{i}} = 0$ direction in "plane-wave" configuration (i.e., aligned at an initial moment on a planar "wavefront" perpendicular to the direction of motion) approaches the time machine. The particles scatter on the collision circle and move toward the corresponding points on the rotated collision circle. Here, they are deflected in the directions coming from the center S' of the rotated collision circle. The dotted curve depicts the wavefront after the scattering in the totally covering space. The particles do not scatter on the collision circle at the same time; however, for large final times the wavefront after scattering approaches the circle. The real wavefront projected back to the conical space is drawn as dashed curves. Segments projected from various sheets of the totally covering space gain additional time shift thanks to the passage through the time machine. Therefore, these parts of the wavefront are larger since the particle had more time for their motion. Inner trajectories focus at one focusing point; for $\omega \in (-\frac{\gamma}{2}, \frac{\gamma}{2})$, they pass through this point. The diagram shows only part of the totally covering space, given approximately by $\varphi \in (-\frac{\gamma}{2}, 2\pi - \frac{\gamma}{2})$.

4.7 Negative velocity parametrization

Let us mention an equivalent parametrization which differs by the sign of the initial velocity u, i.e., the particle moves along initial trajectories with negative velocity $u < 0$. This results into transformation of the initial parameters ρ and φ_{i} on one hand, and the parameters of self-collision ω and r on the other hand. This transformation can be formulated as

$$\begin{pmatrix} u \\ \rho \\ \varphi_{\mathrm{i}} \\ \omega \\ r \end{pmatrix} \leftrightarrow \begin{pmatrix} -u \\ -\rho \\ \varphi_{\mathrm{i}} \pm \pi \\ \omega \pm \pi \\ r \end{pmatrix} . \tag{4.11}$$

Both parametrizations are illustrated in figures 4.4 and 4.5: Solutions corresponding to $u > 0$ and $\omega \in (-\pi/2, \pi/2)$ are drawn by solid lines while solutions corresponding to $u < 0$ and $\omega \in [-\pi, -\pi/2) \cup (\pi/2, \pi]$ are depicted by dashed lines.

This transformation can be interpreted as change from the incoming $\varphi_{\mathrm{i}} > 0$ ($\varphi_{\mathrm{i}} < 0$)

counterclockwise $\rho > 0$ (clockwise $\rho < 0$) trajectory along which the particle moves with the initial positive velocity $u > 0$ into the outgoing clockwise (counterclockwise) trajectory along which the particle moves with negative initial velocity $u < 0$. In other words, to say that the particle gets nearer the vertex with positive velocity $u > 0$ along the initial trajectory characterized by parameters ρ and φ_{i} is the same as to say that the particle recedes the vertex with negative velocity $u < 0$ along the initial trajectory characterized by parameters $-\rho$ and $\varphi_{\mathrm{i}} \pm \pi$.

Remind relation (4.4) which expresses momentum (or velocity) conservation law after the projection of inner and outer velocities into the radial line. Clearly, if the particle moves with positive velocity $v > 0$ along the inner trajectory and $-\pi < \omega < -\pi/2$ or $\pi/2 < \omega > \pi$ then the outer velocity u must be negative, $u < 0$, in order to satisfy equation (4.4). Therefore, a trajectory given by $u < 0$ and $\omega \in [-\pi, -\pi/2) \cup (\pi/2, \pi]$ can be interpreted as identical to the trajectory determined by $\omega \in (-\pi/2, \pi/2)$ and $u > 0$. Accordingly, we can find interpretation for any real value of ω which enter periodic functions (4.7) and (4.8). However, henceforward we will consider parametrization with the positive magnitude of the initial velocity $u > 0$, if not said otherwise.

Notice that the sign of the radial distance r of the self-collision from the vertex is not affected by the change of the parametrization, i.e., it remains positive $r > 0$, as can be verified by substitution of corresponding values of u, ρ and ω into eqs. (4.2) and (4.8). However, looking at figures 4.5(a) and 4.5(b), which illustrate the parametric curve $[\rho(\omega), r(\omega)]$ in both parametrizations, we can see that corresponding graphs are mirror reflected. Although positiveness of the radial distance r seems to be natural, in the chapter concerning finite billiard balls we will see that there are domains where the radial distance r is negative.

Chapter 5

Finite ball: one self-collision

In this chapter we will consider non-relativistic, freely moving billiard ball with finite diameter, $R > 0$. Since we study the self-intersection, or self-collision, following the only innermost loop, the range of the vertex angle γ is confined within the interval $(\pi/2, \pi)$ again.[1] Derivation and analysis of relations for one self-collision will follow. Subsequently, we will proceed in interpretation of the set of dangerous trajectories, and then we will discuss the number and types of solutions. Finally, we will express geometrical restrictions which impose constraints on the initial values and guarantee that the ball fits in the conical space.

5.1 Derivation of equations for self-collisions

Let us derive relations for self-collisions in analogy with the point-like case. However, in the case of finite ball, we have to account for finite radius R of balls: the collision occurs not at the moment when the trajectories of the center of the ball intersect but when the ball touches itself by its surface.

Hence, we have to introduce other quantities characterizing the radial distance of self-collisions. First, we distinguish the radius $\widetilde{r}$ from the radius r to take into account the difference between the self-intersection of the *inner* trajectory and the intersection of *outer* trajectories (incoming from and outgoing to infinity) of the center of the ball. Thus, r measures the radial distance of the intersection of outer trajectories from the axis, while $\widetilde{r}$ gives the radial distance of the self-intersection of the inner trajectory from the axis, cf. figs. 5.1. By $\widetilde{\rho}$ we denote the corresponding impact parameter.

Further on, let us introduce the difference $\triangle r$ between radial distances r and $\widetilde{r}$. We distinguish two positions of the self-colliding particle which correspond to two types I and II: Either the point of impact occurs further from the axis than $\widetilde{r}$

$$\triangle r_{\mathrm{I}} = r - \widetilde{r}, \tag{5.1}$$

and hence the difference is denoted by $\triangle r_{\mathrm{I}}$, cf. figs. 5.1(a) and 5.3. Or the touch point

[1] This system has been considered mainly in [21] (appendix H).

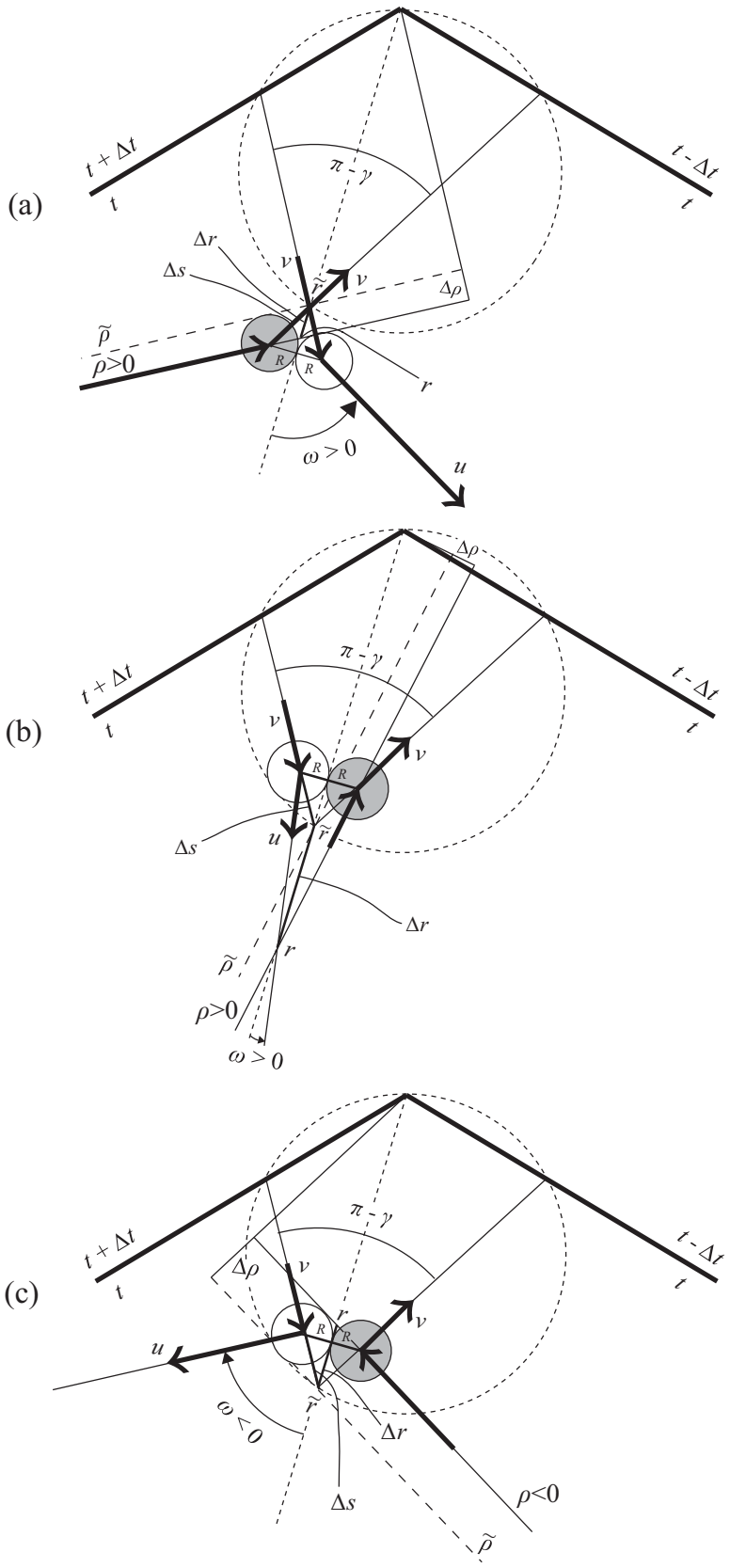

Figure 5.1: **Three situations illustrating two types of self-collisions.** (a) The older version of the ball touches the younger one by its rare part – type I. (b) and (c) The older version touches the younger version by its frontal part – type II. In the case (b) the ball comes from positive direction $\omega > 0$ and $r < \widetilde{r}$ while in the case (c) the ball comes from negative direction $\omega < 0$ and $r > \widetilde{r}$. The older version is white while the younger one is gray.

is located closer to the axis than $\widetilde{r}$

$$\triangle r_{\mathrm{II}} = \widetilde{r} - r,$$

and then $\triangle r_{\mathrm{II}}$ corresponds to the self-collision of type II, see figs. 5.1(b,c) and 5.3.

The geometry of the inner trajectory of a finite ball is identical to that of a point-particle with the modified impact parameter $\widetilde{\rho}$ and radial distance $\widetilde{r}$: $\widetilde{\rho} = \widetilde{r}\sin\omega$. The path s travelled during time Δt gained in the time machine must be corrected due to finite radius of the ball

$$s = \widetilde{s} \pm 2\triangle s,$$

where, analogously to the point-like case, $\widetilde{s} = 2\widetilde{r}\sin\gamma/2$ is the length of the inner trajectory between its self-collision. The upper sign corresponds to type I and the lower sign to type II. The correction is given by $\triangle s = \frac{R}{\cos\gamma/2}$ as can be verified in figs. 5.1.

Thus, to determine the inner path s, we need to add/subtract the correction $2\Delta s$, and to compute the path $\widetilde{s}$ we have to assign the radial distance $\widetilde{r}$. Obviously, both quantities differ according to the concerned type of the self-collision, so we will treat the two cases separately. This will result into two different equations for types I and II, cf. also section 3.1.1.

5.1.1 Equation for self-collisions of type I

From the geometry depicted in figures 5.1(a) and 5.3, we express the quantity $\triangle r_{\mathrm{I}}$ as

$$\triangle r_{\mathrm{I}}(\rho, u) = R(\tan\frac{\gamma}{2} - \cot\omega_{\mathrm{I}}(\rho, u)), \tag{5.2}$$

where we indicated dependence on initial parameters u, ρ and we denoted the solution for the collision angle by ω_{I}. With the help of the constraint (4.2) we obtain final expression for the radius $\widetilde{r}_{\mathrm{I}}$ for type I by combination of equations (5.1) and (5.2)

$$\widetilde{r}_{\mathrm{I}}(\rho, u) = \frac{\rho}{\sin\omega_{\mathrm{I}}(\rho, u)} - R(\tan\frac{\gamma}{2} - \cot\omega_{\mathrm{I}}(\rho, u)). \tag{5.3}$$

Now, we can complete expression for the path s_{I}

$$s_{\mathrm{I}}(\rho, u) = \widetilde{s}_{\mathrm{I}} + 2\triangle s = 2\widetilde{r}_{\mathrm{I}}(\rho, u)\sin\frac{\gamma}{2} + \frac{2R}{\cos\frac{\gamma}{2}},$$

thereby we can write formula for the velocity on the inner path

$$v_{\mathrm{I}}(\rho, u) = \frac{2}{\triangle t}\left(\widetilde{r}_{\mathrm{I}}(\rho, u)\sin\frac{\gamma}{2} + \frac{R}{\cos\frac{\gamma}{2}}\right).$$

Analogously to the point-like case, we compare the projection of the inner velocity onto the radial line (on which the ball self-interacts), $u_{\mathrm{in}} = v_{\mathrm{I}}(\rho, u)\sin\frac{\gamma}{2}$, with the projection of the outer velocity $u_{\mathrm{out}} = u\cos\omega_{\mathrm{I}}(\rho, u)$ and we obtain relation

$$u\triangle t\cos\omega_{\mathrm{I}}(\rho, u) = 2\widetilde{r}_{\mathrm{I}}(\rho, u)\sin^2\frac{\gamma}{2} + 2R\tan\frac{\gamma}{2}, \tag{5.4}$$

cf. eqs. (3.6) and (4.4). Finally, from equations (5.3) and (5.4) we get equation for self-collisions of type I

$$u\triangle t \sin 2\omega_{\rm I}(\rho,u) = 4\rho\sin^2\frac{\gamma}{2} + 4R\sin\frac{\gamma}{2}\sin(\frac{\gamma}{2}+\omega_{\rm I}(\rho,u)), \tag{5.5}$$

which determines $\omega_{\rm I}$ in terms of initial parameters ρ and u.

5.1.2 Equation for self-collisions of type II

The difference $\triangle r$ is expressed in the same form as in the case of type I

$$\triangle r_{\rm II}(\rho,u) = R(\tan\frac{\gamma}{2} - \cot\omega_{\rm II}(\rho,u)),$$

where we denote the solution by $\omega_{\rm II}$ figures 5.1(b,c) and 5.3. In analogy with the case I, we substitute equations (5.1) and (5.1.2) into the constraint (4.2) and express the radius $\widetilde{r}_{\rm II}$ for type II

$$\widetilde{r}_{\rm II} = \frac{\rho}{\sin\omega_{\rm II}(\rho,u)} + R(\tan\frac{\gamma}{2} - \cot\omega_{\rm II}(\rho,u)), \tag{5.6}$$

in terms of ρ and u. We complete expressions for the path $s_{\rm II} = \widetilde{s}_{\rm II} - 2\triangle s$ and for the velocity on the inner path $v_{\rm II} = \frac{s_{\rm II}}{\triangle t}$ we get

$$v_{\rm II}(\rho,u) = \frac{2}{\triangle t}(\widetilde{r}_{\rm II}(\rho,u)\sin\frac{\gamma}{2} - \frac{R}{\cos\frac{\gamma}{2}}). \tag{5.7}$$

Next, we relate the projection of the inner velocity onto the radial line, $u_{\rm in} = v_{\rm II}(\rho,u)\sin\frac{\gamma}{2}$, to the projection of the outer velocity, $u_{\rm out} = u\cos\omega_{\rm II}(\rho,u)$, whereby we obtain equation

$$u\triangle t\cos\omega_{\rm II}(\rho,u) = 2\widetilde{r}_{\rm II}(\rho,u)\sin^2\frac{\gamma}{2} - 2R\tan\frac{\gamma}{2}, \tag{5.8}$$

for eq. (3.6). From equations (5.6) and (5.8) we gain the equation of self-collisions of type II

$$u\triangle t \sin 2\omega_{\rm II}(\rho,u) = 4\rho\sin^2\frac{\gamma}{2} - 4R\sin\frac{\gamma}{2}\sin(\frac{\gamma}{2}+\omega_{\rm II}(\rho,u)), \tag{5.9}$$

which determines $\omega_{\rm II}$ in terms of initial parameters ρ and u.

5.1.3 Notes to just derived equations

Having the scattering angle $\omega_{\rm I,II}$ defined by u and ρ the position of self-collision – determined by the radius r – is given by eq. (4.2). Notice, moreover, that both just derived equations reduce to the same equation of self-collision (4.5)

$$u\Delta t \sin 2\omega = 4\rho\sin^2\frac{\gamma}{2}\,.$$

for the point-like particle as the ball's radius approaches zero, $R \to 0$.

Note also that equations (5.5) and (5.9) can be reformulated in such a way that the impact parameter ρ and the radial distance r depend on the initial velocity u and the angle ω

$$\rho_{\mathrm{I,II}}(u,\omega) = \frac{1}{4\sin^2\frac{\gamma}{2}}(u\triangle t \sin 2\omega \mp 4R\sin\frac{\gamma}{2}\sin(\frac{\gamma}{2}+\omega)), \tag{5.10}$$

and

$$r_{\mathrm{I,II}}(u,\omega) = \frac{1}{2\sin^2\frac{\gamma}{2}}(u\triangle t\cos\omega \mp 2R\tan\frac{\gamma}{2}) \pm R(\tan\frac{\gamma}{2} - \cot\omega), \tag{5.11}$$

and thus form single-valued functions.

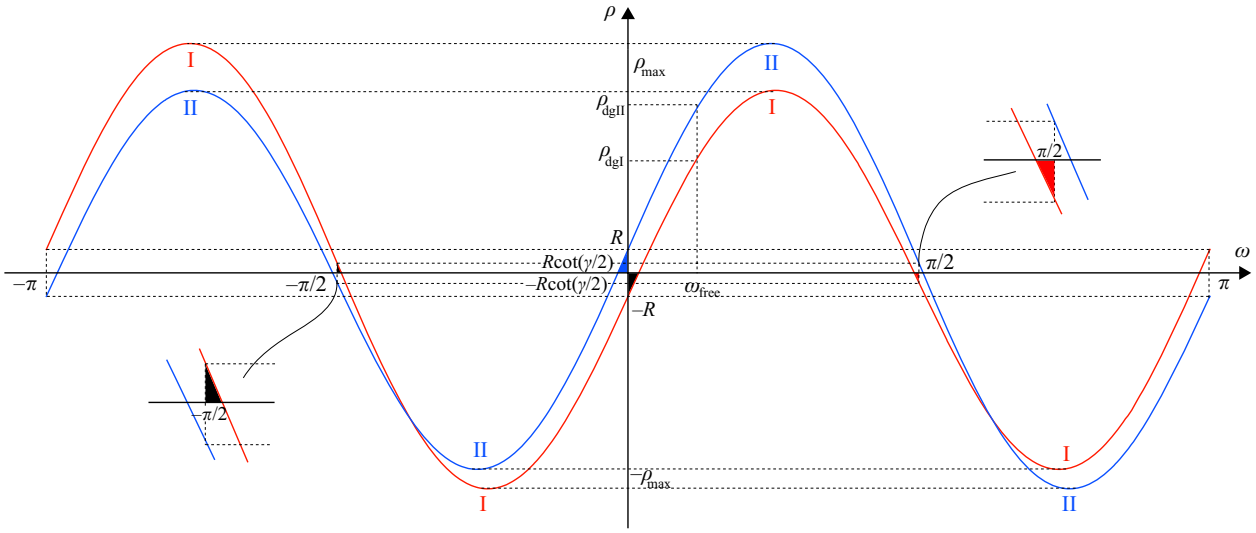

Figure 5.2: **Dependence $\rho_{\mathrm{I,II}} = \rho_{\mathrm{I,II}}(u,\omega)$ for $\omega \in (-\pi,\pi)$.** The diagram depicts the dependence $\rho_{\mathrm{I,II}} = \rho_{\mathrm{I,II}}(u,\omega)$, with $\omega \in (-\pi,\pi)$ and u is fixed. The red graph represents the solution of type I and the blue graph represents the solution of type II. Obviously, both dependencies are periodical with the period 2π. Moreover, the graph of the solution I is identical with the graph of the solution II but shifted by π along the ω-axis. In order to interpret solutions on the extended domain $(-\pi,\pi)$ we realize that the solution of type I within $\omega \in (-\pi,-\pi/2)$, and $\omega \in (\pi/2,\pi)$ respectively, with the negative initial velocity $u < 0$ determines the same velocity vectors as the solution of type II within $(0,\pi/2)$, and $(-\pi/2,0)$ respectively, with the positive initial velocity $u > 0$ (and analogically for the solution of type II). Notice that there are subintervals of $\omega \in [-\pi/2,\pi/2]$ violating equality $\mathrm{sign}(\rho) = \mathrm{sign}(\omega)$ which causes that the radial distance r is negative. These intervals are located in the neighborhood of values $-\pi/2$, 0 and $\pi/2$, and they are emphasized by colored "triangles".

Clearly, we cannot eliminate the dependence on u, just by dividing by $u\Delta t$ as it was possible for a point-like particle, since the radius R of the ball represents an additional length scale in the system. Although various quantities depend on u in a more complicated way than just a rescaling we will fix the value of the initial velocity to discuss the structure of the corresponding solutions. Thus, we can draw diagrams of the dependencies $\rho_{\mathrm{I,II}} = \rho_{\mathrm{I,II}}(u,\omega)$, figure 5.2, with the help of equations (5.10), analogous to those used in the point-like case, see figs. 4.4 and 4.5.

5.1.4 Polynomial form of equations for types I and II

Let us transform equations (5.5) and (5.9) into polynomial form setting $t = \sin\omega$

$$t^4 + a_1 t^3 + a_2 t^2 + a_3 t + a_4 = 0.$$

It has just four roots for both types and the coefficients differ only by signs

$$a_1 = \mp\frac{4R}{u\triangle t}\sin^2\frac{\gamma}{2} \qquad a_2 = \frac{4R^2}{(u\triangle t)^2}\sin^2\frac{\gamma}{2} - 1$$

$$a_3 = \pm\frac{4R}{u\triangle t}\sin^2\frac{\gamma}{2}(1 + \frac{\rho}{u\triangle t}\sin\gamma) \quad a_4 = \frac{4\sin^4\frac{\gamma}{2}}{(u\triangle t)^2}(\rho^2 - R^2)\ .$$

If we eliminate the angle ω from equations (5.4) and (5.8) we receive polynomial equation for radius r

$$b_0 r^4 + b_1 r^3 + b_2 r^2 + b_3 r + b_4 = 0,$$

with coefficients

$$b_0 = 4\sin^4\frac{\gamma}{2}(R^2 - \rho^2) \qquad b_1 = \mp 4R\rho\sin\frac{\gamma}{2}(u\triangle t - \rho\sin\gamma)$$

$$b_2 = \rho^2[(u\triangle t)^2 - 4R^2\sin^2\frac{\gamma}{2}] \qquad b_3 = \pm 4R\rho^3 u\triangle t\sin^2\frac{\gamma}{2} \qquad b_4 = -\rho^4(u\triangle t)^2.$$

5.2 Physical versus spurious self-collisions

Solutions of equations (5.5) and (5.9) can be divided into physical and non-physical solutions. By physical solutions we mean self-collisions in which the particle exchanges positive momentum, while by *spurious* (non-physical) solutions we mean self-collisions in which the particle exchanges negative momentum.

Physical self-collisions of type I or II are restricted by the conditions

$$\omega > \omega_{\rm free} \qquad \text{for physical solutions of type I ,}$$
$$\omega < \omega_{\rm free} \qquad \text{for physical solutions of type II ,}$$

otherwise the ball would deflect to a wrong side of the free trajectory and the momentum transfer from the younger to older version of the ball would be negative. The corresponding difference $\triangle r_{\rm I}$ determined by eq. (5.2), respective $\triangle r_{\rm II}$ determined by eq. (5.1.2), is bounded within the interval $(0, R\tan\frac{\gamma}{2})$, fig. 5.3(a,b,c), respective within the interval $(-\infty, 0) \cup (R\tan\frac{\gamma}{2}, +\infty)$, fig. 5.3(e',f',g'). Intervals for the difference Δr corresponding to physical self-collisions of both types can be read from graphs 5.4 – red and blue curves.

Consequently, spurious solutions correspond to the complement range of the scattering angle ω: $\omega_{\rm I} \in (-\pi/2, \pi/2 - \gamma/2)$ and $\omega_{\rm II} \in (\pi/2 - \gamma/2, \pi/2)$. The corresponding difference $\triangle r_{\rm I}$, respective $\triangle r_{\rm II}$ is bounded within the interval $(-\infty, 0) \cup (R\tan\frac{\gamma}{2}, +\infty)$, fig. 5.3(d,e,f,g), respective within the interval $(0, R\tan\frac{\gamma}{2})$, fig. 5.3(a',b',c',d'). Intervals

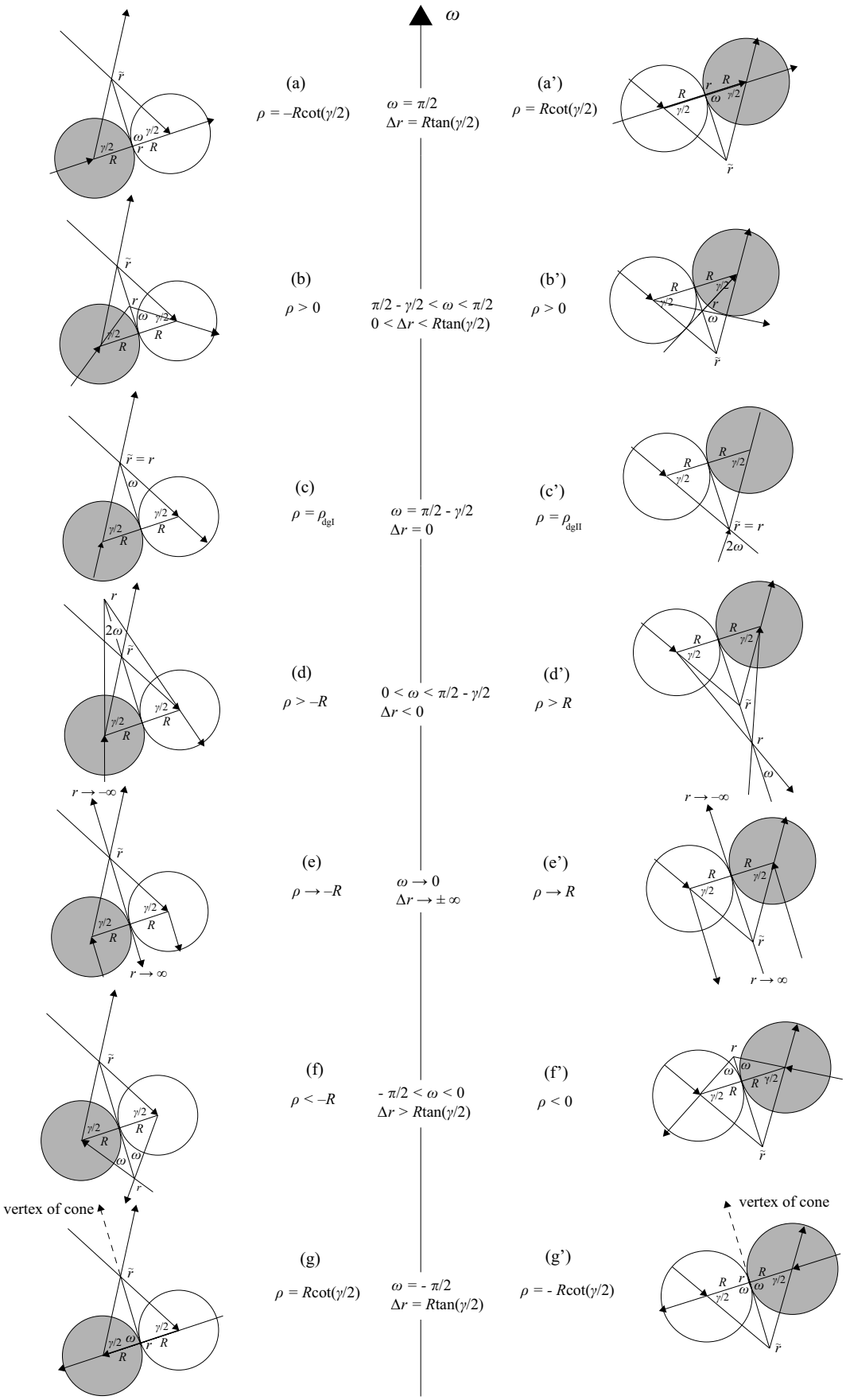

Figure 5.3: **Local structure of self-collisions.**

Figure 5.3: **Legend of figure 5.3.** Diagrams of all interesting collision configurations depending on values of ω from the interval $[-\pi/2, \pi/2]$. On the left there are situations corresponding to type I, while on the right there are situations corresponding to type II. Physical solutions of type I are represented by situations (a), (b) and (c) for which $\omega_{\mathrm{I}} \in (\pi/2 - \gamma/2, \pi/2)$ and $\triangle r_{\mathrm{I}} \in (0, R\tan\frac{\gamma}{2})$ (red curve in figure 5.4(a)). Spurious solutions of type I are represented by configurations (d), (e), (f) and (g) for which $\omega_{\mathrm{I}} \in (-\pi/2, \pi/2 - \gamma/2)$ and $\triangle r_{\mathrm{I}} \in (-\infty, 0) \cup (R\tan\frac{\gamma}{2}, +\infty)$ (gray curve in fig. 5.4(a)). Physical situations of type II are represented by situations (e'), (f') and (g') for which $\omega_{\mathrm{II}} \in (-\pi/2, \pi/2 - \gamma/2)$ and $\triangle r_{\mathrm{II}} \in (-\infty, 0) \cup (R\tan\frac{\gamma}{2}, +\infty)$ (blue curve in figure 5.4(b)). Spurious solutions are represented by positions (a'), (b'), (c') and (d') for which $\omega_{\mathrm{II}} \in (\pi/2 - \gamma/2, \pi/2)$ and $\triangle r_{\mathrm{II}} \in (0, R\tan\frac{\gamma}{2})$ (gray curve in fig. 5.4(b)). To distinguish local geometries of both types (regardless to physicality or spuriousity of solutions) we notice that self-collisions (the point where the ball touch itself) of type I take place farther from the vertex (of the cone) with respect to the radius $\widetilde{r}_{\mathrm{I}}$ while self-collisions of type II occur nearer to the vertex with respect to the radius $\widetilde{r}_{\mathrm{II}}$.

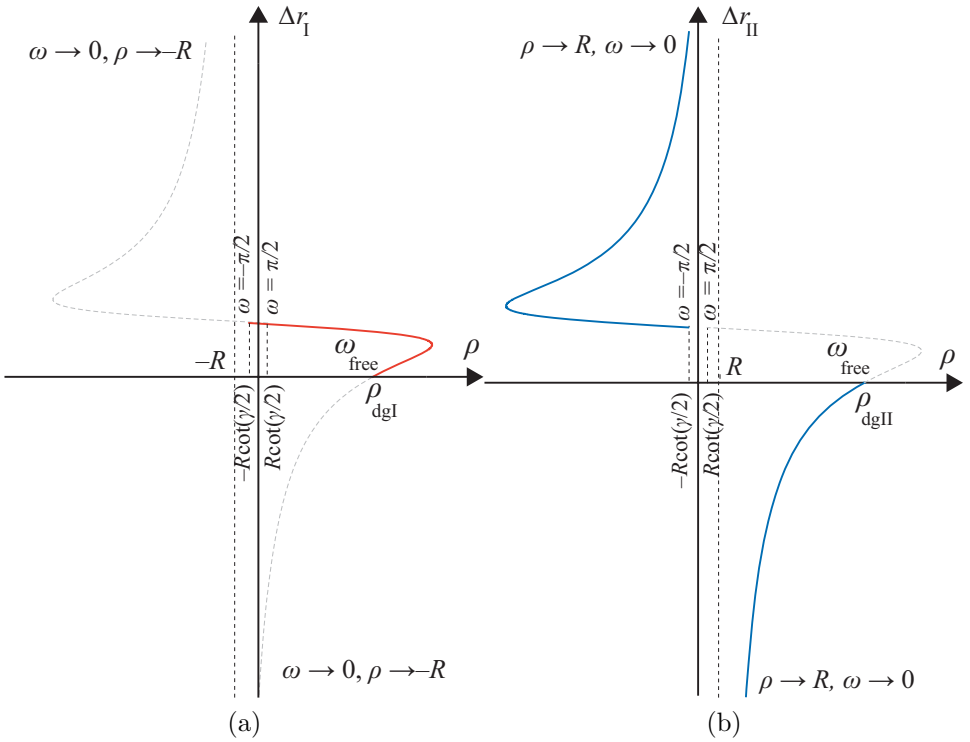

Figure 5.4: **Graphs for differences Δr.** (a) Graph for the difference Δr_{I} is determined by equation (5.2): Physical solutions are bound within domain $\triangle r_{\mathrm{I}} \in (0, R\tan\frac{\gamma}{2})$ (red part of the curve) while spurious solutions are limited to $\triangle r_{\mathrm{I}} \in (-\infty, 0) \cup (R\tan\frac{\gamma}{2}, +\infty)$ (gray dashed part of the curve). (b) Graph for the difference Δr_{II} is determined by equation (5.1.2): Physical solutions are bound within domain $\triangle r_{\mathrm{II}} \in (-\infty, 0) \cup (R\tan\frac{\gamma}{2}, +\infty)$ (blue part of the curve) while spurious solutions are restricted to $\triangle r_{\mathrm{II}} \in (0, R\tan\frac{\gamma}{2})$ (gray dashed part of the curve). If both graphs were merged together we would see three physical self-colliding solutions within the interval $\rho \in (\rho_{\mathrm{dg_I}}, \rho_{\mathrm{dg_{II}}})$ represented by intersections of vertical lines with colored parts of graphs.

for the difference Δr corresponding to spurious self-collisions of both types can be read from graphs 5.4 – gray curves.

Using relations (5.10) and (5.11) we can draw graphs for $\rho_{\mathrm{I,II}}(u,\omega)$ and $r_{\mathrm{I,II}}(u,\omega)$, cf. figs. 5.5 and 5.6, which represent the solutions with at most one self-collision where the initial velocity u is fixed and $\omega \in [-\frac{\pi}{2}, \frac{\pi}{2}]$. The physical solutions (in red and blue) lie on the solid lines while the spurious ones (in gray) on the dashed lines.

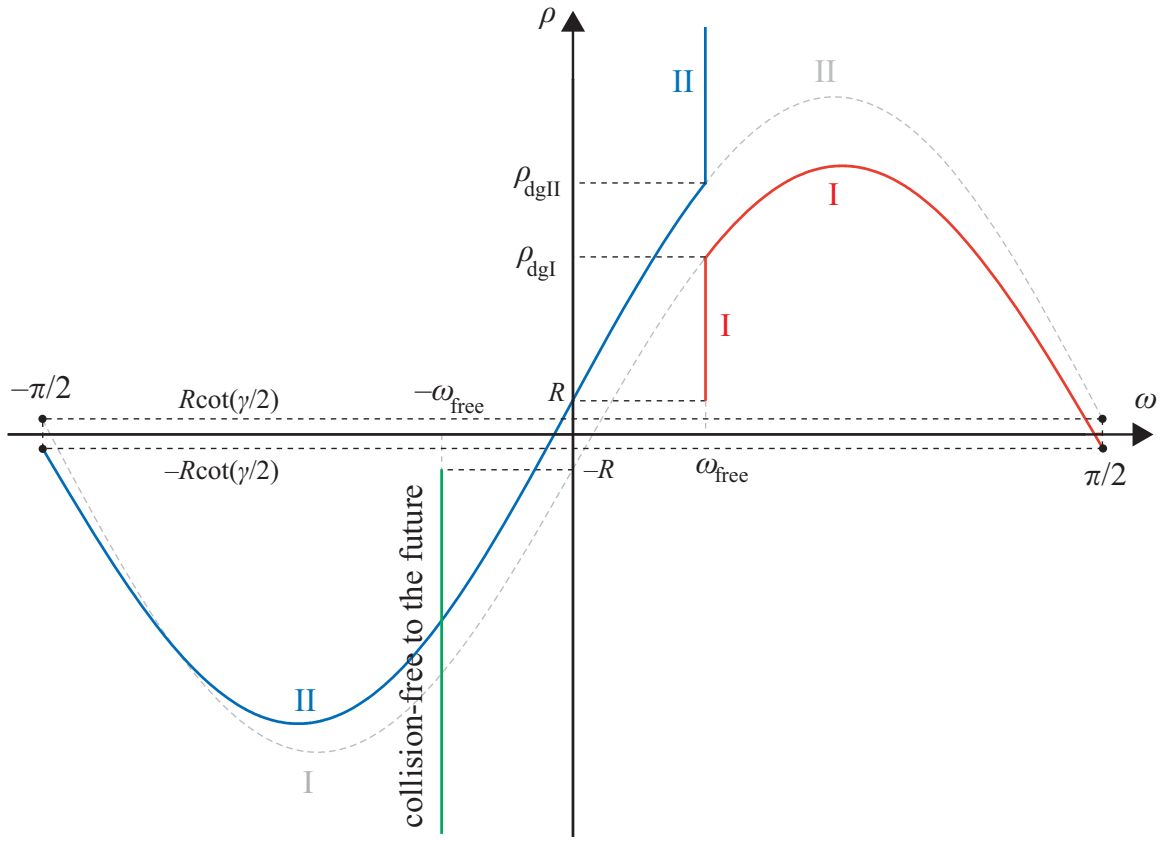

Figure 5.5: **Physical solutions in the ρ-ω plane.** The solutions with at most one self-collision in the ρ-ω plane, analogously to fig. 4.4. The initial velocity u is fixed and $\omega \in [-\frac{\pi}{2}, \frac{\pi}{2}]$. The physical solutions (in red and blue) lie on the solid lines while the spurious ones (in gray) on the dashed lines. The straight vertical lines $\omega = \pm\omega_{\mathrm{free}}$ represent the collision-free solutions. The line $\omega = \omega_{\mathrm{free}}$ corresponds to collision-free trajectories to the past and the line $\omega = -\omega_{\mathrm{free}}$ (in green) corresponds to collision-free trajectories to the future. The collision-free solutions with $\rho < \rho_{\mathrm{dg}}$ (in red) are of type I while the solutions with $\rho > \rho_{\mathrm{dg}}$ (in blue) are of type II. The sinusoidal curves, given by eq. (5.10), correspond to the solution with one self-collision. The part with $\omega > \omega_{\mathrm{free}}$ (in red) represents physical self-collisions of type I while the part with $\omega < \omega_{\mathrm{free}}$ (in blue) represents physical self-collisions of type II. We can see how the collision-free solution of type I changes into the self-colliding one of type I at the point $(\rho_{\mathrm{dg_I}}, \omega_{\mathrm{free}})$ and the collision-free solution of type II changes into self-colliding one of type II at the point $(\rho_{\mathrm{dg_{II}}}, \omega_{\mathrm{free}})$. The values $\rho = \pm R$ and $\rho = \pm R\cot\frac{\gamma}{2}$ correspond to the situation with small ρ when the ball aims toward the axis.

In figure 5.5 we can see physical solutions in the ρ-ω plane. The straight vertical lines $\omega = \pm\omega_{\mathrm{free}}$ represent the collision-free solutions. The line $\omega = \omega_{\mathrm{free}}$ corresponds to collision-free trajectories to the past and the line $\omega = -\omega_{\mathrm{free}}$ (in green) corresponds to collision-free trajectories to the future. The collision-free solutions with $\rho < \rho_{\mathrm{dg}}$ (in red)

are of type I while the solutions with $\rho > \rho_{\mathrm{dg}}$ (in blue) are of type II. The sinusoidal curves, given by eq. (5.10), correspond to the solution with one self-collision. The part with $\omega > \omega_{\mathrm{free}}$ (in red) represents physical self-collisions of type I while the part with $\omega < \omega_{\mathrm{free}}$ (in blue) represents physical self-collisions of type II. The values $\rho = \pm R$ and $\rho = \pm R \cot \frac{\gamma}{2}$ correspond to the situation with small ρ when the ball aims toward the axis.

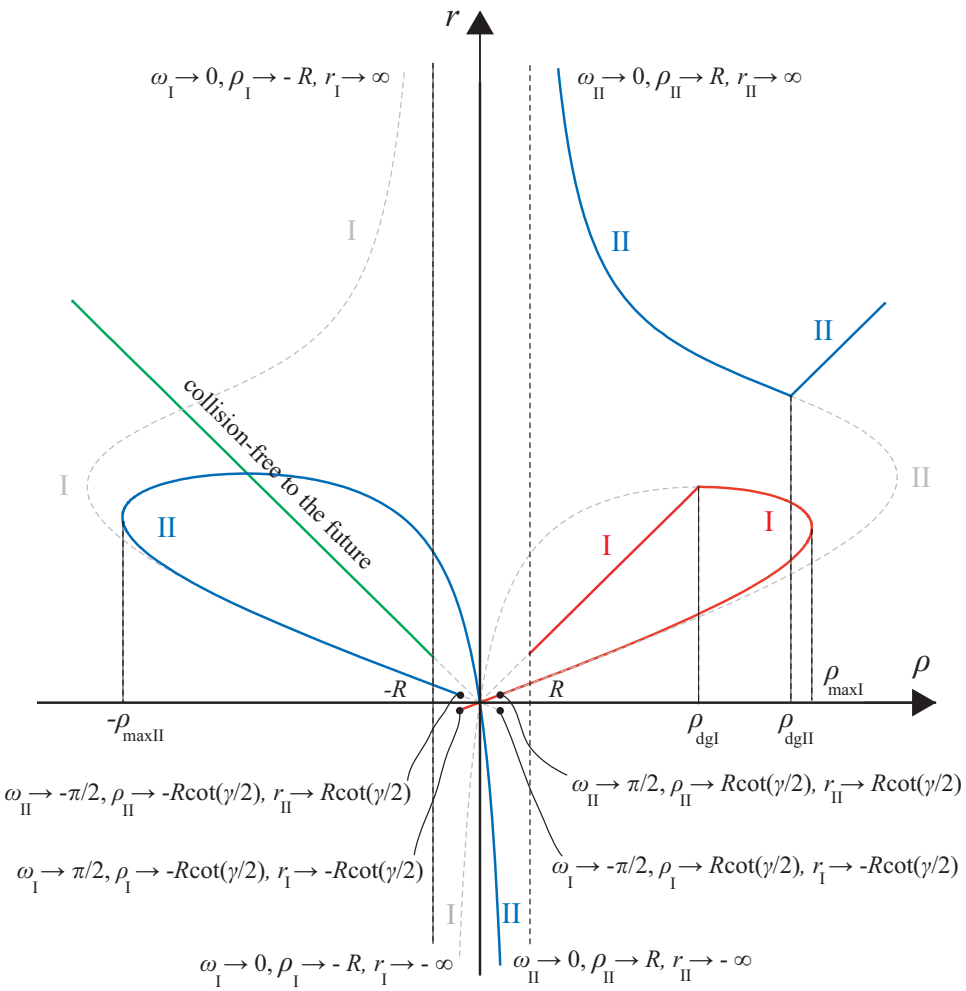

Figure 5.6: **Physical solutions in the r-ρ plane.** The solutions with at most one self-collision in the r-ρ plane, analogously to fig. 4.5. The scattering angle $\omega \in [-\pi/2, \pi/2]$ represents the parameter of the curves defined by eqs. (5.10) and (5.11). The initial velocity u is fixed. The physical solutions (in red and blue) lie on the solid lines while the spurious ones (in gray) on the dashed lines. The radial lines $\omega = \pm\omega_{\mathrm{free}}$ represent the collision-free solutions. The self-colliding solutions are depicted by the parametric curves $[\rho(\omega), r(\omega)]$. The type of the solutions is indicated in a similar way as in fig. 5.5. The infinities in the direction of the r-axis and the boundary points near the origin are given by geometrical constraints for a ball directed very closely toward the axis, see paragraphs 5.2.2 and 5.6 for details.

In figure 5.6 we can see physical solutions in the r-ρ plane. The radial lines $\omega = \pm\omega_{\mathrm{free}}$ represent the collision-free solutions. The self-colliding solutions are depicted by the parametric curves $[\rho(\omega), r(\omega)]$ with the parameter ω, cf. eqs. (5.10) and (5.11). The type of the solutions is indicated in a similar way as in fig. 5.5. The infinities in the direction of the r-axis and the boundary points near the origin correspond to

the situation when the ball is directed very closely toward the axis. The infinite peaks are interpreted as regular self-colliding solutions in paragraph 5.2.2. The end-points near the origin correspond to geometrical restrictions on motion of the particle. These restrictions concern the problem of fitting of the ball into the conical space and preventing it from hitting the axis, see section 5.6. Clearly, the two mentioned phenomena are consequences of a finite size of the ball.

5.2.1 Limits of the impact parameter interval

We can see that each type of self-collisions is represented by its own graph, cf. fig. 5.5. Hence, there are two maximal (minimal) values which determine two impact parameter intervals allowing self-collisions. In order to compute these limits we look for extremals of equation (5.10) with respect to ω

$$\frac{\mathrm{d}\rho}{\mathrm{d}\omega} = 0.$$

Thus, we obtain the relations

$$\triangle tu \cos 2\omega = 2R \sin\frac{\gamma}{2} \cos(\frac{\gamma}{2} + \omega) \ , \tag{5.12a}$$

for type I, and

$$\triangle tu \cos 2\omega = -2R \sin\frac{\gamma}{2} \cos(\frac{\gamma}{2} + \omega) \ , \tag{5.12b}$$

for type II. Solving these equations and substituting ω's back into equations (5.10) we obtain two maximums $\rho_{\max_{\mathrm{I,II}}}$ (minimums $\rho_{\min_{\mathrm{I,II}}}$). However, only one of them corresponds to a physical solution. It is obvious that the minimal value of the impact parameter must correspond to the solution of type II since type I is always spurious for $\omega < 0$. In contrast, the maximal value of ρ (corresponding to the physical self-collision) can be of both types I and II depending on the vertex angle γ: The maximal impact parameter is of type I for $\gamma > \pi/2$, and type II for $\gamma < \pi/2$. Since we have restricted to the vertex angle $\gamma \in (\gamma/2, \pi/2)$ in this chapter, we will employ only the maximal limit of type I, i.e., $\rho_{\max_{\mathrm{I}}}$.

Notice that just derived maximums (minimums) approach values of the point-like case given by relation (4.9). More accurately, from equations (5.10) we can infer that for $\rho \gg R$ is $\omega_{\max} \sim \frac{\pi}{4}$ and $\omega_{\min} \sim -\frac{\pi}{4}$. For $R \to 0$ is $\omega \to \pi/4$, and hence also $|\rho_{\max_{\mathrm{I,II}}}| \to \frac{u\Delta t}{4\sin^2\gamma/2}$.

5.2.2 Solutions with negative radius r

Notice that there are subintervals of $\omega \in [-\pi/2, \pi/2]$ where the radial distance r is negative or diverges. These intervals are located in the neighborhood of values $-\pi/2$, 0 and $\pi/2$, figure 5.2.

The first such subinterval $-\delta < \omega_{\mathrm{II}} < 0$ corresponds to $\rho \in (0, R)$ and it is emphasized by the blue "triangle" in the neighborhood of the origin in diagram 5.2. However,

we can project it on the opposite semi-line, and thus we obtain the physical self-collision, cf. figure 5.7(a).

Even the limit situation $\rho \to R$, for which the radial distance diverges, we can interpret as the physical self-collision, depicted in figs. 5.7(b) and 5.3(e'). More accurately, as ρ approaches R from the left, $\rho \to R_-$, and ω tend to zero from the left, $\omega_{\rm II} \to 0_-$, the difference $\triangle r_{\rm II} \to \infty$ and the radial distance $r_{\rm II} \to -\infty$, situation (f') in figure 5.3. And as ρ approaches R from the right, $\rho \to R_+$, and ω tend to zero from the right, $\omega_{\rm II} \to 0_+$, the difference $\triangle r_{\rm II} \to -\infty$ and the radial distance $r_{\rm II} \to \infty$, situation (d') in figure 5.3. However, the radius $\widetilde{r}_{\rm II} = r_{\rm II} + \triangle r_{\rm II}$ remains finite since both infinities cancel each other.

In contrast, the subinterval $\delta > \omega_{\rm I} > 0$ corresponding to $\rho \in (-R, 0)$ (highlighted by the black "triangle" in the neighborhood of the origin in fig. 5.2) represents the self-collisions with exchange of negative momentum, i.e., spurious solutions.

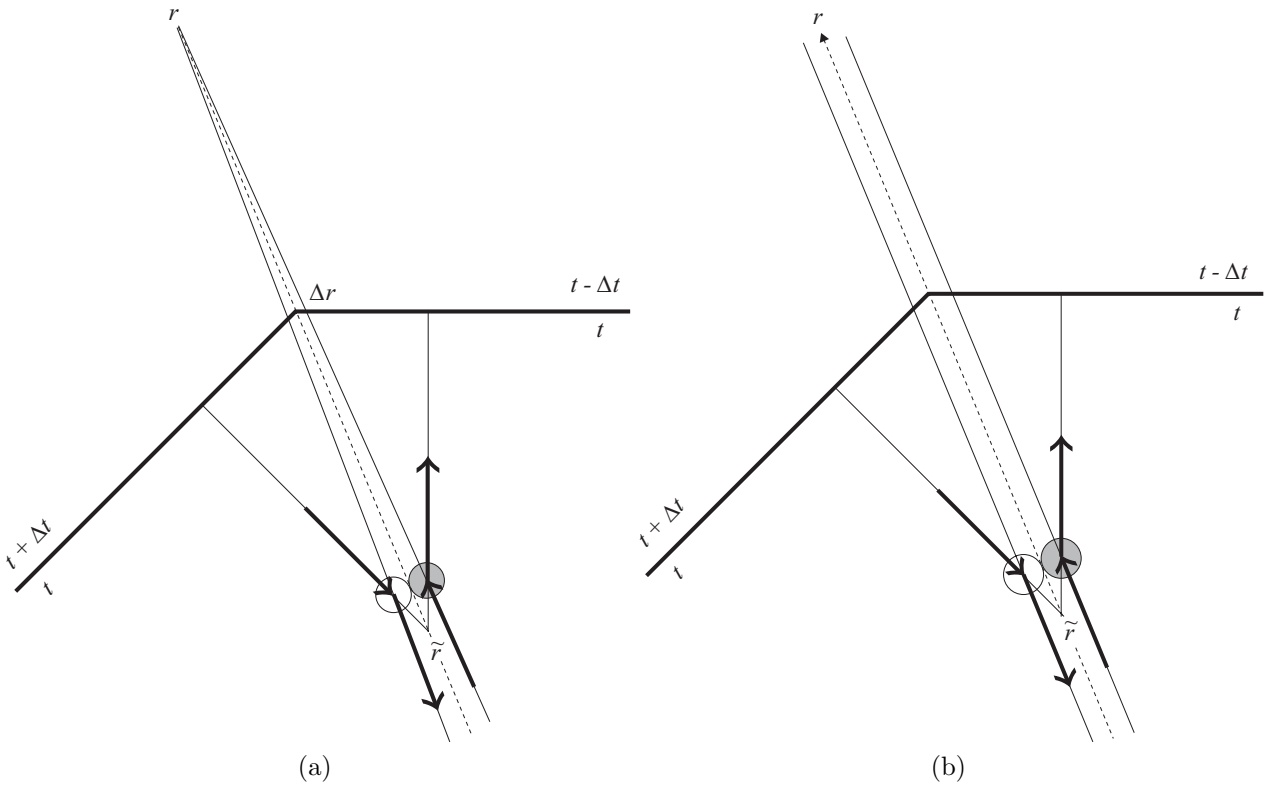

Figure 5.7: **Interpretation of the negative, respectively diverging, radius r.** Although the radial distance r of the self-collision is negative, fig. (a), or diverging, fig. (b), both situations represent regular self-collisions. Specifically, the radial distance r can be projected on the opposite semi-line to obtain interpretation of physical self-collisions. In the case of the limit situation, $\rho \to R$, the radius $\widetilde{r}_{\rm II}(= r_{\rm II} + \triangle r_{\rm II})$ remains finite because both infinite quantities $r_{\rm II}(\to \infty)$ and $\triangle r_{\rm II}(\to -\infty)$ cancel each other.

Interpretation of subintervals in the neighborhood of values $-\pi/2$ and $\pi/2$ will be given in paragraph 5.6 concerning geometrical restrictions on initial parameters. The corresponding intervals $\omega_{\rm I} \in [\pi/2 - \epsilon, \pi/2]$ and $\rho \in (-R\cot\frac{\gamma}{2}, 0)$ represent self-collisions with exchange of positive momentum, respective $\omega_{\rm I} \in [-\pi/2, -\pi/2 + \epsilon]$ and $\rho \in [0, R\cot\frac{\gamma}{2}]$ represent self-collisions with exchange of negative momentum, see the

red, respective black, "triangle" in figure 5.2.

5.3 Dangerous trajectories

Now we want to show that there exist consistent self-collisions along so called dangerous incoming trajectories which supersede paradoxical self-intersections, cf. discussion in chapter 3. Dangerous trajectories are determined by special values of initial parameters u and ρ given by the condition of arrival under the collision-free angle $\omega = \omega_{\text{free}}$, cf. section 4.4. Substituting this value into equations (5.11) we obtain two values of ρ (for given initial velocity u)

$$\rho_{\text{dg}_{\text{I,II}}} = \frac{u\triangle t}{2\tan\frac{\gamma}{2}} \mp \frac{R}{\sin\frac{\gamma}{2}}, \tag{5.13}$$

corresponding to each type of self-collisions. These two values define the interval of the impact parameter ρ for which the collision-free trajectories would become paradoxical, i.e., the ball would self-collide inconsistently. Such a paradoxical situation is illustrated in figure 3.1 where $\rho_{\text{dg}} = \frac{\rho_{\text{dg}_\text{I}}+\rho_{\text{dg}_\text{II}}}{2} = \frac{u\Delta t}{2\tan\gamma/2}$ which represents the value into which degenerates the above interval in the case of the point-like particle.

Therefore, the ball cannot follow a collision-free trajectory to the past for $\rho \in [\rho_{\text{dg}_\text{I}}, \rho_{\text{dg}_\text{II}}]$, in contrast to the only value ρ_{dg} in the point-like case. This interval can be used to separate two types I and II of free trajectories to the past: Collision-free trajectories of type I for $\rho < \rho_{\text{dg}_\text{I}}$, and collision-free trajectories of type II for $\rho > \rho_{\text{dg}_\text{II}}$, cf. paragraph 4.2. In diagrams 5.5 and 5.6 collision-free solutions to the past are represented by straight (red for type I, and blue for type II) lines, while collision-free trajectories to the future drawn as green straight lines (for which $\omega = -\omega_{\text{free}}$).

Notice that self-collisions of either type change continuously into collision-free trajectories at the angle ω_{free}, cf. figs. figures 5.5 and 5.6. Namely, the self-colliding solution of type I changes continuously into the collision-free solution of type I (red curves) at $\rho_{\text{dg}_\text{I}}$, and the self-collision of type II turns continuously into the self-intersection of type II (blue curves) at $\rho_{\text{dg}_\text{II}}$. Clearly, values $\rho_{\text{dg}_{\text{I,II}}}$ represent two limiting solutions when the ball just touches itself but it does not exchanges any momentum. Thus, local geometry of the self-collision changes continuously as we vary the impact parameter through the interval $[\rho_{\text{dg}_\text{I}}, \rho_{\text{dg}_\text{II}}]$.

However, the self-collision of type I does not change continuously into the self-collision of type II which is illustrated, e.g., in fig. 5.5, but by the jump from $\rho_{\text{dg}_\text{I}}$ to $\rho_{\text{dg}_\text{II}}$ for the angle ω_{free}. In other words, in the point of transition, $\omega = \omega_{\text{free}}$, the physical solution of one type is replaced by the physical solution of the other type.

5.4 Number of solutions

In figure 5.5 we can see that for the initial conditions with $\rho \notin (-\rho_{\text{max}_\text{II}}, \rho_{\text{max}_\text{I}})$ there exists just one consistent solution. It is typically a collision-free trajectory, however, for certain values of parameters it can also be a self-colliding solution, cf. fig. 5.8(b).

Specifically, for $\rho_{\mathrm{max_I}} > \rho_{\mathrm{dg_{II}}}$ it is the collision-free solution, while for the reversed inequality it represents the self-collision.

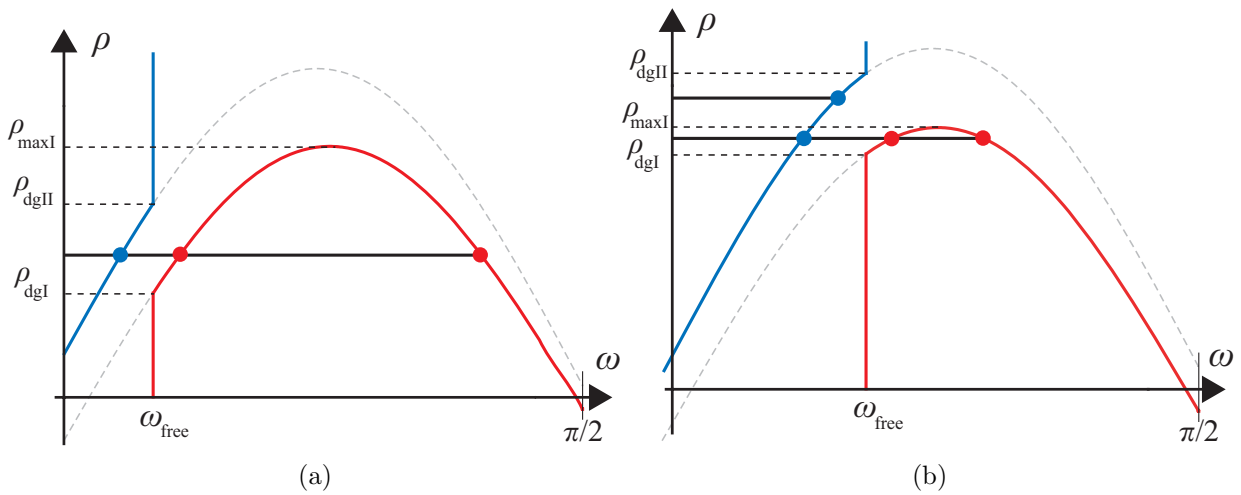

Figure 5.8: **Structure of solutions in the dangerous interval for $\gamma \in (\pi/2, \pi)$.** The number of solutions for chosen initial parameter ρ can be determined by intersecting the graph with the horizontal line corresponding to ρ. The choice of the initial velocity u can slightly modify a shape of the diagrams. As we vary the impact parameter ρ there is one physical solution for $\rho < \rho_{\mathrm{min_{II}}}$ (the collision-free trajectory to the future) and for $\rho > \rho_{\mathrm{max_I}}$ (the collision-free or self-colliding solution of type II), while there are three physical solution in the interval $\rho \in (\rho_{\mathrm{min_{II}}}, \rho_{\mathrm{max_I}})$. Because the structure of solutions can change in the dangerous interval only the part with $\omega > 0$ is depicted – it corresponds approximately to the initial conditions with $\rho > 0$. However, in the dangerous interval $(\rho_{\mathrm{dg_I}}, \rho_{\mathrm{dg_{II}}})$ the number of solutions remains the same. Only the character of solutions changes: the collision-free solution is superseded by the self-colliding solution. (a) Three self-colliding solutions in the dangerous interval occur when inequality $\rho_{\mathrm{max_I}} > \rho_{\mathrm{dg_{II}}}$ holds. (b) For $\rho_{\mathrm{max_I}} < \rho_{\mathrm{dg_{II}}}$, the dangerous interval falls into two subintervals with different number of self-colliding solutions: In the subinterval $(\rho_{\mathrm{dg_I}}, \rho_{\mathrm{max_I}})$ there are three self-colliding solutions, while in the subinterval $(\rho_{\mathrm{max_I}}, \rho_{\mathrm{dg_{II}}})$ there exists just one self-colliding solution.

For $\rho \in (-\rho_{\mathrm{max_{II}}}, \rho_{\mathrm{max_I}})$ there are three physical solutions; typically one collision-free and two self-colliding. However, for the dangerous initial conditions, i.e., $\rho \in (\rho_{\mathrm{dg_I}}, \rho_{\mathrm{dg_{II}}})$, the (missing) collision-free solution is superseded by a self-colliding solution, cf. fig. 5.8. In this case, we obtain two self-colliding solutions of type I and one solution of type II. This continuous replacement of the collision-free trajectory for one extra self-collision represents a resolution of the degenerated situation in the point-like case, cf. section 4.4. Thus, the number of physical solutions in the interval $(-\rho_{\mathrm{max_{II}}}, \rho_{\mathrm{max_I}})$ is conserved from which we can conclude that the dangerous initial conditions are not paradoxical. In other words, the number of solutions for given initial data is the same for dangerous initial data as for generic ones. All three self-collisions for ρ from the dangerous interval are illustrated in figure 5.9.

Let us analyze the structure of solutions with respect to the apex angle γ varying the initial parameters in more detail. Suppose the initial velocity u is fixed though the choice of u can slightly modify a shape of the solution. As we vary the impact parameter ρ there is one physical solution for $\rho < \rho_{\mathrm{min_{II}}}$ (the collision-free trajectory to

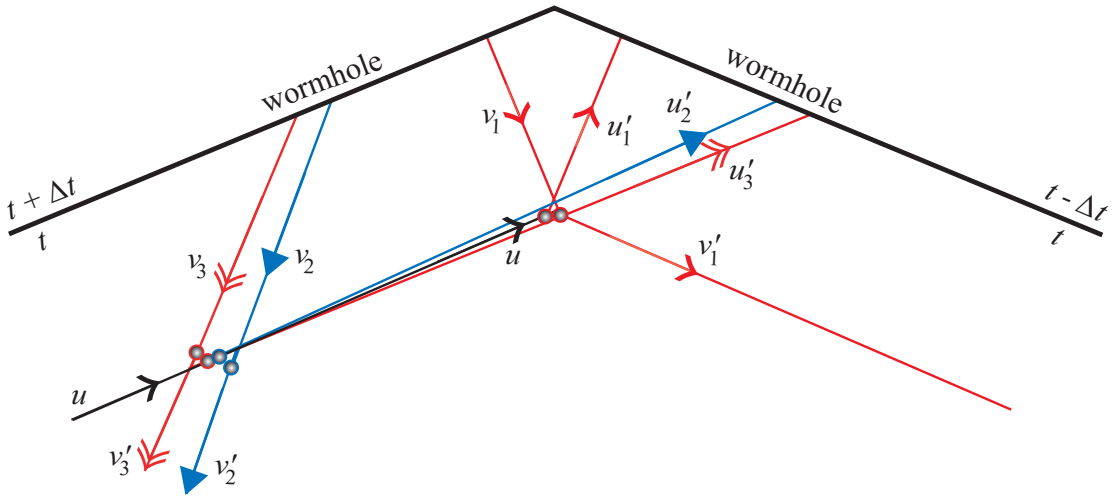

Figure 5.9: **Three self-colliding solutions for ρ from the dangerous interval.** Unlike the point-like case, there is a whole interval $[\rho_{\mathrm{dg_I}}, \rho_{\mathrm{dg_{II}}}]$ – bounded by dangerous values defined in eq. (5.13) – where collision-free trajectories do not exist. As we can see from diagrams 5.5 and 5.6, any such collision-free trajectory is replaced by a self-collision, and thus the number of physical solutions within the interval $[-\rho_{\mathrm{max_{II}}}, \rho_{\mathrm{max_{IorII}}}]$ remains conserved, cf. figure 5.8. Specifically, there are two self-collisions of type I (in red) and one self-collision of type II (in blue).

the future), cf. fig. 5.5, and $\rho > \rho_{\mathrm{max_I}}$ (the collision-free or self-colliding solution of type II), while there are three physical solution in the interval $\rho \in (\rho_{\mathrm{min_{II}}}, \rho_{\mathrm{max_I}})$, cf. fig. 5.8.

The number of solutions remains the same even in the dangerous interval $(\rho_{\mathrm{dg_I}}, \rho_{\mathrm{dg_{II}}})$. Only the character of solutions changes: the collision-free solution is superseded by the self-colliding solution. If the limiting value $\rho_{\mathrm{max_I}}$ belongs to the dangerous interval we can distinguish two cases: For

$$\rho_{\mathrm{max_I}} > \rho_{\mathrm{dg_{II}}},$$

there exist three self-colliding solutions in the dangerous interval, cf. figure 5.8(a), while for

$$\rho_{\mathrm{max_I}} < \rho_{\mathrm{dg_{II}}},$$

the dangerous interval falls into two subintervals with different number of self-colliding solutions: In the subinterval $(\rho_{\mathrm{dg_I}}, \rho_{\mathrm{max_I}})$ there are three self-colliding solutions, while in the subinterval $(\rho_{\mathrm{max_I}}, \rho_{\mathrm{dg_{II}}})$ there exists just one self-colliding solution, cf. figure 5.8(b). [2] Therefore, we can conclude that the structure of solutions does not change for $\gamma \in (\pi/2, \pi)$, i.e., the number of solutions passes from one to three with ρ belonging to the interval $(\rho_{\mathrm{min_{II}}}, \rho_{\mathrm{max_I}})$.

But, till now we have considered the structure of solutions for $\gamma \in (\pi/2, \pi)$ as it is natural for the system with at most one self-collision. However, the structure of solutions (not only within the dangerous interval) changes if the angle γ decreases bellow $\pi/2$. In this case, the collision-free angle

$$\omega_{\mathrm{free}} > \frac{\pi}{4},$$

[2] The limiting value of the vertex angle γ (when the subinterval with only one self-colliding solution appears) could be computed using equality $\rho_{\mathrm{dg_{II}}} = \rho_{\mathrm{max_I}}$, i.e., employing eqs. (5.13) and (5.12a).

and we find a gap in the solution curves in the dangerous interval $\rho \in (\rho_{\mathrm{dg_I}}, \rho_{\mathrm{dg_{II}}})$, cf. fig. 5.10. In other words, collision-free trajectories *are not superseded* by another self-collision. Moreover, for such a ρ, there exists only one self-colliding solution. In this case, we can indeed speak about the paradoxical initial conditions, since the solutions evolved from these conditions are really restricted. However, for $\gamma < \pi/2$ the discussion is more complicated, since the particle can self-interact in a more complex way: there is the possibility of multiple self-intersections between several self-collisions. The multiple self-interactions of the point-particle will be the topic of the next chapter. But it is far from clear if these more complex processes will resolve this problem.

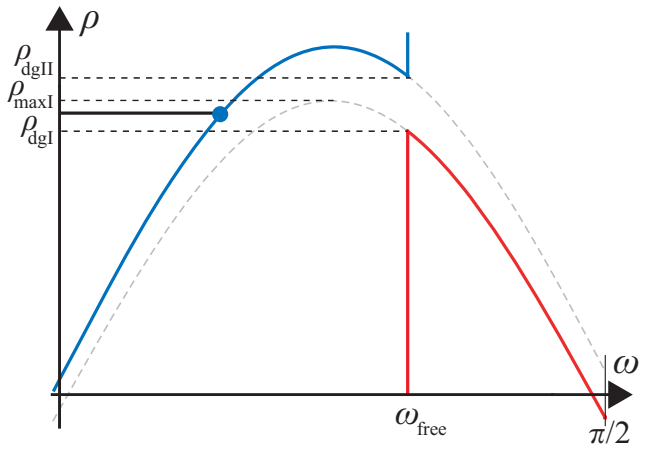

Figure 5.10: **Solutions from the dangerous interval for $\gamma < \frac{\pi}{2}$.** In this case, the collision-free angle is $\omega_{\mathrm{free}} > \frac{\pi}{4}$. For the impact parameter ρ from the corresponding dangerous interval $\rho \in (\rho_{\mathrm{dg_I}}, \rho_{\mathrm{dg_{II}}})$, we find a gap in the solution curves. For such a ρ there exists only one self-colliding solution. Moreover, this solution corresponds to a value of ω which is substantially different from ω_{free}.

5.5 Periodicity and negative velocity parametrization

Let us look at figure 5.2. We see that the dependencies $\rho_{\mathrm{I,II}} = \rho_{\mathrm{I,II}}(u, \omega)$ are periodical with the period 2π, i.e. $\rho_{\mathrm{I,II}}(u, \omega) = \rho_{\mathrm{I,II}}(u, \omega + 2k\pi)$, $k \in \mathbf{Z}$. The curve describing the solution I is identical with the curve of the solution II but shifted by $(2k-1)\pi$ along the ω-axis

$$\rho_{\mathrm{I}}(u, \omega) = \rho_{\mathrm{II}}(u, \omega + (2k-1)\pi).$$

In order to interpret solutions on the extended domain $(-\pi, \pi)$ we realize that the solution of type I within $\omega_{\mathrm{I}} \in (-\pi, -\pi/2)$ respective $\omega_{\mathrm{I}} \in (\pi/2, \pi)$ with the negative initial velocity $u < 0$ determines the same velocity vectors as the solution of type II within $\omega_{\mathrm{II}} \in (0, \pi/2)$ respective $\omega_{\mathrm{II}} \in (-\pi/2, 0)$ with the positive initial velocity $u > 0$ (and analogically for the solution of type II). In other words, in $u < 0$ parametrization solutions within $(-\pi, -\pi/2)$ respective $(\pi/2, \pi)$ represent the same physical situations as solutions in $u > 0$ parametrization within $(0, \pi/2)$ respective $(-\pi/2, 0)$, see transformation (4.11).

5.6 Geometrical restriction on initial parameters

Finally, we solve the question of confinement of the ball within the conical space which results in additional conditions (to solutions of equations of self-collisions) which constrain set of trajectories with physical self-collisions. We formulate such constraints on initial parameters u and ρ that ensure that the ball fits in the conical space, respectively that it does not hit the vertex.

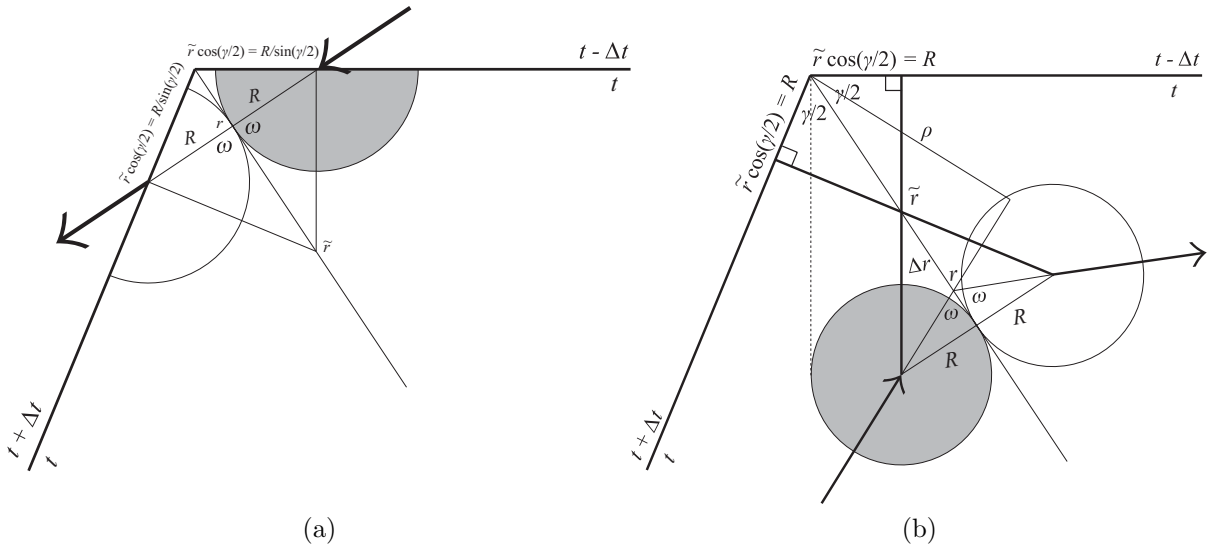

Figure 5.11: **Geometrical restriction on initial parameters in the conical space.** (a) The constraint imposed on the impact parameter ρ by the condition that guarantee that the ball (i.e., its both versions) fits in the conical space at the time of the self-collision. This condition is valid only for self-collisions of type II and can be expressed as inequality $\widetilde{r}_{\mathrm{II}} \cos\frac{\gamma}{2} \geq \frac{R}{\sin\gamma/2}$. (b) In the case of self-collisions of type I, we have to use a stronger condition. Notice that the ball would hit the vertex if we employed the "fitting" condition only. To avoid hitting the vertex we require that another inequality $\widetilde{r}_{\mathrm{I}} \cos\frac{\gamma}{2} \geq R$ holds.

First we consider the constraint imposed on the impact parameter ρ (u is fixed) by the condition which guarantees that the ball (i.e., its both versions) fits in the conical space at the time of the self-collision. The condition is illustrated in figure 5.11(a) by the self-collision of type II, and can be formulated as inequality

$$\widetilde{r}_{\mathrm{II}} \cos\frac{\gamma}{2} \geq \frac{R}{\sin\frac{\gamma}{2}}. \tag{5.14}$$

If we express $\widetilde{r}_{\mathrm{II}}$ from equation (5.8) as $\widetilde{r}_{\mathrm{II}} = \frac{u\triangle t\cos\omega + 2R\tan\gamma/2}{2\sin^2\gamma/2}$, we obtain the constraint

$$\cos\omega \geq 0 \qquad \text{or} \qquad u \geq 0, \tag{5.15}$$

i.e., $\omega \leq \pi/2$, respectively $\omega \geq -\pi/2$.

Let us focus on the limiting "fitting" configuration depicted in figure 5.11(a). Equality in (5.15) occurs either if $\omega_{\mathrm{fit_{II}}} = \pm\pi/2$, or if $u = 0$. Using eq. (5.10) the first equality implies that u is arbitrary and the lowest boundary for ρ is given by $\rho_{\mathrm{fit_{II}}} = \pm R\cot(\gamma/2)$ for self-collisions of type II. Accordingly, if we plug $u = 0$ into eq. (5.10) we receive

arbitrary ω and ρ within $[-R\cot(\gamma/2), \frac{R}{\sin(\gamma/2)}]$, cf. diagrams 5.15. Thus, we can see that the condition (5.14) which guarantees that the ball fits in the conical space does not impose any additional constraint on the range of initial parameters, and gives values determined also by the equation for self-collisions of type II (5.9) for $\omega = \pm\pi/2$.

To demonstrate the limiting 'fitting" configuration depicted in figure 5.11(a) for $\rho_{\mathrm{fit_{II}}} = -R\cot(\gamma/2)$ we have illustrated few moments previous, respectively following the self-collision as seen by a local observer, figure 5.12. The local observer reads the external time t_i of the i-th event where $i = 1, ..., 9$. Events within a column are separated by unit of time while columns of these events are separated by the time shift Δt where $\Delta t \gg 1$. The younger version is represented by the gray ball and its proper time τ differ from the proper time of the older version by Δt. The younger version is halted by the self-collision, waits the period Δt to become the older version, and then gets hit by the other version to leave to the future and the distant region. Thus, in this case, the difference Δt corresponds to the time of motionless waiting at the wormhole, i.e., the inner velocity is zero, $v_{\mathrm{II}} = 0$ (by substitution of $\omega_{\mathrm{fit_{II}}} = -\pi/2$ into eq. (5.7)).

In the case of self-collisions of type I, we have to use a stronger condition. Notice that the ball would hit the vertex if we employed the "fitting" condition only. To avoid hitting the vertex we require that another inequality

$$\widetilde{r}_{\mathrm{I}} \cos\frac{\gamma}{2} \geq R, \tag{5.16}$$

holds, see figure 5.11(b). If we express $\widetilde{r}_{\mathrm{I}}$ from equation (5.4) as $\widetilde{r}_{\mathrm{I}} = \frac{u\triangle t\cos\omega - 2R\tan\gamma/2}{2\sin^2\gamma/2}$, we get the condition

$$u\triangle t\cos\omega \geq 2R\tan\frac{\gamma}{2}(1+\sin\frac{\gamma}{2}). \tag{5.17}$$

Now, we can see that the above constraint represents the additional condition which limits the range of the initial parameters. It has been (numerically) verified that the solution $\pm\omega_{\mathrm{fit_I}}$ computed from (5.17) is always greater (respectively smaller) than ω's determined by the equation for self-collision of type I (5.9) for $\rho = 0$. Thus the lowest boundary $\rho_{\mathrm{fit_I}}$ is always positive for $\omega_{\mathrm{fit_I}} > 0$ (respectively negative for $\omega_{\mathrm{fit_I}} < 0$). It follows that the range violating equality of signs of ω and ρ around $\pm\pi/2$, emphasized by colored "triangles" in figure 5.2, can be interpreted as trajectories (with self-collisions of type I) along which the ball would hit the vertex, cf. section 5.2.2.

In conclusion of this section we mention that there are expected constraints even in the case of collision-free trajectories. Namely, balls moving along collision-free trajectories may not hit the vertex as well, i.e., $\rho > R$ for counterclockwise (to the past) oriented trajectories, respectively $\rho < -R$ for clockwise (to the future) oriented trajectories, cf. figure 5.5.

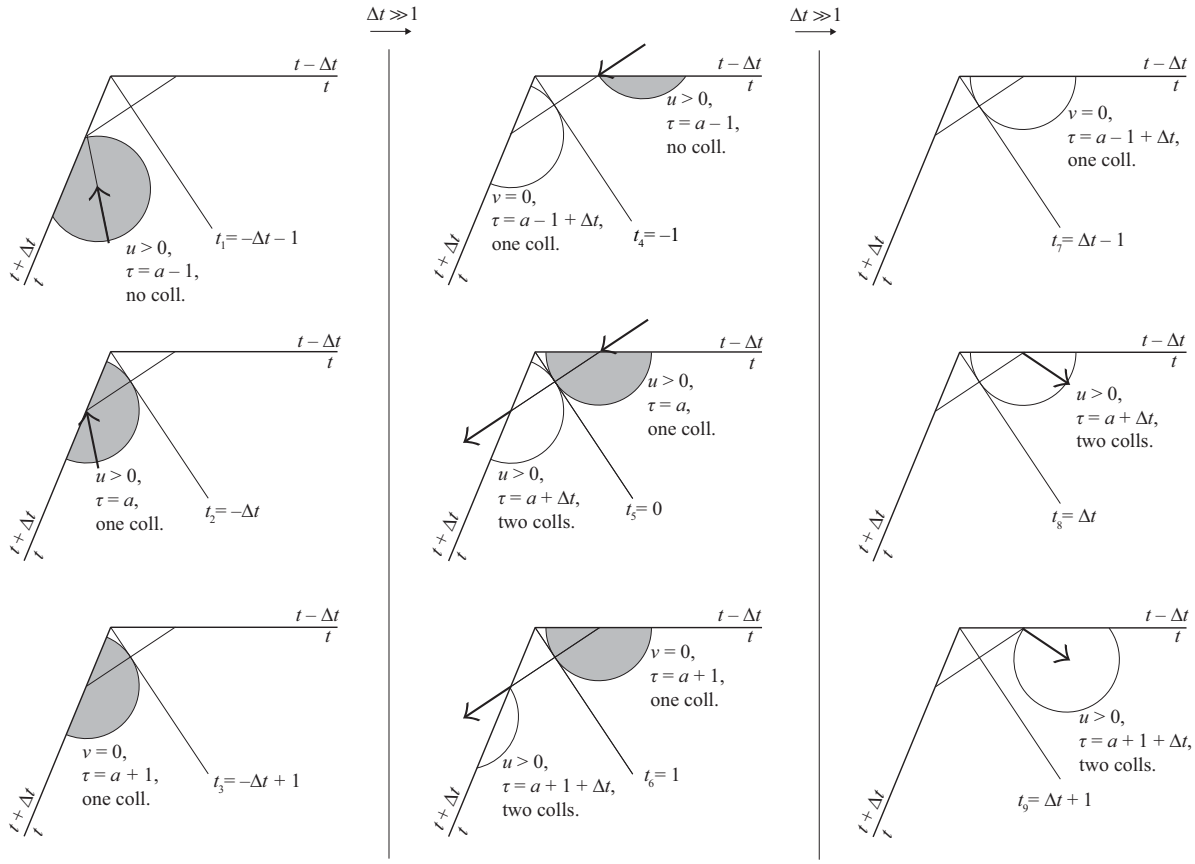

Figure 5.12: **Sequence of "movie pictures" corresponding to the "fitting" condition.** We illustrate few moments previous, respectively following the self-collision as seen by a local observer. The local observer reads the external time t_i of the i-th event where $i = 1, ..., 9$. Events within a column are separated by unit of time while columns of these events are separated by the time shift Δt where $\Delta t \gg 1$. The younger version is represented by the gray ball and its proper time τ differ from the proper time of the older version by Δt. The younger version is halted by the self-collision, waits the period Δt to become the older version, and then gets hit by the other version to leave to the future and the distant region. Thus, in this case, the difference Δt corresponds to the time of motionless waiting at the wormhole, i.e., the inner velocity is zero, $v_{\rm II} = 0$.

5.7 Domains of solutions defined by parameters ρ and u

Let us consider domains of self-colliding solutions over the half-plane of initial parameters $u > 0$ and $\rho \in (-\infty, +\infty)$. The half-plane is divided by specific curves $\rho = \rho(u, \omega)$ (the initial velocity cannot scaled out as in the point-like case). These curves determine regions with self-collisions, impose geometrical constraints (i.e., mark out "forbidden" subregions), and separate physical solutions from spurious solutions. To illustrate all domains and regions properly we draw diagrams for types I and II separately. Moreover, we plot the diagram for $\omega \in (\omega_{\rm min}, \omega_{\rm max})$ apart from the diagram for $\omega \in (-\pi/2, \omega_{\rm min}) \cup (\omega_{\rm max}, \pi/2)$ for each type since there are two values ω for any $\rho \in (\rho_{\rm min}, \rho_{\rm max})$. Finally, we merge all diagrams into one to see regions of different

numbers and types of solutions.

5.7.1 Domains for collision-free solutions

Finally, consider collision-free trajectories, see figure 5.13. The collision-free tra-

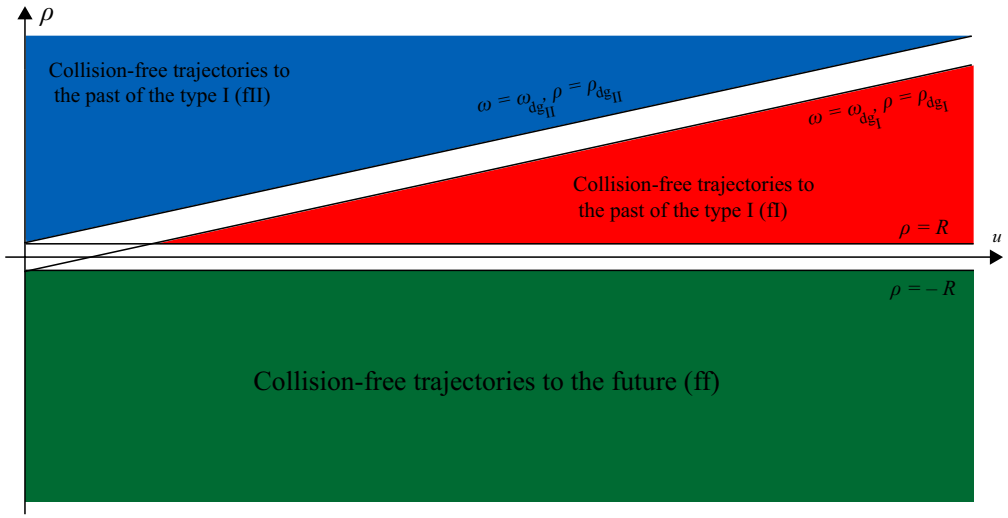

Figure 5.13: **Domains of collision-free solutions.** The collision-free trajectories to the future (labeled by "ff") are contained in the rectangle $\rho < -R$ and $u > 0$ (green region). The collision-free trajectories to the past of type I (labeled by "fI") are contained in the triangle determined by $\rho > R$ and $\rho < \rho(\omega_{\mathrm{dg_I}}, u)$ (red region). The collision-free trajectories to the past of type II (labeled by "fII") are contained in the triangle: $\rho > \rho(\omega_{\mathrm{dg_{II}}}, u)$ (blue region). Notice that the regions of collision-free trajectories to the past are separated by a strip inside which there are no collision-free trajectories. Solutions located on the boundary lines of the strip can be interpreted either as self-collisions with zero momentum exchange or as the extreme collision-free trajectories.

jectories to the future (labeled by "ff") are contained in the rectangle $\rho < -R$ and $u > 0$ (green region). The collision-free trajectories to the past of type I (labeled by "fI") are contained in the triangle determined by $\rho > R$ and $\rho < \rho(\omega_{\mathrm{dg_I}}, u)$ (red region). The collision-free trajectories to the past of type II (labeled by "fII") are contained in the triangle: $\rho > \rho(\omega_{\mathrm{dg_{II}}}, u)$ (blue region). Notice that the regions of collision-free trajectories to the past are separated by a strip inside which there are no collision-free trajectories. Solutions located on the boundary lines of the strip can be interpreted either as self-collisions with zero momentum exchange or as the extreme collision-free trajectories.

5.7.2 Domains for solutions of type I

In figure 5.14 we can see two diagrams which represent domains of initial parameters u and ρ for solutions of type I. The region with self-collisions is bounded by the curve implied by eq. (5.12a) – initial values outside this region determine trajectories located *too far* from the vertex (fixed u) to enable self-collisions. In contrast, the white range

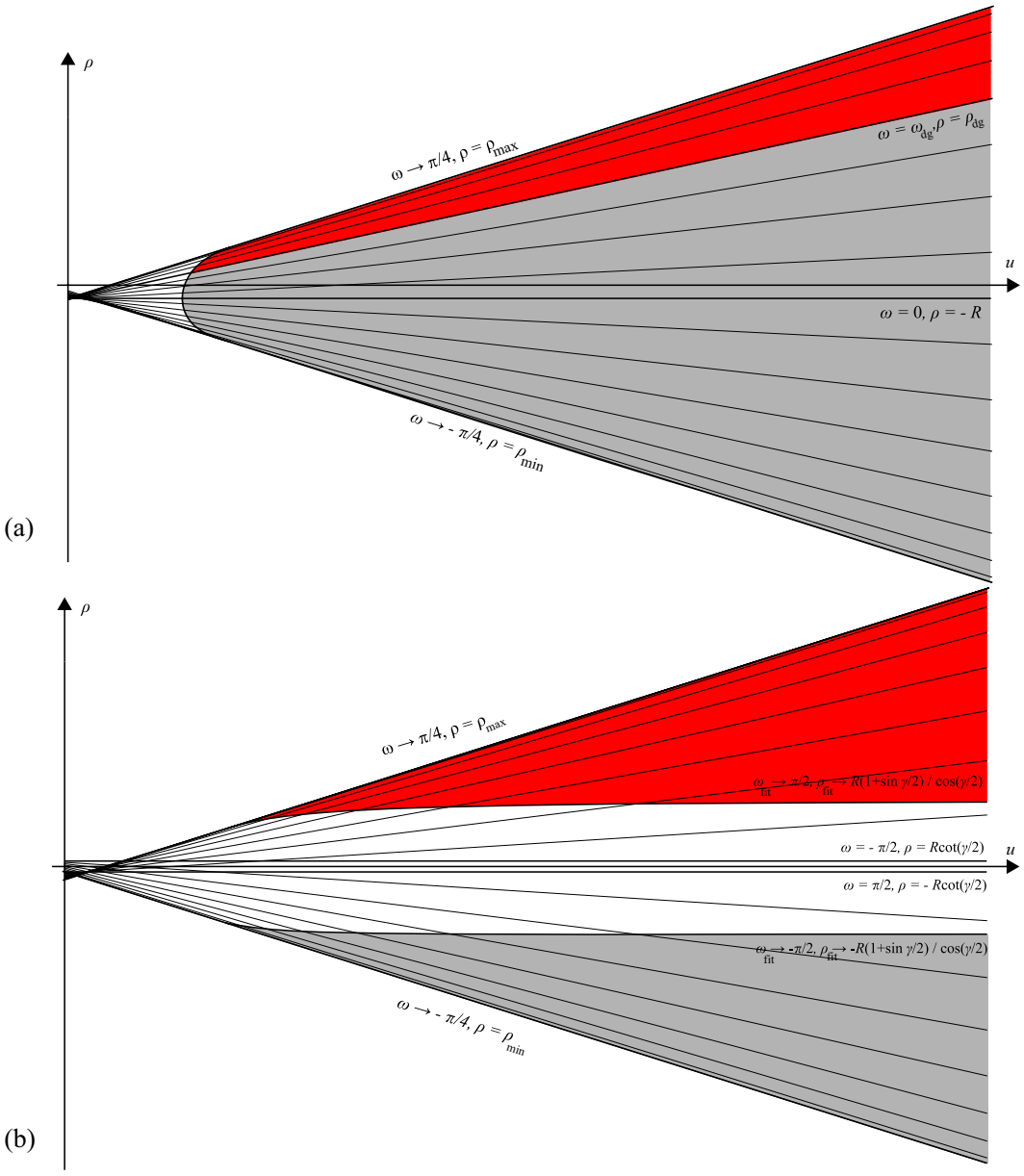

Figure 5.14: **Domains of initial parameters u and ρ for solutions of type I.** The region with self-collisions – filled in with inclined lines $\omega = \text{const.}$ – is bounded by the curve implied by eq. (5.12a). Initial values outside this region determine trajectories located *too far* from the vertex (fixed u) to enable self-collisions. In contrast, the white range within the region with self-collisions (determined by inequality (5.16)) corresponds to solutions which would cause the ball to hit the vertex, i.e., it would self-collide *too close* to the vertex. Physical self-collisions occupy red domains while spurious self-collisions occur within gray regions. (a) The diagram represents self-collisions farther from the vertex with smaller angle ω, i.e., $\omega \in (\omega_{\min_{\mathrm{I}}}, \omega_{\max_{\mathrm{I}}})$. Physical solutions are separated from spurious solutions by the critical direction $\omega = \omega_{\mathrm{free}}$ represented by the straight line (ω_{free} is fixed value). (b) The diagram represents self-collisions nearer the vertex with greater angle ω, i.e., $\omega \in (-\pi/2, \omega_{\min_{\mathrm{I}}}) \cup (\omega_{\max_{\mathrm{I}}}, \pi/2)$. Physical solutions are separated from spurious solutions by the white range (determined by geometrical restrictions).

within the region with self-collisions (determined by inequality (5.16)) corresponds to solutions which would cause the ball to hit the vertex, i.e., it would self-collide *too close* to the vertex. The diagram 5.14(a) represents self-collisions farther from the vertex with smaller angle ω, i.e., $\omega \in (\omega_{\min_{\mathrm{I}}}, \omega_{\max_{\mathrm{I}}})$, while the diagram 5.14(b) represents self-collisions nearer the vertex with greater angle ω, i.e., $\omega \in (-\pi/2, \omega_{\min_{\mathrm{I}}}) \cup (\omega_{\max_{\mathrm{I}}}, \pi/2)$.

Physical self-collisions occupy red domains while spurious self-collisions occur within gray regions. Physical solutions are separated from spurious solutions either by the white range (determined by geometrical restrictions), cf. 5.14(b), or by the critical direction $\omega = \omega_{\mathrm{free}}$ represented by the straight line (ω_{free} is fixed value), cf. 5.14(a).

5.7.3 Domains for solutions of type II

Domains of initial parameters u and ρ for solutions of type II are depicted in figure 5.15. The region with self-collisions is bounded by the curve implied by eq. (5.12b). Geometrical restrictions for type II concern only "fitting" of the ball in the conical space and do not impose any additional constraint on the range of initial parameters except narrow strip around zero, $(-R\cot(\gamma/2), R\cot(\gamma/2))$, given by the equation for self-collisions of type II (5.9) (for $\omega = \pm\pi/2$). Moreover, physical solutions exist even for $u = 0$, cf. small blue triangle region in figure 5.14(b).

The mentioned strip separates physical solutions (blue) from spurious solutions (gray) in figure 5.14(b). In diagram 5.14(a), i.e. for $\omega \in (\omega_{\min_{\mathrm{I}}}, \omega_{\max_{\mathrm{I}}})$, physical solutions are separated from spurious solutions by the critical direction $\omega = \omega_{\mathrm{free}}$ represented by the straight line. However, the critical line for type II is different from the critical line for type I, see eq. (5.13).

5.7.4 Diagram for both self-colliding and collision-free solutions

Finally, we draw diagram consisting of regions with physical solutions of all above diagrams, figure (5.16). Physical self-collisions are restricted within regions determined by curves (5.12a) and (5.12b). Colors of different domains change from blue (prevalence of solutions of type II) to red (type I). The strip-like region of dangerous trajectories determined by two straight lines for $\omega = \omega_{\mathrm{dg_I}}$ and $\omega = \omega_{\mathrm{dg_{II}}}$ contains two self-collisions of type I and one solution of type II. Obviously, one of self-colliding solutions of type I replaces the collision-free trajectory in this area. Geometrical restrictions for type I, which exclude solutions which would cause the ball to hit the vertex, are represented by the curve $\rho_{\mathrm{fit_I}}$. Geometrical restrictions for type II do not impose any additional constraint on the range of initial parameters except narrow strip around zero, $(-R\cot(\gamma/2), R\cot(\gamma/2))$. Collision-free solutions are limited by the value $\rho = \pm R$.

However, we can match this diagram to the graphs 5.5 if we consider greater initial velocities, $u \gg 0$, to avoid more complicated situation near zero initial velocity. When we take a slice through the diagram 5.16 we obtain a sequence of strips corresponding to particular intervals of the impact parameter ρ in figure 5.17.

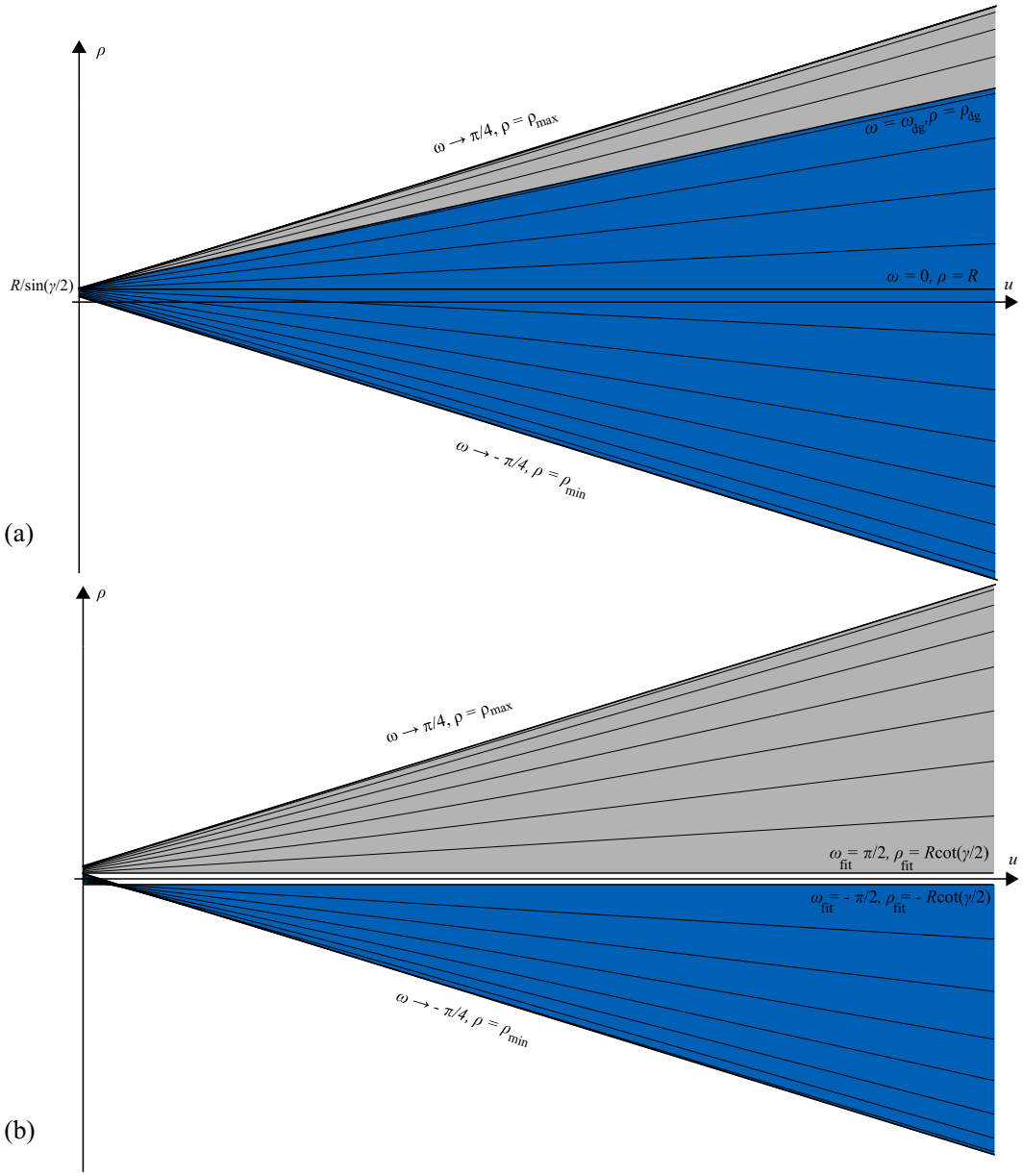

Figure 5.15: **Domains of initial parameters u and ρ for solutions of type II.** The region with self-collisions – filled in with inclined lines $\omega = \text{const.}$ – is bounded by the curve implied by eq. (5.12b). Geometrical restrictions for type II concern only "fitting" of the ball in the conical space and do not impose any additional constraint on the range of initial parameters except narrow strip around zero, $(-R\cot(\gamma/2), R\cot(\gamma/2))$, given by the equation for self-collisions of type II (5.9) (for $\omega = \pm\pi/2$). This strip separates physical solutions (blue) from spurious solutions (gray) in diagram (b). For $\omega \in (\omega_{\min_{\mathrm{I}}}, \omega_{\max_{\mathrm{I}}})$, diagram (a), physical solutions are separated from spurious solutions by the critical direction $\omega = \omega_{\mathrm{free}}$ represented by the straight line. However, the critical line for type II is different from the critical line for type II, see eq. (5.13).

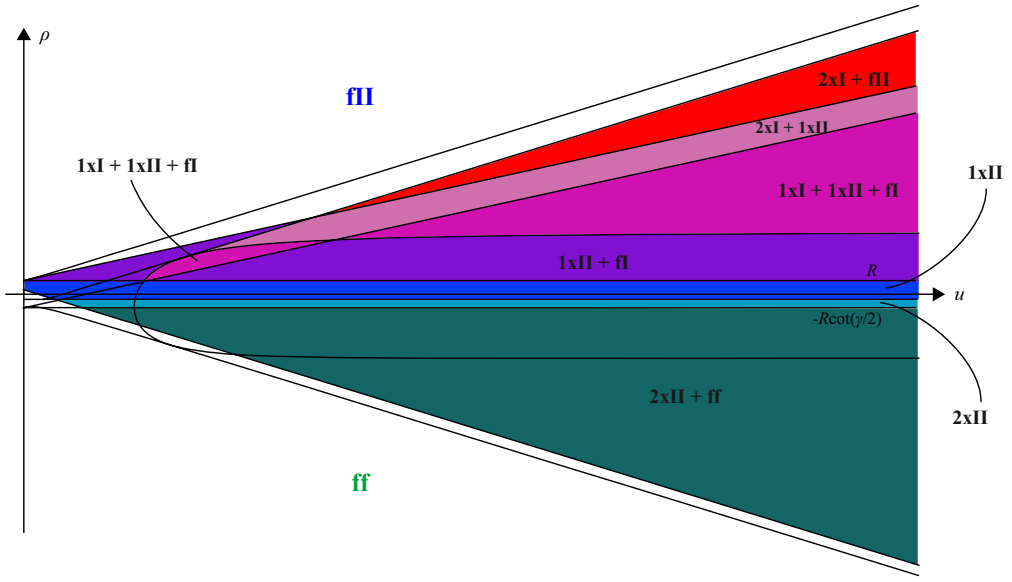

Figure 5.16: **Domains of physical solutions of both types in one diagram.** This diagram consists of regions with physical solutions of above diagrams 5.14 and 5.15. Physical self-collisions are restricted within regions determined by curves (5.12a) and (5.12b). Colors of different domains change from blue (prevalence of solutions of type II) to red (type I). The strip-like region of dangerous trajectories determined by two straight lines for $\omega = \omega_{\mathrm{dg_I}}$ and $\omega = \omega_{\mathrm{dg_{II}}}$ contains two self-collisions of type I and one solution of type II. Obviously, one of self-colliding solutions of type I replaces the collision-free trajectory in this area. Geometrical restrictions for type I are represented by the curve $\rho_{\mathrm{fit_I}}$, and for type II by the narrow strip around zero, $(-R\cot(\gamma/2), R\cot(\gamma/2))$. Collision-free solutions are limited by the value $\rho = \pm R$.

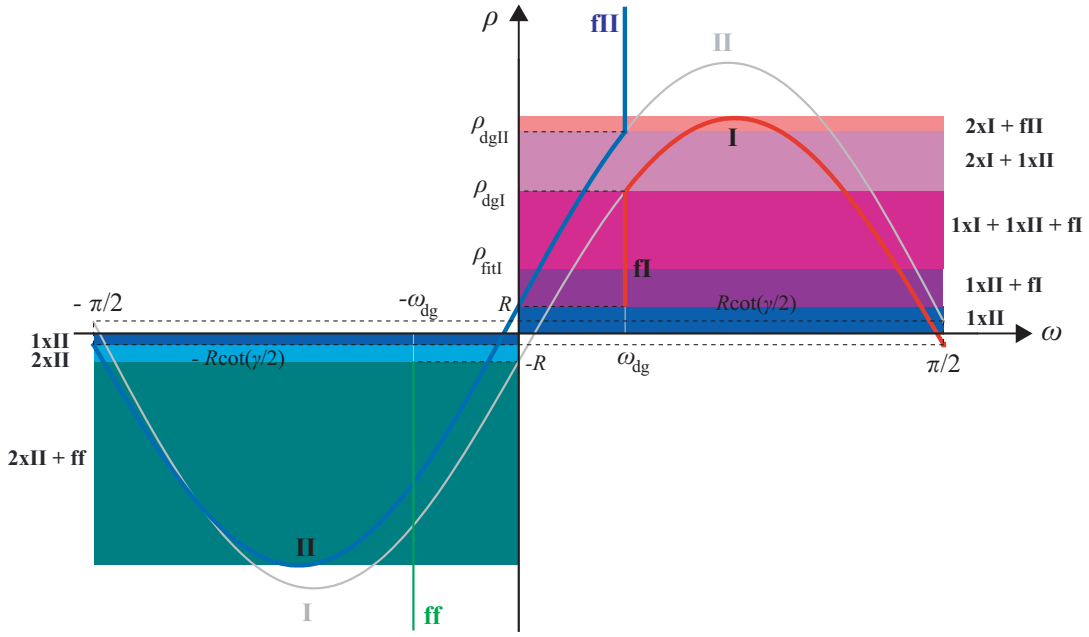

Figure 5.17: **Diagram of $\rho(\omega)$ as cross section of the digram $\rho(u, \omega)$ for a constant initial velocity u.** We can match diagram 5.16 to the graphs 5.5 if we consider greater initial velocities, $u \gg 0$, to avoid more complicated situation near zero initial velocity. When we take a slice through the diagram 5.16 we obtain a sequence of strips corresponding to particular intervals of the impact parameter ρ.

Chapter 6

Point particle: multiple self-collisions

In chapter 4, we have considered a point-particle which comes from a distant region of the conical space, passes through the wormhole just once, and after a self-intersection, or a self-collision leaves to the distant region. However, by tuning the direction ω another self-collision can happen. Moreover, for $\gamma < \pi/i_{\max}$ ($i_{\max}$ is a natural number) there can occur up to $i_{\max}$ self-intersections separating two successive self-collision.

In this chapter we will study multiple self-collisions interpolated by multiple self-intersections. Let us point out that a local geometry of the self-collision, depicted in figures 5.1 and 5.3, holds for each self-collision of multiple self-collisions as well. However, in this chapter, we will consider only a point-like case for which both types of self-collisions are represented by the same equation and dangerous trajectories reduce just into one degenerated case.

6.1 Sequences describing multiple self-events

To abbreviate "events" of self-collisions and/or self-intersections we will call them *self-events* although for self-intersections these are not events represented by one position and one time. Indeed, each self-event can be characterized by two values of the global time t and t', where the first value t corresponds to the time of free passage of the younger version of the particle (approaching the vertex), and the second value t' correspond to the time of free passage of the older version of the particle (receding the vertex). The difference $t' - t$ between these two times determines the type of the self-event. We get it by comparison of the time of motion following a self-collision with the time contribution gained along the corresponding path. If $t' < t$ we speak about the self-intersection of type I, while if $t' > t$ the self-intersection is of type II. In the case that these values equal each other, $t = t'$, the self-event stands for the self-collision. Notice that for the free trajectory to the future the time contribution is added to the time of motion.

The self-events will be numerated by the index variable $p = 0, ..., P$. It will be useful to denote by $p = 0$ the point of the particle trajectory nearest to the vertex of

the cone although it does not represent neither self-intersection, nor self-collision. It can be understood as a *fictive* self-collision of the innermost loop. Let us introduce sequences of different quantities associated with every self-collision or self-intersection: We define the sequence of radial distances r^p from the vertex

$$\{r^p\}_{p=0}^{P} ,$$

and the sequence of angles ω^p between radial lines and trajectories outgoing from p-th self-collision/self-intersection

$$\{\omega^p\}_{p=0}^{P} ,$$

where $\omega^0 = \pi/2$ (by the conical geometry). Note that the angle ω^p corresponding to a self-intersection (i.e., $p \neq n_k$) is uniquely given by the angle ω^{p-1} of the previous self-event as $\omega^p = \omega^{p-1} - \gamma/2$, see appendix A.

The indexes of self-collisions form the sequence

$$\{n_k\}_{k=0}^{N} ,$$

with $n_k < n_{k+1}$, and where ω^{n_k} represent angles corresponding to self-collisions. By definition we set $n_0 = 0$, and N stands for the total number of self-collisions. We can also define another sequence $\{i_k\}_{k=0}^{N-1}$ which determines the number of wormhole passages between two successive self-collisions

$$i_k = n_{k+1} - n_k, \tag{6.1}$$

where inequality $i_k \leq i_{\max}$ must hold. But, relation (6.1) does not allow to define the number i_N of self-intersection occurring beyond the outer self-collision, but see eq. (6.26) for its introduction. Thus, the i_k defines amount of time $i_k \Delta t$ which the particle gains between n_k-th and n_{k+1}-th self-collision which consists of contributions of all versions of the particle occurring between these two self-collisions.

Notice that the *number of wormhole passages i_k exactly corresponds to the number of path segments* between any two successive self-collisions. Generally, the number of wormhole passages between any two self-events corresponds to the number of path segments between these two self-events. This fact is demonstrated within figure 6.1a where we can compare, for instance, the number of path segments between the first self-event (r^1, ω^1) and the fifth self-event (r^5, ω^5) which is equal to four as well as the number of wormhole passages.

There are five self-events, $P = 5$, in figure 6.1. The sequence of self-collisions is described by $\{n_k\}_{k=0}^{N} = \{0, 1, 3, 5\}$ where $N = 3$. The sequence of wormhole passages between two successive self-collisions is $\{i_k\}_{k=0}^{N-1} = \{1, 2, 2\}$ where no self-intersection occur beyond the outer self-collision. In comparison to two cases considered in section 4: one self-collision is described by the sequence $\{n_k\}_{k=0}^{1} = \{0, 1\}$, while one self-intersection is determined by the sequences $\{n_k\}_{k=0}^{0} = \{0\}$. Sequences can be also denoted by listing of self-collisions C and self-intersections I. Thus, five self-events from figure 6.1 is represented by 5-tuple CICIC, while two sequences of section 4 are described by 1-tuple C, and by 1-tuple I respectively.

The sequence of outgoing directions ω^p is given by $\{\omega^p\}_{p=0}^{P} = \{\frac{\pi}{2}, \omega^1, \omega^2, \omega^3, \omega^4, \omega^5\}$ where $\omega^2 = \omega^1 - \gamma/2$ and $\omega^4 = \omega^3 - \gamma/2$ correspond to self-intersections following

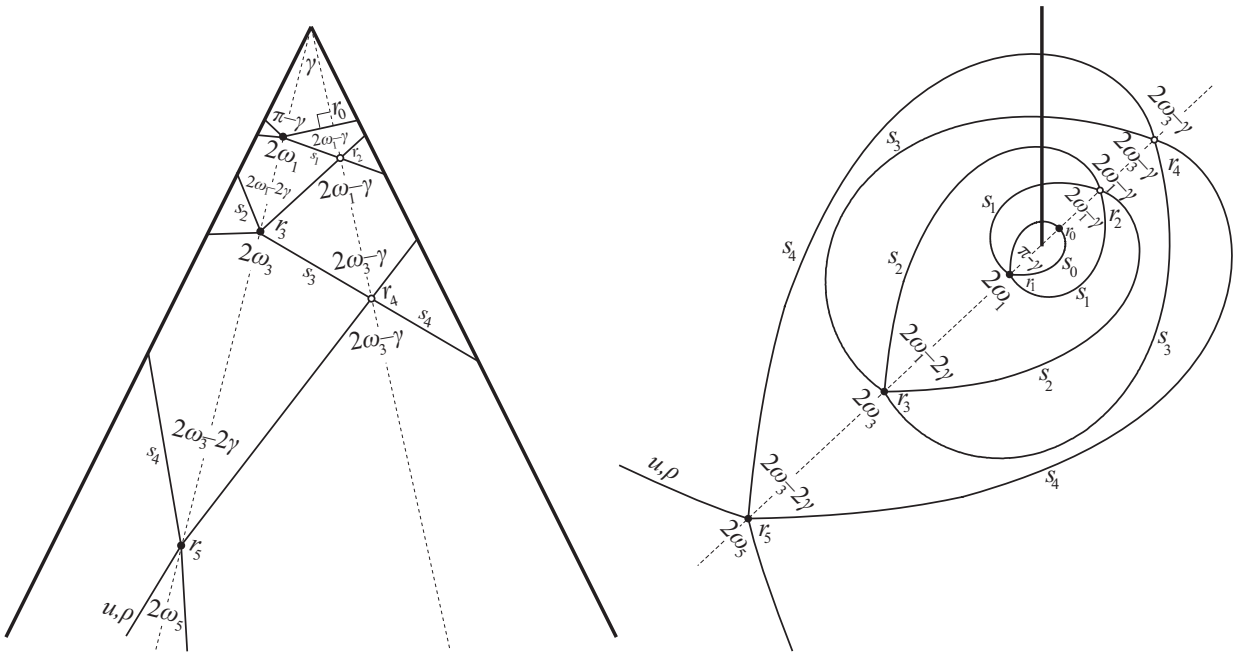

Figure 6.1: **Multiple self-collisions with multiple free traversals.** The number of all self-events is $P = 5$ excluding the "fictive" self-collision $p = 0$. The sequence of self-collisions is $\{n_k\}_{k=0}^{N} = \{0, 1, 3, 5\}$ where $N = 3$ and the sequence of path segments between two successive self-collisions is $\{i_k\}_{k=0}^{N-1} = \{1, 2, 2\}$ with no self-intersection occurring beyond the outer self-collision. The angles ω^p form in the sequence $\{\omega^p\}_{p=0}^{P} = \{\frac{\pi}{2}, \omega^1, \omega^1 - \frac{\gamma}{2}, \omega^3, \omega^3 - \frac{\gamma}{2}, \omega^5\}$ where $\omega^2 = \omega^1 - \frac{\gamma}{2}$ and $\omega^4 = \omega^3 - \frac{\gamma}{2}$ correspond to self-intersections following immediately after self-collisions ω^1 and ω^3. Lengths of path segments are denoted by s^p for $p = 0, ..., 4$ and radial distances of self-events are labeled by r^p, $p = 0, ..., 5$. (a) Conical space is unfolded into an angle in the plane. (b) Conical space as seen from the bird's eye view with the angular coordinate rescaled to range of 2π.

immediately after self-collisions ω^1 and ω^3, for more detail see appendix A. Lengths of path segments are denoted as s^p for $p = 0, ..., P-1$ and radial distances of self-events are labeled by r^p for $p = 0, ..., P$. Thus, there are $P + 1$ different values for r^p and P different values for s^p since the last segment extends to infinity. The number of different velocities is equal $N + 1$, i.e., it corresponds to the number of inner self-collisions $u^{n_0}, ..., u^{n_N}$ with $u^{n_k+i} = u^{n_k}$ for $0 \leq i < i_k$. Clearly, for the initial and final velocity is $u = u^P = u^{n_N}$.

6.2 Derivation of equations for self-collisions

Let us derive equations for scattering angles ω^{n_k}, $k = 1, ..., N$, of multiple self-collisions in terms of the initial parameters u and ρ. From equality of the radial projections of the incoming and outgoing velocities $u_{\text{in}_{p-1}} = u_{\text{out}_p}$ we obtain

$$u^{p-1} \cos(\omega^{p-1} - \frac{\gamma}{2}) = u^p \cos \omega^p, \tag{6.2}$$

for $p = 1, ..., P$. Notice that along any path segment with the self-intersection is $u_{p-1} = u_p$ and $\omega^p = \omega^{p-1} - \gamma/2$, and therefore equation (6.2) is identity for self-intersections. It becomes nontrivial for two successive self-collisions

$$u^{n_{k-1}} \cos(\omega^{n_{k-1}} - i_{k-1}\frac{\gamma}{2}) = u^{n_k} \cos \omega^{n_k}, \tag{6.3}$$

for $k \leq N$.

The conditions of self-collisions say that the time that the particle spent on its way between two successive self-collisions equals to the time contribution it gained by wormhole passages,

$$2 \sum_{j=n_k}^{n_{k+1}-1} \frac{s^j}{u^{n_k}} = i_k \Delta t, \tag{6.4}$$

for $k = 0, ..., N-1$. These relations guarantee that the self-collision with ω^{n_k} is followed by another self-collision after i_k wormhole passages. Then we express the velocity from (6.4) as

$$u^{n_k} = \frac{2 \sum_{j=n_k}^{n_{k+1}-1} s^j}{i_k \Delta t}, \tag{6.5}$$

and substitute the length $\sum_{j=n_k}^{n_{k+1}} s^j$ of the whole path between two self-collisions

$$\sum_{j=n_k}^{n_{k+1}-1} s^j = r^{n_N} \frac{\sin(i_k \frac{\gamma}{2})}{\sin(\omega^{n_k} - i_k \frac{\gamma}{2})} \prod_{j=k}^{N-1} \frac{\sin(\omega^{n_j} - i_j \frac{\gamma}{2})}{\sin \omega^{n_j}}, \tag{6.6}$$

derived in appendix A.2, which is directly related to the radial distance r^{n_k}

$$r^{n_k} = r^{n_N} \prod_{j=k}^{N-1} \frac{\sin(\omega^{n_j} - i_j \frac{\gamma}{2})}{\sin \omega^{n_j}}, \tag{6.7}$$

provided in appendix A.1. Then we project the velocity u^{n_k} into the radial line – more precisely, we plug expressions for velocities $u^{n_{k-1}}$ and u^{n_k} into both sides of equation (6.3).

6.2.1 Geometrical nature of inner directions ω^{n_k}

For inner directions, $k < N$, we obtain $N - 1$ equations

$$i_k \sin(\omega^{n_k} - i_k \frac{\gamma}{2}) \cos(\omega^{n_{k-1}} - i_{k-1} \frac{\gamma}{2}) \sin(i_{k-1} \frac{\gamma}{2}) = i_{k-1} \cos \omega^{n_k} \sin \omega^{n_{k-1}} \sin(i_k \frac{\gamma}{2}), \tag{6.8}$$

where parameters u, ρ and Δt cancel out themselves since they occur on both sides. These relations allow to express dependency of two successive angles in the form of the recurrent formula

$$\tan(\omega^{n_k}) = \tan(i_k \frac{\gamma}{2}) + \frac{i_{k-1} \sin(i_k \frac{\gamma}{2}) \sin(\omega^{n_{k-1}})}{i_k \cos(i_k \frac{\gamma}{2}) \sin(i_{k-1} \frac{\gamma}{2}) \cos(\omega^{n_{k-1}} - i_{k-1} \frac{\gamma}{2})}. \tag{6.9}$$

Starting from $\omega^0 = \pi/2$ eq. (6.9) enable us to compute all inner self-collisions. In other words, the inner self-collision is determined only by the conical geometry (i.e.,

by the vertex angle γ) given the sequence $\{i_k\}_{k=0}^{N-1}$, while it *does not* depend on initial parameters u and ρ.

Let us also introduce formal notation for the formula (6.9)

$$\omega^{n_k} = \arctan\left[\tan(i_k\frac{\gamma}{2}) + \frac{i_{k-1}\sin(i_k\frac{\gamma}{2})\sin(\omega^{n_{k-1}})}{i_k\cos(i_k\frac{\gamma}{2})\sin(i_{k-1}\frac{\gamma}{2})\cos(\omega^{n_{k-1}} - i_{k-1}\frac{\gamma}{2})}\right] \equiv f(\omega^{n_{k-1}}, i_{k-1}, i_k), \tag{6.10}$$

which simplifies argumentation in later analysis. Thus, evaluation of inner angles proceeds in such a way that function $f(\omega^{n_{k-1}}; i_{k-1}, i_k)$ has to be followed by function $f(\omega^{n_k}; i_k, i_{k+1})$ etc.

6.2.2 Type of inner self-collisions

Now we are interested in the type of the k-th inner self-collision. The type of the k-th self-collision is determined by the angle $\omega^{n_{k-1}} - i_{k-1}\frac{\gamma}{2}$ which separates self-collisions of type I from that of type II. Hence, if

$$\omega^{n_k} > \omega^{n_{k-1}} - i_{k-1}\frac{\gamma}{2}\ , \tag{6.11}$$

then the k-th self-collision would be of type I, while if

$$\omega^{n_k} < \omega^{n_{k-1}} - i_{k-1}\frac{\gamma}{2}\ ,$$

then the k-th self-collision would be of type II. The condition (6.11) can be reformulated into inequality

$$\tan(\omega^{n_k}) > \tan(\omega^{n_{k-1}} - i_{k-1}\frac{\gamma}{2}),$$

using eq. (6.9), which can be farther modified into the form

$$\sin(\omega^{n_{k-1}}) > \frac{i_k\sin(i_{k-1}\frac{\gamma}{2})}{i_{k-1}\sin(i_k\frac{\gamma}{2})}\sin(\omega^{n_{k-1}} - (i_{k-1}+i_k)\frac{\gamma}{2}),$$

which allows to show that all inner self-collisions are of type I, i.e., condition (6.11) holds for any $\omega^{n_{k-1}} \in (i_{k-1}\frac{\gamma}{2}, \frac{\pi}{2})$.

Therefore, we can conclude that all inner self-collisions are of type I which has straightforward interpretation: As the younger version of the particle (which is approaching the vertex) hits the rear part of the older version of the particle (which is receding the vertex), the younger version slows down while the older version speeds up. More accurately, equality of radial projections of velocities (6.3) along with the condition (6.11) imply that velocities u^{n_k} on inner loops slow down as the particle approaches the vertex

$$u^{n_{k-1}} < u^{n_k}.$$

Let us show it by a counterexample: if the inner self-collision were of type II it might not self-collide again in any of successive self-intersections. It can be easily demonstrated for the limiting direction $\omega^{n_k} = \omega^{n_{k-1}} - i_{k-1}\frac{\gamma}{2}$ which separates types I and II: for such an angle the velocity of the outgoing ("older") version would not

change, $u^{n_k} = u^{n_{k-1}}$, but the path segments would increase in length each following self-intersection, i.e., this (outgoing) version would get more and more delayed with respect to the incoming versions with each next self-intersection, and thus it could not self-collide again. In other words, the considered self-collision of type II would not be the *inner* self-collision at all.

6.2.3 The outer direction ω^{n_N}

For $k = N$ equation (6.3) takes the form

$$u^{n_{N-1}} \cos(\omega^{n_{N-1}} - i_{N-1}\frac{\gamma}{2}) = u^{n_N} \cos\omega^{n_N},$$

where the velocity u^{n_N} *is* the initial velocity $u \equiv u^{n_N}$, actually. The magnitude of the velocity preceding the outer self-collision is given by

$$u^{n_{N-1}} = \frac{2\sum_{j=n_{N-1}}^{n_N-1} s^j}{i_{N-1}\Delta t} = \frac{2\rho \sin(i_{N-1}\frac{\gamma}{2})}{i_{N-1}\Delta t \sin(\omega^{n_N})\sin(\omega^{n_{N-1}})},$$

and hence the equation for the outer self-collision contains factors consisting of parameters $\triangle t$, u and ρ. Therefore, we can write down equation for the outer self-collision

$$2\rho \sin(i_{N-1}\frac{\gamma}{2})\cos(\omega^{n_{N-1}} - i_{N-1}\frac{\gamma}{2}) = i_{N-1}u\Delta t \sin(\omega^{n_N})\cos(\omega^{n_N})\sin(\omega^{n_{N-1}}), \quad (6.12)$$

which can be formulated as the dependency $\omega^{n_N}(\rho, u)$ on the initial parameters u and ρ:

$$\sin(2\omega^{n_N}) = \frac{4\rho \sin(i_{N-1}\frac{\gamma}{2})}{i_{N-1}u\Delta t}\frac{\cos(\omega^{n_{N-1}} - i_{N-1}\frac{\gamma}{2})}{\sin(\omega^{n_{N-1}})}. \quad (6.13)$$

Analogically to the case of the point-particle with one self-collision, we can also express the dependency of the radial distance $r^{n_N}(\rho, u)$ on initial parameters u and ρ:

$$r^{n_N} = \frac{i_{N-1}u\Delta t \sin(\omega^{n_{N-1}})}{2\sqrt{2}\sin(i_{N-1}\frac{\gamma}{2})\cos(\omega^{n_{N-1}} - i_{N-1}\frac{\gamma}{2})}\sqrt{1 \pm \sqrt{1 - \frac{16\rho^2 \sin^2(i_{N-1}\frac{\gamma}{2})\cos^2(\omega^{n_{N-1}} - i_{N-1}\frac{\gamma}{2})}{(i_{N-1}u\Delta t)^2 \sin^2(\omega^{n_{N-1}})}}}. \quad (6.14)$$

Notice that both dependences above (6.13) and (6.14) correspond to relations (4.5) and (4.6) for the point-like case with one self-collision except for coefficients.

It will be useful to reformulate the above dependency $\omega^{n_N}(\rho, u)$ as the single-valued function $\rho^{n_N}(\omega, u)$ of the outer angle ω

$$\rho^{n_N}(\omega, u) = \frac{i_{N-1}u\Delta t}{2\sin(i_{N-1}\frac{\gamma}{2})}\frac{\sin(\omega^{n_{N-1}})}{\cos(\omega^{n_{N-1}} - i_{N-1}\frac{\gamma}{2})}\sin(\omega)\cos(\omega), \quad (6.15)$$

which allows us to depict the corresponding graph straightforwardly. Notice that configurations of the point-like particle with different initial velocities u are related just by rescaling as well as for one self-collision, cf. section 4.3. Hence, we will concentrate only on the relation among ρ, r, and ω.

6.2.4 Adding self-collisions

Suppose now that the outer self-collision points direct the particle in such a way that it would self-collide once again at the p-th self-event where $p > n_N$. In other words, we tune the length between the N-th self-collision and the p-th self-intersection in such a way that

$$\frac{2\sum_{j=n_N}^{p-1} s^j}{u} = (p - n_N)\Delta t \ ,$$

cf. equation (6.4). After we substitute the length $2\sum_{j=n_N}^{p-1} s^j$ from equation (6.6) we receive

$$\frac{\sin((p-n_N)\frac{\gamma}{2})}{(p-n_N)\sin(\omega^{n_N} - (p-n_N)\frac{\gamma}{2})\sin(\omega^{n_N})} = \frac{u\Delta t}{2\rho}.$$

However, the angle ω^{n_N} must also satisfy equation for the outer self-collision (6.12) numbered by n_N

$$\frac{\sin(i_{N-1}\frac{\gamma}{2})\cos(\omega^{n_{N-1}} - i_{N-1}\frac{\gamma}{2})}{i_{N-1}\sin(\omega^{n_N})\cos(\omega^{n_N})\sin(\omega^{n_{N-1}})} = \frac{u\triangle t}{2\rho},$$

which after some algebra results in formula

$$i_N \sin(\omega^{n_N} - i_N\frac{\gamma}{2})\cos(\omega^{n_{N-1}} - i_{N-1}\frac{\gamma}{2})\sin(i_{N-1}\frac{\gamma}{2}) = i_{N-1}\cos(\omega^{n_N})\sin(\omega^{n_{N-1}})\sin(i_N\frac{\gamma}{2}),$$

denoting $i_N = p - n_N$. By comparison with equation (6.8) we can immediately see that this relation represents the recurrent formula for $k = N$. Thus, the original outer self-collision becomes the inner self-collision if we construct another one – which replaces the original one as the outer self-collision.

6.2.5 Self-collisions separated by q self-intersections

It is helpful to introduce a subset of the ensemble of all sequences defined by a constant number q of intermediate self-intersections between successive self-collisions. For the relevant case $q = 1$ of N self-collisions with no intermediate self-intersection we receive the only allowed sequences for $\gamma \in (\pi/2, \pi)$: $\{n_k\}_{k=0}^{N} = \{0, 1, 2, 3, ..., N\}$ and $\{i_k\}_{k=0}^{N-1} = \{1, 1, ..., 1\}$. Thus, terms n_k coincide with their indexes k: $n_k = k = p$ for $p = 0, ..., P(= N)$. This sequence can be also expressed as N-tuple CCC...C. By obvious reduction of just derived expressions we can immediately write down the recurrent formula

$$\tan(\omega^{k+1}) = \tan(\frac{\gamma}{2}) + \frac{\sin(\omega^k)}{\cos(\frac{\gamma}{2})\cos(\omega^k - \frac{\gamma}{2})}, \tag{6.16}$$

corresponding to the general formula (6.9) with the same starting value $\omega^0 = \pi/2$. Accordingly, relations (6.13) and (6.14) concerning the outer trajectories are given by

$$\sin(2\omega^N) = \frac{4\rho\sin(\frac{\gamma}{2})}{u\Delta t}\frac{\cos(\omega^{N-1} - \frac{\gamma}{2})}{\sin(\omega^{N-1})} \ , \tag{6.17}$$

and

$$r^N = \frac{u\Delta t \sin(\omega^{N-1})}{2\sqrt{2}\sin(\frac{\gamma}{2})\cos(\omega^{N-1}-\frac{\gamma}{2})}\sqrt{1 \pm \sqrt{1 - \frac{16\rho^2 \sin^2(\frac{\gamma}{2})\cos^2(\omega^{N-1}-\frac{\gamma}{2})}{(u\Delta t)^2 \sin^2(\omega^{N-1})}}}. \qquad (6.18)$$

In section 6.2.1 we have shown that the inner self-collisions are entirely given by the apex angle γ. Let us now demonstrate another relationship between the conical geometry (given by γ) and the (constant) sequences $\{k\}_{k=0}^N$ of inner self-collisions. We spread out the vertex angle as $\gamma \to q\gamma \equiv \Gamma$ and stretch out the time shift as $\Delta t \to q\Delta t \equiv \Delta T$ where q is arbitrary but fixed value from the interval $[1, i_{\max}]$, still for the sequence $\{0, 1, 2, 3, ..., N\}$. Then, after replacements in equations (6.16) and (6.17), we obtain relations

$$\tan(\omega^k) = \tan(\frac{\Gamma}{2}) + \frac{\sin(\omega^{k-1})}{\cos(\frac{\Gamma}{2})\cos(\omega^{k-1}-\frac{\Gamma}{2})},$$

and

$$\sin(2\omega^N) = \frac{4\rho\sin(\frac{\Gamma}{2})}{u\Delta T}\frac{\cos(\omega^{N-1}-\frac{\Gamma}{2})}{\sin(\omega^{N-1})},$$

which can be rewritten as

$$\tan(\omega^{qk}) = \tan(q\frac{\gamma}{2}) + \frac{\sin(\omega^{q(k-1)})}{\cos(q\frac{\gamma}{2})\cos(\omega^{q(k-1)}-q\frac{\gamma}{2})}, \qquad (6.19)$$

and

$$\sin(2\omega^{qN}) = \frac{4\rho\sin(q\frac{\gamma}{2})}{qu\Delta t}\frac{\cos(\omega^{q(N-1)}-q\frac{\gamma}{2})}{\sin(\omega^{q(N-1)})}, \qquad (6.20)$$

where we have exchanged indexes k and N for their multiples qk and qN. Then, however, the second couple of equations represents also equations for inner angles of the sequence $\{n_k\}_{k=0}^N = \{qk\}_{k=0}^N = \{0, q, 2q, 3q, ..., Nq\}$, i.e., sequences of self-collisions separated by q self-intersections. In other words, equations for the sequence $\{0, 1, 2, 3, ..., N\}$ on the extended cone (given by parameters Γ and ΔT) correspond exactly to equations for the sequence $\{0, q, 2q, 3q, ..., Nq\}$ on the original cone (described by parameters γ and Δt).

6.3 Limits of the impact parameter interval

The maximal impact parameter $\rho_{\max}$ defines such a limiting value for a sequence $\{n_k\}_{k=0}^N$ for which the outer self-collision occurs. Relation for $\rho_{\max}$ results from substitution of the angle $\pi/4$ for the outer direction in eq. (6.15). For each sequence $\{n_k\}_{k=0}^N$ there is a (different) value $\rho_{\max}$, and hence these values form a discrete set. Thus, the number of solutions changes by varying the initial impact parameter ρ through $\rho_{\max}$ of different sequences $\{n_k\}_{k=0}^N$. For example, in figure 6.3, we can see the graphs representing constant sequences $\{k\}_{k=0}^N$ with various $N = 1, 2, ...$ where corresponding values of $\rho_{\max}$ are marked out. There occurs infinite number of solutions for any $\rho \in [-\rho_{\max}^\infty, \rho_{\max}^\infty]$, which are illustrated by the gray "strip".

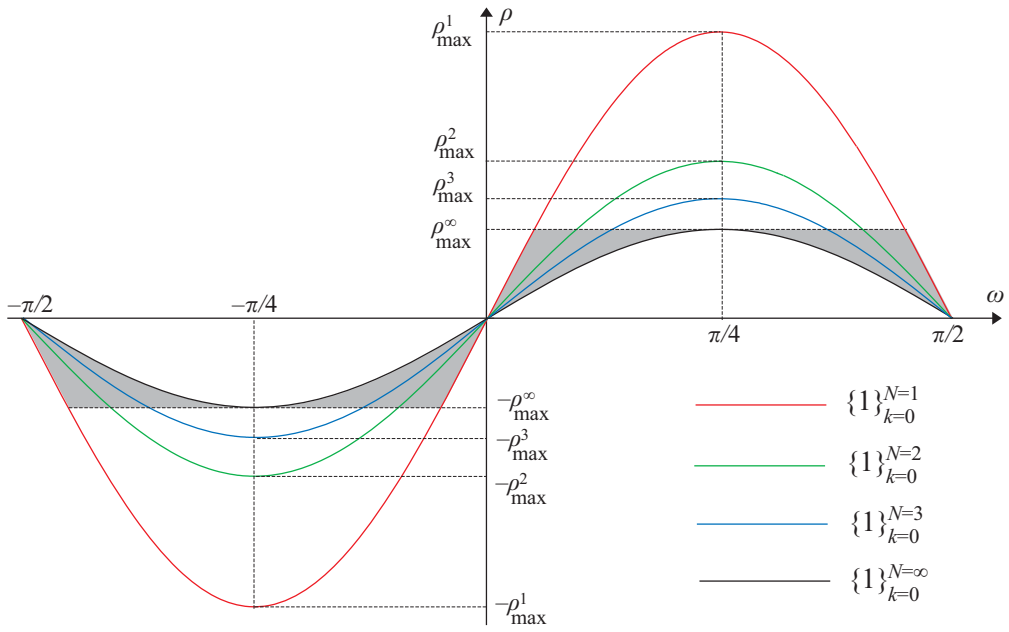

Figure 6.2: **The maximal impact parameter $\rho_{\max}$ for sequences with $i_k = 1$.** In figure we can see graphs representing constant sequences $\{k\}_{k=0}^{N}$ with various $N = 1, 2, \ldots$. The corresponding values $\rho_{\max}$ are marked out. Maximal values $|\rho_{\max}|$ for sequences $\{k\}_{k=0}^{N=1}$ (red), $\{k\}_{k=0}^{N=2}$ (green), $\{k\}_{k=0}^{N=3}$ (blue) and $\{k\}_{k=0}^{N\to\infty}$ (black) can be ordered as $\rho_{\max}|_{N=1} > \rho_{\max}|_{N=2} > \rho_{\max}|_{N=3} > \rho_{\max}|_{N\to\infty}$. There is infinite number of solutions for any $\rho \in [-\rho_{\max}^{\infty}, \rho_{\max}^{\infty}]$, illustrated by the gray "strip", which is represented by intersections of the horizontal line $\rho = \text{const.}$ with the graphs.

Now, let us analyze the maximal impact parameter $\rho_{\max}$ for constant sequences $\{qk\}_{k=0}^{N}$. By substitution of $\omega^{qN} = \pi/4$ into equation (6.20) we obtain the relation

$$\rho_{\max} \equiv \frac{qu\Delta t}{4\sin(q\frac{\gamma}{2})} \frac{\sin(\omega^{q(N-1)})}{\cos(\omega^{q(N-1)} - q\frac{\gamma}{2})}\,, \tag{6.21}$$

The $\rho_{\max}$ decreases for increasing N since inequality $\omega^{qk} < \omega^{qj}$ holds for any two inner angles, where $j > k$ and q is fixed. Thus, the graphs of $\rho_{\max}$ depending on q represented by polylines are nicely arranged and confined by two lines: The graph for $N = 1$, corresponding to solutions with just one self-collision preceded by q self-intersections, described by relation

$$\rho_{\max} = \frac{qu\Delta t}{4\sin^2(q\frac{\gamma}{2})},$$

where $\omega^0 = \pi/2$ has been plugged into eq. (6.21), is placed at the top (red line). The graph for $N \to \infty$ given by relation

$$\rho_{\max} = \frac{qu\Delta t}{4\sin(q\frac{\gamma}{2})}, \tag{6.22}$$

where the limiting inner angle $\omega^{\infty-1} = \frac{\pi+q\gamma}{4}$ has been substituted into eq. (6.21), is located at the bottom (blue line). Moreover, relation (6.22) represents increasing function of q, and hence the limit values can be ordered as

$$\rho_{\max}|_{q=1} < \rho_{\max}|_{q=2} < \ldots < \rho_{\max}|_{q=i_{\max}},$$

cf. graph in figure 6.3.

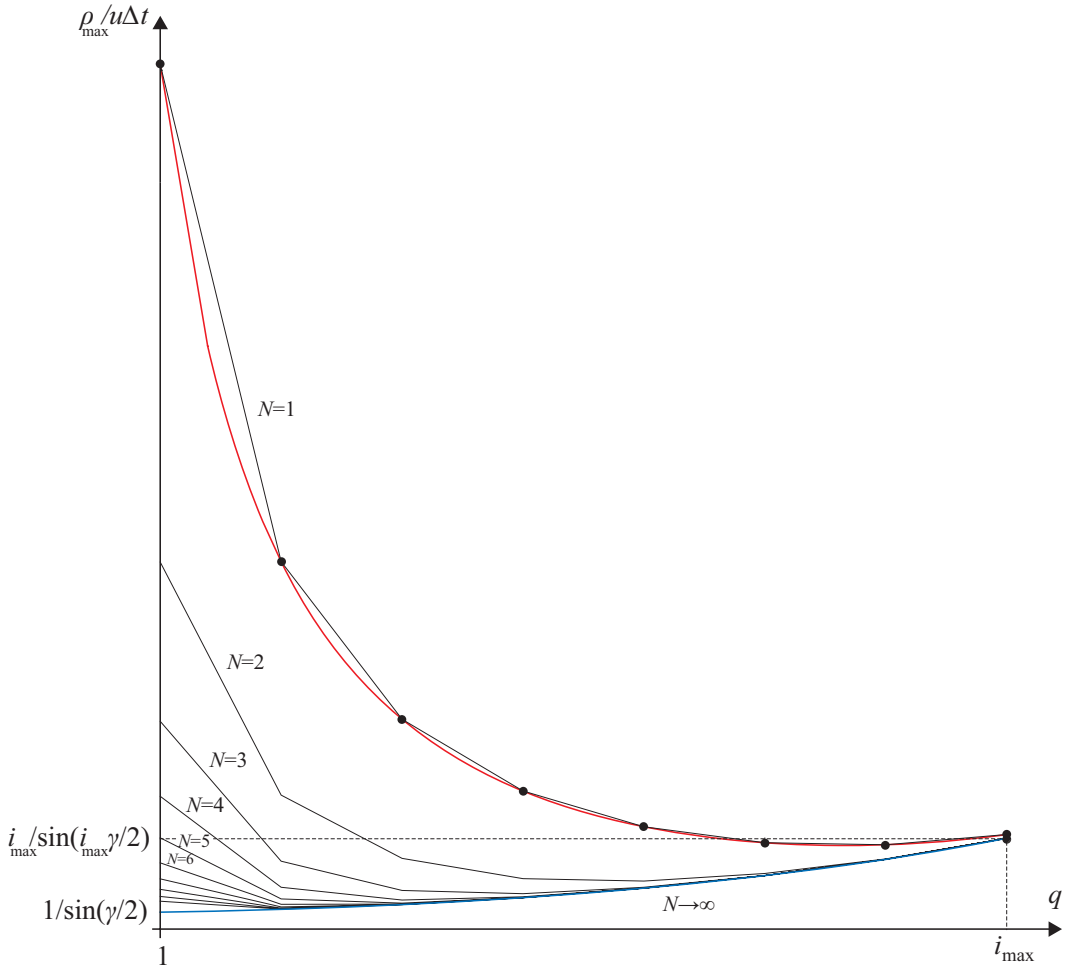

Figure 6.3: **Maximum $\rho_{\max}$ for constant sequences $\{qk\}_{k=0}^{N}$.** The $\rho_{\max}$ decreases for increasing N since inequality $\omega^{qk} < \omega^{qj}$ holds for any two inner angles, where $j > k$ and q is fixed. Thus, graphs of $\rho_{\max}$ depending on q represented by polylines are nicely arranged and confined by two lines: The graph for $N = 1$, corresponding to solutions with just one self-collision preceded by q self-intersections, is placed at the top (red line), while the graph for $N \to \infty$ is located at the bottom (blue line). Since equation (6.22) represents increasing function of q, the limit values can be ordered as $\rho_{\max}|_{q=1} < \rho_{\max}|_{q=2} < \ldots < \rho_{\max}|_{q=i_{\max}}$.

Relation for the maximal impact parameter $\rho_{\max}$ for general sequences

$$\rho_{\max} = \frac{i_{N-1} u\Delta t}{4\sin(i_{N-1}\frac{\gamma}{2})} \frac{\sin(\omega^{n_{N-1}})}{\cos(\omega^{n_{N-1}} - i_{N-1}\frac{\gamma}{2})} , \tag{6.23}$$

results from substitution of $\omega^{n_N} = \pi/4$ into eq. (6.15). We can regard this relation as the function of the number i_{N-1} and the last inner angle $\omega^{n_{N-1}}$, which depends on the sequence $\{n_k\}_{k=0}^{N}$ and lies within the interval $[\frac{\pi+\gamma}{4}, \frac{\pi}{2}]$.

Although there exists (uncountable) infinite variety of sequences $\{n_k\}_{k=0}^{\infty}$ it is numerically evident that limiting inner angles – denoted as $\omega^{\infty-1}$– are bounded within the interval $[\frac{\pi+\gamma}{4}, \frac{\pi+i_{\max}\gamma}{4}]$. Thus, the maximal limiting inner angle is equal to $\omega^{\infty-1} = \frac{\pi+i_{\max}\gamma}{4}$ (for the constant sequence $\{i_{\max}k\}_{k=0}^{\infty}$), while the minimal limiting inner angle is equal

to $\omega^{\infty-1} = \frac{\pi+\gamma}{4}$ (for the constant sequence $\{k\}_{k=0}^{\infty}$). It follows that there exist corresponding values of the maximal impact parameter $\rho_{\max}$ because relation (6.23) is the increasing function of $\omega^{n_{N-1}}$, cf. appendix B.3. Hence, the maximum $\rho_{\max}$ for all infinite sequences is confined within the interval

$$\rho_{\max} \in \left[\frac{u\Delta t}{4\sin(\gamma/2)}, \frac{i_{\max}u\Delta t}{4\sin(i_{\max}\gamma/2)}\right] ,$$

cf. figure 6.3.

Moreover, we can separate three intervals for the impact parameter ρ with qualitatively different sets of solutions: (i) Within the interval

$$\rho \in \left[\frac{u\Delta t}{4\sin^2(\gamma/2)}, \infty\right] ,$$

only one collision-free solution occurs. (ii) Finite number of self-colliding solutions plus one collision-free solution exist for the impact parameter from

$$\rho \in \left[\frac{i_{\max}u\Delta t}{4\sin(i_{\max}\gamma/2)}, \frac{u\Delta t}{4\sin^2(\gamma/2)}\right] .$$

(iii) And, in the interval

$$\rho \in \left[0, \frac{i_{\max}u\Delta t}{4\sin(i_{\max}\gamma/2)}\right] ,$$

there is infinite number of self-colliding solutions and one collision-free solution for the initial parameter ρ. In other words, passage through the value $\rho = \frac{i_{\max}u\Delta t}{4\sin(i_{\max}\gamma/2)}$ represents transition between finite and infinite number of solutions to the defined initial problem. Notice also that this value increases if the vertex angle $\gamma \to 0$ decreases.

6.4 Dangerous solutions

In the point-like case, the geometry of the paradoxical self-intersection is identical to the geometry of the dangerous self-collision, cf. par. 4.4, in contrast to the finite ball, see section 5.3. Thus, the paradoxical self-intersection defined by the collision-free direction $\omega^p_{\text{free}} = \omega^{n_N} - (p - n_N)\frac{\gamma}{2}$ at the p-th self-event, $p > n_N$, is superseded by the $N+1$-th dangerous self-collision determined by the (outer) scattering angle

$$\omega^{n_{N+1}}_{\text{dg}} = \omega^{n_N} - i_N\frac{\gamma}{2}, \tag{6.24}$$

provided $\omega^p_{\text{free}} = \omega^{n_{N+1}}_{\text{dg}}$ and $i_N = p - n_N$. The dangerous impact parameter $\rho^{n_{N+1}}_{\text{dg}}$ results from substitution of the angle $\omega^{n_{N+1}}_{\text{dg}}$ into equation (6.12):

$$\rho^{n_{N+1}}_{\text{dg}} = \frac{i_N u\Delta t}{2\sin(i_N\frac{\gamma}{2})}\sin(\omega^{n_N})\sin(\omega^{n_N} - i_N\frac{\gamma}{2}), \tag{6.25}$$

i.e., the dangerous interval of the finite ball degenerates into one point again. And so the dangerous self-collision defined by the parameters $(\rho^{n_{N+1}}_{\text{dg}}, \omega^{n_{N+1}}_{\text{dg}})$ describes the

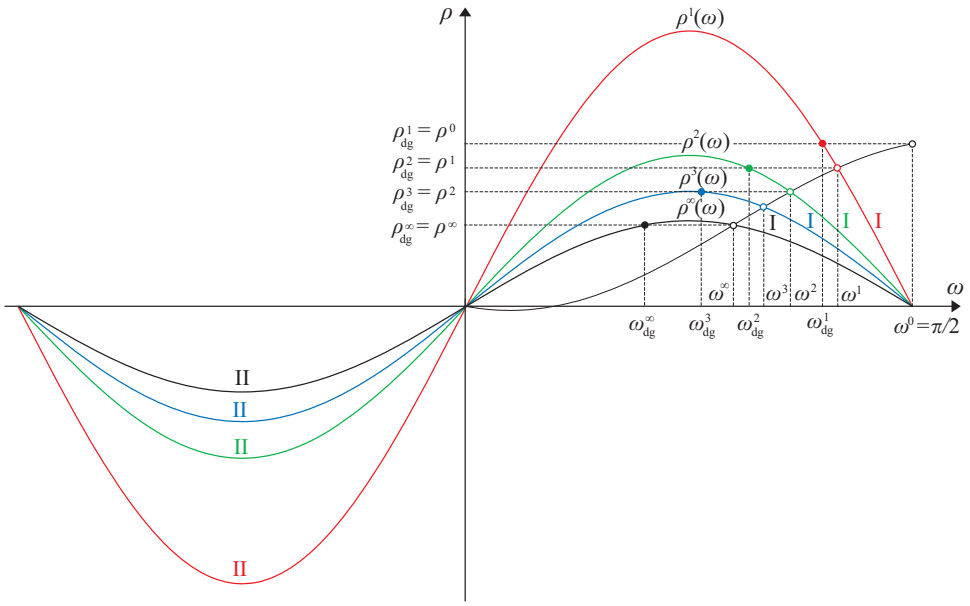

Figure 6.4: **Relation of inner self-collisions to dangerous self-collisions.** Consider the sequence $\{k\}_{k=0}^{N}$ for which $n_N = N$. If the outer direction ω^{n_N} of the sequence $\{n_k\}_{k=0}^{N}$ equals to the inner direction $\omega^{\bar{n}_N}$ of the sequence $\{\bar{n}_k\}_{k=0}^{N+1}$, where $n_k = \bar{n}_k$ for $k = 0, ..., N$, then the dangerous direction $\omega_{\rm dg}^{\bar{n}_{N+1}}$ results from shifting of the inner direction $\omega^{\bar{n}_N}$ by $i_N \frac{\gamma}{2}$. Such shifts take place along horizontals lines corresponding to constant values of the impact parameter $\rho_{\rm dg}^{n_N}$ for $N = 1, 2, ...$ Open dots represent inner directions, while full dots represent dangerous directions. If the outer direction of the sequence $\{k\}_{k=0}^{1}$ is identical to the inner direction of the sequence $\{k\}_{k=0}^{2}$ then the dangerous direction $\omega_{\rm dg}^{2}$ of the sequence $\{k\}_{k=0}^{2}$ results from shifting of the inner direction ω^1 by $\gamma/2$. This shift takes place on the line of the dangerous impact parameter $\rho_{\rm dg}^{2}$ of the sequence $\{k\}_{k=0}^{2}$. Obviously, the value of $\rho_{\rm dg}^{2}$ is identical to the value of the inner impact parameter ρ^1 because there is no change in the direction, or the impact parameter, within the dangerous self-collision (of the sequence $\{k\}_{k=0}^{2}$). Similarly, shifting the inner direction ω^2 of the sequence $\{k\}_{k=0}^{3}$ along the line of the dangerous impact parameter $\rho_{\rm dg}^{3}$ by $\gamma/2$ results into the dangerous direction $\omega_{\rm dg}^{3}$ of the same sequence. In the limit case $N \to \infty$, the inner direction of the sequence $\{k\}_{k=0}^{\infty}$ is shifted by $\gamma/2$ along the line of the dangerous impact parameter $\rho_{\rm dg}^{\infty}$ into the dangerous direction $\omega_{\rm dg}^{\infty}$ of the sequence $\{k\}_{k=0}^{\infty}$. Values of inner angles ω^N preceding the outer $N+1$-th self-collision lie within intersections of particular graphs and the curve determined by eq. (6.25) (in black in the diagram), in which the inner angle ω^N is varied and the initial velocity u remains fixed. Notice also that in the point-like case spurious solutions of one type change into physical solutions of the other type: self-collisions of type I are physical for $\omega > \omega_{\rm dg}^{N}$, and self-collisions of type II are physical for $\omega < \omega_{\rm dg}^{N}$.

particle which self-interacts without exchange of any momentum because of its point-likeness.[1][2]

[1]Notice also that in the point-like case spurious solutions of one type change into physical solutions of the other type: self-collisions of type I are physical for $\omega^{n_{N+1}} > \omega_{\rm free}^{p}$, and self-collisions of type II are physical for $\omega^{n_{N+1}} < \omega_{\rm free}^{p}$, cf. figure 6.4.

[2]Clearly, if the $N+1$-th self-collision is dangerous then the particle does not change its direction or impact parameter as it passes by. Hence, the dangerous impact parameter $\rho_{\rm dg}^{n_{N+1}}$ of the sequence $\{n_k\}_{k=0}^{N+1}$, eq. (6.25), is equal to the inner impact parameter ρ^{n_N} of the sequence $\{n_k\}_{k=0}^{N}$. For other

Notice that replacement of the paradoxical self-intersection at the p-th self-event (following the outer n_N-th self-collision) by the $N+1$-th (dangerous) self-collision at the n_{N+1}-th self-event corresponds to transition from sequence $\{n_k\}_{k=0}^{N}$ to sequence $\{\bar{n}_k\}_{k=0}^{N+1}$, i.e., transition between two different solutions. However, in the point-like case, inner angles are related by recurrence (6.9), and thus their values do not depend on the length of sequences. Therefore, two sequences $\{n_k\}_{k=0}^{N}$ and $\{\bar{n}_k\}_{k=0}^{N+1}$ differ only by occurrence of the last member $\bar{n}_{N+1}$ in the second (longer) sequence, while all other terms remain identical, $n_k = \bar{n}_k$ for $k = 0, ..., N$. We will distinguish sequences $\{n_k\}_{k=0}^{N}$ and $\{\bar{n}_k\}_{k=0}^{N+1}$ only if we need to emphasize that solutions ω correspond to different sequences.

If the outer direction ω^{n_N} of the sequence $\{n_k\}_{k=0}^{N}$ equals to the inner direction $\omega^{\bar{n}_N}$ of the sequence $\{\bar{n}_k\}_{k=0}^{N+1}$, where $n_k = \bar{n}_k$ for $k = 0, ..., N$, then the dangerous direction $\omega_{\rm dg}^{\bar{n}_{N+1}}$ results from shifting of the inner direction $\omega^{\bar{n}_N}$ by $i_N\frac{\gamma}{2}$, cf. eq. (6.24). In diagram 6.4, such shifts take place along horizontals lines corresponding to the constant impact parameter $\rho_{\rm dg}^{n_N}$. Specifically, in the case of the sequence $\{k\}_{k=0}^{N}$, if the outer direction of the sequence $\{k\}_{k=0}^{1}$ is identical to the inner direction of the sequence $\{k\}_{k=0}^{2}$ then the dangerous direction $\omega_{\rm dg}^{2}$ of the sequence $\{k\}_{k=0}^{2}$ results from shifting of the inner direction ω^1 by $\gamma/2$. This shift can be seen in diagram 6.4 on the line of the dangerous impact parameter $\rho_{\rm dg}^{2}$ of the sequence $\{k\}_{k=0}^{2}$. Obviously, the value of $\rho_{\rm dg}^{2}$ is identical to the value of the inner impact parameter ρ^1 because there is no change in the direction, or the impact parameter, within the dangerous self-collision (of the sequence $\{k\}_{k=0}^{2}$).

If a sequence ends with self-intersections then its graph has to be shifted to the left by $i_N\gamma/2$ (by the number of self-intersections preceding the paradoxical self-intersection) which generates intersections with the graphs of other sequences. A trailing (and paradoxical) self-intersection of one sequence is superseded by dangerous (and outer) self-collision of the other sequence if the intersection of graphs corresponds to the same self-event. For example, in figure 6.5 we can see few illustrating examples for $p = 0, 1, 2, 3$.

The "zero" self-event, $p = 0$, represents the fictive self-collision with $\omega = \pi/2$ for arbitrary ρ as introduced in section 6.1, cf. blue vertical line in fig. 6.5a. After one loop around the cone the self-intersection I (with $\omega = \pi/2 - \gamma/2$) follows, cf. fig. 6.5b, and after two loops "double" self-intersection II (with $\omega = \pi/2 - \gamma$) occurs, cf. fig. 6.5c. In other words, after one loop, the corresponding trajectory is defined by the sequence I, and after two loops is the same trajectory described by the sequence II. At the first self-event, $p = 1$, the paradoxical self-intersection is replaced by the dangerous self-collision, see intersection of graphs I and C in fig. 6.5b. It can be followed by one more self-intersection, since $\frac{\gamma}{2} < \frac{\pi-\gamma}{2} < \gamma$, which changes labeling to II and CI, see intersection of graphs II and CI in fig. 6.5c. Two replacements can occur at the second self-event, $p = 2$: II→IC and CI→CC, cf. fig. 6.5c. Because there are two preceding loops around the cone, the graph II is shifted twice by $\frac{\gamma}{2}$, the replacement II→IC. And analogically, since there is just one preceding loop, the graph CI is shifted by

inner self-collisions, the inner impact parameter is given by

$$\rho^{n_{k+1}} = \frac{i_k u^{n_k} \Delta t}{2\sin(i_k\frac{\gamma}{2})} \sin(\omega^{n_k}) \sin(\omega^{n_k} - i_k\frac{\gamma}{2}),$$

where u^{n_k} represents velocities on inner loops given by eq. (6.5). This relation turn into the dangerous impact parameter $\rho_{\rm dg}^{n_{N+1}}$, eq. (6.25), for $k = N$ and $u^{n_k} = u$.

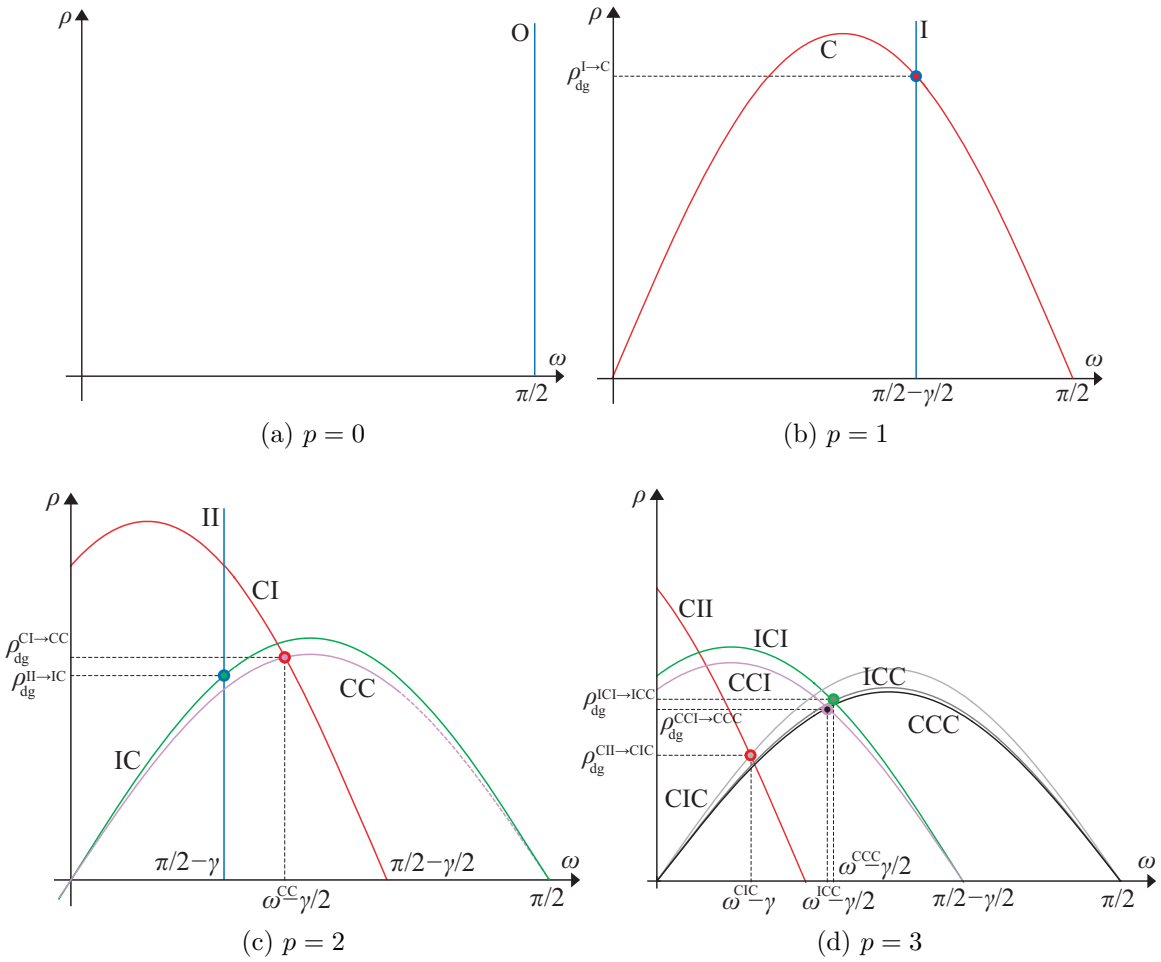

Figure 6.5: **Replacements of paradoxical self-intersections by dangerous self-collisions at the p-th self-event.** Graphs ρ-ω, which illustrate superseding of the paradoxical self-intersections by the dangerous self-collisions. Graphs of sequences ending with self-intersections are shifted by $i_N\gamma/2$ to the left, i.e., by $\gamma/2$ for *each* trailing self-intersection. The emphasized intersections of the graphs correspond to the dangerous parameters $\rho_{\rm dg}$ and $\omega_{\rm dg}$ for which we cannot distinguish dangerous self-collisions from paradoxical self-intersections. Assume that the vertex angle $\gamma \in (\pi/3, \pi/2)$, i.e., self-collision can be followed at the most by two self-intersections. (a) The "zero" self-event, $p = 0$, represents the fictive self-collision with $\omega = \pi/2$ for arbitrary ρ, as introduced in section 6.1. After one loop around the cone the self-intersection I (with $\omega = \pi/2 - \gamma/2$) follows, cf. blue vertical line (b), and after two loops double self-intersection II (with $\omega = \pi/2 - \gamma$) occurs, cf. blue vertical line (c). (b) At the first self-event, $p = 1$, the paradoxical self-intersection is replaced by the dangerous self-collision, see intersection of graphs I and C (red graph). It can be followed by one more self-intersection which changes labeling to II and CI, see intersection of graphs II and CI in diagram (c). (c) Two replacements can occur at the second self-event, $p = 2$: II→IC (blue to green) and CI→CC (red to purple). Depending on number of self-intersections preceding the paradoxical self-intersection, the graph II in the replacement II→IC is shifted twice by $\frac{\gamma}{2}$, while the graph CI in the replacement CI→CC is shifted by $\frac{\gamma}{2}$ only once. There occur another two intersections of graphs II and CC, and graphs IC and CI, in the diagram (c), which both represent two regular solutions which only coincide in the location and direction, cf. corresponding situations in figure 6.4. (d) Three replacements can occur at the third self-event, $p = 3$: CII→CIC (red to light gray), CCI→CCC (purple to black) and ICI→ICC (green to dark gray). Also here shifting of the graphs differ according to the number of preceding loops around the cone.

$\frac{\gamma}{2}$ only once, the replacement CI→CC . Geometry of collisions corresponding to just mentioned replacements, i.e., I→C (fig. 6.5b), II→IC and CI→CC, (fig. 6.5c), can be seen in figure 6.4. Finally, three replacements can occur at the third self-event, $p = 3$: CII→CIC, CCI→CCC and ICI→ICC. Again, shifting of the graphs differ according to the number of preceding loops around the cone.

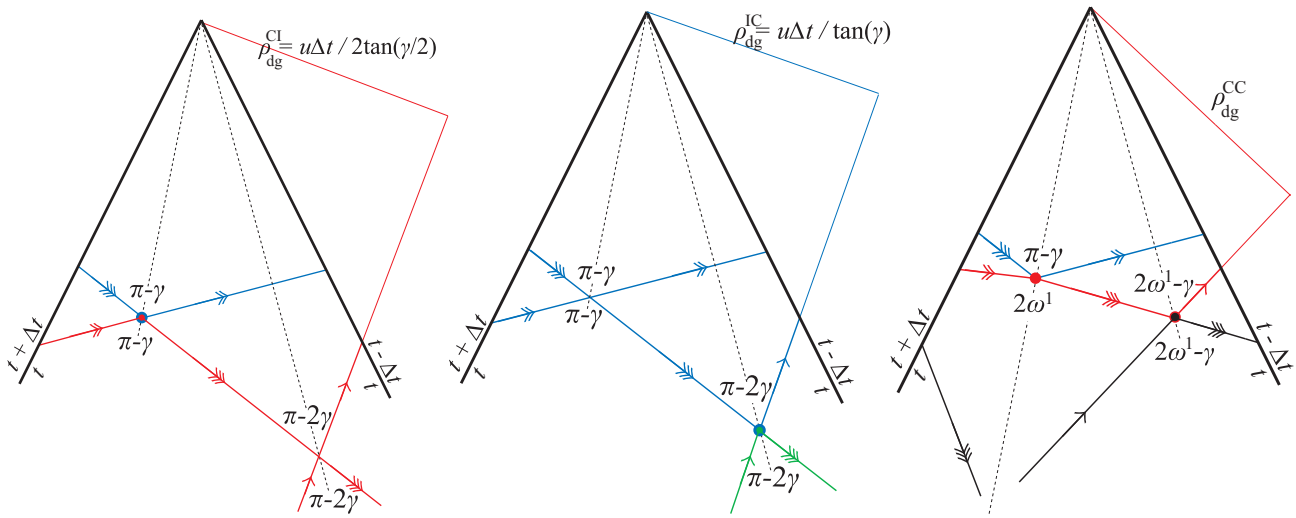

(a) II→CI (b) II→IC (c) CI→CC

Figure 6.6: **Paradoxical self-intersections and dangerous self-collisions – viewpoint of the observer located at the 2-th self-event.** Paradoxical trajectories are such trajectories along which the particle would enter time machine without self-collision and would pass through it in such a way that it would self-collide inconsistently. Paradoxical (and inconsistent) self-intersections – when the particle moves along the paradoxical trajectory without self-collision – are replaced by dangerous (and consistent) self-collisions – when the particle moving along the dangerous trajectory self-collides. Geometry of paradoxical self-intersections and dangerous self-collisions is identical in the case point-like particle, i.e., incoming directions equal to outgoing directions. The first figure (a) demonstrates the replacement at the first self-event: II→CI. The point of the paradoxical situation consists of two colors to symbolize that the free passage through the self-intersection is replaced by the self-collision (red to blue). Figures (b) and (c) represent replacements (of paradoxical self-intersections by self-collisions) at the second self-event: II→IC (green to blue), and CI→CC (black to red) respectively.

Notice that there are other intersections of graphs: The intersection of graphs II and CC, and of graphs IC and CI, cf. fig. 6.5b. Such intersections represent two regular solutions which have the same initial data (u, ρ) and final data (ω, r), and correspond to two different self-events which coincide only in locations, but not in times of self-events, see corresponding situations in figure 6.4.[3]

[3]Generally, the replacement at the p-th self-event occurs in the intersection of two graphs if the first graph represents the sequence of the form $\{X\}^{p-1}\mathrm{I}\{I\}^{P-p}$, and the second graph represents sequence of the form $\{X\}^{p-1}\mathrm{C}\{I\}^{P-p}$ where P is the length of both sequences, and $\{X\}^{p-1}$ stands for any arbitrary sequence of the length $p-1$ and $\{I\}^{P-p}$ is sequence of I's only of the length $P-p$. The first graph describes the sequence with $N-1$ self-collisions and it is shifted about $(p-n_{N-1})\frac{\gamma}{2}$ to the left to the origin, while the other graph corresponds to the sequence with N of self-collisions $(p = n_N)$.

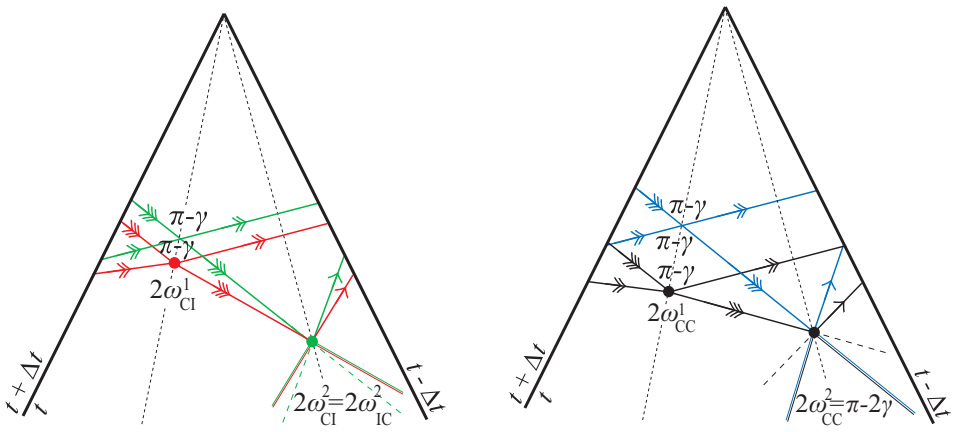

(a) CI versus IC (b) II versus CC

Figure 6.7: **Regular solutions – viewpoint of the observer located at the 2-th self-event.** There are another two intersections, namely, the intersection (a) of graphs CI and IC, and (b) of graphs II and CC. Such intersections represent two regular solutions which have the same initial data (u, ρ) and final data (ω, r), and correspond to two different self-events which coincide only in locations, but not in times of self-events. In figure (a) the sequence CI is represented by the red trajectory, while the sequence IC corresponds to the green path. In figure (b) the sequence II is represented by the blue trajectory, while the sequence CC corresponds to the black path.

6.5 Asymptotic behavior of the outer trajectories

Considering multiple self-collisions complicates slightly the asymptotic behavior of the outer trajectories. The asymptotic observer measures the angle $2\omega^P$ between the trajectory along which the youngest version of the particle moves to its first self-collision and the trajectory along which the oldest version of the particle leaves its last self-collision for infinity. Range of the asymptotic angle ω^P, i.e., span of trajectories incoming toward the asymptotic observer, is limited by the interval $[-\frac{\gamma}{2}, \frac{\gamma}{2}]$ regardless of the sequence $\{n_k\}_{k=0}^N$.

This angle can correspond either to the outer self-collision ($P = n_N$ and $-\frac{\gamma}{2} \leq \omega^{n_N} \leq \frac{\gamma}{2}$), or to the self-intersection following the outer self-collision ($P > n_N$ and $\omega^{n_N} > \frac{\gamma}{2}$ or $\omega^{n_N} < -\frac{\gamma}{2}$) in which case we can introduce the additional term i_N to sequence $\{i_k\}_{k=0}^{N-1}$ as quotient

$$i_N = \mathrm{Q}(|\omega^{n_N}|, \frac{\gamma}{2}), \tag{6.26}$$

which indicates the number of self-intersections following the outer self-collision. Thus, the total number of all self-events P can be written down as the sum $P = \sum_{k=0}^{N} i_k$. As the outer direction ω^{n_N} depends on the initial parameters u and ρ, so it does the i_N. Depending on the sign of ω^{n_N} the asymptotic angle can be expressed as

$$\omega^P = \omega^{n_N} - i_N \frac{\gamma}{2}\,,$$

for the particle traveling to the past beyond its outer self-collision

$$\omega^P = \omega^{n_N} + i_N \frac{\gamma}{2}\,,$$

for the particle which shifts to the future. To illustrate relation between the angle ω^P and the impact parameter ρ we cut the graph for ω^{n_N}, given by equation (6.15), into $i_{\max}$ parts, and then shift these partial graphs by $i_N\frac{\gamma}{2}$ toward the origin where each part of the graph corresponds to a number i_N. For instance, for $\gamma \in [\frac{\pi}{3}, \frac{\pi}{2})$, each graph is divided into three parts as we can see in fig. 6.8. Thus, multiple values of final parameters (ω, r) are assigned to initial parameters u and ρ from the asymptotic viewpoint. Moreover, intersections of the partial graphs represent indistinguishable solutions with identical both initial data (u, ρ) and final data (ω, r).

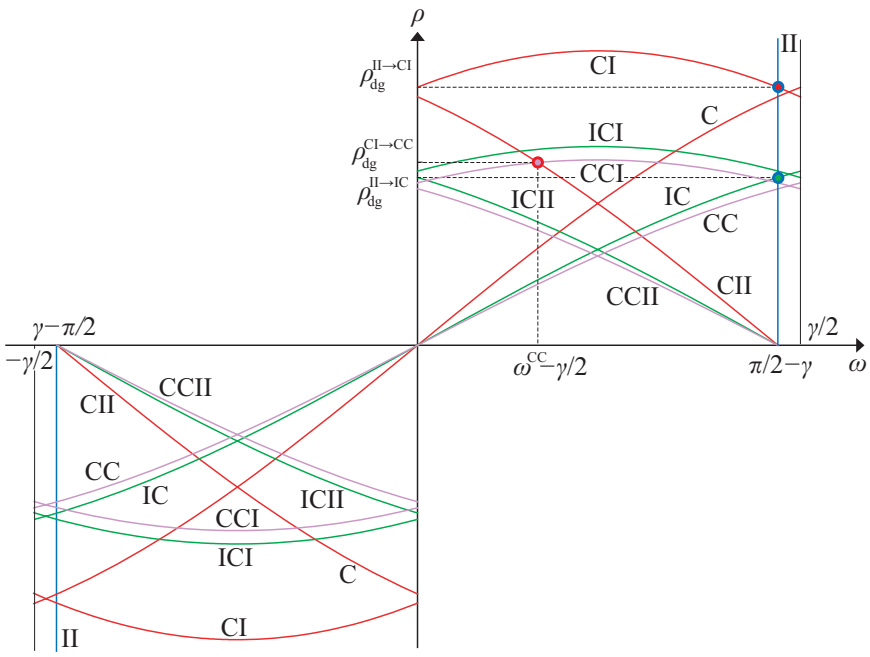

Figure 6.8: **Relation of initial and final data from the asymptotic viewpoint.** Range of the asymptotic angle ω^P, i.e., span of trajectories incoming toward the asymptotic observer, is limited by the interval $[-\frac{\gamma}{2}, \frac{\gamma}{2}]$ regardless of the sequence $\{n_k\}_{k=0}^N$. Graphs for sequences ending with the self-collision, given by equation (6.15), have to be cut and shifted by integer multiple of $\frac{\gamma}{2}$ in such a way that they fit in the interval $[-\frac{\gamma}{2}, \frac{\gamma}{2}]$. The number i_N of self-intersections beyond the outer self-collision determines the number of shifts of parts of these graphs. Obviously, the number of parts of a graph is given by the magnitude of the vertex angle γ. For instance, for $\gamma \in [\frac{\pi}{3}, \frac{\pi}{2})$, each graph is divided into three parts. Asymptotic viewpoint assigns multiple values of final parameters (ω, r) to initial parameters u and ρ. Intersections of cut and shifted graphs represent such indistinguishable solutions which share both initial data (u, ρ) and final data (ω, r).

In order to determine how many times outer trajectories pass through the wormhole we have to take into account also the angular position of the N-th self-collision with respect to the wormhole. The motion with respect to the orientation of the wormhole can be investigated again by employing the covering space for the conical space. Analogously to the case with at most one self-collision we assume that the angular coordinate of the incoming trajectory is $\varphi_{\mathrm{i}} = 0$ with the impact parameter ρ and the initial velocity u. Let us denote each self-collision by C_k for $k = 1, ..., N$.

The outer self-collision C_N lies on the collision circle which has the center S on the radial line $\varphi = 0$, the circle passes through the axis, and its radius is given by the

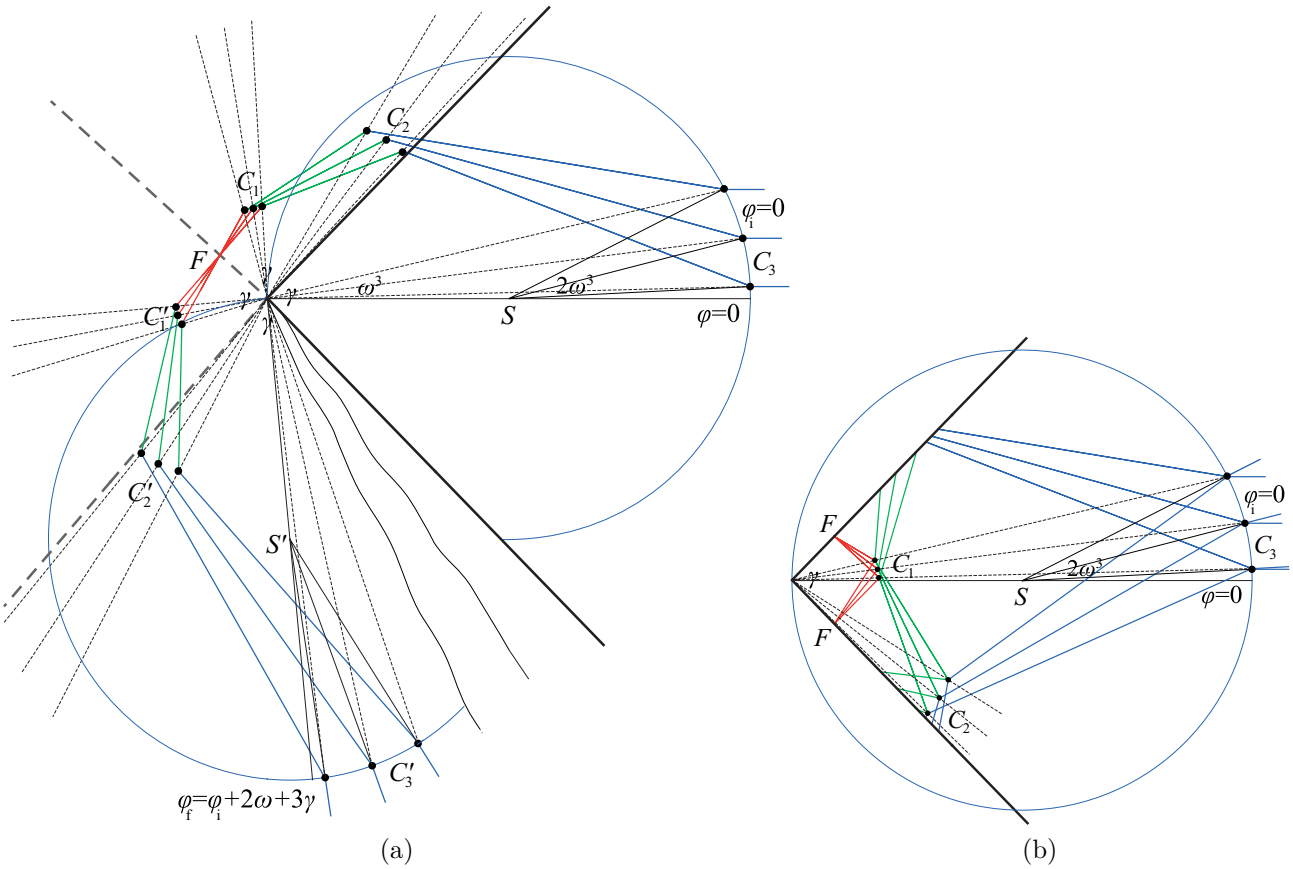

Figure 6.9: **Multiply self-colliding trajectories in the totally covering space for $\{k\}_{k=0}^{3}$.** Thanks to the parametrization $\varphi_{\rm i}=0$ the angular coordinate φ of the *outer* self-collision is given exactly by the scattering angle ω^3. At the point of outer self-collision C_3 the trajectory is deflected, and it continues toward the points of inner self-collisions C_2 and C_1. These points are defined by inner angles ω^2 and ω^1, and rotated subsequently by $\frac{\gamma}{2}$ around the axis (in the counterclockwise direction). When the trajectory reaches the innermost self-collision C_1, it is rotated by angle γ to its image point C_1'. Then the trajectory continues on through the other image point C_2' (deflected by ω^2 and rotated by $\frac{\gamma}{2}$) in the covering space, till it approaches the image point C_3' of the outer self-collision. From C_3' the particle continues through the covering space in the direction which aims from the center S' of the rotated collision circle with the angular parameter $\varphi_{\rm f}=\varphi_{\rm i}+2\omega^3+3\gamma$ of the outgoing (outer) trajectory. This procedure is illustrated for sequence $\{i_k\}_{k=0}^{3}=\{1,1,1,0\}$, (a) in the covering space, and (b) in the original conical space after the different points C_k and C_k' of the covering space have been identified as the "twofold" point C_k. The total time shift of the trajectory is $\Delta T=-(3-0-0)\Delta t$ given by three inner loops (always directed to the past). Clearly, the focusing point F is passed through by all three innermost trajectories (belonging to the same congruence). The diagram (a) shows only a part of the totally covering space.

maximal impact parameter $\rho_{\max}$ determined by a sequence $\{n_k\}_{k=0}^{N}$, cf. fig. 6.9. Thanks to the parametrization $\varphi_{\rm i}=0$ the angular coordinate φ of the *outer* self-collision is given exactly by the scattering angle ω^{n_N}. At the point of outer self-collision C_N the trajectory is deflected, and it continues toward the points of inner self-collisions C_{N-k} (for $k=1,...,N-1$). These points are defined by inner angles $\omega^{n_{N-k}}$ and rotated subsequently by $i_{N-k}\frac{\gamma}{2}$ around the axis (in the counterclockwise direction). When the

trajectory reaches the innermost self-collision C_1, it is rotated by angle $i_0\gamma$ to its image point C_1' (and it focuses at the point F which occurs between C_1 and C_1'). Then the trajectory continues on through the other image points C_k' (deflected at every inner self-collision by ω^{n_k} and rotated subsequently by $i_k\frac{\gamma}{2}$) in the covering space, till it approaches the image point C_N' of the outer self-collision. From C_N' the particle continues through the covering space in the direction which aims from the center S' of the rotated collision circle with the angular parameter

$$\varphi_{\rm f} = \varphi_{\rm i} + 2\omega^{n_N} + \gamma\sum_{k=0}^{N-1} i_k = \varphi_{\rm i} + 2\omega^{n_N} + n_N\gamma,$$

of the outgoing (outer) trajectory. This procedure is illustrated in figure 6.9, for sequence $\{i_k\}_{k=0}^3 = \{1,1,1,0\}$, (a) in the covering space, and (b) in the original conical space after the different points C_k and C_k' of the covering space have been identified as the "twofold" point C_k.

The total time ΔT gained in the wormhole during the whole scattering process, which depends on the angular position of the outer self-collision, characterizes the asymptotic behavior of the outer trajectory as it determines the proper time spent between the start time $t_{\rm i}$ and final time by $t_{\rm f}$. Thus, if the angular coordinate $\varphi_{\rm f}$ of the outgoing trajectory belongs to n-th copy of the wormhole in the covering space, $n \in \mathbf{Z}$, the particle gains the time-shift $\Delta T = -n\Delta t$:

$$\varphi_{\rm f} \in \Big(-\frac{\gamma}{2} + \psi + n\gamma, \frac{\gamma}{2} + \psi + n\gamma\Big) \;\Rightarrow\; \Delta T = -n\Delta t\ ,$$

where $\psi \in (-\gamma/2, \gamma/2)$ defines the orientation of the wormhole, cf. section 4.6.3. Taking into account the restrictions on γ, ψ and ω, the total time-shift can be

$$-\Delta t(n_N + i_N + 1) \le \Delta T \le -\Delta t(n_N - i_N - 1).$$

Thus, the total time shift ΔT consists of three contributions: the term

$$n_N\Delta t = \Delta t\sum_{k=0}^{N-1} i_k,$$

is given by the number n_N of all inner loops, the second quantity $\pm i_N\Delta t$ is defined by the number of the self-intersections following the outer N-th self-collision, and the unit contribution $\pm\Delta t$ is determined by the orientation of the wormhole ψ. Thus, the total time shift of the trajectory in figure 6.9 is $\Delta T = -(3-0-0)\Delta t$ since three inner loops (always directed to the past). Finally, the proper time τ as measured by the particle is given by

$$\tau = t_{\rm f} - t_{\rm i} + \Delta T\ . \tag{6.28}$$

By analogy to section 4.6.4 the congruence with "plane-wave" wavefront can be formed for $\rho \in (-\rho_{\max}, \rho_{\max})$ corresponding to a sequence $\{n_k\}_{k=0}^N$. Similarly to the case of one self-collision, particles approaching the time machine along the null direction $\varphi_{\rm i} = 0$ self-collide on the *outer* collision circle and, after all inner self-collisions occur, leave in the directions which point out from the common point S'. Thus, the original plane-wave congruence of particles scatters to the circular-wave congruence with phase

shifted trajectories in the covering space. The congruence focuses at a point F when it passes its innermost loop, i.e., all inner multiply self-colliding trajectories (between the corresponding outer self-collisions) have a direction going through one focusing point F at its innermost loop, cf. fig. 6.9. Obviously, detailed analysis multiply self-colliding congruences would turn out to be complicated and it would deserve another chapter.

6.6 Analysis of inner angles for infinite sequences

Let us study sequences of inner angles. First we notice that recurrent function (6.10) is single-valued, i.e., there exists just one inner angle ω^{n_k} given the preceding inner direction $\omega^{n_{k-1}}$ and numbers i_{k-1} and i_k, see appendix B.1. Then we introduce the limit of infinite sequences with $N \to \infty$ and investigate the last inner angle $\omega^{n_{N-1}}$ for the external observer located near the outer N-th self-collision. Next, we analyze limiting inner angles for constant sequences $\{i_k\}_{k=0}^{N-1} = \{q\}_{k=0}^{N-1}$, where q is arbitrary but fixed value from the interval $[1, i_{\max}]$. Finally, we extend our consideration to periodical sequences where the notion of the "attractor" will be introduced and identified with the set of limiting inner angles.

6.6.1 Infinite sequences

Till now we have considered sequences of finite length N. Surprisingly, also infinite sequences represent solutions to the initial problem. Although infinite sequences are partly disqualified, since they imply infinite proper time τ along the whole inner path, given by eq. (6.28) with $N \to \infty$, they can be used for approximation of behavior of very long sequences. Moreover, even for infinite sequences the particle leaves the interacting region (wormhole) in a finite external time.

When we compute inner angles we proceed from the first inner self-collision (given by $\omega^0 = \pi/2$) to the last inner self-collision (given by $\omega^{n_{N-1}}$) using relations (6.9). Thus, increasing N means adding another self-collision far from the vertex. However, it seems natural to assume that the external observer standing at the outer self-collision "sees" outer self-events labeled by large indexes, i.e., the numbers i_{N-1}, i_{N-2}, ..., of path segments separating the last self-collisions. Therefore, in contrast to the direction of computation of the angles ω^{n_k} we should number inner self-collision from the last inner self-collision to the first one. It reflects the fact that other quantities as radial distances of the self-collisions r^{n_k} and impact parameters ρ^{n_k}, or lengths of path segments $\sum_j s^j$ between two successive self-collisions, are computed using recurrent formulas, cf. eqs. (6.7) and (6.6), from the outer side of the sequences.

However, we will not relabel the numbering of the sequences explicitly, instead, we will use a formal notation in which the outermost self-collisions of the infinite sequences ($N \to \infty$) are labeled as $\{...n_{\infty-3}n_{\infty-2}n_{\infty-1}\}$ and corresponding segments $\{...i_{\infty-3}i_{\infty-2}i_{\infty-1}\}$. This reversed point of view has sense if there exist limiting values $\omega^{\infty-1}$, $\omega^{\infty-2}$, $\omega^{\infty-3}$ for the inner angles near the outer end of the sequences. In that case we can fix these limiting values as the initiate values of the reversed sequences. The limiting values of the inner angles $\omega^{n_{N-1}}$, $\omega^{n_{N-2}}$, $\omega^{n_{N-3}}$ can be found for special

kind of infinite sequences, namely for *periodical* sequences

$$\{...q_{N-2}q_{N-1}q_{N-a}...q_{N-2}q_{N-1}q_{N-a}...q_{N-2}q_{N-1}\},$$

with the period $\{q_k\}_{k=1}^{a}$ of the length a.

This class of sequences could be generalized to *asymptotically periodical* sequences which consist of an arbitrary finite sequence at the outermost end, $\{...i_{\infty-3}i_{\infty-2}i_{\infty-1}\}$, preceded by a infinite periodical sequence with the period a

$$\{q_{N-1}q_{N-2}...q_{N-a}q_{N-1}q_{N-2}...q_{N-a}q_{N-1}...\}.$$

However, we will study just periodical sequences, the asymptotically periodical sequences should be straightforward but cumbersome generalization.

For periodical sequences one can show that values of inner angles ω^{n_k} limit to asymptotically well defined values $\omega^{\infty-1}, ..., \omega^{\infty-a}$ with the period a. We can thus take these values as fixed values of the inner angles for the reversed infinite sequences starting at the outermost self-collision.

6.6.2 Inner angles of constant sequences

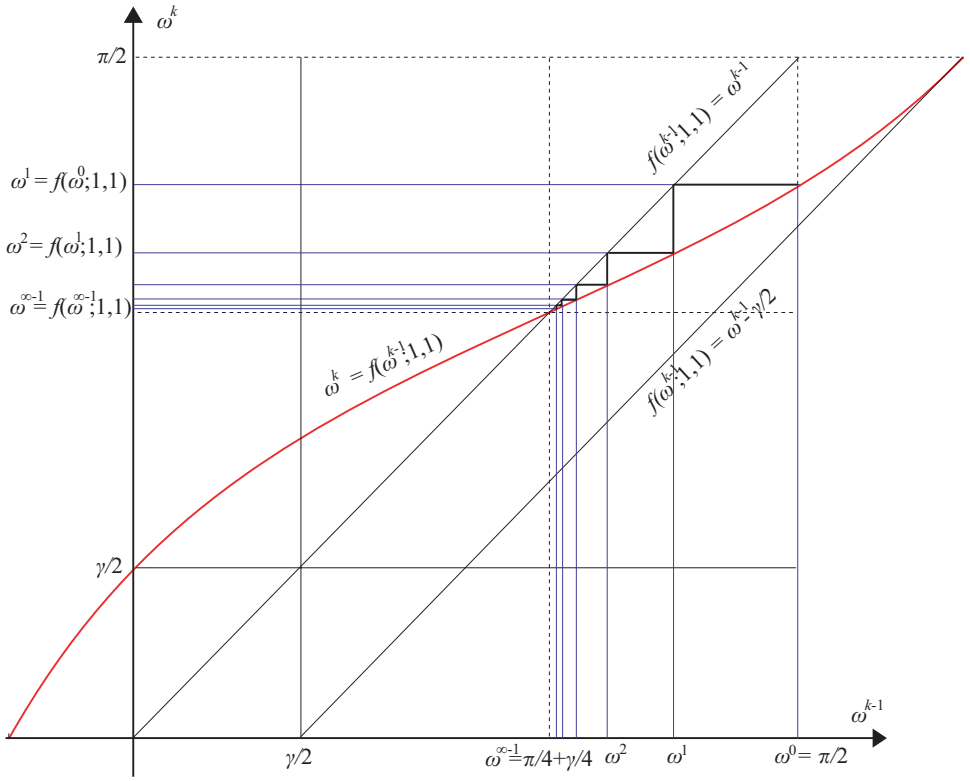

Figure 6.10: **Algorithm for generating of the inner angles for the sequence $\{i_k\} = \{1\}$.** Equation (6.16) determines certain increasing function $f(\omega)$ (the red line) defining the recurrence relation $\omega^k = f(\omega^{k-1}; 1, 1)$ for $k = 0, ..., N-1$. There is the fixed point $f(\omega^{\infty-1}; 1, 1) = \omega^{\infty-1}$ within $(\frac{\gamma}{2}, \frac{\pi}{2})$, namely $\omega^{\infty-1} = \frac{\pi}{4} + \frac{\gamma}{4}$, which represents the limiting value of the sequence $\{\omega^k\}_{k=0}^{\infty-1}$. Couple of first steps of the recurrent calculation of values ω^k is also illustrated.

In this paragraph we will study inner angles of constant sequences for $\{i_k\}_{k=0}^{N-1} = \{q\}_{k=0}^{N-1}$ with a trivial period of the length $a = 1$, where $q \in [1, i_{\max}]$. Thus, inner angles ω^{qk} are described by a single function $\omega^{qk} = f(\omega^{q(k-1)}; q, q)$, cf. definition (6.10). This function determines the monotonic convergent sequence $\{\omega^{qk}\}$ which results from inequality of derivatives

$$0 < \frac{\mathrm{d}f(\omega^{q(k-1)}; q, q)}{\mathrm{d}\omega^{q(k-1)}} < 1,$$

for any $\omega^{qk} \in (q\frac{\gamma}{2}, \frac{\pi}{2})$ as demonstrated in appendix C. More accurately, the sequence $\{\omega^{qk}\}_{k=0}^{N-1}$ *decreases* from the starting value $\omega^0 = \frac{\pi}{2}$.

Moreover, the sequence determined by recurrent relation (6.16) contains the fixed point

$$\omega^{q(N-1)} \xrightarrow{N\to\infty} \frac{\pi + q\gamma}{4},$$

within the interval $(q\frac{\gamma}{2}, \frac{\pi}{2})$, i.e., the point that is mapped to itself by the function f:

$$\frac{\pi + q\gamma}{4} = f(\frac{\pi + q\gamma}{4}; q, q).$$

First few steps of the recurrence calculation are illustrated in figure 6.10. Obviously, in the case $i_k = q =$ constant we need not to distinguish if self-collisions are added at the innermost end, or at the outermost end. The existence of the fixed point which is limiting value for $N \to \infty$ guarantees that for large N the values $\omega^{q(N-k)}$ for the trailing terms in the sequence $\{\omega^0, \omega^q, ..., \omega^{q(N-2)}, \omega^{q(N-1)}\}$ will be essentially equal to this limiting value, i.e., $\omega^{q(N-k)} \approx \omega^{\infty-1}$ for $N \gg k$.

6.6.3 Inner angles of periodical sequences

The recurrent formula (6.9) for inner self-collisions describes up to $(i_{\max})^2$ different functions $f(\omega^{n_{k-1}}; i_{k-1}, i_k)$ as i_{k-1} and i_k vary through $[1, 2, ..., i_{\max}]$. It can be verified that formula (6.9) represents increasing functions, see appendix B.1. Moreover, their slope can be constrained similarly to the case of constant $i_k = q$, and thus inequality

$$0 < \frac{\mathrm{d}f(\omega^{n_{k-1}}; i_{k-1}, i_k)}{\mathrm{d}\omega^{n_{k-1}}} < 1,$$

holds within the interval $\omega^{n_{k-1}} \in (i_{k-1}\gamma/2, \pi/2)$ as shown in appendix B.2. This condition implies that all functions $f(\omega^{n_{k-1}}; i_{k-1}, i_k)$ represent monotonic convergences with fixed points on the line $f(\omega^{n_{k-1}}; i_{k-1}, i_k) = \omega^{n_{k-1}}$.

Monotonic convergence of periodically applied functions allow us to formulate a hypothesis that a periodical sequence with a period a possess an *attractor* consisting of a values $\omega_1^{\&}, ..., \omega_a^{\&}$. Here, the term attractor is used to label a stable loop, which is approached by repeating the subsequence made just of a values $\omega_1^{\&}, ..., \omega_a^{\&}$ corresponding to particular $q_1, ..., q_a$. The attractors, or loops, cf. diagram 6.11, develop in process of computation which starts with a fixed q_k and evaluates a functions $f(\omega^{n_{k-1}}; q_{k-1}, q_k)$ successively. In diagram 6.11 there are illustrated periodical sequences with periods $\{p, q\}$ and $\{p, q, r, p, q, s\}$, analogically to fig. 6.10.

However, the value $\omega_{q_k}^{\&}$ of an attractor represents just the desired limiting inner angle $\omega^{\infty-k}$, described above in paragraph 6.6.1, at the outer end of the infinite sequence.

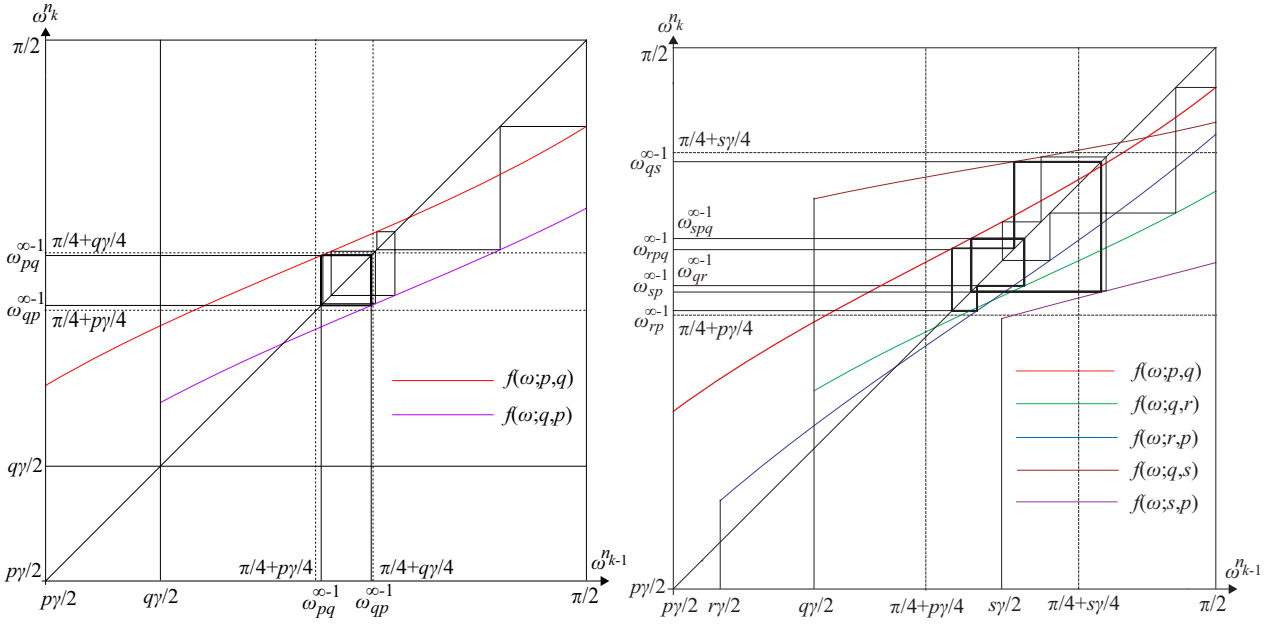

(a) Sequence with period $\{pq\}$ where $p < q$ (b) Sequence with period $\{pqrpqs\}$ where $p < r < q < s$

Figure 6.11: **Attractors for periodical sequences.** In the case of general sequences, values ω^{n_k} "jumps" since various functions $f(\omega^{n_{k-1}}; i_{k-1}, i_k)$ are used in recurrence calculation of ω^{n_k}. However, if a sequence is periodical with a period a then there exists an *attractor* consisting of a values $\omega_1^{\&}, ..., \omega_a^{\&}$: Here, the term attractor is used to label a stable loop, which is approached by repeating the subsequence made just of a values $\omega_1^{\&}, ..., \omega_a^{\&}$ corresponding to particular $q_1, ..., q_a$. The attractors, or loops, develop in process of computation which starts with a fixed q_k and evaluates a functions $f(\omega^{n_{k-1}}; q_{k-1}, q_k)$ successively. In this diagram there are illustrated periodical sequences with periods $\{p, q\}$, $a = 2$, and $\{p, q, r, p, q, s\}$, $a = 6$, analogically to fig. 6.10.

Thus, each limiting angle $\omega^{\infty-k} \equiv \omega_{q_k}^{\&}$ included in an attractor corresponds to the sequence of segments *ending* with the term q_k. Obviously, in the case of sequences with a trivial period of the length $a = 1$, the attractor consists of the only value identical to the limiting inner angle, $\omega^{\infty-1} \equiv \omega_q^{\&}$ where q is fixed, cf. previous paragraph 6.6.2.

We can plot a graph of the last inner angles $\omega^{n_{N-1}}$ for all sequences *ending* with the same term as N increases. Depending on the final q_k (of the period $\{q_k\}_{k=1}^{a}$) which closes these sequences we can distinguish a sets/lines for sequences of the length N. Similarly to the case of constant sequences, the existence of limiting inner angles guarantees that for large N the values $\omega^{n_{N-k}}$ for the trailing terms within periodical sequences $\{\omega^0, \omega^{n_1}, ..., \omega^{n_{N-2}}, \omega^{n_{N-1}}\}$ will be essentially equal to these limiting values, i.e., $\omega^{n_{N-k}} \approx \omega^{\infty-\mathrm{Mod}(N-k,a)}$ (respectively $\omega^{n_{N-k}} \approx \omega^{\infty-a}$ for $\mathrm{Mod}(N-k, a) = 0$) for $N \gg k$, where Mod is the modulo function and a is the period.

Two lines in diagram 6.12, which connect the last inner angles $\omega^{n_{N-1}}$, correspond to two set of sequences ending with the same terms: The first (purple) line, which ends with $\{...pqpqp\}$, approaches the limiting angle $\omega_p^{\infty-1}$, while the second (red) line, which ends with $\{...qpqpq\}$, approaches the limiting angle $\omega_q^{\infty-1}$, as calculated in eq. (6.29). In contrast, two zig-zag lines, which connect the last inner angles, correspond to two set of sequences – as computed – *starting with the same terms*: Thus, the first zig-zag (red) line starts with $\{pqpqp...\}$, while the second zig-zag (purple) line starts with $\{qpqpq...\}$.

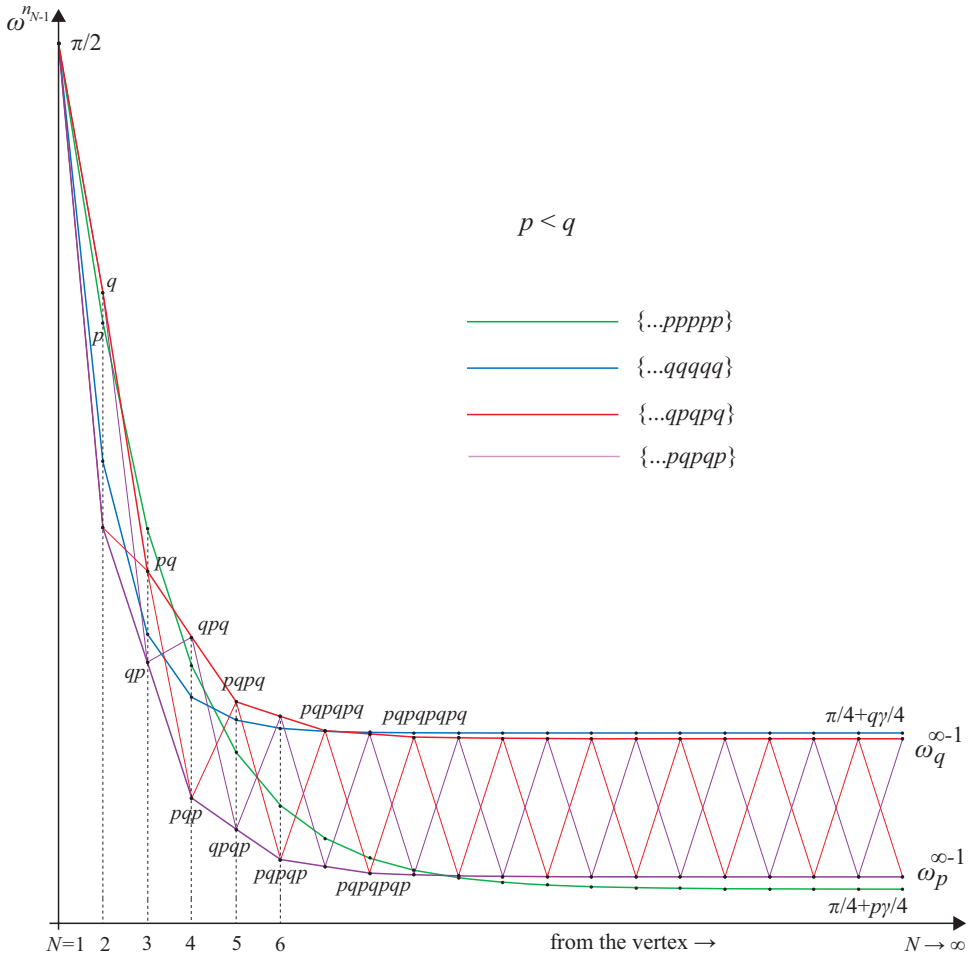

Figure 6.12: **Limiting inner angles of sequences {...*pqpqp*} and {...*qpqpq*}.** Obviously, last inner angles $\omega^{n_{N-1}}$ of sequences {...*pqpqp*} and {...*qpqpq*} approach limiting values $\omega_p^{\infty-1}$ and $\omega_q^{\infty-1}$ as calculated in eq. (6.29). Thus, limiting angles $\omega_p^{\infty-1}$, respectively $\omega_q^{\infty-1}$, correspond to sequences *ending with the same terms*: The first (purple) line ends with {...*pqpqp*}, while the second (red) line ends with {...*qpqpq*}. In contrast, two zig-zag lines connect the last inner angles which correspond to two different sequences – as computed – *starting with the same terms*: Thus, the first zig-zag (red) line starts with {*pqpqp*...}, while the second zig-zag (purple) line starts with {*qpqpq*...}. For comparison, lines corresponding to sequences with the constant value of i_k have been depicted: Namely, the sequence {...*ppppp*} with the limit value $\frac{\pi+p\gamma}{4}$ (green line), and the sequence {...*qqqqq*} with the limit value $\frac{\pi+q\gamma}{4}$ (blue line).

For comparison, lines corresponding to sequences with the constant value of i_k have been also depicted in fig. 6.12: Namely, the sequence {...*ppppp*} with the limit value $\frac{\pi+p\gamma}{4}$ (green line), and the sequence {...*qqqqq*} with the limit value $\frac{\pi+q\gamma}{4}$ (blue line).

For example, if a pair of numbers $p \neq q$ repeats periodically within a sequence $\{i_k\}_{k=0}^{\infty}$, i.e., $i_{2k} = p$ and $i_{2k-1} = q$ for any k, the sequence of inner angles ω^{n_k} is determined by two functions $f(\omega^{n_{k-1}}; p, q)$ and $f(\omega^{n_k}; q, p)$. In order to determine its attractor for this periodical sequence we substitute p and q into eq. (6.8) to obtain

system of two equations

$$q\sin(\omega_p^{\&} - q\frac{\gamma}{2})\cos(\omega_q^{\&} - p\frac{\gamma}{2})\sin(p\frac{\gamma}{2}) = p\cos(\omega_p^{\&})\sin(\omega_q^{\&})\sin(q\frac{\gamma}{2}),$$

$$p\sin(\omega_q^{\&} - p\frac{\gamma}{2})\cos(\omega_p^{\&} - q\frac{\gamma}{2})\sin(q\frac{\gamma}{2}) = q\cos(\omega_q^{\&})\sin(\omega_p^{\&})\sin(p\frac{\gamma}{2}).$$

where solutions $\omega_p^{\&}$ and $\omega_q^{\&}$ denote two limiting inner angles $\omega_p^{\infty-1}$ and $\omega_q^{\infty-1}$ for sequences ending by p $(= i_{N-1})$, respectively by q $(= i_{N-1})$, self-intersections, and are expressed in appendix D. Analogously, an attractor consisting of limiting inner angles could be computed for any periodical sequence $\{...q_N q_{N-a}...q_{N-1}q_N q_{N-a}...q_{N-1}q_N\}$.

In the case of general (non-periodic) sequences, exact values of limiting inner angles cannot be found. However, we expect that limiting inner angles should be represented by converging lines analogical to instances of constant sequences or periodical sequences: If we assume a long enough arbitrary sequence, starting at the outermost end, then adding self-collisions at the innermost end should not influence values of last inner angles, radial distances, etc. In other words, limiting inner angles should be invariant with respect to the extending and/or changing of general sequences at the innermost end. It is numerical evidence that there exists the maximal, respectively minimal, value which fixes the upper, respectively lower, boundary on limit inner angles. The upper boundary is equal to $\frac{\pi+i_{\max}\gamma}{4}$, while the lower boundary is equal to $\frac{\pi+\gamma}{4}$. In the case of periodical sequences, we can specify even the range of limit inner angles within the attractors: $[\frac{\pi+q_{\min}}{4}, \frac{\pi+q_{\max}}{4}]$ where $q_{\max}$, $q_{\min}$ denote the maximal, respectively minimal, term of the repeating subsequence $\{q_k\}_{k=1}^{a}$.

6.7 Behavior of other quantities for $N \to \infty$

In our study of behavior of other quantities for $N \to \infty$ we start with the outer radial distance r^{n_N} since all other explored quantities are directly proportional to it.

6.7.1 The outer radial distance r^{n_N}

From equation (6.14), respectively (6.18), it follows that the outer radial distance r^{n_N} is finite for any sequence $\{i_k\}_{k=0}^{N}$ with the impact parameter from the range $\rho \in [-\rho_{\max}, \rho_{\max}]$. In the previous section we have shown that last inner angles $\omega^{n_{N-1}}$ approach limiting inner angles $\omega^{\infty-1}$ for arbitrary sequences. Hence, we can conclude that also the outer radial distance r^{n_N} converges to a finite value r^{∞}. More accurately, the outer radial distance r^{n_N} either decreases, or increases to the limiting value for $N \to \infty$, since there exist two self-colliding solutions for given initial parameters u and ρ.

As we are able to determine the exact limiting inner angles for fixed and periodical sequences, we can specify also corresponding values r^{∞} for such sequences. For example, in the case of constant sequences $\{q\}_{k=0}^{\infty}$, the limit of the outer radial distance r^{∞} can

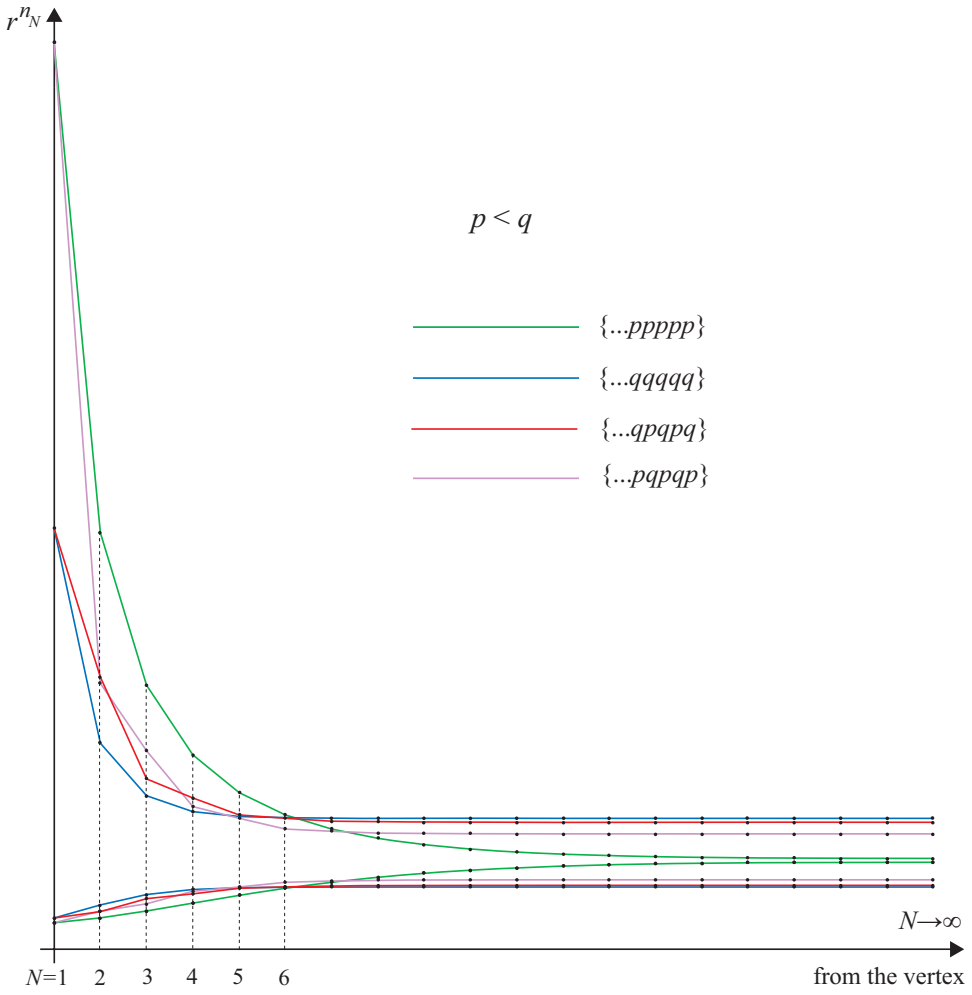

Figure 6.13: **The radial distance r^{n_N} as a function of the number N of self-collisions.** Since we have shown that last inner angles $\omega^{n_{N-1}}$ approach limiting inner angles $\omega^{\infty-1}$ for arbitrary sequences $\{i_k\}_{k=0}^{\infty}$, we can conclude that also the outer radial distances r^{n_N} converges to finite values r^{∞}, cf. relation (6.14). More accurately, the outer radial distance r^{n_N} either decreases, or increases to the limit for $N \to \infty$, since there exist two self-colliding solutions for given initial parameters u and ρ. As we are able to determine exact limiting inner angles for fixed and periodical sequences, we can specify also corresponding values r^{∞} for such sequences. In this diagram we can see values r^{n_N} for increasing N for the constant sequences $\{p\}_{k=0}^{N}$ (green) and $\{q\}_{k=0}^{N}$ (blue), and for the periodical sequences $\{...qpqp\}$ (purple) and $\{...pqpq\}$ (red).

be expressed as

$$r^{\infty} = \frac{qu\Delta t}{2\sqrt{2}\sin(q\frac{\gamma}{2})}\sqrt{1 \pm \sqrt{1 - \frac{16\rho^2 \sin^2(q\frac{\gamma}{2})}{(qu\Delta t)^2}}}\,, \tag{6.30}$$

cf. eq. (6.18). In diagram 6.13 we can see values r^{n_N} for increasing N for constant sequences $\{p\}_{k=0}^{N}$ (green) and $\{q\}_{k=0}^{N}$ (blue), and for periodical sequences $\{...qpqp\}$ (purple) and $\{...pqpq\}$ (red).

Obviously, the limiting outer radius r^{∞} is maximal for $q = i_{\max}$ and $\rho = 0$. Thus,

the value

$$r^{\infty} = \frac{i_{\max} u \Delta t}{2\sqrt{2}\sin(i_{\max}\frac{\gamma}{2})} ,$$

separates the region with finite number of solutions

$$r \in \left[\frac{i_{\max} u \Delta t}{2\sqrt{2}\sin(i_{\max}\frac{\gamma}{2})}, \infty \right] ,$$

from the region with infinite number of solutions

$$r \in \left[0, \frac{i_{\max} u \Delta t}{2\sqrt{2}\sin(i_{\max}\frac{\gamma}{2})} \right] ,$$

cf. paragraph 6.3.

6.7.2 Inner radial distances and lengths of paths between two self-collisions

In this paragraph we will look at the behavior of radial distances r^{n_k} of inner self-collisions, cf. eq. (6.7), and lengths of paths between two inner self-collisions $\sum_{j=n_k}^{n_{k+1}-1} s^j$, cf. eq. (6.6). First, we have to distinguish two types of limits taken for $N \to \infty$: (i) Either we evaluate inner radial distances and paths for n_k with fixed k, or (ii) we figure out radii and paths for n_{N-k} with constant k. Let us investigate both types separately.

The first limit determines behavior of radial distances and lengths of segments in the vicinity of the vertex since k is fixed while $N \to \infty$. In diagram 6.14 we can see how inner radii r^{n_k} and paths $\sum_j s^j$ quickly approach zero, i.e.,

$$r^{n_k} \xrightarrow{N\to\infty} 0, \qquad \sum_{j=n_k}^{n_{k+1}-1} s^j \xrightarrow{N\to\infty} 0.$$

because the product, in equations (6.7) and (6.6), is over terms smaller than one. Hence, most of the inner loops are cumulated next to the vertex. Notice that the path between inner self-collisions is shortened as it approaches the vertex while time to pass the loop remains the same Δt. This implies that velocities u^{n_k} reduce for $k \to 0$, or also

$$u^{n_k} \xrightarrow{N\to\infty} 0,$$

which is in accord with conclusion of section 6.2.2. Moreover, vanishing values of lengths $\sum_{j=n_k}^{n_{k+1}-1} s^j$, when k is fixed and $N \to \infty$, guarantee that the length of the whole path can be finite even for infinite number of self-collisions.

The second limit describes radial distances and lengths of segments from the view of the external observer, i.e., in the neighborhood of the outer self-collision. Indeed, the $N-k$ self-collision is separated from the outer one just by (fixed) k self-collisions for $N \to \infty$. The radial distance $r^{n_{N-k}}$ is equal to the outer radial distance r^{n_N} multiplied by a constant factor smaller than one. As the outer radius converges to a limit for $N \to \infty$ the value $r^{n_{N-k}}$ remains virtually constant, cf. graph 6.13.

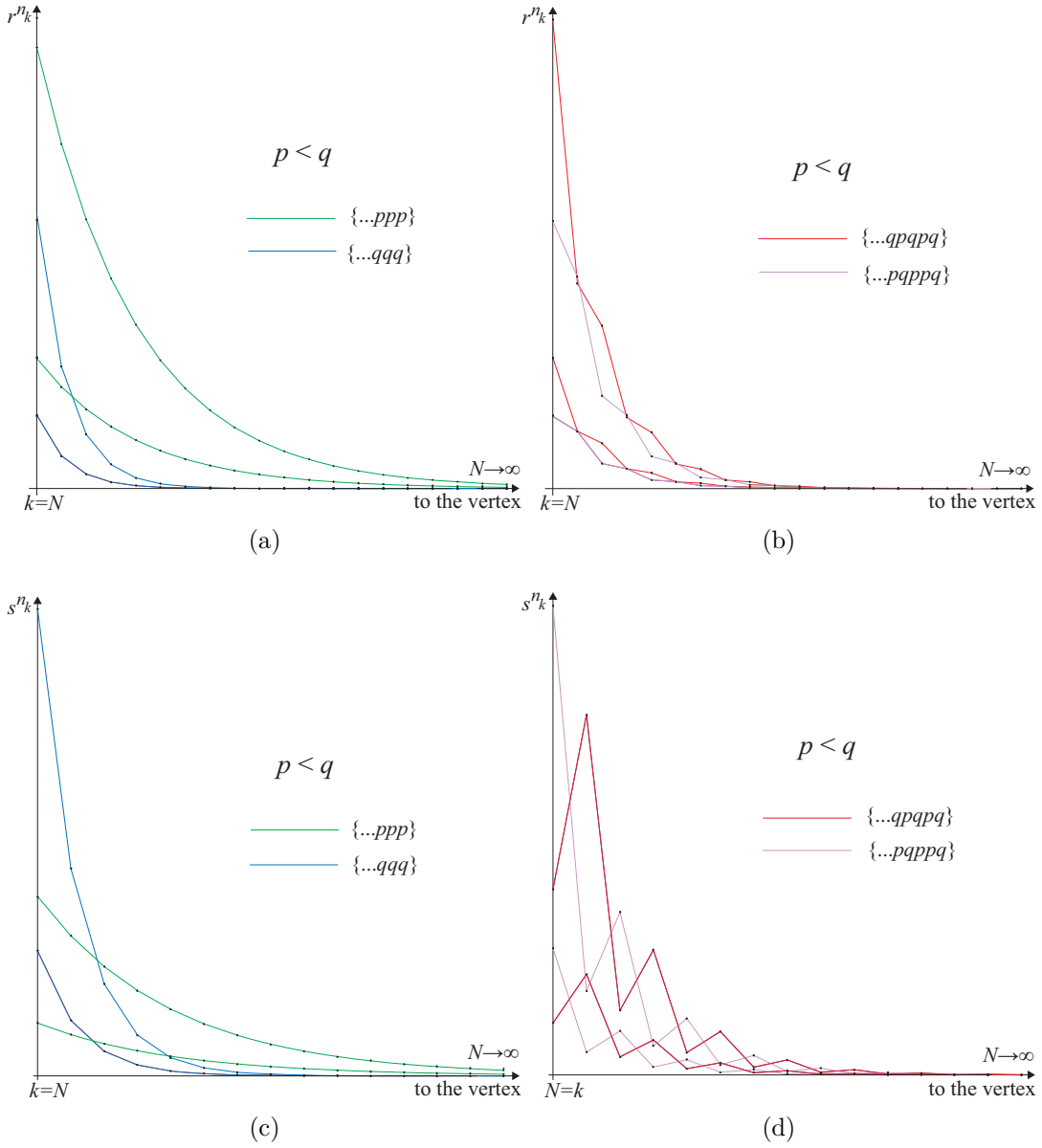

Figure 6.14: **Inner radial distances and lengths of paths between two self-collisions when n_k is fixed and $N \to \infty$.** We can see how radial distances r^{n_k} (upper diagrams) and lengths $\sum_{j=n_k}^{n_{k+1}-1} s^j$ (bottom diagrams) quickly approach zero because of the product in eqs. (6.7) and (6.6). Hence, most of inner loops are cumulated next to the vertex when $N \to \infty$. Moreover, vanishing values of lengths $\sum_{j=n_k}^{n_{k+1}-1} s^j$ guarantee that the length of the whole path can be finite even for infinite number of self-collisions.

Starting from the outer self-collision, the following inner radial distances are given by multiplying by a factor

$$\frac{\sin(\omega^{\infty-k} - i_{\infty-k}\frac{\gamma}{2})}{\sin\omega^{\infty-k}},$$

where $\omega^{\infty-k}$ denotes a limiting inner angle and $i_{\infty-k}$ its separation from $\omega^{\infty-k-1}$, cf.

eq. (6.7). Moreover, in the case of periodical sequences, there is a constant factor

$$\prod_{j=1}^{a} \frac{\sin(\omega^{\infty-j} - i_{\infty-j}\frac{\gamma}{2})}{\sin \omega^{\infty-j}}, \tag{6.31}$$

which transforms a radial distances $r^{\infty-1}, ..., r^{\infty-a}$ into $r^{\infty-a-1}, ..., r^{\infty-2a}$. Because radial distances r^{n_k} and lengths of paths between the k-th and $k+1$-th self-collision are related by the factor

$$\frac{\sin(i_k\frac{\gamma}{2})}{\sin(\omega^{n_k} - i_k\frac{\gamma}{2})},$$

cf. eq. (6.6), lengths $s^{\infty-1}, ..., s^{\infty-a}$ are rescaled in the same way within periodical sequences, where $s^{\infty-1}$ represent sum of segments between the last inner self-collision and the outer self-collision.

In other words, thanks to the conical geometry and the fact that the last inner angles converge to fixed values, pattern made of a self-collisions, where a is a period, is periodically reproduced as receding the outer self-collision. Of course, the pattern is scaled down by constant factor (6.31) in each repetition. Finally, notice that nonvanishing values of lengths $\sum_{j=n_{N-k}}^{n_{N-k+1}-1} s^j$ coming from outermost loops, when k is fixed and $N \to \infty$, guarantee nontrivial contributions into the sum for the whole path, see the next paragraph.

6.7.3 Length S of the whole inner path

The formula for the length of the whole inner path is given by sum over all inner path segments

$$S^N = \sum_{k=0}^{N-1} \sum_{j=n_k}^{n_{k+1}-1} s^j = r^{n_N} \sum_{k=0}^{N-1} \frac{\sin(i_k\frac{\gamma}{2})}{\sin(\omega^{n_k} - i_k\frac{\gamma}{2})} \prod_{j=k}^{N-1} \frac{\sin(\omega^{n_j} - i_j\frac{\gamma}{2})}{\sin(\omega^{n_j})}\,. \tag{6.32}$$

In diagram 6.15a we can see that the length of the whole inner path S^N is an increasing function of N converging to the limiting value $\sum_{k=0}^{N\to\infty} s^{n_k} \equiv S^\infty$. Specifically, blue and green lines represent lengths of constant sequences while red and purple lines correspond to periodical sequences.

In the previous paragraph 6.7.2 we have shown that most of inner loops cumulates next to the vertex for $N \to \infty$ which guarantees that the sum S^∞ over infinite number of inner path segments (connecting infinite number of self-collisions) is finite. Obviously, the sum is determined by contributions from outermost loops. The value S^∞ can be computed by two methods: Either by limiting the recurrent formula derived from the sum (6.32), or by summing the infinite geometric progression resulting from the sum (6.32) after substitution of limiting inner angles $\omega^{\infty-1}$, see calculations in appendices E and F.

For constant sequences, $\{q\}_{k=0}^N$, the formula (6.32) reduces into

$$S^N = \sum_{k=0}^{N-1} s^{qk} = r^{qN} \sum_{k=0}^{N-1} \frac{\sin(q\frac{\gamma}{2})}{\sin(\omega^{qk} - q\frac{\gamma}{2})} \prod_{j=k}^{N-1} \frac{\sin(\omega^{qj} - q\frac{\gamma}{2})}{\sin(\omega^{qj})}\,. \tag{6.33}$$

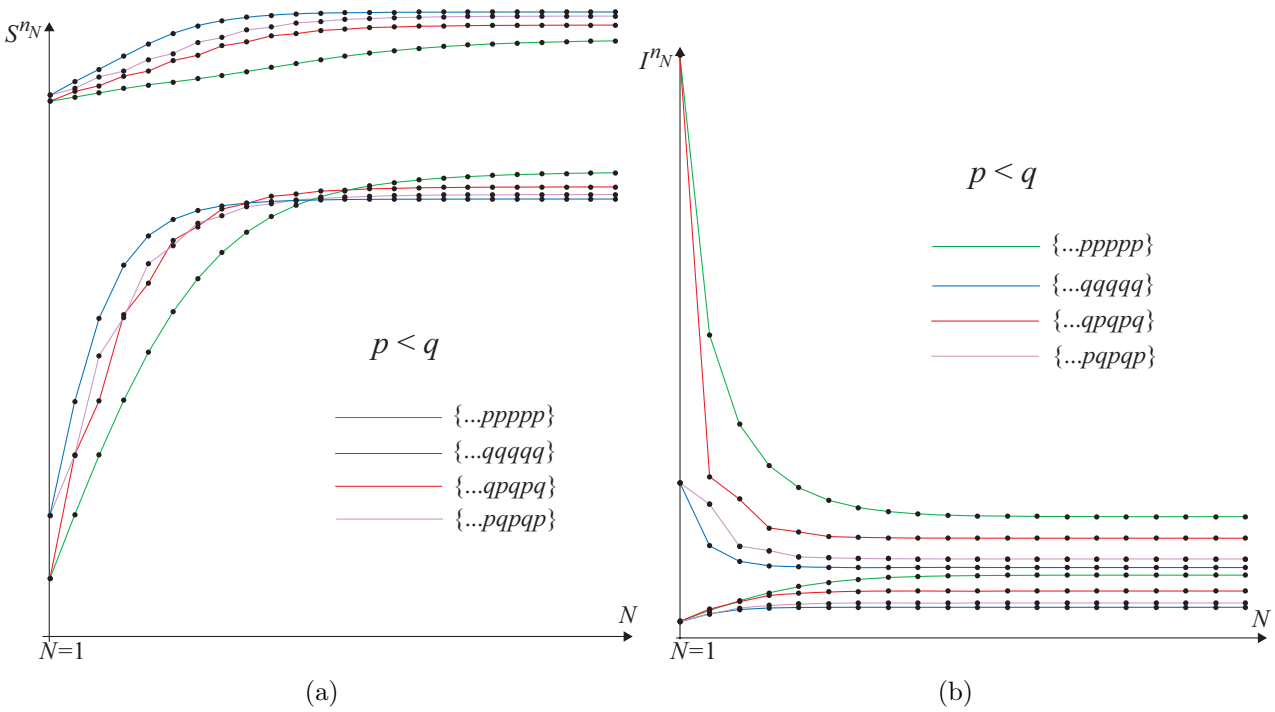

Figure 6.15: **Length S and action I of the whole inner path.** (a) The length of the whole inner path S^N is an increasing function of N converging to the limiting value $\sum_{k=0}^{N\to\infty} s^{n_k} \equiv S^\infty$. It can be shown that the sum S^∞ over infinite number of inner path segments is finite. Blue and green lines represent lengths of constant sequences while red and purple lines correspond to periodical sequences. (b) The action of the whole inner path I^N partly reproduces behavior of the outer radial distance r^{n_N}. As the radius r^{n_N} is finite for each N the action I^N of the inner path for $N \to \infty$ self-collisions is finite as well. In diagram (b) we can see the action I^N for constant sequences (blue and green lines) and for periodical sequences (red and purple lines).

The corresponding infinite sum S^∞ is equal to

$$S^\infty = \sqrt{2}\ r^\infty \cos(q\frac{\gamma}{4})\ ,$$

cf. appendix E, where the radial distance r^∞ is defined by eq. (6.30). Accordingly, the length S^∞ is finite and can be exactly computed for periodical sequences. In appendix F the sum S^∞ is expressed for the periodical sequence with the period $a = 2$, i.e., consisting of the subsequence $\{pq\}$.

6.7.4 Action I of the whole inner path

We define the action I^N of the whole inner path with N self-collisions and derive

the formula for it:

$$I^N = \frac{m}{2}\int v^2 \mathrm{d}t = \frac{m}{2}\sum_{k=0}^{N-1}\int \left(\frac{2\sum_{j=n_k}^{n_{k+1}-1} s^j}{i_k \Delta t}\right)^2 \mathrm{d}t = 2m\sum_{k=0}^{N-1}\left(\frac{\sum_{j=n_k}^{n_{k+1}-1} s^j}{i_k \Delta t}\right)^2 \Delta t =$$

$$= \frac{2m}{\Delta t}\sum_{k=0}^{N-1}\left(\sum_{j=n_k}^{n_{k+1}-1}\frac{s^j}{i_k}\right)^2 = \frac{2m}{\Delta t}\left(r^{n_N}\right)^2 \sum_{k=0}^{N-1}\left[\frac{\sin(i_k\frac{\gamma}{2})}{i_k \sin(\omega^{n_k} - i_k\frac{\gamma}{2})}\prod_{j=k}^{N-1}\frac{\sin(\omega^{n_j} - i_j\frac{\gamma}{2})}{\sin(\omega^{n_j})}\right]^2, \tag{6.34}$$

The sum of squares represents increasing function of N which approaches a limit value for $N \to \infty$. This is shown in appendix G for constant sequences. As the radial distance r^{n_N} is finite for each N the action I^N of the inner path for $N \to \infty$ self-collisions is finite as well. Notice that behavior of the action I^N corresponds directly to the behavior of the radius r^{n_N}: increasing r^{n_N} results in rising I^N, while decreasing r^{n_N} leads to falling I^N, cf. diagrams 6.13 and 6.15b. In diagram 6.15b we can see the action I^N for constant sequences, blue and green lines, and for periodical sequences, red and purple lines.

For constant sequences formula (6.34) reduces to

$$I^N = \frac{2m}{\Delta t}\left(r^{qN}\right)^2 \sum_{k=0}^{N-1}\left[\frac{\sin(q\frac{\gamma}{2})}{q\sin(\omega^{qk} - q\frac{\gamma}{2})}\prod_{j=k}^{N-1}\frac{\sin(\omega^{qj} - q\frac{\gamma}{2})}{\sin(\omega^{qj})}\right]^2. \tag{6.35}$$

It is derived in appendix G that the action I^∞ for infinite number of self-collision is equal to

$$I^\infty = \frac{2m}{\Delta t}\left(r^\infty\right)^2 \sin(q\frac{\gamma}{2}),$$

where the radial distance r^∞ is expressed in eq. (6.30). From comparison of formulas (6.32) and (6.34) it follows that both methods used for computation of the length S^∞ can be used to determine the I^∞, see appendix G. Obviously, calculation of I^∞ for periodical sequences would be analogical to that of S^∞ as well.

Conclusion

Recapitulation

In this work we have investigated a simple interacting system in the space with a nontrivial causal structure, cf. [21, 22]. We have considered model of an elastically interacting particle in the non-relativistic space with a time machine realized by a wormhole with a time shift. We have required that standard local physical laws hold and searched for their globally consistent solutions, i.e, we have assumed the validity of the principle of self-consistency. If there were a nontrivial set of initial conditions which would violate this principle, the system would be logically inconsistent. We have shown that the investigated system is not inconsistent in this sense and thus confirmed results obtained for similar systems studied, e.g., in [14]. Specifically, we have found that a globally consistent evolution exists for all natural initial conditions, and, moreover, that more than one solution exists for a wide class of initial conditions. Thus, the evolution of the described system is not unique. Thanks to the chosen model we have been able carry out a detailed explicit analysis of the structure of solutions even for multiply interacting system.

The content of the first chapter is partly a review of the known problems related to time machines and partly a very brief introduction to the wormhole time machines. In the second chapter we have defined the (non-relativistic) conical spacetime with induced time shift which provided the background for a study of trajectories in the presence of the time machine. The main reason for the restriction to the non-relativistic case is the billiard character of collisions, i.e., collisions of rigid spherical balls, which allowed us to formulate the problem explicitly. The third chapter was devoted to formulation of the rules of motion. Also, the dangerous initial conditions which could lead to the paradoxical situations have been defined. Next, the rules of self-collisions have been analyzed and possible types of self-collisions have been found. At last, we have specified geometry of self-collisions and investigated another symmetry resulting from the conical geometry.

In the fourth chapter we have considered the limit of the point-like particle, $R \to 0$, which has turned out to be scale invariant. First, we have introduced parameters for initial trajectories and defined quantities describing self-collisions on these trajectories. Then we have looked at collision-free trajectories and specified the conditions for the self-collisions. We have concentrated on the self-collision occurring closest to the axis on the cone on which only one self-intersection is allowed. Next, we have demonstrated

that there exist globally consistent evolutions for this system in the presence of the time machine and shown that these evolutions are not unique. Finally, we have investigated the asymptotic behavior of the initial and final trajectory as it differs in the total time contribution due to the distinct angular and temporal location of the self-collision.

However, the point particle model is not rich enough to investigate structure of trajectories corresponding to the dangerous initial conditions. Hence, in the fifth chapter the discussion has been extended to the case of non-relativistic, freely moving solid balls with finite radius, $R > 0$. We have focused again on the self-collision occurring closest to the apex. After we derived and analyzed relations for such a self-collision, we have separated two types of self-collisions indistinguishable in the point-like case. Next, we have shown that the free trajectories given by the dangerous initial conditions can be replaced by the trajectories possessing self-collisions to avoid paradoxical situations. Thus we have found that a number of solutions for given initial data is conserved, i.e., it is the same for the dangerous initial data as for the generic ones. Finally, we have expressed geometrical restrictions imposing constraints on initial values u and ρ which ensure that the ball fits in the conical space.

Till the last chapter we have considered only trajectories with at most one self-collision. However, in principle, it can happen that the particle self-collides more times and it really happens. Such a possibility enlarges a number of solutions for given initial data and thus complicates the discussion of all possible particle motions. Because of the complexity of the system – determined by the number of occurrence of the particle – we have switched back to the point-like (and scale invariant) case. We have found that geometry of the inner self-collisions is entirely given by the apex angle γ and the chosen sequence of self-events and that the inner self-collisions are always of type I. Next, we have derived the equation for the outer self-collisions and explicated the way of addition of extra self-collisions into the sequences. This equation has allowed us to formulate the explicit expressions for the limits on the impact parameter $\rho_{\max}$ (admitting the outer self-collisions) for various classes of sequences. On this basis we have been able to separate the range of ρ with finite number of solutions from the interval with an infinite number of solutions. Analogously to the case of one self-collision of the point-particle, we have shown that any paradoxical self-intersection occurring at the end of the sequence can be superseded by the corresponding (and geometrically indistinguishable in the point-like case) dangerous self-collision and we have illustrated mechanism of such replacements (between pairs of sequences) in diagrams. Because of plurality of solutions for the given initial conditions we have investigated asymptotic behavior of solutions in the following paragraph and calculated relations for the total time contribution gained along trajectories passing through the time machine. Finally, we have concentrated on infinite sequences of self-collisions since they serve as a good approximation of very long sequences and studied behavior of all relevant quantities. We have found that the periodical sequences play especially important role in understanding of this behavior. We have obtained that sequences with infinite self-collisions define finite inner path and finite action along this path.

Let us summarize our work. We have studied the system of a (billiard) particle moving in a non-relativistic space with the time machine which is very close to that of [14]. We have confirmed that all initial conditions have globally consistent and non-unique evolutions in the presence of time machine. However, since we have chosen a different time-machine configuration (which significantly simplifies the analysis) we

have been able to solve the equations of motion explicitly which has allowed us a very detailed study of various attributes of motion within the time machine spacetime. At the same time, the model is sufficiently nontrivial to reproduce the most important features of systems with time machines. Moreover, this elaborated model can be reused for another analysis, for example, study of systems with multiple self-collisions of the finite ball which can be necessary for resolution of some of open problems, see paragraph bellow.

Open problems and future prospects

We have found that a number of solutions for given initial data is the same for dangerous initial data as for generic ones in the natural configuration, $\gamma > \pi/2$, for one self-collision. But, when we have considered the structure of solutions for the *finite ball* for $\gamma < \pi/2$ we have found a gap in the solution curves, cf. par. 5.4. This could indicate that there could exist a nontrivial set of paradoxical initial conditions when the solutions evolved from these conditions are really restricted. However, in this case, $\gamma < \pi/2$, there is the possibility of multiple self-intersections between several self-collisions which remains as open problem. It is supposed that such analysis of multiple self-collisions would complicate the discussion significantly though it is treatable due to the simplicity of the model. However, from the obtained results of multiple self-collisions of the point-particle it is far from clear if it resolved this problem.

The problem complicates even more when we realize that a role in filling the solution gap could play evolutions with the so-called ghost particle. Such a particle appears from the time machine, hits the particle coming from infinity, and deflects itself back to the time machine so as to reappear it in the mentioned way. This evolution posses actually two particles. Generalized evolutions with multiple self-collisions involve multiple particles occurring on variety of inner loops, in opposition to multiple versions of one particle examined in this work.

It would also be interesting to derive such a quantity as the action with respect to the initial and final time and position. Along with the action of the inner trajectory we would obtain the total action which would allow to compute corresponding probabilities for different evolutions for given initial and final points. This task is, however, complicated by the fact that trajectories given by the same initial position diverges from each other and thus the particle occurs at the final time at different locations. However, this problem could be resolved by an appropriate reformulation of the model. And if we were able to assign probabilities to different evolutions we would have a better insight to indeterminism implied by the multiplicity of solutions for given initial conditions.

Bibliography

[1] R. Penrose. *The Emperor's New Mind*. Oxford University Press, 1990.

[2] K. Gödel. An example of a new type of cosmological solution of Einstein's field equation of gravitation. *Rev. Mod. Phys.*, 21:447, 1949.

[3] F. J. Tipler. Rotating cylinders and the possibility of global causality violation. *Phys. Rev. Lett.*, 9:2203, 1974.

[4] M. S. Morris and K. S. Thorne. Wormholes in Spacetime and Their Use for Interstellar Travel: A Tool for Teaching General Relativity. *Am. J. Phys.*, 56:395, 1988.

[5] III Gott, J. R. Closed Timelike Curves Produced by Pairs of Moving Cosmic Strings: Exact Solutions. *Phys. Rev. Lett.*, 66:1126, 1991.

[6] M. Visser. *Lorentzian Wormholes: From Einstein to Hawking*. AIP Series in Computational and Applied Mathematical Physics, New York, 1995.

[7] K. S. Thorne. *Black Holes and Time Warps: Einstein's Outrageous Legacy*. W.W. Norton & Company, New York, 1994.

[8] J. R. III Gott. *Time Travel in Einstein's Universe: The Physical Possibilities of Travel Through Time*. Mariner Books, Boston, 2002.

[9] S. V. Krasnikov. Time Machine (1988-2001). *ArXiv General Relativity and Quantum Cosmology e-prints*, 2003.

[10] S. V. Krasnikov. Time travel paradox. *Phys. Rev. D*, 65:064013, 2002.

[11] I. Novikov. Time machines and self-consistent evolution in problems with self-interaction. *Phys. Rev. D*, 45:1989, 1992.

[12] J. L. Friedman, M. S. Morris, I. D. Novikov, F. Echeverria, G. Klinkhammer, K. S. Thorne, and U. Yurtsever. Cauchy Problem in Spacetimes with Closed Timelike Curves. *Phys. Rev. D*, 42:1915, 1990.

[13] A. Carlini, V. P. Frolov, M. B. Mensky, I. D. Novikov, and H. H. Soleng. Time Machines: the Principle of Self-Consistency as a consequence of the Principle of Minimal Action. *Int. J. Mod. Phys. D*, 4:557, 1995.

[14] F. Echeverria, G. Klinkhammer, and K. S. Thorne. Billiard Balls in Wormhole Spacetimes with Closed Timelike Curves: Classical Theory. *Phys. Rev. D*, 44:1077, 1991.

[15] M. B. Mensky and I. D. Novikov. Three-Dimensional Billiards with Time Machine. *Int. J. Mod. Phy. D*, 5:179, 1996.

[16] J. L. Friedman and M. S. Morris. The Cauchy Problem for the Scalar Wave Equation is Well Defined on a Class of Spacetimes with Closed Timelike Curves. *Phys. Rev. Lett.*, 66:401, 1991.

[17] K. Schleich and D. M. Witt. Topological Censorship. *ArXiv General Relativity and Quantum Cosmology e-prints*, 1999.

[18] J. L. Friedman, K. Schleich, and D. M. Witt. Topological Censorship. *Phys. Rev. Lett.*, 71:1486, 1993.

[19] M. S. Morris, K. S. Thorne, and U. Yurtsever. Wormholes, Time Machines, and the Weak Energy Condition. *Phys. Rev. Lett.*, 61:1446, 1988.

[20] V. P. Frolov and I. D. Novikov. Physical Effects in Wormholes and Time Machines. *Phys. Rev. D*, 42:1057, 1990.

[21] J. Dolanský and P. Krtouš. Billiard ball in the space with a time machine. *Phys. Rev. D*, 82:124056, 2010.

[22] J. Dolanský and P. Krtouš. Trajectories in presence of the time machine. *in Proceedings of the 16-th Conference of Czech and Slovak Physicists*, 2008.

Appendix A

Lengths of paths between self-collisions

In order to derive equations for self-collisions we have to determine lengths of paths between two self-collisions. These can be easily derived in the parametrization with $\varphi = 0$ and $\psi = 0$, when self-intersections and self-interactions are located either on the wormhole, or on the opposite radial line, cf. figure A.1.

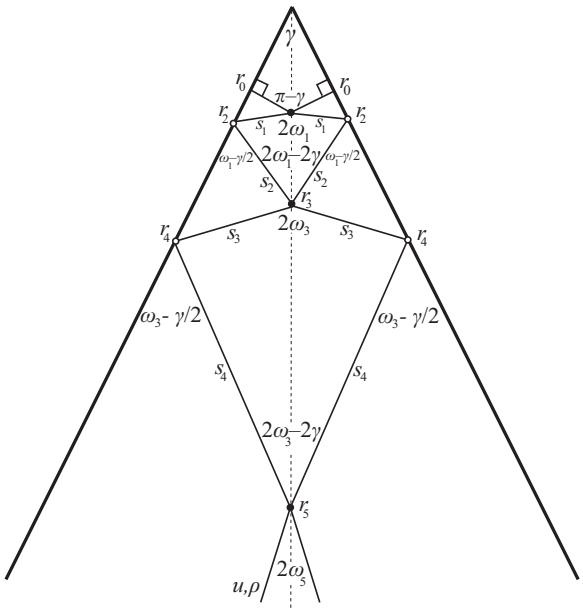

Figure A.1: **The parametrization with $\varphi = 0$.** This parametrization is convenient for deriving relations which determine lengths of paths between two self-collisions.

First, we realize that the particle has to travel to the past along all inner loops, otherwise it would prevent itself from another self-collision. In other words, the angles ω^p, for $p = 0, ..., n_N - 1$, have to be positive. Hence, the angle ω^p assigned to the p-th self-intersection following the $(p-1)$-th self-event decreases by $\frac{\gamma}{2}$

$$\omega^p = \omega^{p-1} - \frac{\gamma}{2},$$

as the self-intersections (as well as self-collisions) occur alternately on two opposite radial lines, cf. section 2.2. Generally, to determine any angle ω^p for $n_{k+1} > p \geq n_k$ corresponding to a self-intersection which follows the n_k-th self-collision and precedes the n_{k+1}-th self-collision we have to *subtract* multiples of $\frac{\gamma}{2}$ to receive

$$\omega^p = \omega^{n_k} - (p - n_k)\frac{\gamma}{2}, \tag{A.1}$$

for $k = 1, ..., N$. As an example see figure 6.1 with just one free passage after the first ($\omega^2 = \omega^1 - \frac{\gamma}{2}$) and third self-collision ($\omega^4 = \omega^3 - \frac{\gamma}{2}$).

A.1 Length of a particular path segment

Let us first express relations for lengths of particular path segments between two self-collisions. For radial distances r^p, $p = 0, ..., P$, and path segments s^p, $p = 0, ..., P-1$, we obtain

$$\frac{s^p}{\sin\frac{\gamma}{2}} = \frac{r^{p+1}}{\sin\omega^p} = \frac{r^p}{\sin(\omega^p - \frac{\gamma}{2})}, \tag{A.2}$$

due to the sinus theorem, cf. fig. A.1. We can thus relate all radial distances r^p, lengths s^p and directions ω^p are related to the radial distance of the outer self-collision r^{n_N} which is defined by the constraint

$$r^{n_N} = \frac{\rho}{\sin\omega^{n_N}}, \tag{A.3}$$

cf. equation (4.2).

Indeed, the second equality in eq. (A.2) implies the recurrent formula for radial distances

$$r^p = r^{p+1}\frac{\sin(\omega^p - \frac{\gamma}{2})}{\sin\omega^p},$$

for both self-intersections and self-collisions. Moreover, for $n_k \leq p \leq q < n_{k+1}$ we can generalize the above formula as

$$r^p = r^q\frac{\sin(\omega^p - (q-p)\frac{\gamma}{2})}{\sin\omega^p}, \tag{A.4}$$

where both natural numbers p and q lie between the n_k-th and the n_{k+1}-th self-collision, cf. figure A.2.

If we substitute $p = n_k$ and $q = n_{k+1} = n_k + i_k$ into eq. (A.4) we obtain

$$r^{n_k} = r^{n_{k+1}}\frac{\sin(\omega^{n_k} - i_k\frac{\gamma}{2})}{\sin\omega^{n_k}}.$$

Step-by-step multiplication from the outer, i.e., most remote, n_N-th self-collision to the n_k-th radial distance gives

$$r^{n_k} = r^{n_N}\prod_{j=k}^{N-1}\frac{\sin(\omega^{n_j} - i_j\frac{\gamma}{2})}{\sin\omega^{n_j}}. \tag{A.5}$$

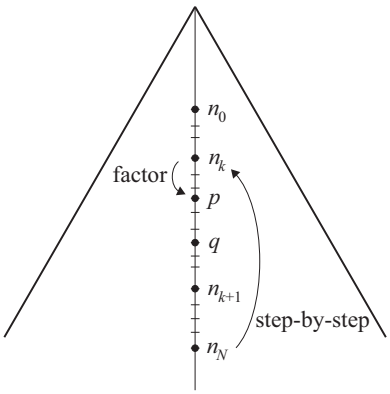

Figure A.2: **Schema of computing r^p respective s^p.** Two direction of computation: First, step-by-step multiplication from the outer, i.e., most remote, n_N-th self-collision to the n_k-th radial distance. Second, multiplying the result of the first step by the factor corresponding to the passage from n_k-th self-collision to the p-th radial distance where $p > n_k$.

in accord with the arrow of computation in schema A.2.

For arbitrary $n_k \leq p < n_{k+1}$ and $k < N$ we must multiply expression (A.5) by factor $\frac{\sin\omega^{n_k}}{\sin(\omega^{n_k}-(p-n_k)\gamma/2)}$ corresponding to formula (A.4) for $q = p$ and $p = n_k$ to get radial distances r^p

$$r^p = r^{n_N}\frac{\sin\omega^{n_k}}{\sin(\omega^{n_k}-(p-n_k)\frac{\gamma}{2})}\prod_{j=k}^{N-1}\frac{\sin(\omega^{n_j}-i_j\frac{\gamma}{2})}{\sin\omega^{n_j}}, \tag{A.6}$$

for both self-intersections and self-collisions. Notice that for $k = N$ we have assumed $\prod = 1$.

The second equality in eq. (A.2) enable us to express relation between r^p and s^p

$$s^p = r^p\frac{\sin\frac{\gamma}{2}}{\sin(\omega^p-\frac{\gamma}{2})}, \tag{A.7}$$

which together with relations for arbitrary ω^p, eq. (A.1), and r^p, eq. (A.6), yield final formula for arbitrary path segment s^p

$$s^p = r^{n_N}\frac{\sin\frac{\gamma}{2}}{\sin(\omega^{n_k}-(p-n_k+1)\frac{\gamma}{2})}\frac{\sin\omega^{n_k}}{\sin(\omega^{n_k}-(p-n_k)\frac{\gamma}{2})}\prod_{j=k}^{N-1}\frac{\sin(\omega^{n_j}-i_j\frac{\gamma}{2})}{\sin\omega^{n_j}}. \tag{A.8}$$

A.2 Length of the whole path between two self-collisions

The path between two self-collisions is the straight line (on the cone) since intermediate self-intersections do not change its direction. If we unfold the trajectory together with the cone, see figure A.3, we receive a number of copies of the cone depending on the number of intersections of the path and the wormhole. The two concerned self-collisions become connected by the straight line (in the unfolded plane), and thus we can express the whole path between them using the ordinary sinus theorem.

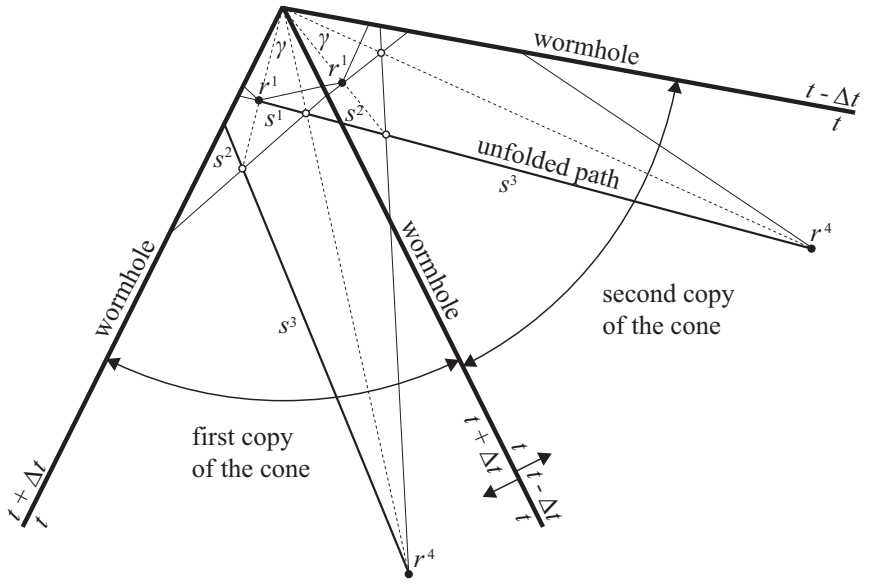

Figure A.3: **The length of the unfolded path between two successive self-collisions.** If we unfold the trajectory together with the cone we receive a number of copies of the cone depending on the number of intersections of the path and the wormhole. The two self-collisions become connected by the straight line (in the unfolded plane), and thus we can express the whole path between them using the ordinary sinus theorem. The length of the unfolded path between the first self-collision, given by (ω^1, r^1), and the second self-collision, given by (ω^4, r^4), is determined by formula (A.2). However, this expression still depends on values of all inner angles with $1 < j < N$.

Analogically to the equation (A.2) we can write down

$$\frac{\sum_{j=n_k}^{n_{k+1}-1} s^j}{\sin(i_k\frac{\gamma}{2})} = \frac{r^{n_{k+1}}}{\sin\omega^{n_k}} = \frac{r^{n_k}}{\sin(\omega^{n_k} - i_k\frac{\gamma}{2})},$$

which after substitution from eq. (A.5) leads to the relation

$$\sum_{j=n_k}^{n_{k+1}-1} s^j = r^{n_N}\frac{\sin(i_k\frac{\gamma}{2})}{\sin(\omega^{n_k} - i_k\frac{\gamma}{2})}\prod_{j=k}^{N-1}\frac{\sin(\omega^{n_j} - i_j\frac{\gamma}{2})}{\sin\omega^{n_j}}, \tag{A.9}$$

cf. formula for the path segment (A.8). Using this relation we can write down a sum formula of inverse sine. Notice that by summing separate segments of equation (A.8) we obtain formula for the whole path between two self-collisions

$$\sum_{j=n_k}^{n_{k+1}-1} s^j = \sum_{j=n_k}^{n_{k+1}-1} r^{n_N}\frac{\sin\frac{\gamma}{2}}{\sin(\omega^{n_k} - (j-n_k+1)\frac{\gamma}{2})}\frac{\sin\omega^{n_k}}{\sin(\omega^{n_k} - (j-n_k)\frac{\gamma}{2})}\prod_{j=k}^{N-1}\frac{\sin(\omega^{n_j} - i_j\frac{\gamma}{2})}{\sin\omega^{n_j}}.$$

Comparing this expression with equation (A.9) we receive

$$\frac{\sin(i_k\frac{\gamma}{2})}{\sin(\frac{\gamma}{2})\sin(\omega^{n_k})\sin(\omega^{n_k} - i_k\frac{\gamma}{2})} = \sum_{j=n_k}^{n_{k+1}-1}\frac{1}{\sin(\omega^{n_k} - (j-n_k)\frac{\gamma}{2})\sin(\omega^{n_k} - (j-n_k+1)\frac{\gamma}{2})},$$

which can be modified into the formula for the sum of inverse sines

$$\frac{\sin(k\alpha)}{\sin(\alpha)\sin(\omega)\sin(\omega - k\alpha)} = \sum_{i=0}^{k-1}\frac{1}{\sin(\omega - i\alpha)\sin(\omega - (i+1)\alpha)}.$$

Here we changed the variable $\omega^{n_k} \to \omega$, the constant $\frac{\gamma}{2} \to \alpha > 0$, and indexes $j - n_k \to i$ and $i_k = n_{k+1} - n_k \to k$. This formula holds for any ω: $\omega \neq i\alpha$, $i = 0, ..., k$ and $\alpha \neq 0$.

To demonstrate the above formula we compute the length of the path between the first self-collision (given by (ω^1, r^1)) and the second self-collision (given by (ω^4, r^4)) as depicted in figure A.3. This length is determined by formula

$$\sum_{j=1}^{3} s^j = r^{n_N} \frac{\sin(\frac{3\gamma}{2})}{\sin(\omega^1 - \frac{3\gamma}{2})} \prod_{j=1}^{N-1} \frac{\sin(\omega^{n_j} - i_j \frac{\gamma}{2})}{\sin \omega^{n_j}},$$

which still depends on values of all inner angles with $1 < p < N$, see schema in fig. A.2.

A.3 Length of the path segments beyond the outer self-collision

It is obvious that the length of the path segments beyond the outer self-collision has no end point. However, we can take closer look at expressions for lengths of path segments following the outer self-collision and preceding the last and infinite path segment. Thus, formulas for radial distances for $p \geq n_N$ corresponding to self-intersections following the outer self-collision are given by

$$r^p = r^{n_N} \frac{\sin \omega^{n_N}}{\sin(\omega^{n_N} - (p - n_N)\frac{\gamma}{2})}, \tag{A.10}$$

which we receive replacing n_k by n_N in eq. (A.6) and supposing $\prod = 1$. Or, we can replace (A.1) and (A.3) in the generalized constraint $r^p = \frac{\rho}{\sin \omega^p}$, cf. eq. (4.2), which relates quantities ω^p and r^p even after the outer self-collision. Furthermore, substituting (A.1) and (A.10) into (A.7) we obtain

$$s^p = r^{n_N} \frac{\sin \frac{\gamma}{2}}{\sin(\omega^{n_N} - (p - n_N + 1)\frac{\gamma}{2})} \frac{\sin \omega^{n_N}}{\sin(\omega^{n_N} - (p - n_N)\frac{\gamma}{2})}. \tag{A.11}$$

Sum of path segments following the outer n_N-th self-collision and preceding the last P-th self-intersection is given by

$$\sum_{j=n_N}^{p-1} s^j = r^{n_N} \frac{\sin((p - n_N)\frac{\gamma}{2})}{\sin(\omega^{n_N} - i_N \frac{\gamma}{2})},$$

using straightened path where $n_N < p \leq P$ and definition (6.26). Notice, however, that for the last segment s^P is the value given by (A.11) negative, $s^P < 0$.

Appendix B

Behavior of the inner angles

In this appendix we account for some important attributes of formula (6.9) for the inner angles ω^{n_k}.

B.1 Uniqueness of inner angles $\boldsymbol{\omega^{n_k}}$

We want find out if eq. (6.9) determines *unique* relationship between two successive inner directions $\omega^{n_{k-1}}$ and ω^{n_k} given numbers i_{k-1} and i_k. We carry out derivative

$$\frac{\mathrm{d}\omega^{n_k}}{\mathrm{d}\omega^{n_{k-1}}} = \left[1 + \left(\tan(i_k\frac{\gamma}{2}) + \frac{i_{k-1}\sin(\omega^{n_{k-1}})\sin(i_k\frac{\gamma}{2})}{i_k\cos(\omega^{n_{k-1}} - i_{k-1}\frac{\gamma}{2})\cos(i_k\frac{\gamma}{2})\sin(i_{k-1}\frac{\gamma}{2})}\right)^2\right]^{-1} \times$$

$$\times\left(\frac{i_{k-1}\sin(i_k\frac{\gamma}{2})\cos(\omega^{n_{k-1}})}{i_k\sin(i_{k-1}\frac{\gamma}{2})\cos(\omega^{n_{k-1}} - i_{k-1}\frac{\gamma}{2})\cos(i_k\frac{\gamma}{2})} + \frac{i_{k-1}\sin(i_k\frac{\gamma}{2})\sin(\omega^{n_{k-1}})\sin(\omega^{n_{k-1}} - i_{k-1}\frac{\gamma}{2})}{i_k\sin(i_{k-1}\frac{\gamma}{2})\cos^2(\omega^{n_{k-1}} - i_{k-1}\frac{\gamma}{2})\cos(i_k\frac{\gamma}{2})}\right),$$

whereby we receive product of two positive brackets since $\omega^{n_{k-1}} \in (i_{k-1}\frac{\gamma}{2}, \frac{\pi}{2})$. Thus, relation (6.9) defines increasing function $\omega^{n_k} = f(\omega^{n_{k-1}})$

$$\frac{\mathrm{d}\omega^{n_k}}{\mathrm{d}\omega^{n_{k-1}}} > 0,$$

and hence we can also conclude that there is always just one ω^{n_k} for any $\omega^{n_{k-1}}$ given i_k and i_{k-1}.

B.2 Confinement to the slope

To show that the slope of functions $\omega^{n_k} = f(\omega^{n_{k-1}}; i_{k-1}, i_k)$ can be constrained we

differentiate formula (6.9)

$$\frac{\mathrm{d}\omega^{n_k}}{\mathrm{d}\omega^{n_{k-1}}} = \left[1 + \left(\tan(i_k\frac{\gamma}{2}) + \frac{i_{k-1}\sin(\omega^{n_{k-1}})\sin(i_k\frac{\gamma}{2})}{i_k\cos(\omega^{n_{k-1}} - i_{k-1}\frac{\gamma}{2})\cos(i_k\frac{\gamma}{2})\sin(i_{k-1}\frac{\gamma}{2})}\right)^2\right]^{-1} \times$$

$$\times\left(\frac{i_{k-1}\sin(i_k\frac{\gamma}{2})\cos(\omega^{n_{k-1}})}{i_k\sin(i_{k-1}\frac{\gamma}{2})\cos(\omega^{n_{k-1}} - i_{k-1}\frac{\gamma}{2})\cos(i_k\frac{\gamma}{2})} + \frac{i_{k-1}\sin(i_k\frac{\gamma}{2})\sin(\omega^{n_{k-1}})\sin(\omega^{n_{k-1}} - i_{k-1}\frac{\gamma}{2})}{i_k\sin(i_{k-1}\frac{\gamma}{2})\cos^2(\omega^{n_{k-1}} - i_{k-1}\frac{\gamma}{2})\cos(i_k\frac{\gamma}{2})}\right),$$

and modify it into the form

$$\frac{\mathrm{d}\omega^{n_k}}{\mathrm{d}\omega^{n_{k-1}}} =$$

$$\frac{i_{k-1}i_k\sin(i_{k-1}\frac{\gamma}{2})\cos(i_{k-1}\frac{\gamma}{2})\sin(i_k\frac{\gamma}{2})\cos(i_k\frac{\gamma}{2})}{i_k^2\sin^2(i_{k-1}\frac{\gamma}{2})\cos^2(\omega^{n_{k-1}} - i_{k-1}\frac{\gamma}{2}) + 2i_{k-1}i_k\sin^2(i_k\frac{\gamma}{2})\sin(i_{k-1}\frac{\gamma}{2})\sin(\omega^{n_{k-1}})\cos(\omega^{n_{k-1}} - i_{k-1}\frac{\gamma}{2}) +}$$

$$\frac{\ldots}{+i_{k-1}^2\sin^2(i_k\frac{\gamma}{2})\sin^2(\omega^{n_{k-1}})},$$

which results in the desired inequality

$$\frac{\mathrm{d}\omega^{n_k}}{\mathrm{d}\omega^{n_{k-1}}} < 1,$$

that holds even in the general case within the interval $\omega^{n_{k-1}} \in (i_{k-1}\frac{\gamma}{2}, \frac{\pi}{2})$. Notice, moreover, that the derivatives can be ordered into inequalities according to the parameters i_{k-1} and i_k

$$0 < \frac{\mathrm{d}f(\omega^{n_{k-1}}; i_{\max}, i_{\max})}{\mathrm{d}\omega^{n_{k-1}}} < \frac{\mathrm{d}f(\omega^{n_{k-1}}; q_{\max}, q_{\max})}{\mathrm{d}\omega^{n_{k-1}}} < \frac{\mathrm{d}f(\omega^{n_{k-1}}; i_{k-1}, i_k)}{\mathrm{d}\omega^{n_{k-1}}} <$$

$$< \frac{\mathrm{d}f(\omega^{n_{k-1}}; q_{\min}, q_{\min})}{\mathrm{d}\omega^{n_{k-1}}} < \frac{\mathrm{d}f(\omega^{n_{k-1}}; 1, 1)}{\mathrm{d}\omega^{n_{k-1}}} < 1,$$

for $\omega^{n_{k-1}} \in (\gamma/2, \pi/2)$ which suggests behavior of boundaries for limit inner angles.

B.3 The maximum $|\rho_{\max}|$ is increasing function of the last inner angle $\omega^{n_{N-1}}$

The maximum $|\rho_{\mathrm{m}}|$ (corresponding to a sequence $\{n_k\}_{k=0}^{N}$) is increasing function of the angle $\omega^{n_{N-1}}$ (while we fix the number i_{N-1}) as can be verified by carrying out derivative

$$\frac{\mathrm{d}\rho_{\mathrm{m}}^{n_N}}{\mathrm{d}\omega^{n_{N-1}}} = \frac{i_{N-1}u\Delta t}{4\sin(i_{N-1}\frac{\gamma}{2})}\left[\frac{\cos(\omega^{n_{N-1}})}{\cos(\omega^{n_{N-1}} - i_{N-1}\frac{\gamma}{2})} + \frac{\sin(\omega^{n_{N-1}})\sin(\omega^{n_{N-1}} - i_{N-1}\frac{\gamma}{2})}{\cos^2(\omega^{n_{N-1}} - i_{N-1}\frac{\gamma}{2})}\right] > 0,$$

for any $\omega^{n_{N-1}} \in (i_{N-1}\frac{\gamma}{2}, \frac{\pi}{2})$.

Appendix C

Behavior of the inner angles for the constant sequences

Let us consider the case of the constant sequences $i_k = q$. We will show that the inner angles form decreasing sequence $\{\omega^{qk}\}_{k=0}^{N}$ with fixed point $\frac{\pi+q\gamma}{4}$ for $N \to \infty$, i.e., that the formula (6.19) represents the fixed point iteration. The sequence $\{\omega^{qk}\}_{k=0}^{N}$ is described by a single increasing function $\omega^{qk} = f(\omega^{q(k-1)}; q, q)$, cf. paragraph B.1. Furthermore, we can rearrange the corresponding derivative

$$\frac{\mathrm{d}\omega^{qk}}{\mathrm{d}\omega^{q(k-1)}} = \left[1 + \left(\tan(q\frac{\gamma}{2}) + \frac{\sin(\omega^{q(k-1)})}{\cos(\omega^{q(k-1)} - q\frac{\gamma}{2})\cos(q\frac{\gamma}{2})}\right)^2\right]^{-1} \times$$

$$\times \left(\frac{\cos(\omega^{q(k-1)})}{\cos(\omega^{q(k-1)} - q\frac{\gamma}{2})\cos(q\frac{\gamma}{2})} + \frac{\sin(\omega^{q(k-1)})\sin(\omega^{q(k-1)} - q\frac{\gamma}{2})}{\cos^2(\omega^{q(k-1)} - q\frac{\gamma}{2})\cos(q\frac{\gamma}{2})}\right),$$

into the form

$$\frac{\mathrm{d}\omega^{qk}}{\mathrm{d}\omega^{q(k-1)}} = \frac{1}{1 + 4\sin^2(\omega^{q(k-1)})\tan^2(q\frac{\gamma}{2}) + 4\sin^2(\omega^{q(k-1)})\cos(\omega^{q(k-1)})\tan^2(q\frac{\gamma}{2})} < 1,$$

for any $\omega^{qk} \in (q\frac{\gamma}{2}, \frac{\pi}{2})$. Thus, we have proved inequality

$$0 < \frac{\mathrm{d}\omega^{qk}}{\mathrm{d}\omega^{q(k-1)}} < 1,$$

which defines monotonic convergence within the interval $(q\frac{\gamma}{2}, \frac{\pi}{2})$. Moreover, it can be verified that

$$\frac{\pi + q\gamma}{4} = f(\frac{\pi + q\gamma}{4}, q),$$

i.e., a fixed point occurs within the same interval. Finally, we compare two successive values of inner angles

$$\tan(\omega^{q(k-1)}) > \tan(\omega^{qk}),$$

and after some algebra we receive that inner angles form decreasing sequence $\{\omega^{qk}\}$ for $k \to \infty$ (or we realize that the starting value $\omega^0 = \frac{\pi}{2}$ is also the maximal value) with the fixed point limit $\frac{\pi+q\gamma}{4}$.

Appendix D

Attractor of the periodical sequence with the period $a = 2$

Let us compute attractor of periodical sequence with the period $a = 2$, i.e., sequence consisting of the repeating subsequence of two terms: $\{p, q\}$. Substituting into eq. (6.8) we obtain system of two equations

$$q \sin(\omega^q - q\frac{\gamma}{2}) \cos(\omega^p - p\frac{\gamma}{2}) \sin(p\frac{\gamma}{2}) = p \cos\omega^q \sin\omega^p \sin(q\frac{\gamma}{2}),$$

$$p \sin(\omega^p - p\frac{\gamma}{2}) \cos(\omega^q - q\frac{\gamma}{2}) \sin(q\frac{\gamma}{2}) = q \cos\omega^p \sin\omega^q \sin(p\frac{\gamma}{2}),$$

where ω^p and ω^q represent desired fixed points defining the attractor. Expressing $\tan(\omega^q)$ from both equations and comparing them we receive the quadratic equation with variable $\tan(\omega^p)$

$$\begin{aligned}\tan^2(\omega^p) \Big[-pq \sin^2(p\frac{\gamma}{2}) \cos(p\frac{\gamma}{2}) - p^2 \sin^2(q\frac{\gamma}{2}) \cos(p\frac{\gamma}{2})\Big] + \\ \tan(\omega^p) \Big[q^2 \sin^3(p\frac{\gamma}{2}) + 2pq \sin^3(p\frac{\gamma}{2}) + p^2 \sin^2(q\frac{\gamma}{2}) \sin(p\frac{\gamma}{2})\Big] + \\ \Big[q^2 \sin^2(p\frac{\gamma}{2}) \cos(p\frac{\gamma}{2}) + pq \sin^2(p\frac{\gamma}{2}) \cos(p\frac{\gamma}{2})\Big] = 0.\end{aligned}$$

This equation posses one positive root ω^p which can be plugged into explicit formula (6.9) to obtain the other value ω^q. Thus, we have determined two limiting values of the periodical sequence made of the repeating subsequence $\{p, q\}$

$$\omega^p = f(\omega^q; p, q),$$

$$\omega^q = f(\omega^p; q, p),$$

which form the attractor.

Appendix E

Length S^N of the inner path for $N \to \infty$ self-collisions for the constant sequences

Let us compute the length of the whole path for $N \to \infty$, i.e., sum (6.33) over infinite number of inner path segments, for the case of sequences with constant number q of intermediate self-intersections. The sum S^∞ can be computed by two methods: Either by limiting the recurrent formula (E.2) bellow, or by summing the infinite geometric progression. The first method consists in summing of increasing number of self-collisions N. While the second method uses the fact that known limiting inner angles $\omega^{\infty-1}$ are virtually constant for $N \to \infty$ which results in geometrical series easily to evaluate (for constant sequences). Let us rewrite sum (6.33)

$$S^N = \sum_{k=0}^{N-1} s^{qk} = r^{qN} \sin(q\frac{\gamma}{2}) \sum_{k=0}^{N-1} \frac{1}{\sin(\omega^{qk} - q\frac{\gamma}{2})} \prod_{j=k}^{N-1} \frac{\sin(\omega^{qj} - q\frac{\gamma}{2})}{\sin(q\omega^j)} \ ,$$

where the term $\sin(q\frac{\gamma}{2})$ has been factored out.

Now, we derive the length S^∞ made of infinite number of inner path segments by the first method. We introduce the sum $\sigma^N \equiv \frac{S^N}{r^{qN}\sin(q\gamma/2)}$ and write it down in matrix-like

form

$$\sigma^{N-1} =$$

$$\frac{1}{\sin(\omega^0 - q\frac{\gamma}{2})}\left[\frac{\sin(\omega^0 - q\frac{\gamma}{2})}{\sin(\omega^0)} \times \frac{\sin(\omega^q - q\frac{\gamma}{2})}{\sin(\omega^q)} \times ... \times \frac{\sin(\omega^{qk} - q\frac{\gamma}{2})}{\sin(\omega^{qk})} \times ... \times \frac{\sin(\omega^{q(N-1)} - q\frac{\gamma}{2})}{\sin(\omega^{q(N-1)})}\right] +$$

$$\frac{1}{\sin(\omega^q - q\frac{\gamma}{2})}\left[\frac{\sin(\omega^q - q\frac{\gamma}{2})}{\sin(\omega^q)} \times ... \times \frac{\sin(\omega^{qk} - q\frac{\gamma}{2})}{\sin(\omega^{qk})} \times ... \times \frac{\sin(\omega^{q(N-1)} - q\frac{\gamma}{2})}{\sin(\omega^{q(N-1)})}\right] +$$

.

.

$$\frac{1}{\sin(\omega^{qk} - q\frac{\gamma}{2})}\left[\frac{\sin(\omega^{qk} - q\frac{\gamma}{2})}{\sin(\omega^{qk})} \times ... \times \frac{\sin(\omega^{q(N-1)} - q\frac{\gamma}{2})}{\sin(\omega^{q(N-1)})}\right] +$$

.

.

$$\frac{1}{\sin(\omega^{q(N-1)} - q\frac{\gamma}{2})}\left[\frac{\sin(\omega^{q(N-1)} - q\frac{\gamma}{2})}{\sin(\omega^{q(N-1)})}\right], \tag{E.1}$$

from which the recurrent formula follows

$$\sigma^N = \sigma^{N-1}\frac{\sin(\omega^{qN} - q\frac{\gamma}{2})}{\sin(\omega^{qN})} + \frac{1}{\sin(\omega^{qN} - q\frac{\gamma}{2})}\frac{\sin(\omega^{qN} - q\frac{\gamma}{2})}{\sin(\omega^{qN})}. \tag{E.2}$$

For $N \to \infty$ we obtain

$$\sigma^\infty = \sigma^\infty\frac{\sin(\omega^\infty - q\frac{\gamma}{2})}{\sin(\omega^\infty)} + \frac{1}{\sin(\omega^\infty)},$$

from which we can easily express the sum

$$\sigma^\infty = \frac{1}{\sin(\omega^\infty) - \sin(\omega^\infty - q\frac{\gamma}{2})},$$

where $\omega^\infty = \frac{\pi + q\gamma}{4}$ is the fixed point for the sequence $\{q\}_{k=0}^\infty$. Finally, we substitute σ^∞ back into (6.33) to receive the length S^∞ of the path composed from infinite number of path segments

$$S^\infty = \sigma^\infty r^\infty \sin(q\frac{\gamma}{2}) = \sqrt{2}\ r^\infty \cos(q\frac{\gamma}{4}),$$

where the radial distance r^∞ corresponds to two solutions determined by eq. (6.30)

$$r^\infty = \frac{q\triangle tu}{2\sqrt{2}\sin(q\frac{\gamma}{2})}\sqrt{1 \pm \sqrt{1 - \frac{16\rho^2\sin^2(q\frac{\gamma}{2})}{(q\triangle tu)^2}}}.$$

On the other hand, we can plug the limiting inner angle $\omega^{\infty-1}$ into the sum (6.33) over infinite number of inner path segments to obtain relation

$$S^{\infty} = r^{\infty} \frac{\sin(q\frac{\gamma}{2})}{\sin(\frac{\pi}{4} - q\frac{\gamma}{4})} \sum_{k=0}^{\infty} \left(\frac{\sin(\frac{\pi}{4} - q\frac{\gamma}{4})}{\sin(\frac{\pi}{4} + q\frac{\gamma}{4})} \right)^{k},$$

since the value $\omega^{\infty-1} = \pi/4 + \gamma/4$ remains virtually constant for $N \to \infty$ (it is the fixed value of the sequence $\{q\}_{k=0}^{\infty}$). As the most of inner loops cumulates next to the vertex, and nontrivial contributions come from outermost loops, cf. section 6.7.2, we can evaluate suggested geometric progression, and finally get

$$S^{\infty} = \sqrt{2}\ r^{\infty} \cos(q\frac{\gamma}{4}),$$

which is identical to the result obtained by limiting of the recurrent formula (E.2).

Appendix F

Length S^N of the inner path for $N \longrightarrow \infty$ self-collisions for the periodical sequences

In this paragraph we calculate the length of the whole path for $N \to \infty$ for periodical sequences. We use both methods, introduced in the previous paragraph E, though their application is a little more difficult. To simplify matter, we employ the periodical sequence with the period $a = 2$, i.e., made of the subsequence $\{pq\}$. Let us rewrite sum (6.32)

$$S^N = \sum_{k=0}^{N-1} \sum_{j=n_k}^{n_{k+1}-1} s^j = r^{n_N} \sum_{k=0}^{N-1} \frac{\sin(i_k \frac{\gamma}{2})}{\sin(\omega^{n_k} - i_k \frac{\gamma}{2})} \prod_{j=k}^{N-1} \frac{\sin(\omega^{n_j} - i_j \frac{\gamma}{2})}{\sin(\omega^{n_j})} ,$$

and suppose two limiting inner angles $\omega_p^{\infty-1}$ and $\omega_q^{\infty-1}$.

The first method is based on limiting of recurrent formulas. For the periodical sequence with the period $a = 2$ two formulas have to be arranged

$$\sigma^{2N} = \sigma^{2N-1} \frac{\sin(\omega_q^{\infty-1} - q\frac{\gamma}{2})}{\sin(\omega_q^{\infty-1})} + \frac{\sin(q\frac{\gamma}{2})}{\sin(\omega_q^{\infty-1} - q\frac{\gamma}{2})} \frac{\sin(\omega_q^{\infty-1} - q\frac{\gamma}{2})}{\sin(\omega_q^{\infty-1})},$$

$$\sigma^{2N+1} = \sigma^{2N} \frac{\sin(\omega_p^{\infty-1} - p\frac{\gamma}{2})}{\sin(\omega_p^{\infty-1})} + \frac{\sin(p\frac{\gamma}{2})}{\sin(\omega_p^{\infty-1} - p\frac{\gamma}{2})} \frac{\sin(\omega_p^{\infty-1} - p\frac{\gamma}{2})}{\sin(\omega_p^{\infty-1})},$$

where $\sigma^N \equiv S^N / r^{n_N}$. Notice that the second formulas determines that the sequence $\{i_k\}_{k=0}^{N-1}$ ends with p. Obviously, the first formula can be plugged into the second one in such a way that we get the only relation

$$\sigma^{2N+1} = \left[\sigma^{2N-1} \frac{\sin(\omega_q^{\infty-1} - q\frac{\gamma}{2})}{\sin(\omega_q^{\infty-1})} + \frac{\sin(q\frac{\gamma}{2})}{\sin(\omega_q^{\infty-1})}\right] \frac{\sin(\omega_p^{\infty-1} - p\frac{\gamma}{2})}{\sin(\omega_p^{\infty-1})} + \frac{\sin(p\frac{\gamma}{2})}{\sin(\omega_p^{\infty-1})},$$

For $N \to \infty$ we obtain

$$\sigma_p^{\infty} = \frac{\sin(p\frac{\gamma}{2}) \sin(\omega_q^{\infty-1}) + \sin(q\frac{\gamma}{2}) \sin(\omega_p^{\infty-1} - p\frac{\gamma}{2})}{\sin(\omega_p^{\infty-1}) \sin(\omega_q^{\infty-1}) - \sin(\omega_p^{\infty-1} - p\frac{\gamma}{2}) \sin(\omega_q^{\infty-1} - q\frac{\gamma}{2})},$$

σ_p^∞ where the subscript p denotes that the sequence ends with p. Hence, the sum S_p^∞ is finite where the radial distance r_p^∞ follows from equation (6.14)

$$r^\infty = \frac{pu\Delta t \sin(\omega_p^{\infty-1})}{2\sqrt{2}\sin(p\frac{\gamma}{2})\cos(\omega_p^{\infty-1} - p\frac{\gamma}{2})}\sqrt{1 \pm \sqrt{1 - \frac{16\rho^2 \sin^2(p\frac{\gamma}{2})\cos^2(\omega^{\infty-1} - p\frac{\gamma}{2})}{(pu\Delta t)^2 \sin^2(\omega^{\infty-1})}}}.$$

In order to use the method of summing of the infinite geometric progressions we have to separate the sum into $a = 2$ sub-sums. Let us denote

$$a_p = \frac{\sin(p\frac{\gamma}{2})}{\sin(\omega_p^{\infty-1} - p\frac{\gamma}{2})}\sin(\omega_p), \quad a_q = \frac{\sin(q\frac{\gamma}{2})}{\sin(\omega_q^{\infty-1} - q\frac{\gamma}{2})}\sin(\omega_p),$$

and

$$P = \frac{\sin(\omega_p^{\infty-1} - p\frac{\gamma}{2})}{\sin(\omega_p)}, \qquad Q = \frac{\sin(\omega_q^{\infty-1} - q\frac{\gamma}{2})}{\sin(\omega_q)}.$$

Now, we expand the sum (6.32) for $N \to \infty$

$$a_pP + a_qPQ + a_pP^2Q + a_qP^2Q^2 + a_pP^3Q^2 + a_qP^3Q^3 + ...,$$

starting with terms which correspond to self-collisions next to the outer self-collision and assuming that the sequence $\{i_k\}_{k=0}^{\infty-1}$ ends with p. The first sum with odd terms looks like

$$a_pP + a_pP^2Q + a_pP^3Q^2 + ... = a_pP\sum_{k=0}^{\infty}(PQ)^k,$$

while second sum with even terms is

$$a_qPQ + a_qP^2Q^2 + a_qP^3Q^3 + ... = a_q\sum_{k=0}^{\infty}(PQ)^k - a_q.$$

Hence, the whole sum is equal to

$$a_pP + a_qPQ + a_pP^2Q + a_qP^2Q^2 + ... = (a_pP + a_q)\sum_{k=0}^{\infty}(PQ)^k - a_q,$$

which after some algebra results in σ_p^∞ computed above. Notice that subscripts p and q could be exchanged again.

Appendix G

Action I^N of the inner path for $N \to \infty$ self-collisions for the constant sequences

Comparison of formulas of the length S^N, (6.33), and the action I^N, (6.35), for constant sequences suggests that calculation of both quantities is analogical. We compute the action I^N of the inner path for $N \to \infty$ self-collisions using both methods involved in the case of the length S^N.

First, we derive corresponding recurrent formula:

$$I^N = \frac{2m}{q^2\Delta t}\sin^2(q\frac{\gamma}{2})\left(r^{qN}\right)^2\sum_{k=0}^{N-1}\left[\frac{1}{\sin(\omega^{qk}-q\frac{\gamma}{2})}\prod_{j=k}^{N-1}\frac{\sin(\omega^{qj}-q\frac{\gamma}{2})}{\sin(\omega^{qj})}\right]^2,$$

where we have factored out the term $\sin^2(q\frac{\gamma}{2})/q^2$. Let us denote the sum of squares of

brackets by $\left(\sigma^N\right)^2$ and arrange the sum into matrix-like form

$$\left(\sigma^{N-1}\right)^2 =$$

$$\frac{1}{\sin^2(\omega^0 - q\frac{\gamma}{2})}\left[\frac{\sin^2(\omega^0 - q\frac{\gamma}{2})}{\sin^2(\omega^0)} \times \frac{\sin^2(\omega^q - q\frac{\gamma}{2})}{\sin^2(\omega^q)} \times ... \times \frac{\sin^2(\omega^{qk} - q\frac{\gamma}{2})}{\sin^2(\omega^{qk})} \times ... \times \frac{\sin^2(\omega^{q(N-1)} - q\frac{\gamma}{2})}{\sin^2(\omega^{q(N-1)})}\right] +$$

$$\frac{1}{\sin^2(\omega^q - q\frac{\gamma}{2})}\left[\frac{\sin^2(\omega^q - q\frac{\gamma}{2})}{\sin^2(\omega^q)} \times ... \times \frac{\sin^2(\omega^{qk} - q\frac{\gamma}{2})}{\sin^2(\omega^{qk})} \times ... \times \frac{\sin^2(\omega^{q(N-1)} - q\frac{\gamma}{2})}{\sin^2(\omega^{q(N-1)})}\right] +$$

.

.

$$\frac{1}{\sin^2(\omega^{qk} - q\frac{\gamma}{2})}\left[\frac{\sin^2(\omega^{qk} - q\frac{\gamma}{2})}{\sin^2(\omega^{qk})} \times ... \times \frac{\sin^2(\omega^{q(N-1)} - q\frac{\gamma}{2})}{\sin^2(\omega^{q(N-1)})}\right] +$$

.

.

$$\frac{1}{\sin^2(\omega^{q(N-1)} - q\frac{\gamma}{2})}\left[\frac{\sin^2(\omega^{q(N-1)} - q\frac{\gamma}{2})}{\sin^2(\omega^{q(N-1)})}\right],$$

cf. eq. (E.1), which results in recurrent formula

$$\left(\sigma^N\right)^2 = \left(\sigma^{N-1}\right)^2 \frac{\sin^2(\omega^{qN} - q\frac{\gamma}{2})}{\sin^2(\omega^{qN})} + \frac{1}{\sin^2(\omega^{qN} - q\frac{\gamma}{2})}\frac{\sin^2(\omega^{qN} - q\frac{\gamma}{2})}{\sin^2(\omega^{qN})}.$$

For $N \to \infty$ we obtain relation

$$(\sigma^\infty)^2 = (\sigma^\infty)^2 \frac{\sin^2(\omega^\infty - q\frac{\gamma}{2})}{\sin^2(\omega^\infty)} + \frac{1}{\sin^2(\omega^\infty)},$$

from which we can express the sum

$$(\sigma^\infty)^2 = \frac{1}{\sin^2(\omega^\infty) - \sin^2(\omega^\infty - q\frac{\gamma}{2})},$$

equal to $\sin(q\gamma/2)$ for $\omega^{\infty-1} = \frac{\pi+q\gamma}{4}$. Therefore, the action I^∞ of the inner path for constant sequences is determined by

$$I^\infty = \frac{2m}{q^2\Delta t}\,(r^\infty)^2 \sin(q\frac{\gamma}{2}),$$

where the radial distance r^∞ is fixed in eq. (6.30).

To formulate I^∞ as the geometric progression we replace inner angles in eq. (6.35) by the limiting inner angle $\omega^{\infty-1} = \frac{\pi+q\gamma}{4}$

$$I^\infty = \frac{2m\,(r^\infty)^2}{q^2\Delta t}\frac{\sin^2(q\frac{\gamma}{2})}{\sin^2(\frac{\pi}{4} - q\frac{\gamma}{4})}\sum_{k=0}^{\infty}\left(\frac{\sin^2(\frac{\pi}{4} - q\frac{\gamma}{4})}{\sin^2(\frac{\pi}{4} + q\frac{\gamma}{4})}\right)^k,$$

and finally get

$$I^{\infty} = \frac{2m\left(r^{\infty}\right)^2 \sin(q\frac{\gamma}{2})}{q^2 \Delta t},$$

which is identical to the result obtained by limiting of the recurrent formula above. Analogously, calculations for periodical sequences would reproduce procedures from paragraph F.

Appendix H

Dolanský, J. and Krtouš, P. 2010

PHYSICAL REVIEW D **82,** 124056 (2010)

Billiard ball in the space with a time machine

Jindřich Dolanský* and Pavel Krtouš†

Institute of Theoretical Physics, Faculty of Mathematics and Physics, Charles University in Prague, V Holešovičkách 2, 180 00 Prague 8, Czech Republic

(Received 12 October 2010; published 23 December 2010)

We study a system of an elastic ball moving in the nonrelativistic spacetime with a nontrivial causal structure produced by a wormhole-based time machine. For such a system, it is possible to formulate a simple model of the so-called ''grandfather paradox'': for certain ''paradoxical'' initial conditions, the standard straight trajectory of the ball would self-collide inconsistently. We analyze globally consistent solutions of local equations of motion; namely, we find all trajectories with one self-collision. It is demonstrated that all standard initial conditions have a consistent evolution, including those paradoxical ones, for which the inconsistent collision-free trajectory is superseded by a special consistent self-colliding trajectory. Moreover, it is shown that for a wide class of initial conditions, more than one globally consistent evolution exist. The nontrivial causal structure thus breaks the uniqueness of the classical theory even for locally deterministic physical laws.

DOI: 10.1103/PhysRevD.82.124056 PACS numbers: 04.20.Gz, 45.20.D−, 45.50.Tn

I. INTRODUCTION

Time travel is a phenomenon which has been attracting interest both in fiction and general discussions for a long time. However, only after a formulation of the theory of relativity could such considerations be investigated on a more scientific and solid basis. Already, special relativity shows that different observers experience different times and one of them can ''travel'' to the future of others by means of his relative motion. Thanks to the general theory of relativity a possibility opens that an observer could travel even to his own past—his worldline could pass through a geometrically or topologically nontrivial area to a region where the worldline originally started [1,2]. Worldlines which even cross themselves are called *closed timelike curves* (CTCs), and it is customary to say that spacetimes with CTCs contain *time machines* [3,4].

Spacetimes with time machines are causally nontrivial—in such spacetimes one can send a signal to one's own past or even try to influence the past—which immediately opens a question of consistency of standard physical laws as we know them. On a formal level, it is the question of the existence of solutions of physical equations of motion and the question of whether the initial value problem is well-possessed. On a less formal level, these problems can be phrased as the well-known ''grandfather paradox,'' suggested, e.g., in [5–7]: in spacetimes with time machines, one has to face a logical riddle of what happens if one travels to his own past and kills his grandfather. Consequently, one would never be born, and therefore, one could not travel to the past.

This is a clearly inconsistent situation which suggests that spacetimes with CTCs are pathological and they should be excluded from serious scientific consideration. However, a system containing live beings is too complicated by too many unknown physical laws, and therefore, one cannot be sure that the inconsistency of the grandfather paradox is really inescapable. Therefore, people have tried to formulate analogous situations for much simpler systems which could be studied exactly [8–11].

As an example, in [12], and especially in [13], the system of the billiard balls in spacetime with wormholes has been studied. This system allows a straightforward reformulation of the grandfather paradox: the ball could be sent through the time machine in such a way that it hits itself and thus inconsistently prevents its entry to the time machine, cf. Fig. 1. It seems that such paradoxical initial conditions do not lead to a consistent evolution of the system.

Perhaps surprisingly, the extensive studies of systems with CTCs during the 1980s and the 1990s showed that for a simple physical system, pathology of spacetimes is not so severe and the equations of motion can be consistently solved.

Let us formulate this point more precisely. We consider a spacetime containing a time machine and we want to study a system with well-known local physical laws (e.g., a particle or electromagnetic field). We do not change these local laws, i.e., we require that they hold locally in any small spacetime domain. However, in addition to the local laws, we also require the so-called *principle of self-consistency* [8,10,14]. Namely, a *globally consistent* solution of local laws must exist. It means that we allow the system to propagate to its own past; however, it must be done in a *consistent* way with the original evolution in the past. The past cannot be changed since it has already been changed.

The key question of studies of time machines is whether such globally consistent evolutions exist for given local

*dolanskyy@gmail.com
†Pavel.Krtous@utf.mff.cuni.cz

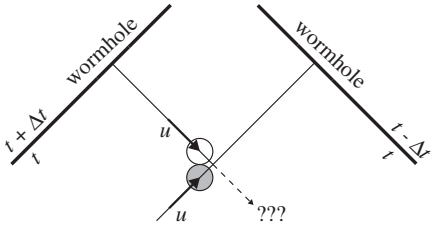

FIG. 1. *The ball self-colliding inconsistently.* The ball (in gray) comes from a distant region and enters the wormhole without any self-collision. It leaves the time machine (now in white) in such a way that it inconsistently hits itself. Thus, this situation represents an inconsistent evolution which is the direct analogue of the grandfather paradox.

laws and whether these global evolutions are sufficiently generic. More accurately, we would like to show that there exist consistent solutions for all, or, at least, for almost all standard initial data. Otherwise, if the local laws have no globally consistent solution, the spacetime would be clearly pathological and we could rule it out from our consideration. Similarly, the pathology would be serious if the local physical laws had only few globally consistent solutions.

As we have said, the studies of different systems show that spacetimes with CTCs are not necessarily causally pathological. Let us mention the results for a system of interacting particles [8,12,13] or the scalar field theory [9,10], where it was shown that standard local laws have generic globally consistent solutions even in the presence of CTCs. Another surprising result of such studies is that the existence of time machines does not usually restrict a number of consistent solutions, but on the contrary, it leads to a possibility of more than one globally consistent solution for given initial values. In spacetimes with time machines, we thus usually lose the uniqueness of the evolution [13].

Especially for the apparently paradoxical initial conditions from the grandfather paradox-like situation, it was shown [13] that a consistent evolution exists, although it can be rather nonintuitive. On less formal level of the human version of the paradox, it could be rephrased as a conjecture of a hidden law which always prevents the grandson from killing his grandfather [15].

In the present work, we want to study the system of a ball moving in a nonrelativistic space with CTCs, which is very close to that of [13]. However, we have chosen a different time-machine configuration which significantly simplifies the analysis. We will be able to solve the equations of motion explicitly and we will confirm the behavior described above: paradoxical initial conditions are not really paradoxical, and the evolution is not, in general, unique. The contribution of our analysis is that it can be done very explicitly, since our model is sufficiently simple; at the same time, it is sufficiently nontrivial to reproduce the most important features of systems with time machines.

Our work proceeds as follows. In the next section, we describe the system of a ball moving in the space with wormhole-based time machine. We derive the equations characterizing trajectories. In Sec. III, we discuss the character and number of solutions for various initial conditions and also the resolution of the ''grandfather paradox''. Section IV describes the geometry of the trajectories, and the paper is summarized in the conclusion.

II. DESCRIPTION OF THE SYSTEM

A. Wormhole time machine

The simplest and most natural way to construct a spacetime with CTCs is to use a wormhole [7,11,13]. The wormhole can be viewed as a shortcut between two location of the spacetime. It forms CTCs if one of the mouths of the wormhole lies in the past of the other mouth.

In the nonrelativistic setting, we can consider spatial wormholes connecting two places in space with an additional time shift. The speed of light is infinite, and it determines a unique notion of simultaneity and thus allows us to define a global time—at least, before introducing the time difference. Introducing the time shift means that traveling through the wormhole not only sends the observer to a different place in space but also to a different time.

A simple spatial wormhole in otherwise Euclidian space can be obtained by the cutting and gluing method. For example, we can cut out two spheres and glue their surfaces together, cf. [3] or [13]. We thus obtain a topologically and geometrically nontrivial space—it is not a simply connected space, and the geometry on the glued surface is not flat.

In this work, we consider an even simpler situation of the wormhole with planar mouths instead of spherical ones. Namely, we cut out from the space two planar sections which we identify, as in Fig. 2. Since we use flat planar sections, their identification is geometrically trivial. The

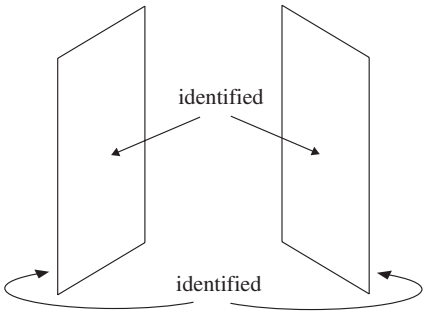

FIG. 2. *Spatial representation of two simple wormholes.* A wormhole obtained by gluing two planar sections cut from otherwise Euclidian space. Planar wormhole mouths could be obtained, e.g., by squeezing the mouths of the spherical wormhole into very thin planes). The external curvature, with the exception of the boundary of the planar sections, is vanishing, and the geometry through the wormhole is thus flat.

whole curvature of the mouths is squeezed to the borders of the planar sections, which can be understood as a kind of solid frames on which the traversable parts of the wormhole are spanned. To avoid a discussion of the wormhole boundary, we assume that the planar sections are much larger than the scales of our experiments. As idealization, we consider the mouths of our wormhole to be two half-planes which form an angle γ with a common boundary line, called the axis.

If we identify these half-planes (first, say, at the same moment of time), the space between them becomes a locally Euclidean space with a conical singularity localized on the axis. Indeed, if we restrict ourselves to the two-dimensional picture and ignore the direction parallel to the axis, our space forms a cone with the angle γ around the vertex.

Of course, this is a overidealized situation. We should keep in mind that the mouths of the wormhole are large but finite, so somewhere very far from the axis, the conical part of the space ends and goes over to the full Euclidean space. But in most of our discussions, we restrict ourselves only to the part of the space between the mouths of the wormhole. We thus effectively work in the conical space with angle γ around the axis.

Let us stress that in our construction, the mouths of the wormhole are special and privileged. However, after enlarging them to the semi-infinite size and restricting ourselves only to the conical space between mouths, we can no longer localize the position of the mouths by local experiments. The geometry through the mouths is locally Euclidean, as it is anywhere else. We thus obtained a space which is axially symmetric with respect to the rotation around the axis (it has also translation symmetry along the axis and it is static). The position of the wormhole can be identified only on scales larger than the wormhole, from the surrounding globally Euclidean space.

Finally, we assume that the angle $\gamma \in (\frac{\pi}{2}, \pi)$. For γ smaller than π, we obtain interesting situations when the straight trajectory of a free particle intersects itself. For $\gamma > \pi/2$, the straight trajectory intersects itself only once. The second condition is not a crucial assumption; it just simplifies the discussion.

Since we want to study a space with a time machine, we have to identify the mouths of the wormhole with a time shift Δt. Of course, it destroys the standard causal structure of the nonrelativistic spacetime (a clear distinction between future and past). Despite this, we will keep using and referring to the original notion of the simultaneity and to the global time of the surrounding space, which is, certainly, reasonable for small wormholes; however, we admit that it can be slightly confusing and less founded in the idealized case considered below.

Indeed, the constructed spacetime is still locally Euclidian (except the axis, of course), but endowed with a strange causal structure. Hypersurfaces of simultaneity (visualized in the standard nonrelativistic spacetime diagram as horizontal planes) propagate through the wormhole and form ''helical'' surfaces winding around the axis. This indicates that the spacetime contains CTCs. The particle moving toward the wormhole reads that the external time t increases continuously until it enters the wormhole mouth. By crossing one of the mouths, the external time t either increases by Δt into $t + \Delta t$, or decreases by $-\Delta t$ into $t - \Delta t$.

This can be visualized in the spacetime diagram in Fig. 3. Here, two spatial directions perpendicular to the axis are shown in horizontal directions; the direction parallel to axis is suppressed. The vertical direction corresponds to time. Semiplanar mouths of the wormhole at one moment are thus depicted as horizontal semilines, their time evolution as vertical half-planes. The identification of two such half-planes is not on the same vertical level, but with the vertical shift Δt. We assume that going through the wormhole in counterclockwise direction takes us time $\Delta t > 0$ to the past, in clockwise direction to the future.

B. Equation of motion

Now, we want to derive equations of motion for a ball moving in the nonrelativistic spacetime which has just been described. We assume that the motion satisfies classical local laws of motion. Additionally, we restrict ourselves to motions perpendicular to the axis of the wormhole because the ball can self-interact only for such a motion.

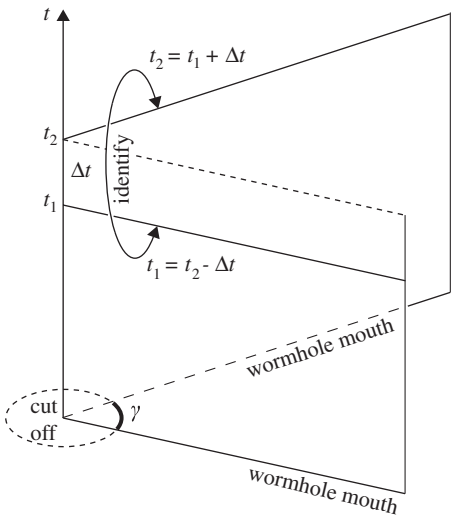

FIG. 3. *A spacetime diagram of the conical time machine.* The vertical direction is temporal; horizontal planes correspond to the hypersurface of simultaneity of the original spacetime (the third spatial direction is suppressed). Two half-planes on the boundary of the conical spacetime represent the history of the mouths of the wormhole, and they are identified with a time shift Δt.

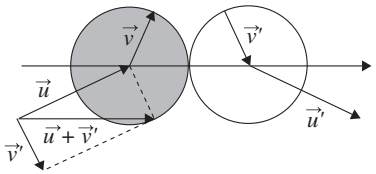

FIG. 4. *Character of self-collision of the ball with itself.* The incoming velocity $\vec{u}$ of the younger version of the ball (in gray) is complementary to mirror reflection of the outgoing velocity $\vec{v}'$ of the older version of the ball (white) and similarly for velocities $\vec{u}'$ and $\vec{v}$.

Clearly, a free particle moves uniformly along a straight line. However, for $\gamma \in (\pi/2, \pi)$, a straight line in a conical space must intersect itself. If the trajectory of the particle crosses itself in different times, we speak about *self-intersection*. If the particle intersects its trajectory exactly at the same time—which is allowed thanks to time shift $-\Delta t$ gained in the wormhole—it hits itself and we speak about *self-collision*. Our goal is to describe trajectories with exactly one consistent self-collision.

We assume that an elastic collision occurs when the ball collides with itself. The classical elastic impact of two balls is determined by the momentum and energy conservation and the assumption that it occurs in one plane. In our case, two versions of the same ball collide: the *younger* version of the ball coming from infinity hits the *older* version coming from the wormhole; after the collision, the younger ball flies to the wormhole and the older one flies away to infinity. Since the traverse of the wormhole does not change the velocity of the ball, magnitude v of the outgoing velocity $\vec{v}$ of the younger ball is the same as the magnitude of the incoming velocity $\vec{v}'$ of the older ball. All these conditions determine [16] that the impact of the ball with itself must have the form depicted in Fig. 4. Namely, in the rest frame of the wormhole, the incoming velocity $\vec{u}$ of the younger ball is complementary to the mirror reflection of the outgoing velocity $\vec{u}'$ of the older ball with respect to the plane tangent to balls at the point of impact. We call this plane the *impact plane*. Similar property holds for velocities $\vec{v}$ and $\vec{v}'$. Moreover, projections of the incoming and outgoing velocities $\vec{u}$ and $\vec{v}$ (respectively, $\vec{v}'$ and $\vec{u}'$) to the impact plane are the same.

Now, we want to find a location of the self-collision in such a way that the outgoing younger ball consistently passes to the incoming older ball. It can be done [16] in two ways, depicted in Fig. 5. The key property is that the impact plane must be radial, i.e., it contains the axis (dashed line in the figure). Type I represents the situation when the older ball touches the younger one by its rear part, i.e., the younger version must collide from the left side.[1]

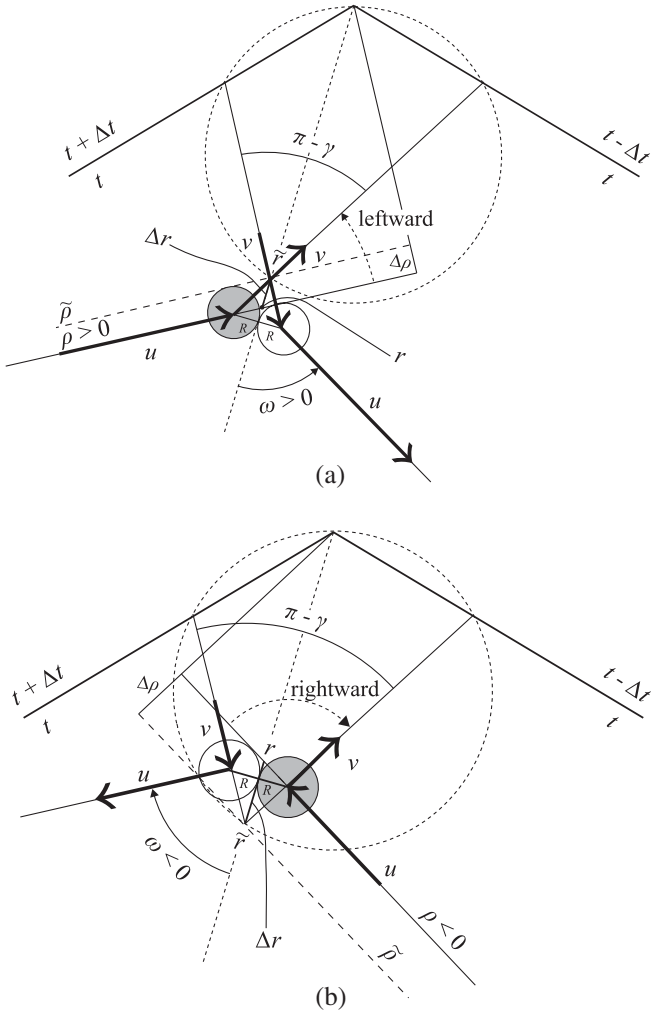

FIG. 5. *Physical self-collisions of types I and II.* (a) The configuration of type I represents a situation in which the younger ball (in gray) is on the left side while the older ball (in white) is on the right side with respect to the radial line. The self-collision is physical when the momentum transfer is positive and the trajectory of the particle is deflected leftward. (b) The configuration of type II represents a situation in which the older ball is on the left side while the younger ball is on the right side with respect to the radial line. The self-collision is physical if the trajectory of the particle is deflected rightward.

For type II, the younger ball touches its older version by its front part and is incoming from the right side.

For both types, we can distinguish the physical collisions with a positive momentum transfer from the younger ball to the older ball from ''spurious'' collisions which would need a negative momentum transfer. The latter are unphysical not only for the sign of the exchanged momentum but also because the ball would not fit geometrically into space for such collisions—it would have to fly through itself. For the physical self-collision of type I, the younger ball must deflect leftward, i.e., closer to the vertex than if it followed the collision-free trajectory. For the physical

[1]Left and right side are selected by our choice of time shift of the time machine.

self-collisions of type II, the trajectory of the younger ball is deflected rightward, cf. Fig. 5.

C. Pointlike particle

To determine parameters of the self-collision, we start with a simpler case of a point particle, i.e., taking radius of the ball $R \to 0$. In this case, the distinction between the two types described above disappears[2] and the geometry of the self-collision is depicted in Fig. 6. The trajectory of the incoming particle can be determined by two initial parameters: the *impact parameter* ρ, which gives the distance of the incoming trajectory from the vertex of the cone, and the *magnitude of incoming velocity* $u > 0$. We adopt the convention that the impact parameter ρ is positive if the particle circles the cone in the counterclockwise direction, and it is negative if it circles the cone in the clockwise direction.

Of course, the parameters u and ρ do not determine the incoming trajectory uniquely since they do not specify its angular location around the axis and its temporal location—we would need two additional parameters for that.[3] However, the conical space has the rotational symmetry and is static, so the exact angular and temporal location are irrelevant for the character of solutions. Therefore, we can ignore the additional initial parameters when we investigate the geometry of the self-collision.

The self-collision can be parametrized by its *radial distance* $r > 0$ from the axis and by the oriented *scattering angle* $\omega \in (-\frac{\pi}{2}, \frac{\pi}{2})$ between the outgoing trajectory and the radial direction; see Fig. 6(a).

Thanks to the symmetry of the self-collision with respect to the radial direction, the angle ω also determines the direction of incoming trajectory. For the same reason, the outgoing particle also has velocity u and impact parameter ρ. The angle between the inner trajectory and the radial direction is determined by the conical geometry and it is equal to $\frac{\pi}{2} - \frac{\gamma}{2}$, cf. Fig. 6(b). The length s of the inner trajectory is then $s = 2r\sin\gamma/2$.

The collision parameters r and ω encode the same information as the initial parameters u and ρ. Indeed, ρ in terms of r and ω is given by the simple geometry

$$\rho = r\sin\omega. \tag{2.1}$$

Since the radial projection of the particle velocity before and after the collision is the same (as a consequence of the laws of the elastic impact, as we discussed for finite balls), the incoming velocity u is related to the inner velocity v along the trajectory between the self-collision as

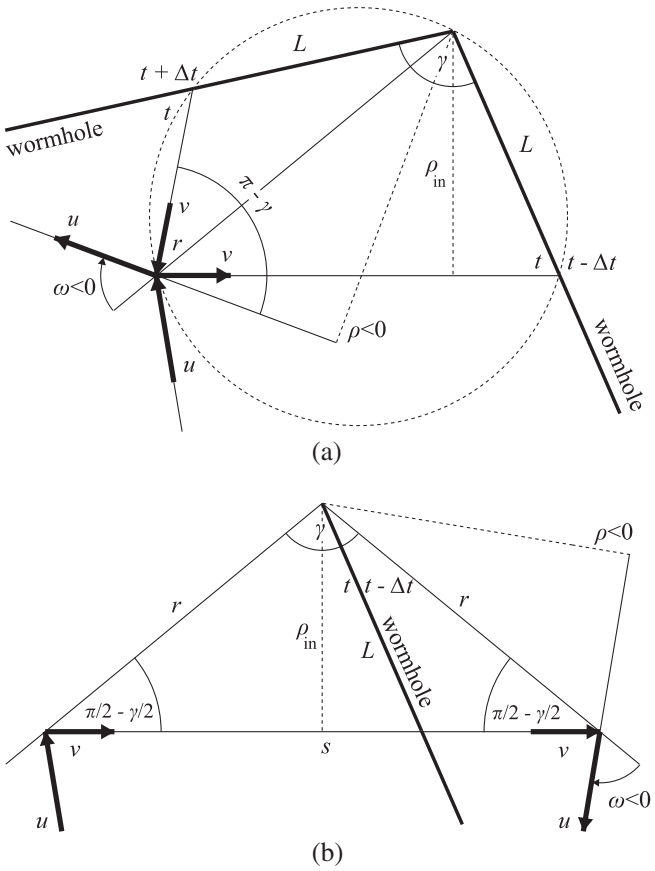

FIG. 6. *Geometry of self-colliding point-particle trajectory.* (a) A point particle is approaching the wormhole from infinity with a velocity u and impact parameter ρ; it collides with the version of itself which has already passed through the time machine, and with a velocity v moves toward the wormhole. After passing the wormhole and self-colliding with itself, it moves with the velocity u back to infinity. The self-collision occurs at the distance r from the axis, and the outgoing trajectory forms with the radial direction the orientated angle ω. Thanks to symmetry of the self-collision with respect to radial direction, the angle ω is half of the angle between the incoming and outgoing trajectory. (b) The same situation depicted in a map which cuts the conical space not along the wormhole but along the radial direction through the self-collision. The length s of the straight trajectory between its self-intersection is given by $s = 2\rho\tan\frac{\gamma}{2} = 2r\sin\frac{\gamma}{2}$.

$$u\cos\omega = v\sin\frac{\gamma}{2}. \tag{2.2}$$

However, the inner velocity must be such that the particle passes the inner trajectory exactly in the time Δt gained in the wormhole,

$$v = \frac{s}{\Delta t} = \frac{2r\sin\frac{\gamma}{2}}{\Delta t}. \tag{2.3}$$

We thus obtain relation for u:

$$u = \frac{2r\sin^2\frac{\gamma}{2}}{\Delta t\cos\omega}. \tag{2.4}$$

[2]More precisely, the physical solutions of type I are geometrically identical to spurious solutions of type II and vice versa. Of course, for a point particle we cannot distinguish from which side the particle hits itself.

[3]Here, we completely ignore motion along the axis of the wormhole.

It will be also useful to write down the relation for ρ as a function of ω and u:

$$\rho = \frac{u\Delta t}{4\sin^2\frac{\gamma}{2}}\sin(2\omega). \tag{2.5}$$

Eqs. (2.1) and (2.4) thus relate the parameters of the incoming trajectory u, ρ and the parameters of the self-collision r, ω. Their consequences will be discussed in more detail in Sec. IV.

Before we return to the case of finite balls, let us note that we can introduce similar parameters for the free trajectory. The only difference is that r and ω refer, in general, to self-intersection (i.e., not necessarily to self-collision) of the free trajectory. Clearly, the angle ω is now given just by the conical geometry

$$\omega = \omega_{\text{free}} \equiv \frac{\pi - \gamma}{2}. \tag{2.6}$$

The solutions, for which the younger version of the particle passes through the point of self-intersection later than the older version (coming from the time machine), are the solutions of type I. When the younger particle passes the point of self-intersection earlier, we speak about the solutions of type II.

The self-intersection threatens to become a self-collision if time spent on the inner part of the free trajectory is equal to the time shift of the time machine. Because $u = v$ for a free trajectory , conditions (2.1) and (2.3) give

$$u_{\text{px}}\Delta t = 2\rho_{\text{px}}\tan\frac{\gamma}{2}. \tag{2.7}$$

Such values u_{px}, ρ_{px} correspond to the paradoxical free trajectory for which the particle occurs at the point of self-intersection twice at the same time. For a point particle, it is not possible to decide plausibly what happens in such a situation. We can only observe that the same parameters u_{px}, ρ_{px} also describe the trajectory with one self-collision, which is given by the same parameters as paradoxical self-intersection of the free trajectory, namely $r = \rho_{\text{px}}/\cos\frac{\gamma}{2}$ and $\omega = \omega_{\text{free}}$. A detailed analysis of this situation will be done for finite balls in Sec. III.

The direction ω_{free} is also the boundary value between physical collisions of types I and II. Physical self-collisions of type I, for which the trajectory deflects leftward from the free trajectory, are bounded within the interval $\omega \in (\omega_{\text{free}}, \frac{\pi}{2})$; while physical self-collisions of type II (with rightward deflection) sweep out the interval $\omega \in (-\frac{\pi}{2}, \omega_{\text{free}})$.

D. Finite ball

We have to be more precise to define the parameters of the self-collision for a finite ball. Let r be the radial distance from the axis of the intersection of the incoming and outgoing trajectories (extended beyond the actual self-collision), and let $\tilde{r}$ be the radial distance from the axis of the self-intersection of the inner trajectory (for type II extended beyond the self-collision); see Fig. 5. Clearly, Eq. (2.1) still holds, and $r = \tilde{r} \pm R(\tan\gamma/2 - \cot\omega)$, with upper sign for type I and lower sign for type II. The geometry of the inner trajectory of the finite balls is identical with that of a point particle with modified impact parameter $\tilde{\rho} = \tilde{r}\sin\omega$. The path s traveled during time Δt gained in the time machine must be corrected due to a finite radius of balls, $s = \tilde{s} \pm \frac{2R}{\cos\gamma/2}$, where, analogously to the point-particle case, $\tilde{s} = 2\tilde{r}\sin\gamma/2$ is the length of the inner trajectory between its self-intersection. The corrected relation (2.3) together with (2.2) finally leads to equation between u, ρ, and ω:

$$\rho = \frac{1}{4\sin^2\frac{\gamma}{2}}\left(u\,\triangle\, t\sin 2\omega \mp 4R\sin\frac{\gamma}{2}\sin\left(\frac{\gamma}{2} + \omega\right)\right), \tag{2.8}$$

again, with upper/lower sign for types I/II, respectively.

Physical self-collisions of type I or II are restricted by the conditions

$$\omega > \omega_{\text{free}} \qquad \text{for physical solutions of type I,} \tag{2.9}$$

$$\omega < \omega_{\text{free}} \qquad \text{for physical solutions of type II;} \tag{2.10}$$

otherwise the ball would deflect to a wrong side of the free trajectory and the momentum transfer from the younger to older version of the ball would be negative.

Equation (2.8) supersedes relation (2.5) for the point particle, as can be also seen by taking the limit $R \to 0$. This can be regarded as the key equation of motion which determines the scattering angle ω in terms of the initial conditions u and ρ. The position of the self-collision is then determined by the parameter r, which is given by Eq. (2.1).

III. NUMBER AND CHARACTER OF SOLUTIONS

A. Pointlike particle

In the case of the point particle, there is only one length scale $u\Delta t$ given by the initial velocity u and the time shift Δt. The velocity u thus changes only the scale of the whole experiment. Therefore, we can fix u and study only the relations among ρ, r, and ω.

The relation between ω and ρ is given by Eq. (2.5) and depicted in Fig. 7; the relation to the parameter r is given by (2.1) [or, alternatively, implicitly by Eq. (2.4)].

We immediately see that the self-collision can happen only for

$$|\rho| < \rho_{\max} \equiv \frac{u\Delta t}{4\sin^2\frac{\gamma}{2}}. \tag{3.1}$$

For larger $|\rho|$, the particle would not be fast enough to travel through the wormhole and hit itself consistently—it would be too far from the axis of the wormhole, and the path through the wormhole would be too long.

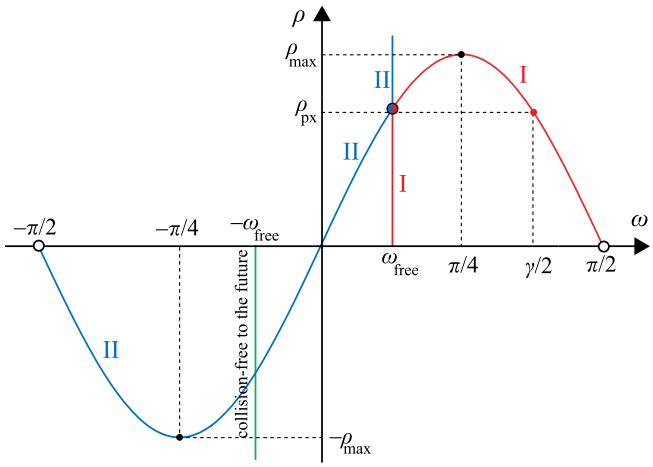

FIG. 7 (color online). *The ρ-ω diagram of consistent solutions for a point particle*. Each point of the graph in the ρ-ω plane represents a consistent solution for a point particle with at most one self-collision. The velocity u is fixed (it changes only a scale of the solutions), and the parameter r is given by Eq. (2.1). Collision-free solutions are represented by the straight vertical lines. The line $\omega = -\omega_{\text{free}}$ (in green) represents collision-free trajectories to the future; the line $\omega = \omega_{\text{free}}$ represents free trajectories to the past. The points below the value ρ_{px} (in red) corresponds to the solutions of type I, for which the younger particle passes the point of self-intersection later than that coming from the wormhole. The solutions with $\rho > \rho_{\text{px}}$ (in blue) are of type II. The sinusoidal part of the graph represents solutions with one self-collision. The part with $\omega > \omega_{\text{free}}$ (in red) represents self-collisions of the type I; the part with $\omega < \omega_{\text{free}}$ (in blue) represents self-collisions of type II. Self-colliding solutions are thus possible only for $|\rho| < \rho_{\text{max}}$. The point $(\rho_{\text{px}}, \omega_{\text{free}})$ represents both the paradoxical collision-free solutions for which younger and older versions of the particle meet at the point of intersection at the same moment, and the consistent self-colliding solution (which is geometrically identical to the paradoxical solutions). Exact relation of these solutions is clarified in the case of balls with a finite radius.

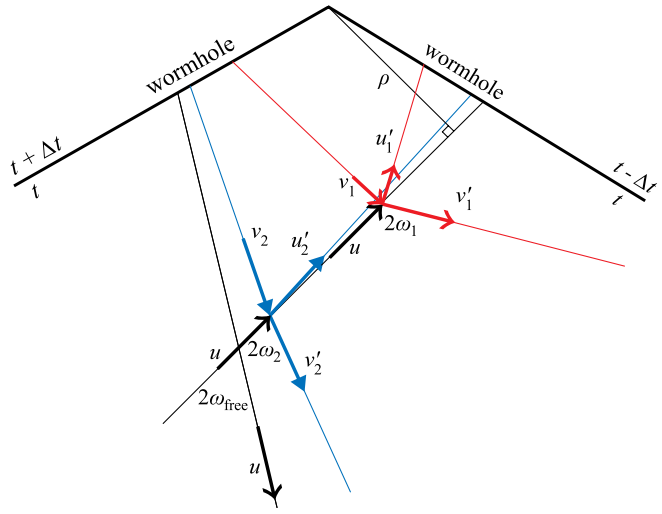

FIG. 8 (color online). *Three possible solutions for given initial conditions of a pointlike particle*. For $|\rho| < \rho_{\text{max}}$, $\rho \neq \rho_{\text{px}}$ there exist three possible solutions: the collision-free trajectory (black) and two self-colliding trajectories (red/gray and blue/light-gray). One of the self-colliding trajectories is close to the free trajectory (it coincides in the limit $\rho \to \rho_{\text{px}}$); another is rather different.

For $|\rho| < \rho_{\text{max}}$, the map $\rho \to \omega$ is not a unique relation: for a given ρ we have, in general, two ω satisfying (2.5). For the given initial conditions, we thus obtain, in addition to the collision-free trajectory, two self-colliding solutions. These two solutions have the scattering angles complementary to $\pm\frac{\pi}{2}$ and represent completely different evolutions of the system. Note that the self-colliding solutions exist even if $\rho < 0$, i.e., if the free trajectory passes the wormhole to the future.

All three possible solutions for the given initial conditions (with $\rho < \rho_{\text{max}}$) are shown in Fig. 8.

For the paradoxical value $\rho = \rho_{\text{px}}$, Eq. (2.7), the "paradoxical" collision-free solution geometrically coincides with one of the self-colliding solutions. It is called paradoxical because, for these initial values, the free-moving particle meets itself at the point of self-intersection exactly at the same moment, so it cannot be the collision-free solution. However, since for a pointlike particle we cannot distinguish the noncolliding solution from the colliding one, it is dubious to study the nature of this paradoxical situation. Therefore, we will discuss the details of the paradoxical initial conditions in the case of finite balls. After that, we will return to the simpler case of a pointlike particle to study the geometry of the trajectories in more detail.

B. Paradoxical situations for a finite ball

In the case of finite balls, the system has an additional length scale given by the radius R of the ball. Therefore, the dependence on the velocity u is not trivial any more. Nevertheless, we still fix the value of the initial velocity and discuss the structure of the corresponding solutions. The values of various quantities can, however, depend on u in a more complicated way than just a rescaling.

Collision-free trajectories of a finite ball are again characterized by the angle ω_{free}, and they can be also divided into types I and II; see Fig. 9. However, due to the finite radius of the balls, there is a whole interval of the impact parameter ρ, for which the collision-free trajectory becomes paradoxical—if the ball hits itself inconsistently. Checking the geometry of the free trajectory of a ball, it turns out [16] that the boundary of this interval is given by values of ρ determined by Eqs. (2.8) for types I and II with $\omega = \omega_{\text{free}}$,

$$\rho \text{ paradoxical} \Leftrightarrow \rho \in (\rho_{\text{pxI}}, \rho_{\text{pxII}}). \tag{3.2}$$

Explicitly, the paradoxical values of the impact parameter are given by

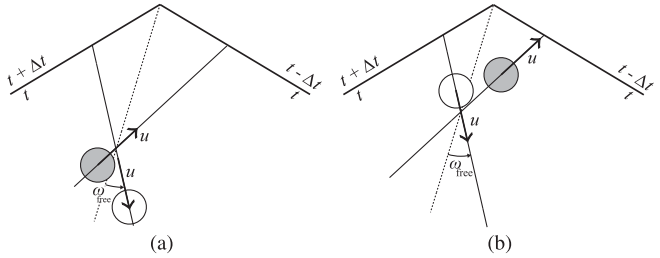

FIG. 9. *Two types of collision-free trajectories passing the time machine to the past.* (a) Trajectory of type I. For $\rho < \rho_{\mathrm{pxI}}$, time s/v spent by the ball between the self-collision is smaller than the time shift Δt, i.e., the younger version of the ball goes through the point of self-intersection later than the older version. (b) Trajectory of type II. For $\rho > \rho_{\mathrm{pxII}}$, the younger version of the ball goes through the point of intersection earlier than the older version.

$$\rho_{\mathrm{pxI,II}} = \frac{u \triangle t}{2 \tan\frac{\gamma}{2}} \mp \frac{R}{\sin\frac{\gamma}{2}}. \tag{3.3}$$

For $\rho < \rho_{\mathrm{pxI}}$, the collision-free trajectory is of type I, i.e., the older version of the ball overtakes the younger one at the point of intersection. If $\rho > \rho_{\mathrm{pxII}}$, the collision-free trajectory is of type II, cf. Fig. 9.

The parameters of the self-colliding trajectories are characterized by relations (2.8) and (2.1). We can depict the physical solutions (cf. conditions (2.9)) with at most one self-collision in a diagram analogous to the one we used in the point-particle case; see Fig. 10.

We see here that the solutions split into two branches: the physical self-colliding solutions of type I together with collision-free solutions of type I, and self-colliding and collision-free solutions of type II. The collision-free solution of type I becomes the self-colliding solution of type I for $\omega = \omega_{\mathrm{free}}$, $\rho = \rho_{\mathrm{pxI}}$. It is a limiting case when the ball on the free trajectory just touches itself but does not exchange any momentum. It is thus identical to the limiting case of physical self-colliding solutions of type I. Similarly, for $\omega = \omega_{\mathrm{free}}$, $\rho = \rho_{\mathrm{pxII}}$ the ball on the free trajectory just touches itself, now from the other side, and it becomes the self-colliding solution of type II.

Inspecting Fig. 10, we can also conclude that for the initial conditions with $\rho \notin (-\rho_{\mathrm{maxII}}, \rho_{\mathrm{maxI}})$ (where $\rho_{\mathrm{maxI,II}}$ are given by the maximal values of the expression (2.8) for types I and II, respectively), there exists just one consistent solution. It is typically a collision-free trajectory; however, for certain values of parameters it can also be a self-colliding solution, cf. Fig. 11(b).

For initial conditions with $\rho \in (-\rho_{\mathrm{maxII}}, \rho_{\mathrm{maxI}})$, there are three possible solutions; typically, one collision-free and two self-colliding. However, for the paradoxical values of the impact parameter $\rho \in (\rho_{\mathrm{pxI}}, \rho_{\mathrm{pxII}})$, the collision-free solution is superseded by a self-colliding solution,

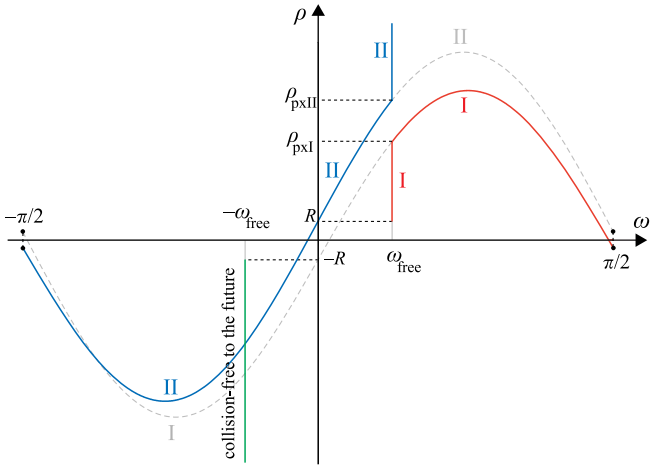

FIG. 10 (color online). *Physical solutions in the ρ-ω plane.* The points on the curves represent solutions characterized by the parameters ρ and ω. The initial velocity u is fixed. The physical solutions correspond to the solid curves, the spurious one to the dashed curves. Vertical lines are collision-free solutions. Sinusoidal curves, determined by Eqs. (2.8), represent the solution with one self-collision. The type of the solution is indicated in a similar way as in Fig. 7.

cf. Fig. 11. In this case, we obtain two self-colliding solutions of type I and one solution of type II; see Fig. 12.

We can conclude that the paradoxical initial conditions are not paradoxical in any dangerous way. These initial conditions lead to the same number of solutions as other sufficiently close initial conditions. Only the character of solutions is different: the collision-free solution

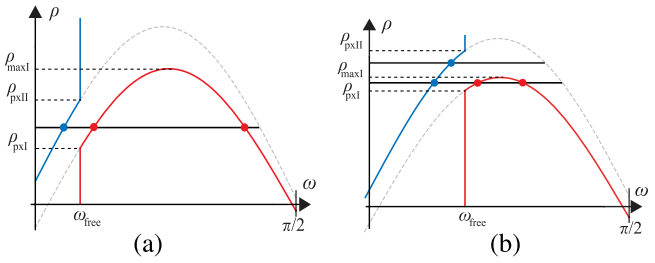

FIG. 11 (color online). *Number of solutions for given initial conditions.* The number of solutions for chosen initial parameter ρ can be determined from Fig. 10 by intersecting the graph with the horizontal line corresponding to ρ. The choice of the initial velocity u can slightly modify a shape of the diagrams. Here, two representative cases are shown. Only the part with $\omega > 0$ is depicted—it corresponds approximately to the initial conditions $\rho > 0$ with the ball directed to the time machine toward the past. Clearly, the number of solutions steps from one to three, with ρ becoming smaller than ρ_{maxI}. In the paradoxical interval $(\rho_{\mathrm{pxI}}, \rho_{\mathrm{pxII}})$ the number of solutions remains the same. Only the character of the solutions is different: the collision-free solution is superseded by the self-colliding solution. In the case (b), the limiting value ρ_{maxI} belongs to the paradoxical interval. For $\rho \in (\rho_{\mathrm{maxI}}, \rho_{\mathrm{pxII}})$ there exists just one self-colliding solution.

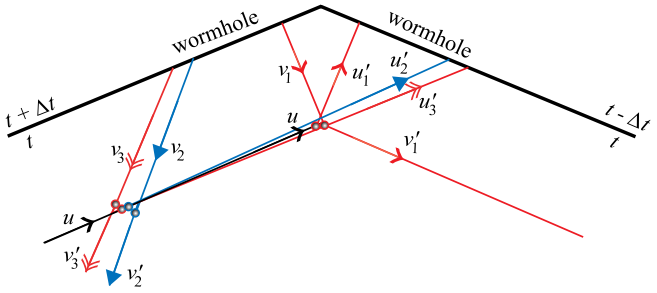

FIG. 12 (color online). *Three self-colliding solutions for ρ from the paradoxical interval*. Unlike the pointlike case, there is a whole interval $(\rho_{\mathrm{pxI}}, \rho_{\mathrm{pxII}})$ where collision-free trajectories do not exist. As we can see from Fig. 11(a), the collision-free trajectory is replaced by a self-colliding one. The diagram depicts all three self-colliding solutions, two of type I (in light and dark red) and one of type II (in blue).

changes to the self-colliding solution. The number of solutions depends on other characteristics, namely, if $\rho \in (-\rho_{\mathrm{maxII}}, \rho_{\mathrm{maxI}})$: for a large $|\rho|$, only the collision-free solution is admissible.

However, it should be said that the situation changes if the angle between the wormhole mouths is smaller. For $\gamma < \frac{\pi}{2}$, the equations for the trajectory remain the same but the value of the angle ω_{free} is larger than $\frac{\pi}{4}$. The structure of the solutions thus changes, as depicted in Fig. 13. Clearly, for $\rho \in (\rho_{\mathrm{pxI}}, \rho_{\mathrm{pxII}})$, the collision-free trajectory is not possible, and it is not superseded by another solution. Moreover, for such ρ, there exists only one self-colliding solution. In this case, we can indeed speak about paradoxical initial conditions, since the solutions evolved from these conditions are really restricted. However, in the case $\gamma < \frac{\pi}{2}$ the whole discussion is more complicated, since the particle can self-interact in a more complicated way (there is the possibility of self-intersection between several self-collisions, etc.). We do not have any indications that these more complicated processes could improve

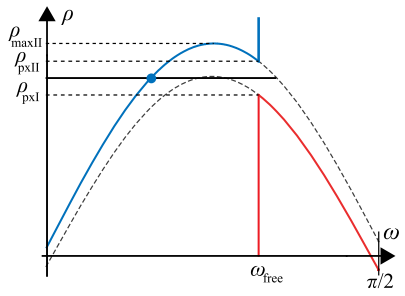

FIG. 13 (color online). *Solutions from paradoxical interval for* $\gamma < \frac{\pi}{2}$. In this case, the collision-free angle is $\omega_{\mathrm{free}} > \frac{\pi}{4}$. For the impact parameter ρ from the corresponding paradoxical interval $\rho \in (\rho_{\mathrm{pxI}}, \rho_{\mathrm{pxII}})$, we find a gap in the solution curves. For a paradoxical ρ, we obtain only one self-colliding solution. Moreover, this solution corresponds to a value of ω which is substantially different from ω_{free}.

the discussed behavior; however, we have not excluded it completely [16]. In the following, we restrict again to the larger angles, $\gamma > \frac{\pi}{2}$.

IV. MOTION OF A POINTLIKE PARTICLE

To clarify the character of solutions with paradoxical initial conditions, in this section we describe the motion of a pointlike particle in more detail.

The geometry of the inner trajectory is given only by the parameter r and by the angular position of the self-collision with respect to the wormhole—i.e., it is independent of the scattering angle ω. The geometry is such that the point of self-collision, the point of the entry to wormhole, the point of the departure from the wormhole, and the axis itself all belong to a common circle, cf. Fig. 6(a). The inner particle velocity v is given by Eq. (2.3). For the fixed point of self-collision, one can then choose any $\omega \in (-\frac{\pi}{2}, \frac{\pi}{2})$, which determines ρ through Eq. (2.1), and calculate the initial velocity using Eq. (2.2).

Taking into account the rotational symmetry of the conical space between the mouths of the wormhole, we can ignore the angular position with respect to the wormhole in the discussion about many features of the motion. But, when discussing the asymptotic behavior of the incoming and outgoing trajectories, the angular information must be taken into account. Namely, one has to track if the outer trajectories pass through the wormhole. Clearly, it must occur for the scattering angle $\omega > \frac{\gamma}{2}$, but depending on the angle between the self-collision and wormhole, it can happen also for smaller angles ω.

However, we first describe the motion without a reference to the wormhole mouths. It can be done in the simplest way employing the totally covering space for our conical space. Namely, instead of the conical space with angular coordinate $\varphi \in (-\frac{\gamma}{2}, \frac{\gamma}{2})$, we use the space without any restriction on φ, i.e., a helical surface winding around the axis infinitely. The original conical space is then obtained by the identification of points which differ in coordinate φ by an integer multiple of γ.

In this covering space, the trajectory can be described as follows. Let us assume a particle incoming along the direction $\varphi_{\mathrm{in}} = 0$ with the impact parameter ρ and the initial velocity u. The self-collision C for such a trajectory always happens on the circle which we call the *collision circle*. It has the center S on the radial line $\varphi = 0$, it passes through the axis, and its radius is ρ_{max}, cf. Fig. 14. For $\rho \in (-\rho_{\mathrm{max}}, \rho_{\mathrm{max}})$, the incoming trajectory intersects this circle twice, which corresponds to two possible self-colliding solutions. The angular coordinate φ of self-collision is given exactly by the scattering angle ω. At the point of self-collision C, the trajectory is deflected, and it continues toward the point C', which can be obtained by a counterclockwise rotation of the point C around the axis by angle γ, cf. Fig. 14. In the covering space, C and C' are different points; however, in the original conical space these points

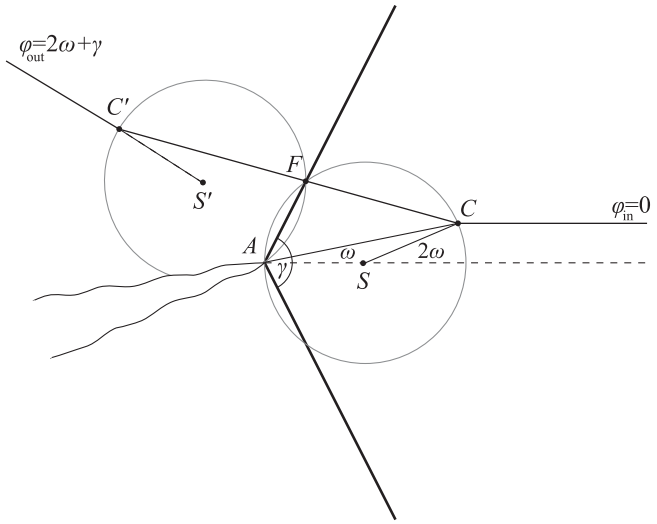

FIG. 14. *Self-colliding trajectory in the totally covering space.* The particle incoming along the direction $\varphi_{\text{in}} = 0$ with the impact parameter ρ is deflected at the point of self-collision C. The point C must lie on the collision circle with the center S on the radial line $\varphi = 0$, it passes through the axis A, and its radius is $\rho_{\max}$. The trajectory continues toward the point C', which is obtained by a counterclockwise rotation of the point C around A by angle γ. In the original conical space, points C and C' are identified and correspond to the point of self-collision. From C', the trajectory continues in the direction which aims from the center S' of the rotated collision circle. The direction of the inner trajectory goes through the focusing point F. The diagram shows only a part of the totally covering space.

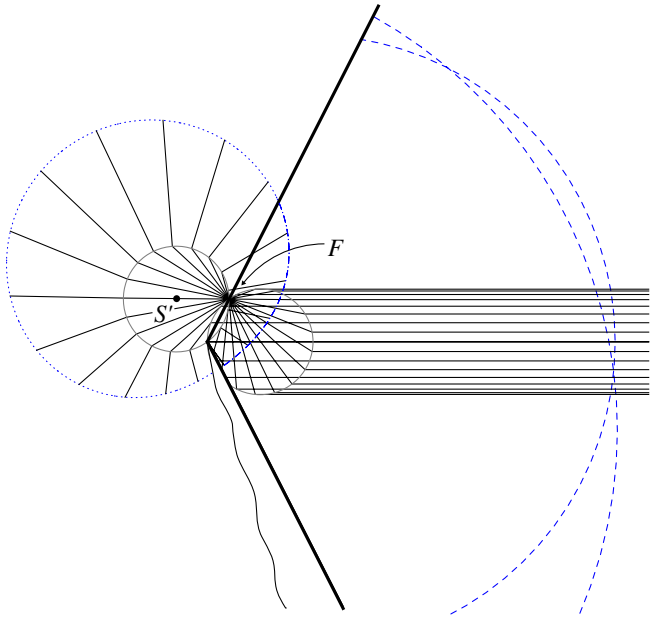

FIG. 15 (color online). *Scattering of the plane-wave congruence of particles in the totally covering space.* Congruence of particles coming along $\varphi_{\text{in}} = 0$ direction in "plane-wave" configuration (i.e., aligned at an initial moment on a planar "wave front" perpendicular to the direction of motion) approaches the time machine. The particles scatter on the collision circle and move toward the corresponding points on the rotated collision circle. Here, they are deflected in the directions coming from the center S' of the rotated collision circle. The dotted curve depicts the wave front after the scattering in the totally covering space. The particles do not scatter on the collision circle at the same time; however, for large final times the wave front after scattering approaches the circle. The real wave front projected back to the conical space is drawn as dashed curves. Segments projected from various sheets of the totally covering space gain additional time shift thanks to the passage through the time machine. Therefore, these parts of the wave front are larger since the particle had more time for their motion. Inner trajectories focus at one focusing point; for $\omega \in (-\frac{\gamma}{2}, \frac{\gamma}{2})$, they pass through this point. The diagram shows only part of the totally covering space, given approximately by $\varphi \in (-\frac{\gamma}{2}, 2\pi - \frac{\gamma}{2})$.

are identified as the point of self-collision—of course, the particle must pass the point of self-collision twice. Finally, from C' the particle continues through the covering space in the direction which aims from the center S' of the rotated collision circle, cf. Fig. 14.

Notice that particles which approach the time machine along the same direction $\varphi = 0$ [with various $\rho \in (-\rho_{\max}, \rho_{\max})$, thus forming congruence with "plane-wave" wave front] self-collide on the common colliding circle and, in the end, leave in the directions which point out from the common point S', cf. Fig. 15. In the covering space, the original plane-wave congruence of particles scatters to the circular-wave congruence, but the particles are phase shifted. They fly in radial directions, but the wave front of the congruence at one moment does not form a circle since the particles start to move in the radial directions in various times. Indeed, the incoming particles reach the collision circle in various times and, therefore, their self-collisions do not occur simultaneously.

Let us mention an interesting feature of the trajectories of the discussed congruence: all inner trajectories (between the self-collisions) have the direction going through one focusing point F, cf. Fig. 15. For $\omega \in (-\frac{\gamma}{2}, \frac{\gamma}{2})$, they even pass through this point. The congruence thus focuses in this point; however, the particles do not pass the focusing point at the same moment.

We have obtained a simple picture of the motion in the covering space. It complicates slightly if we return to the conical space by choosing the orientation of the wormhole [i.e., setting mouths at the angles $-\frac{\gamma}{2} + \psi$ and $\frac{\gamma}{2} + \psi$ with $\psi \in (-\frac{\gamma}{2}, \frac{\gamma}{2})$] and making the identification of points with φ differ by an integer multiple of γ. The resulting picture depends on the values of γ, ψ and of the impact parameter ρ; some of the representative trajectories are depicted in Fig. 16.

The typical quantity, which depends on the angular position of the self-collision, is the total time T gained in the wormhole during the whole scattering process. It can be read out in the covering space from the angular coordinate

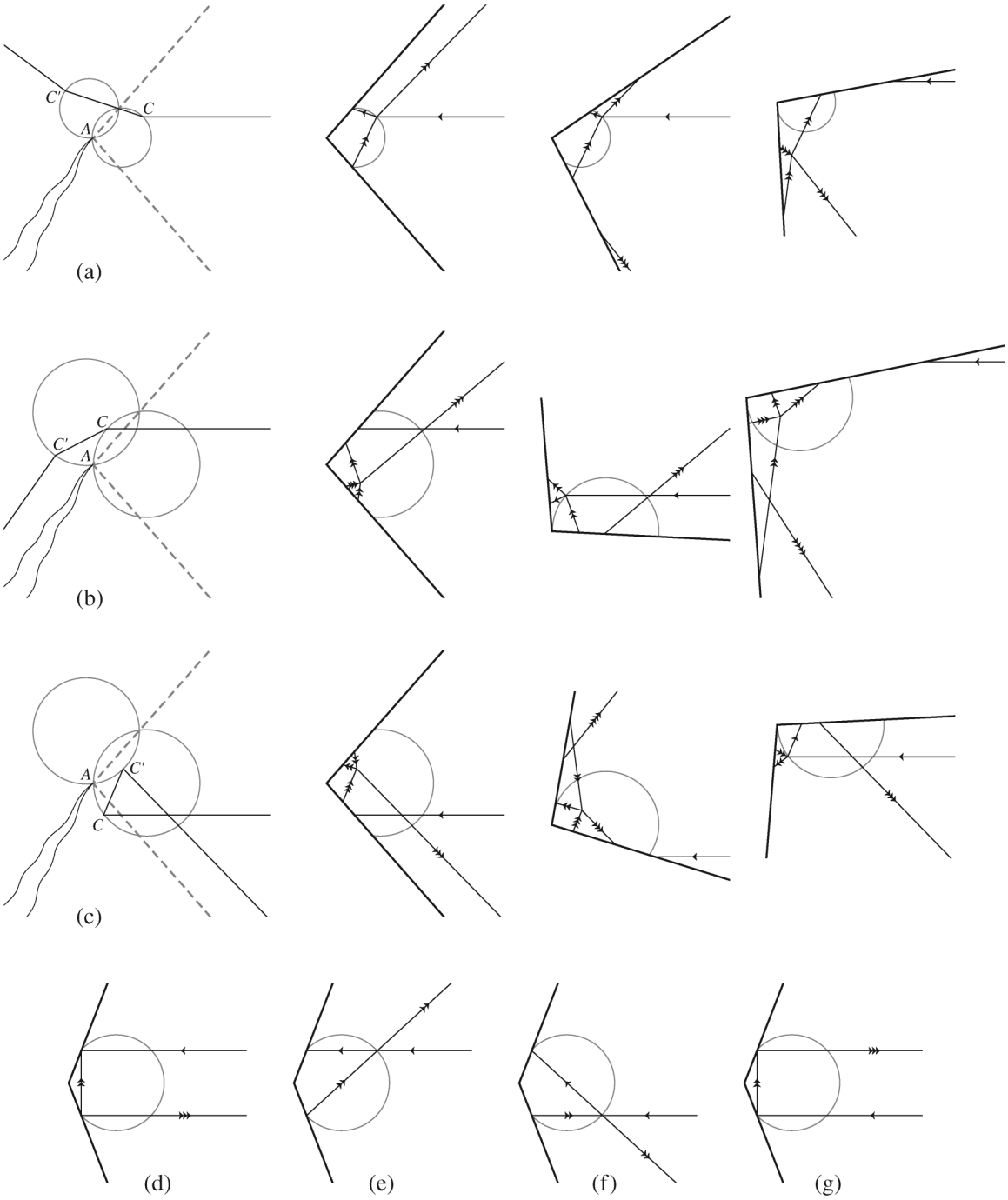

FIG. 16. *Examples of the self-colliding trajectories.* Diagrams show trajectories with various choices of the impact parameter ρ, or, equivalently, with a different scattering angle ω. The angle ω also parameterizes the position of the self-collision on the collision circle. Diagrams (a, b, c) represent typical cases $\omega \in (0, \frac{\pi}{4})$, $\omega \in (\frac{\gamma}{2}, \frac{\pi}{2})$, and $\omega \in (-\frac{\pi}{2}, -\frac{\gamma}{2})$, respectively. The diagram in the first column depicts the trajectory in the totally covering space, the second column shows the trajectory in the conical space with the wormhole centered on the direction of the incoming trajectory ($\psi = 0$), and the third and the fourth columns correspond to other orientations of the wormhole. The diagrams (d, e, f, g) depict special choices of the trajectory, namely, those with $\omega = \frac{\gamma}{2}$, $\omega = \omega_{\text{free}}$, $\omega = -\omega_{\text{free}}$, and $\omega = -\frac{\gamma}{2}$, respectively, in all of them with the wormhole centered on the incoming trajectory. The arrows indicate passages through the wormhole; however, they do not count the time shift, since the particle can travel through the time machine in both directions. We can observe that the structure of the trajectory can change substantially with various choices of the impact parameter and of the incoming direction with respect to the wormhole. For example, the particle can self-collide after passing through the wormhole, both into the past and future, or it can move through the wormhole after the self-collision.

$\varphi_{\text{out}} = 2\omega + \gamma$ of the outgoing trajectory[4]—if it belongs to nth copy of the wormhole in the covering space, $n \in \mathbf{Z}$, the particle gains the time shift $T = -n\Delta t$:

$$\varphi_{\text{out}} \in \left(-\frac{\gamma}{2} + \psi + n\gamma, \frac{\gamma}{2} + \psi + n\gamma\right) \Rightarrow T = -n\Delta t. \tag{4.1}$$

Taking into account the restrictions on γ, ψ, and ω, the total time shift can be $-3\Delta t \leq T \leq \Delta t$. See Fig. 16 for examples.

The total time shift can be similarly calculated for the collision-free trajectories. In this case, the direction of the outgoing trajectory in the covering space is $\varphi_{\text{out}} = \pi$ for the trajectories passing the wormhole to the past, and $\varphi_{\text{out}} = -\pi$ for the trajectories passing the wormhole to the future. The condition (4.1) gives that the trajectory traveling to the past, $\rho > 0$, gains the time shift $T = -\Delta t$ for $\psi \in (-\frac{\gamma}{2}, \frac{3}{2}\gamma - \pi)$, or it can pass the wormhole twice, $T = -2\Delta t$, if $\psi \in (\frac{3}{2}\gamma - \pi, \frac{\gamma}{2})$. Similarly, for $\rho < 0$, the particle gains the time shift $T = \Delta t$ for $\psi \in (\pi - \frac{3}{2}\gamma, \frac{\gamma}{2})$ and $T = 2\Delta t$ for $\psi \in (-\frac{\gamma}{2}, \pi - \frac{3}{2}\gamma)$.

V. CONCLUSION

We have analyzed a simple interacting system in the space with a nontrivial causal structure. We have assumed the principle of self-consistency, i.e., we have required the validity of standard local physical laws and we have searched for consistent global solutions. In such a setting, one can formulate the analogue of the so-called ''grandfather paradox'' as a question of whether all natural initial conditions lead to the globally consistent solutions of the local physical laws. Initial conditions which do not lead to such solutions would be paradoxical, and the system with a nontrivial set of paradoxical initial conditions would be logically inconsistent.

We have shown that the investigated system of finite billiard balls in the nonrelativistic space with a time machine realized by a wormhole with a time shift is not logically inconsistent in this sense. A naïve guess can identify potentially paradoxical initial conditions for which the ball sent through the time machine hits itself and inconsistently changes its own motion. The detailed analysis has shown that even for such initial conditions there exists a global solution satisfying locally all physical laws.

This result was anticipated, since it agrees with the previous results obtained for various other systems—in particular, for the very closely related system studied in [13]. Our results thus endorse one of the main messages of the study of the system with a nontrivial causal structure: that the presence of time machines does not necessarily imply a drastic reduction of space of the classical solutions of the equations of motion. However, the previous results have been obtained mainly for linear (noninteracting) systems or through a rather complicated and cumbersome analysis of interacting systems. Therefore, the confirmation for the interacting system allowing a detailed explicit analysis is valuable.

We have also confirmed another similarly interesting result discussed in [13]. The presence of the nontrivial causal structure in our system has enlarged the space of solution. We have found that for a wide class of initial conditions (namely for $|\rho| < \rho_{\max}$ with given u), more than one classical evolutions exist. In addition to the ''standard'' collision-free trajectory, the particle can also move along two different self-colliding trajectories; see Fig. 8. The evolution of the system thus fails to be deterministic, and the classical theory does not have any means to determine which of the different evolutions would be realized.

One can speculate that the quantum theory would be a more complete description. It does not determine exact trajectory of the particle—it just estimates a probability for various possible evolutions (specified up to a quantum uncertainty). In the classical limit, only evolutions close to the solutions of the classical laws would have a nontrivial probability. In systems with standard causal structure, there is usually only one such solution. However, in our system, one can expect that all three classical solutions would have nontrivial probabilities and a semiclassical approximation could give an estimate for these probabilities.

Nevertheless, one has to emphasize that it is not trivial at all to complete this program. The status of quantum theory in the presence of time machines is unclear. The common formulations of the quantum theory are heavily based on the standard notion of time, so a nontrivial causal structure would change the theory substantially.[5] It would be extremely interesting to find a modification of the quantum mechanics for a space with time machines, but it is a hard challenge for further work. The simplicity of our model could give hope that such a challenge is treatable.

However, one could ask what a key ingredient is for the existence of more solutions of the classical equations of motion. Is it really the presence of the time machine? One could also suspect a peculiar geometrical structure of our conical space. The conical space breaks the uniqueness of the classical solutions even without the time machine.

[4]We have chosen the incoming trajectory with $\varphi_{\text{in}} = 0$, and its angular position with respect to the wormhole is given by the parameter ψ. Alternatively, we could set $\psi = 0$ and admit $\varphi_{\text{in}} \neq 0$.

[5]As an example of possible difficulties, let us mention that one would have to take into account the quantum space for degrees of freedom ''hidden inside'' the time machine, i.e., the degrees of freedom which are not encoded in the standard initial conditions. We ignored them on the classical level—they correspond, e.g., to a mysterious particle which appears from the wormhole, hits the particle coming from infinity, and deflects itself back to the time machine in such a way that it reappears from it exactly as the introduced mysterious particle. On a quantum level, such degrees of freedom cannot be easily ignored or separated.

Indeed, for given initial and final points, in the conical space there exist more trajectories which join them. This effect is purely geometrical and does not need a nontrivial causal structure. However, we have identified a different kind of uniqueness: we have found that the specification of both the initial position and the momentum (the complete initial conditions) admits more different evolutions, which is certainly surprising when the local evolution is given by standard differential equations which are generally accepted as deterministic. Nonuniqueness appears here as a strange result of the interplay between a local deterministic evolution and a nontrivial causal structure on a global scale for which the time machine is the key ingredient.

Let us finally mention that further study [16] of our system revealed that, if one takes into account a possibility of multiple self-collisions, the situation gets even more interesting. In this work, we have studied only the collision-free trajectories, and the trajectories with one self-collision. However, the incoming and outgoing trajectories from the self-collision can easily self-intersect and, for a special choice of parameters, even self-collide again. It is possible to show that when the impact parameter ρ gets smaller (with fixed u), there exist more and more multi-self-colliding solutions. For a pointlike particle, there exists a finite value $\rho^{\infty}_{\mathrm{max}}$ under which there exist an infinite number of possible evolutions for single initial parameters ρ and u, cf. [16]. We leave further details to the subsequent publication of [16].

To summarize, the studied system with a wormhole-based time machine does not suffer from the paradoxical initial conditions. On the contrary, it breaks the deterministic character of the theory and offers more solutions for single initial conditions.

ACKNOWLEDGMENTS

P. K. was supported by Grant No. GAČR-202/09/0772 and by Project No. MSM0021620860. The authors also thank Prof. Jiří Langer for reading the manuscript.

[1] K. Gödel, Rev. Mod. Phys. **21**, 447 (1949).
[2] F. Tipler, Phys. Rev. D **9**, 2203 (1974).
[3] M. S. Morris and K. S. Thorne, Am. J. Phys. **56**, 395 (1988).
[4] J. R. Gott, Phys. Rev. Lett. **66**, 1126 (1991).
[5] K. S. Thorne, *Black Holes and Time Warps: Einstein's Outrageous Legacy* (W. W. Norton & Company, New York, 1994).
[6] J. R. Gott, *Time Travel in Einstein's Universe: The Physical Possibilities of Travel Through Time* (Mariner Books, Boston, 2002).
[7] M. Visser, *Lorentzian Wormholes: From Einstein to Hawking*, AIP Series in Computational and Applied Mathematical Physics (AIP, New York, 1995).
[8] I. Novikov, Phys. Rev. D **45**, 1989 (1992).
[9] J. L. Friedman and M. S. Morris, Phys. Rev. Lett. **66**, 401 (1991).
[10] J. L. Friedman *et al.*, Phys. Rev. D **42**, 1915 (1990).
[11] M. S. Morris, K. S. Thorne, and U. Yurtsever, Phys. Rev. Lett. **61**, 1446 (1988).
[12] M. B. Mensky and I. D. Novikov, Int. J. Mod. Phys. D **5**, 179 (1996).
[13] F. Echeverria, G. Klinkhammer, and K. S. Thorne, Phys. Rev. D **44**, 1077 (1991).
[14] A. Carlini *et al.*, Int. J. Mod. Phys. D **4**, 557 (1995).
[15] S. V. Krasnikov, arXiv:gr-qc/0305070.
[16] J. Dolanský, thesis, Charles University, Prague, Czech Republic (unpublished, in English).

Appendix I

Dolanský, J. and Krtouš, P. 2008

Trajectories of particles in presence of the time machine

J. Dolanský[1], **P. Krtouš**[1]

[1] *Faculty of Mathematics and Physics, Charles University in Prague*

I Introduction

Time travel is a phenomenon which has been attracting interest in literature or in a general discussion for a long time. However, only after a formulation of the theory of relativity such considerations could be investigated on a more scientific and solid basis. Even the special relativity shows that different observers experience different times and one of them can "travel" to the future of the other by means of his relative motion (e.g., an astronaut returning from a trip to the centre of our galaxy after spending 40 years in a spaceship comes to the Earth where more than 50,000 years have elapsed). The general theory of relativity describes the gravitation as a curved spacetime and that opens a possibility to consider spacetimes with even more complicated geometrical and topological structures. It allows one to study a possibility that an observer could travel even to his own past – his worldline could pass through a geometrically or topologically nontrivial area to a region where the worldline originally started. Worldlines which even cross themselves are called *closed timelike curves (CTCs)* and it is customary to say that spacetimes with CTCs contain *time machines*.

Spacetimes with time machines are causally nontrivial – in such spacetimes you can send a signal to your own past or even try to influence the past – which immediately opens a question of consistency of standard physical laws as we know them. On a formal level it is the question of the existence of solutions of physical equations of motion and the question whether the initial value problem is well possessed. On a less formal level these problems can be phrased as well-known "grandfather paradox": in spacetimes with time machines you have to face a logical riddle what happens if you travel to your own past and kill your grand-father (just for scientific reasons). It would cause that you would not be born and therefore you could not travel to the past – which is clearly inconsistent.

However, a system containing live beings is too complicated with too many unknown physical laws. For this reason in the last two decades physicists have considered various spacetimes with CTCs and studied the consistency of different physical systems in these spacetimes. Surprisingly, such studies showed that for a simple physical system pathology of spacetimes is not so severe and the equations of motion can be consistently solved.

Let us formulate this point more precisely. We consider a spacetime containing a time machine and we want to study a system with well known local physical laws (e.g.,a point particle, or electromagnetic field). We do not change these local laws, i.e., we require that they hold locally in any small spacetime domain. However, in addition to the local laws we also require so-called *principle of consistency*: there must exist a *global consistent* solution of local laws. It means that we allow the system to propagate itself to its own past, however, it must be done in a *consistent* way with the original evolution in the past.

The key question of studies of time machines is whether such globally consistent evolutions exist for given local laws and whether these global evolutions are sufficiently generic. If the local laws did not have any consistent global solution, the spacetime would be clearly pathological and we could rule it out from our consideration. Similarly, the pathology would be serious if the local physical laws had only few globally consistent solutions.

As we said, extensive studies of different systems showed that spacetimes with CTCs are not necessarily causally pathological. Let us mention results for a system of interacting particles [1] or the scalar field theory [2] where it was shown that standard local laws have globally consistent solutions even in the presence of CTCs.

Another surprising result of such studies is that the existence of time machines does not usually restrict a number of consistent solution, but in opposite, it leads to a possibility of more than one globally consistent solutions for given initial values. In spacetimes with time machines we thus usually lose the uniqueness of the evolution.

In our work, we consider a very simple toy model of an elastically interacting point particle in non-relativistic spacetime with a simple time machine. In this model we demonstrate just discussed features. We show that any initial conditions have globally consistent evolutions, that this solution of local laws is not unique, and that a number of solutions is the same even for the initial conditions which lead to an apparently inconsistent solution which mimics discussed "grandfather" paradox. Namely, we consider a situation in which we send a particle through the time machine to its past in such a way that the particle hits itself and prevents thus itself from entering the time machine.

In the next section we shortly discuss the wormhole based time machines and we specify the details of our toy model. In section III we formulate equations of motion for a point particle and discuss globally consistent solutions. In the last section before Summary we shortly discuss the behavior of balls of finite radii. We present only the main results, their derivations will be presented in a more thorough publication [3].

II Conical spacetime with time machine

The simplest way how to construct spacetimes with CTCs is to consider a wormhole which can be then deformed to a time machine – such a procedure is described in detail , e.g., in reference [4]. The wormhole can be viewed as a shortcut between two spatial places. A simple spatial wormhole can be obtained by cutting out two spheres in a three dimensional space and gluing the surfaces of these holes together, cf. figure 1a. We thus obtain a topologically and geometrically nontrivial space – it is not a simply connected space and the geometry on the glued surface is not flat. In the full spacetime picture, a nontrivial geometry according to Einstein equations corresponds to a the presence of the stress-energy tensor – it means that the wormhole would be filled with some kind of matter. However, it is possible to deform the wormhole in such a way that some of its parts are flat, without matter.

The wormhole thus connects two places, which could be very distant in the surrounding space. The entries into the wormhole are called *mouths*.

In the spacetime picture, we have to specify also the moments of time when both mouths are identified. It seems natural to assume that they are identified at the same time, but it is not

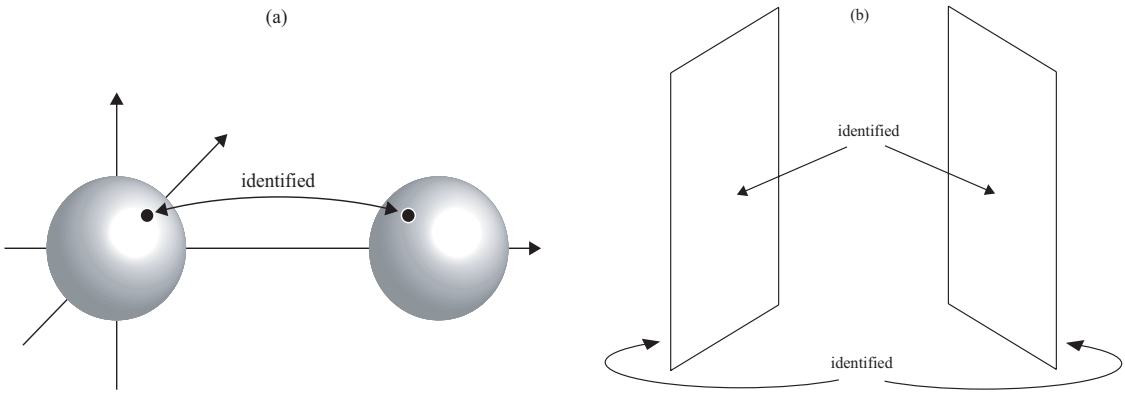

Figure 1: **Spatial representation of two simple wormholes.** (a) A wormhole formed by identification of two spherical holes in surrounding Euclidian space. Surfaces of both spheres are isometrically identified. Since the external curvature of these surfaces is non-vanishing, the geometry near the glued spherical surface is not flat. (b) A wormhole obtained by gluing two planar sections (which, could be obtained from (a) by squeezing the spheres into very thin planes). The external curvature is vanishing with the exception of the boundary of the planar sections and the geometry through the wormhole is thus flat.

necessary. In the relativistic setup, it is even not clear what "at the same moment means." Times of identification of both mouths must be specified explicitly on both sides. Of course, we have the restriction, that time must run continuously through the wormhole, i.e., locally, for the observer sitting in the wormhole, clocks on both sides must tick at the same rate without any jumps.

Let us assume as an example two mouths in the Minkowski spacetime which are at rest with respect to the same inertial frame,but they are identified with a time shift Δt equal, say, to one hour. Time on both sides of the wormhole runs in the same rate, so going through the wormhole does not affect an observer in any specific way. However, going through the wormhole, the observer arrives one hour to the future (or to the past, depending on the direction) with respect to the global inertial frame. Depending on the distance of both mouths in the surrounding space such a configuration may form the time machine: if the observer travelling through the wormhole one hour into the past is able to return through the surrounding space to his original position in less than one hour, he can form CTC, i.e., he can return to his own past and meet himself.

In our work we will consider even a simpler model of a time machine. We assume only *non-relativistic* situation, i.e., we assume that the speed of light is infinite and it determines a unique notion of simultaneity and if we use it we can define a global time – at least, before introducing a time machine. We also assume that the space is locally Euclidian.

The wormhole can be constructed in the non-relativistic spacetime in the same way as we discussed above – only in this case, thanks to the global simultaneity, we uniquely know what it means when both mouths of the wormhole are identified at the same time. If we identify them with any nonvanishing time shift Δt we immediately obtain the time machine, since the passage through the wormhole takes us to a different moment of time with respect to the global time of the surrounding spacetime. Of course, it destroys the standard causal structure of the non-relativistic spacetime (a clear distinction between future and past), but despite this we will keep using and referring to the original notion of the simultaneity and to the global time of the

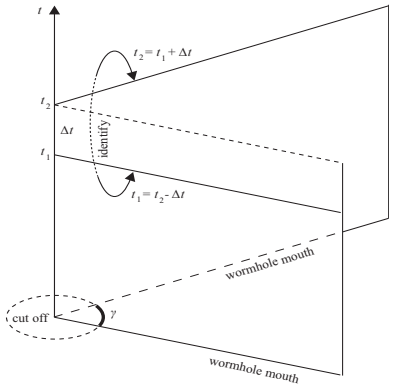

Figure 2: **A spacetime diagram of the conical time machine.** The vertical direction is temporal, horizontal planes correspond to the hypersurface of simultaneity of the original spacetime (the third spatial direction is suppressed). Two half-planes on forming the boundary of the conical spacetime represent the history of the mouths of the wormhole and they are identified with a time shift Δt.

surrounding space.

Our second simplification is that we use the wormhole with planar mouths instead of spherical ones. Namely, we cut out from the space two planar sections which we identify as in figure 1b. Since we use *flat planar* sections their identification is geometrically trivial – spacetime in them is flat everywhere, the space is locally Euclidian, without matter. Here we ignored problematic boundaries of our planar sections. The whole curvature of the mouths is squeezed to these borders which can be understood as a kind of solid frames on which the traversable parts of the wormhole are spanned.

To avoid a discussion of the wormhole boundary we assume that the planar sections are much larger than the scales of our experiments. In this approximation we can even assume that the planar sections are infinite. To simplify the geometry even more we consider the mouths of our wormhole to be two half-planes with a common boundary line. These two half-planes form an angle γ. If we identify them (first, say, at the same moment of time) the space between them becomes a locally Euclidian space with a conical singularity localized on the axis – at the intersection of the half-planes. Indeed, if we restrict ourselves to the two dimensional picture and ignore the direction parallel to the axis, our space forms a cone with the angle γ around the vertex. Since we restrict our study only to particles moving perpendicularly to the axis, it will be sufficient to consider only this two dimensional cone.

Of course, this is over-idealized situation. We should keep in mind that the mouths of the wormhole are large but finite, so somewhere very far from the axis the conical part of the space ends and goes over to the full Euclidian space. But in our consideration we restrict ourselves only to the part of the space between the mouths of the wormhole. We thus effectively work in the conical space with angle γ around the axis.

Let us stress, that in our original construction the mouths of the wormhole are special and privileged – given by the position of the wormhole. However, after enlarging them to the semi-infinite size and restricting ourselves only to the conical space between mouths, we can no longer localise the position of the mouths by local experiments. Geometry through the mouths is locally Euclidian as everywhere else. We thus obtained a space which is axially symmetric with respect

to the rotation around the axis (it has also translation symmetry along the axis). The position of the wormhole can be identified only on scales larger than the wormhole, from the surrounding globally Euclidian space – however, this region is very far and we do not consider it.

In the last three paragraphs we assumed the identification of both mouths at the same moment of global time. Since we want to study a space with a time machine, we have to identify the mouths of the wormhole with a time shift Δt. This can be visualized in the three-dimensional spacetime diagram in figure 2 where we draw two important spatial directions in horizontal directions. The vertical direction corresponds to time. Semi-planar mouths of the wormhole at one moment are thus depicted as horizontal semi-lines, their time evolution as vertical half-planes. The identification of such two half-planes is not on the same vertical level, but with the vertical shift Δt. We assume that going through the wormhole in anticlockwise direction takes us time $\Delta t > 0$ to the past, in clockwise direction to the future.

After such an identification the spacetime is still locally Euclidian, even through the wormhole, (of course, except the axis), but endowed with a strange causal structure. Hypersurfaces of simultaneity (originally horizontal planes) propagate through the wormhole and form "helical" surfaces winding around the vertex. This explicitly demonstrates that the spacetime contains CTCs.

In the just described conical spacetime with the time machine we investigate a motion of a particle which can interact with a similar particle by elastic collisions described by the standard non-relativistic local laws. Namely, we assume the validity of the local conservation of energy and momentum. To study elastic collisions we consider finite solid spherical balls of radius R (this is also the main reason for the restriction to the non-relativistic case). However, in this paper we concentrate mainly on the simpler limit $R \to 0$ for which the discussion simplifies considerably since it turns out to be scale invariant. The case of finite balls will be shortly discussed at the end and thoroughly presented elsewhere [3].

III Point particle

As we described above, we consider a point particle moving in two dimensional conical space with a positive time shift Δt when going in the clockwise direction around the vertex of the cone. We also assume that the angle γ around the vertex of the cone is smaller than π since only for such angles we obtain interesting situations of self-collisions of the particle. Indeed, on the cone with $\gamma < \pi$ a straight line intersects itself at least once. Since a free particle is moving along the straight line, after passing through the time machine its trajectory must intersect the trajectory along which the same particle approached the time machine. If the trajectory crosses itself in different times we will speak about *self-intersection*. If the particle intersects its trajectory exactly at the same times, it hits itself and we speak about *self-collision*. In the following we will specify the conditions for the self-collision and find consistent solutions of a particle motion with one self-collision.

A trajectory of the particle is determined by two initial parameters: the *impact parameter* ρ which gives the distance of the initial trajectory from the vertex of the cone, and the *magnitude of initial velocity* $u > 0$, see figure 3a. We adopt the convention that the impact parameter ρ is positive if the particle circles the cone in the counterclockwise direction and it is negative if it

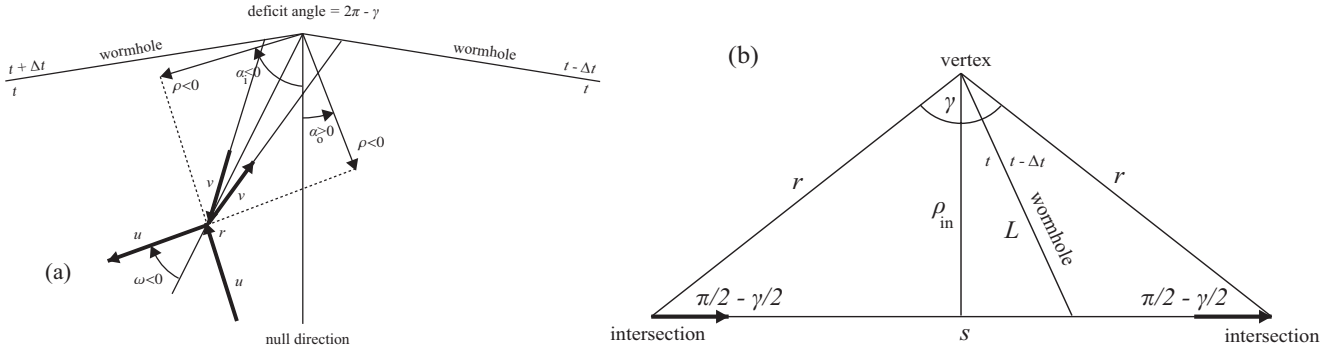

Figure 3: **Geometry of self-colliding trajectory.** (a) A typical self-colliding trajectory in the conical space with a time machine. A point particle is approaching the wormhole from infinity with a velocity u, it collides with the version of itself which already passed through the time machine, and with a velocity v moves toward the wormhole. After passing it and self-colliding with itself, it moves with the velocity u back to infinity. The conical space is illustrated as an angle boundary of which represent mouths of the wormhole and should be identified. (b) The trajectory between the self-collision is a straight line, which can be clearly demonstrated if we cut the conical space not along the wormhole but along the radial line going through the self-collision. The wormhole is than depicted as another radial line. Since the particle passes the wormhole freely, its trajectory must be straight across the wormhole line. It starts and ends at the self-collision which is represented as two points on the boundary semi-lines at the distance r from the vertex. The same geometry applies also for a segment of the collision-free trajectory between its self-intersection. We immediately see that length between the self-intersection is $2r \sin \frac{\gamma}{2}$.

circles the cone in the clockwise direction.

The parameters u and ρ do not determine the initial trajectory uniquely since these parameters do not distinguish between trajectories which are just rotated around the vertex of the cone. We should specify also an angle $\alpha_{\rm i}$ of the incoming trajectory with respect to some chosen "null" direction. However, since the conical space is symmetric under rotations, the angle $\alpha_{\rm i}$ does not affect a character of the motion and we can ignore it.

A generic physical solution to initial data is represented by a collision-free trajectory. A particle which moves along such a trajectory intersects itself without a self-collision. The collision-free trajectory can take the particle to the past, or to the future, according to the direction in which it passes the wormhole. If the collision-free trajectory is determined by a negative impact parameter $\rho < 0$ the time machine takes the particle to the future, if the collision-free trajectory is defined by positive impact parameter $\rho > 0$ it takes the particle back in time by $-\Delta t$.

The length s of the straight trajectory between its self-intersection is given by the conical geometry as can be seen in figure 3,

$$s = 2\rho \, \tan \frac{\gamma}{2} \, . \tag{1}$$

The time needed to circle the cone is thus $s/u = \frac{2\rho \tan \gamma/2}{u}$.

Now, there are two ways in which the particle can travel back in time without self-collision. (a) Either the movement around the cone takes longer time than the time thus gained, namely $\Delta t < s/u$, in which case the older version of the particle (i.e., the one that already passed the wormhole) gets late with respect to the younger version of the particle which moves through the point of intersection as the first. (b) Or the orbit around the cone takes shorter time than time

thus gained, $\Delta t > s/u$, in which case the older version of the particle moves through the point of intersection as the first.

For a special choice of parameters ρ and u the particle self-interacts. In this case while the older version of the particle passes through the time machine and leaves it, the younger version of the same particle moves from a distant region toward the time machine exactly in such a way that both versions of the particle collide. Such an initial condition is potentially *dangerous* since the self-collision could prevent the particle from passing the wormhole which would be inconsistent. However, for the same dangerous initial condition we could still find a consistent solution with a self-collision which would be fine-tuned in such a way that the self-interacting particle consistently moves through the time machine. To convince ourselves that it is really true we first investigate a general particle motion with one self-collision.

Let us assume that the self-collision takes place on a radial ray at the distance r from the vertex of the cone, see figure 3a. For a symmetry reason (justified also by a detailed study of collision of finite balls [3]) the self-collision will be symmetric with respect to the radial line. We will define the oriented angle $\omega \in [-\pi/2, \pi/2]$ between the radial ray and the outgoing trajectory – it is thus a half of the angle between ingoing and outgoing trajectories. We will see that the initial parameters u and ρ are uniquely related to the quantities ω and r and can be interchanged mutually. We also denote v the magnitude of the particle velocity between the self-collision and $\rho_{\rm in}$ the impact parameter of the trajectory between the self-collision.

For the collision-free trajectories we can define analogous quantities r and ω which refer to the point of self-intersection instead of self-collision. In this case $\rho_{\rm in} = \rho$ and the angle ω is given just by the conical geometry, namely

$$\omega = \omega_{\rm crit} \equiv \frac{\pi - \gamma}{2} \,. \tag{2}$$

From the definition of ρ, r, and ω we immediately find that for both self-interacting and collision-free trajectories the radial distance r is related to ρ by

$$\rho = r\, \sin\omega \,, \qquad \rho_{\rm in} = r\, \sin\omega_{\rm crit} = r\, \cos\frac{\gamma}{2} \,. \tag{3}$$

For a trajectory between the self-collision the "inner" velocity v is given by the condition that the particle has to travel the distance s in time Δt, i.e.,

$$v = \frac{s}{\Delta t} = \frac{2r \sin\frac{\gamma}{2}}{\Delta t} = \frac{2\rho}{\Delta t} \frac{\sin\frac{\gamma}{2}}{\sin\omega} \,, \tag{4}$$

where we expressed the length s using the radial distance r, see figure 3, which is given in terms of ρ and ω by equation (3).

The remaining relation between parameters ρ, u, and r, ω follows from the equations for the self-collision, namely from the momentum and energy conservation during the self-collision. A detailed study [3] of the self-collision of a finite ball of radius R shows that the particle can self-collide in two ways and the type of the self-collision is determined by the angle ω. For $\omega > \omega_{\rm crit}$ the trajectory of the particle after the self-collision is directed to the wormhole closer to the vertex than if it followed the collision-free trajectory. Thus the older version of the ball touches the younger one by its rear part. Let us denote such a case as the self-collision of the *type I*. If

$\omega < \omega_{\rm crit}$ then the trajectory of the particle is directed to the wormhole farther from the vertex than if it moved along the collision-free trajectory and the older version touches the younger version by its frontal part. We denote this case as the self-collision of the *type II*.

In the limit $R \to 0$ of the point particle the self-collision of the first type changes continuously into the self-collision of the second type and both types are described by the same equation. It turns to be equivalent to the conservation of the radial momentum during the self-collision. Comparing radial momentum of the particle between the self-collision given by $v \sin \frac{\gamma}{2}$ and radial momentum of the incoming trajectory $u \cos \omega$ we find

$$u \cos \omega = v \sin \frac{\gamma}{2} \,. \tag{5}$$

Substituting expression (4) we obtain ω in terms of ρ and u

$$\sin(2\omega) = \frac{4\rho \sin^2 \frac{\gamma}{2}}{u\Delta t} \,. \tag{6}$$

Finally, inserting the expression for ω into (3) we get r in terms of ρ and u.

Before a discussion of these relation let us return to the dangerous initial conditions mentioned above. Clearly, the dangerous initial parameters would be those for which the self-intersection becomes the self-collision. It means that $\omega = \omega_{\rm crit}$ and $v = u$. For the given initial velocity u we denote the dangerous value of the impact parameters as $\rho_{\rm px}$. Substituting $\omega = \omega_{\rm crit}$ and $v = u$ into (4) we find

$$\rho_{\rm px} = \frac{u\,\Delta t}{2 \tan \frac{\gamma}{2}} \,. \tag{7}$$

Let us reformulate equations (6) and (3) in such a way that the radial distance and the impact parameter are expressed as functions of the angle ω and of the velocity u

$$\rho(\omega) = \frac{u\Delta t \sin\omega \cos\omega}{2 \sin^2 \frac{\gamma}{2}} \,, \qquad r(\omega) = \frac{u\Delta t \cos\omega}{2 \sin^2 \frac{\gamma}{2}} \,. \tag{8}$$

Dividing these equations by $u\Delta t$ we obtain relations for dimensionless quantities (distances measured in units of $u\Delta t$) which do not depend on the velocity u anymore. It means that point particle configurations with different initial velocities u are related just by a simple rescaling. Therefore, we will discuss only the relation between ρ, r, and ω. This dependence is depicted in figure 4. On the left we can see the function $\rho = \rho(\omega)$, on the right the parametric curve $[\rho(\omega), r(\omega)]$ in the plane r-ρ, with $\omega \in [-\pi/2, \pi/2]$. From these graphs we can easily read the desired dependence $\omega(\rho)$ and $r(\rho)$.

The first equation of (8) also determines the interval of the impact parameter ρ for which the self-interaction is possible. Clearly, $\rho \in [\rho_{\rm min}, \rho_{\rm max}]$ with $\rho_{\rm min} \equiv -\frac{\Delta t u}{4 \sin^2 \gamma/2}$ and $\rho_{\rm max} \equiv \frac{\Delta t u}{4 \sin^2 \gamma/2}$. Similarly for the radial distance of the self-collision r we find $r \in [0, \frac{\Delta t u}{2 \sin^2 \gamma/2}]$. Trajectories outside this region cross themselves too far from the vertex with the time shift too short to self-interact.

Inspecting figure 4a we thus see that for $\rho \notin [\rho_{\rm min}, \rho_{\rm max}]$ we have exactly one solution for ω, r which corresponds to the collision-free trajectory. However, for $\rho \in (\rho_{\rm min}, \rho_{\rm max})$, $\rho \neq \rho_{\rm px}$ we find three solutions for ω, r – one corresponding again to the collision-free trajectory, and

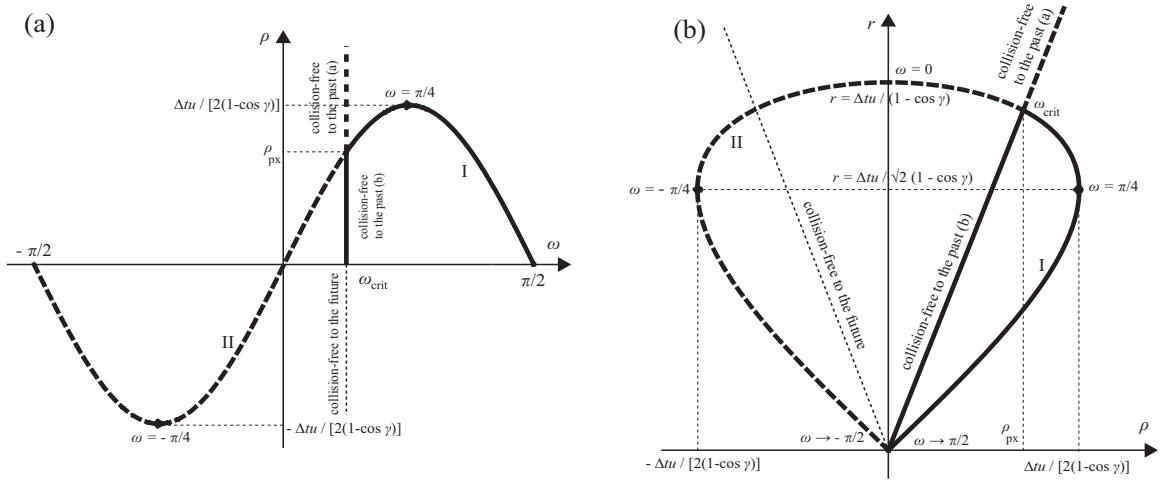

Figure 4: **Relation between ρ, r, and ω for a point particle.** (a) The dependence $\rho = \rho(\omega)$ and (b) the parametric curve $[\rho(\omega), r(\omega)]$. Relations for a self-colliding particle are given by eqs. (8). Relations for collision-free trajectories are given by eqs. (2) and (3). The angle ω runs in the interval $[-\pi/2, \pi/2]$.

two corresponding to trajectories with a self-collision. In the limiting cases $\rho = \rho_{\min}, \rho_{\max}$ two self-colliding solutions coincide.

The special case of the dangerous initial conditions $\rho = \rho_{\rm px}$ seems to have only two solutions with collision-free trajectory degenerating to the paradoxical case. The exact behavior of the particle in this case cannot be solved on the level of a point particle model but can be found by investigating finite balls as we will do in the next section.

IV Balls of a finite radius

In this section we would like to discuss shortly the motion of solid balls of a finite radius. We review only the main results, technical details can be found in [3].

The discussion of this case goes along the same line as for a point particle – we can introduce initial parameters ρ and u and parameters r and ω related to the self-collision. However, the finite radius of balls modifies the description of the self-collision. The radius R introduces a new scale into the theory and a dependence on the initial velocity is not so simple. Moreover, as we discussed above, there are two types of self-collision, however, for $R > 0$ the equations describing them are different.

The solutions of these equations split into two classes – we have physically realistic solutions which resemble those discussed in the case of point particle. Additionally, we also have unphysical solutions for which the particle during the self-collision would have exchange a negative momentum. So, if we do not consider "sticky" balls we have to rule these solutions out. The relation among ρ, r and ω with fixed u for finite balls is shown in figure 5 in a similar manner as we did for a point particle in figure 4. Since the equation for collisions of type I and II are different we have two curves representing dependencies $\rho(\omega)$ and $r(\omega)$ (lines I and II in the figure). However, only a part of these curves correspond to physical solutions (thick lines). Spurious solutions are depicted by thin lines. Similarly as for the case of point particle we also included lines for collision-free

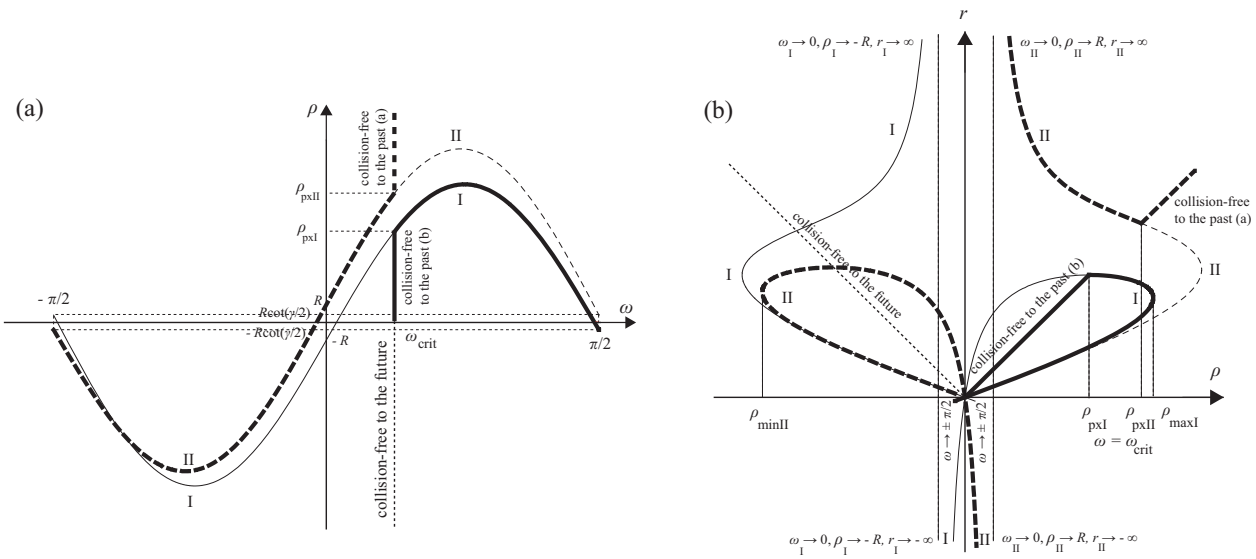

Figure 5: **Relation between ρ, r, and ω for a particle of a finite radius R.** (a) The dependence $\rho = \rho(\omega)$ and (b) the parametric curve $[\rho(\omega), r(\omega)]$ with u fixed and $\omega \in [-\frac{\pi}{2}, \frac{\pi}{2}]$. Curves corresponding to the physical solutions are represented by thick solid (type I) and dashed (type II) lines while curves corresponding to the spurious solutions are represented by thin lines.

trajectories given by $\omega = \omega_{\text{crit}}$ and with ρ not corresponding to paradoxical values.

However, for a finite radius R, instead of only one paradoxical value ρ_{px} as in the case of a point particle we have an entire interval $[\rho_{\text{px}_\text{I}}, \rho_{\text{px}_\text{II}}]$ of dangerous values of ρ (for fixed u) for which a collision-free trajectory is inconsistent, see figure 5. Boundary values $\rho_{\text{px}_\text{I}}$ and $\rho_{\text{px}_\text{II}}$ of the interval of dangerous values of ρ represent solutions for which both versions of the ball just touch each other without exchanging any momentum. Thus they can be considered both collision-free and self-interacting trajectories.

Now, let us discuss a number of consistent solutions for different initial values ρ and u. For fixed u it can be easily read from figure 5. For a large positive or negative ρ we have again only one collision-free trajectory. For ρ sufficiently small but out of the range of dangerous values, $\rho \notin [\rho_{\text{px}_\text{I}}, \rho_{\text{px}_\text{II}}]$, we have one collision-free trajectory and two physical self-colliding trajectories. Surprisingly, for dangerous values $\rho \in [\rho_{\text{px}_\text{I}}, \rho_{\text{px}_\text{II}}]$ we also have three solutions, all of them with a self-collision. One of them is of type II, two other solutions are of type I. An inconsistent collision-free trajectory thus changes to a new self-colliding solution.

The geometry of all these three consistent self-colliding solutions corresponding to a dangerous initial data is explicitly shown in figure 6.

Summary

We have discussed the motion of a point particle and of a solid ball in the non-relativistic conical space with a time machine. The point particle model documents a non-uniqueness of the evolutions in the presence of time machines. However, this model is not rich enough to investigate structure of trajectories corresponding to dangerous initial values. Such a discussion can be done

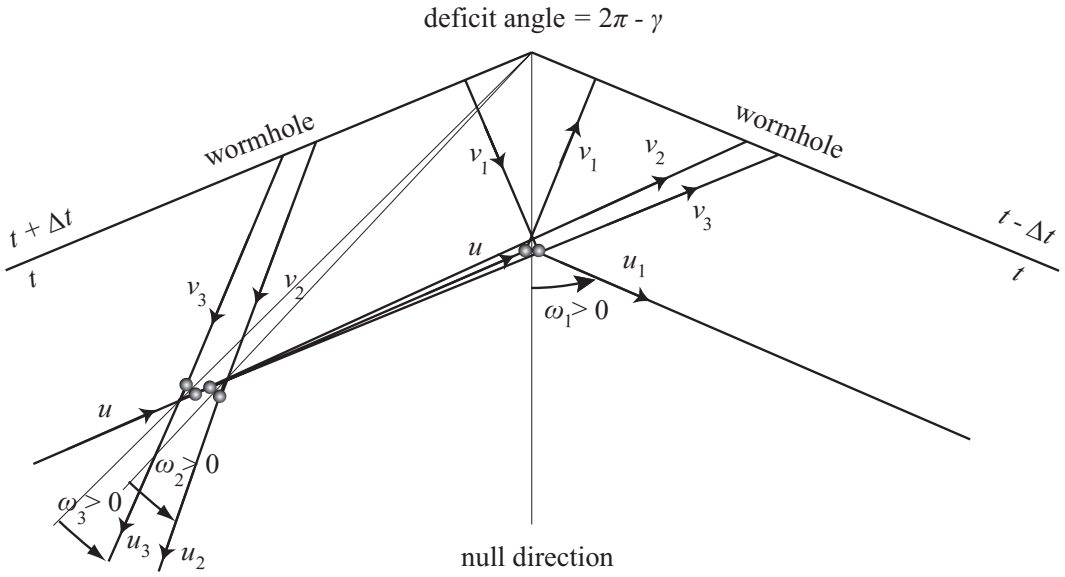

Figure 6: **Solutions for "paradoxical" initial data.** Figure shows three consistent solutions 1, 2, and 3 for "paradoxical" or "dangerous" initial data. We can identify three solutions with a self-collision, two of them are similar to the case of generic initial data. However, for the paradoxical initial data there is no collision-free solution. Instead, it is compensated by the third self-colliding solution.

in the case of finite balls for which we found that a number of solutions for given initial data is the same for dangerous initial data as for generic ones. An inconsistent collision-free trajectory is replaced by a new self-colliding solution.

Finally, let us mention that we considered only trajectories with one self-collision or no collision at all. In principle, it can and it does happen that the particle self-collides or self-intersects more times. Such a possibility enlarges a number of solutions for given initial data and complicates a discussion of all possible particle motions. For a point particle such the discussion is done in [3].

Acknowledgement

This work was supported by MŠMT ČR MSM0021610860 (J.D.) and GAR202/06/0041 (P.K.). We would like to thank J. Langer for useful discussions and reading the manuscript.

References

[1] Echeverria F, Klinkhammer G, Thorne K, *Physical Review D* **44** (1991), 1077–..

[2] Friedman J, Morris M, *Physical Review Letters*, **66** (1991)

[3] Dolanský J, Krtouš P, in preparation

[4] Thorne K, Black holes and time warps, (1994)